EFFECTS OF HIGH-DILUTED COLLOIDAL SILICA MIXTURES ON THE MECHANICAL BEHAVIOR OF POTENTIALLY LIQUEFIABLE SAND

Dissertation

submitted to and approved by the

Faculty of Architecture, Civil Engineering and Environmental Sciences
Technische Universität Braunschweig

and the

Department of Civil and Environmental Engineering
University of Florence

in candidacy for the degree of a
Doktor-Ingenieur (Dr.-Ing.) /
Dottore di Ricerca in Civil and Environmental Engineering[*)]

by
Giovanni Ciardi
born 05 May 1989
from Empoli, Italy

Submitted on	16 August 2019
Oral examination on	06 November 2019
Professorial advisors	Prof. Joachim Stahlmann
	Prof. Claudia Madiai

2019

*) Either the German or the Italian form of the title may be used.

Contents

List of Figures

List of Tables

List of Symbols

a_{max}	peak acceleration at ground surface
α	concentration of accelerant in the grout (by volume)
B	Skempton's coefficient
c'	effective cohesion
CRR	cyclic resistance ratio
CS	colloidal silica
CS_W	silica solids content (by weight)
CSR	cyclic stress ratio
D	specimen diameter
D_0	initial specimen diameter
D_r	relative density
D_x	particle diameter corresponding to x% passing
DA	double amplitude
Δu	excess pore water pressure
e	void ratio
e_0	initial void ratio
e_c	voida ratio after isotropic consolidation
e_{cr}	critical void ratio
e_{max}	maximum void ratio
e_{min}	minimum void ratio
E_0	tangent modulus at small strain (untreated material)
E_x	tangent modulus at small strain (x% treated material)
ϵ_a	axial strain
ϵ_r	radial strain
ϵ_{DA}	double amplitude axial strain
ϵ_q	deviatoric strain
ϵ_v	vertical strain
ϵ_{vol}	volumetric strain
FLS	flow liquefaction surface
ϕ'	effective angle of internal friction
g	gravity acceleration
G_s	specific gravity
γ	shear strain

γ_{DA}	double amplitude shear strain
H	specimen height
H_0	initial specimen height
i	hydraulic gradient
ID	identification code
I_f	improvement factor
$k_{T=10°C}$	hydraulic conductivity (10°C)
MR_{Vol}	concentration of MasterRoc MP 325 (by volume)
MR_W	concentration of MasterRoc MP 325 by (weight)
m_v	compressibility modulus
N	number of loading cycles
ν	Poisson's ratio
p'	mean effective stress
PPR	pocket penetrometer shear resistance
q	deviatoric stress
q_{max}	maximum deviatoric stress
r_d	coefficient of stress reduction
r_u	pore water pressure ratio
ρ_{acc}	density of accelerant (20°C)
ρ_{H_2O}	density of distilled water (20°C)
ρ_{MR}	density of MasterRoc MP 325 (20°C)
s'	$\frac{\sigma'_1+\sigma'_3}{2}$
S_h	horizontal displacement
S_r	degree of saturation
S_v	vertical displacement
SSL	steady state line
σ	total normal stress
σ'	effective normal stress
σ_1	major total stress
σ'_1	major effective stress
σ_3	minor total stress
σ'_3	minor effective stress
σ'_c	consolidation effective stress
σ'_v	vertical effective stress
σ_{v0}	total vertical overburden stress
σ'_{v0}	effective vertical overburden stress
σ'_{vc}	vertical effective consolidation stress
t'	$\frac{\sigma'_1-\sigma'_3}{2}$
t_c	curing time
t_g	gel time
τ	shear stress
τ_f	shear stress at failure

τ_{max}	maximum shear stress in direct shear tests
u	pore water pressure
U	uniformity coefficient
V_{acc}	volume of accelerant
V_{H_2O}	volume of distilled water
V_{MR}	volume of MasterRoc MP 325
V_p	P-waves velocity
V_s	S-waves velocity
V_{tot}	total volume of grout
ψ	state parameter

Acknowledgments

I would like to thank my advisors Claudia Madiai, Giovanni Vannucchi and Joachim Stahlmann, for their constant support. Special thanks to Giuseppe Modoni, who suggested the potential benefits of colloidal silica grout dilution, and to Matthias Rosenberg, who constantly helped me during my period abroad. Laboratory investigations couldn't be carried out without the fundamental help of Roberto Bardotti, Pietro Vannocci, Massimiliano Nocentini, Erminio Salvatore, Martina Fanfani, Eugen Daumlechner, Svenja Wacker, Burcu Sacildi and Edoardo Turco. Thanks to Patrizia Rossi, Paola Paoli, Laura Chelazzi and Samuele Ciattini, who helped me understanding the chemical properties of colloidal silica and performing X-ray micro-tomography tests. Thanks to Sibelco S.p.A. and to BASF SE, that provided our laboratory with Fossanova FO-25 sand and with colloidal silica solution, respectively.

Abstract

Seismic soil liquefaction is one of the greatest hazards of earthquakes of a certain size, and its effects on structures, infrastructures and human lives can be devastating. Liquefaction arises because of the soil shear resistance decrease as a consequence of the pore water pressure build-up in loose saturated cohesionless soil subjected to undrained loading conditions.

If a soil is susceptible to liquefaction, several remedial measures can be considered to reduce the liquefaction hazard. Different mitigation techniques have been proposed over the past years; *colloidal silica grouting* is one of the innovative proposals that have been recently developed. A colloidal silica (CS) mixture is a low-viscosity grout able to provide the soil particles with an artificial cohesion which improves the soil behavior under both static and cyclic loading conditions. Cohesion results from a gelation process, developed within the grout as a consequence of chemical interactions. The amount of cohesion depends on the initial silica content: the higher the silica concentration, the higher the development of silica bonds among the grains. Historically, CS contents no lower than 5% by weight have been considered enough to improve the liquefaction resistance of liquefiable sand. However, the effectiveness of high-diluted CS mixtures has not been exhaustively investigated yet.

The present study aims to evaluate the effects of low-content CS grouts (i.e. CS contents lower than 5% by weight) on the behavior of a clean liquefiable sand by means of an extensive laboratory investigations campaign. Laboratory tests were carried out on treated and untreated material; an in-depth analysis of soil response is presented and discussed.

The performed tests showed that 2% CS content is enough to improve the soil behavior under both cyclic and monotonic loading conditions; however, the compressibility of treated soil is higher than that of the untreated one, and it increases as CS contents increase. For this reason, 2% CS represents the optimal compromise to enhance sand liquefaction resistance by minimizing undesired effects (i.e. increased soil strain) and economic costs of a potential treatment.

Chapter 1

Introduction

1.1 Statement of the problem

Seismic soil liquefaction is one of the greatest hazards related to earthquakes. It can occur in loose saturated cohesionless soils during earthquakes of a certain size, and it appears as a loss of soil shearing resistance and/or as large and accumulated soil strain. Liquefaction phenomena can potentially cause huge damages to human lives, structures and infrastructures.

In order to reduce the liquefaction hazard and mitigate its effects, several remedial measures have been proposed over the years, such as densification, reinforcement, grouting and mixing methods. Among these latter and within the framework of innovative chemical products used to stabilize potentially liquefiable soil, colloidal silica (CS) has recently become one of the most interesting and appealing ones. A colloidal silica solution is an aqueous dispersion of colloidal silica particles: it is a clear, harmless, low-viscosity fluid that, if properly mixed with a reactant, increases its initial viscosity and it becomes a *gel* after a certain time. The gel state reflects the growth of silica-based chains within the product. Gel bonds, therefore, if developed within the soil grains, can stabilize the solid matrix, providing it with a sort of artificial cohesion. In addition, since colloidal silica is durable and not toxic, its use for geotechnical engineering practice would be environmentally safe and economically favorable: its cost is in fact significantly lower than that of other most commonly used grouts, such as cement. A colloidal silica grout can be injected and delivered to a target area without high injection pressures, since the initial viscosity of the mixture can be kept as low as that of water. However, the major concern for a wide practical use of colloidal silica is represented by the need of a specific in-field design to avoid early/late gelation; furthermore, a decrease of the soil hydraulic conductivity is expected, due to the presence of gel within the soil voids.

It has been demonstrated by researchers that the concentration of silica particles in the treatment solution significantly changes the mechanical response of the stabilized soil, since it directly affects the amount of silica chains developed within the colloidal silica gel. Broadly speaking, the higher the silica content, the higher the level of soil improvement, the higher the hydraulic conductivity reduction. However, the use of high CS content in the stabilizing grout for the treatment of a certain soil volume could be expensive and unnecessary for liquefaction mitigation purposes.

Following the work of Gallagher and Mitchell (2002), who suggested that a 5-10% CS con-

tent (by weight in the grout) is enough to improve the undrained cyclic behavior of a loose clean sand, many Authors assumed 5% CS concentration as a sort of lower limit for CS dilution in the stabilizing grout. However, it has been shown that even CS contents lower than 5% are sufficient to reduce the liquefaction potential of a liquefiable sand (Kodaka et al., 2005), and that also 1% CS gel can provide the sand with adequate bonds after a certain time, thus achieving an adequate level of improvement (Hamderi and Gallagher, 2015).These studies, however, do not deal with the effects of high-diluted CS grouts on the mechanical response of treated material. If low CS content grouts are proved to be effective in increasing the liquefaction resistance of sand, the reduction of CS content in the treatment solution would imply significant economic saving; at the same time, the overall treatment would probably have less impact on the pre-existing soil properties, such as its hydraulic conductivity and compressibility. Therefore, the effects of high CS dilution need to be further investigated.

1.2 Scope of research

The present research aims to investigate how high-diluted colloidal silica mixtures affect the mechanical behavior of a potentially liquefiable sand, in order to optimize the CS dilution for practical uses. To date, there are no systematic scientific contributions on this particular topic; therefore, an in-depth study is required to investigate the behavior of sand treated with these mixtures under both static and cyclic loading conditions, and to understand if they can be successfully used as a cost-effective method for reducing the liquefaction susceptibility of cohesionless soils. The main goal of this PhD Thesis is therefore to focus on the effects of high-diluted CS solutions (no more than 5% by weight CS concentration in the grout) on the mechanical properties of the treated material, with emphasis on the undrained cyclic resistance of a clean stabilized sand.

1.3 Methods

A detailed understanding of the mechanical response of treated soil requires an overall analysis of its behavior under both static and cyclic loading conditions; the effects of the treatment on the fundamental geotechnical properties need to be discussed. It is in fact necessary to exhaustively describe the characteristics of the stabilized soil material (i.e. hydraulic conductivity, compressibility) before the analysis focuses on its undrained monotonic and cyclic behavior.

An experimental campaign consisting of laboratory tests on treated and untreated material was carried out to investigate the effects of the CS treatment on the mechanical properties of a uniform grain distributed sand. The untreated material was taken as the reference for comparison of the obtained results. Firstly, X-ray micro tomography tests and analysis of the pure colloidal silica grout were performed, in order to understand the gelation process and to correctly set up the tests on treated soil. Secondly, permeation and permeability tests, direct shear tests, oedometer tests, and monotonic as well as cyclic triaxial tests, were performed on treated and untreated material. The results are presented and discussed pointing out the modifications provided by the CS treatment to the low-CS content treated soil. The reference material con-

sisted of a mainly siliceous sand, named S3, extracted from a quarry and sieved to eliminate any influence of the fine fraction; its grain distribution is entirely within the boundaries of the most liquefiable soils. Direct shear tests were used to determine the drained shear resistance parameter for treated sand, while oedometer tests were used to evaluate the compressibility properties of treated and untreated materials. Finally, monotonic and cyclic triaxial tests were carried out on cylindrical specimens that were previously saturated by colloidal silica grout. The specimen preparation method allowed full gel saturation of the material, but it didn't permit pore pressure measurement; therefore, proper failure criteria were discussed and assumed to interpret test results.

1.3.1 Thesis outline

This study is divided into six Chapters. An overview of the overall topic is presented in Chapter 1; detailed literature reviews on the liquefaction phenomenon, including liquefaction countermeasures, and on colloidal silica grouting are presented in Chapter 2 and Chapter 3, respectively. Experimental procedures are discussed in detail in Chapter 4, while test results are shown and discussed in Chapter 5. Chapter 6 concludes this study, summarizing the main results and pointing out benefits and shortcomings of colloidal silica grouting.

Chapter 2

Seismic soil liquefaction: concepts and definitions

2.1 Introduction

It is common knowledge that *seismic soil liquefaction* can be considered as one of the most impressive and catastrophic effects of earthquakes of a certain size; over the past decades, severe damages to buildings, infrastructures, and human lives have been reported after many great shocks all around the world. Lateral soil movements, subsidence of buildings, high settlements, floating of buried structures, slope and foundation failures are typical effects related to seismic-induced liquefaction. Historically, a systematic scientific interest towards liquefaction has risen up after Niigata (1964, Japan) and Alaska (1964) Earthquakes, after which widespread liquefaction phenomena were observed (Fig. 2.1, 2.2); in recent years, several important liquefaction occurrences have been reported after e.g. Taiwan (1999), Christchurch (New Zealand, 2011), Emilia (Italy, 2012) and Hokkaido (Japan, 2018) Earthquakes.

Broadly speaking, seismic liquefaction indicates the peculiar way of failure of cohesionless saturated soils under cyclic loading conditions: it is characteristic of fully saturated non-plastic soils, such as sandy or silty non-cohesive soils, and it arises due to the build-up of earthquake-induced pore water pressure under undrained loading conditions. As the pore water pressure rises, the soil stiffness and shear strength decrease, thus inducing soil instability; however, the ultimate soil condition, which can be generally referred to as *failure*, can be achieved in very different ways, depending on several factors such as the soil initial void ratio, confining pressure, or the ratio between the existing static shear stress and the residual one after the shake, among many others. The different manners the liquefiable soil fails during or after a seismic event are characteristics of distinct liquefaction phenomena, such as *flow liquefaction* or *cyclic mobility*, that are however triggered by the same mechanism, that is, the generation and build-up of positive pore water pressure under constant volume conditions. For this reason, when it is not specifically required to distinguish among the different aspects of the phenomenon, the term *liquefaction* is generally used to refer to all soil instabilities due to the increased pore water pressure in cohesionless saturated soils with.

Understanding liquefaction mechanisms at the volume element scale (e.g. by means of

laboratory tests) has been helpful in identifying adequate strategies to mitigate its effects at sites prone to liquefaction. For instance, since numerous studies revealed that the amount of the excess pore water pressure in liquefiable soils is related to their volume contraction, prevented under undrained loading, a good strategy to reduce it is to decrease the contractive tendency of soil; this can be easily achieved by reducing the available pore space among soil grains, thus by making the grain packaging denser than in the origin. Consequently, certain *in situ* remedial measures against liquefaction developed over the years, like densification, vibro-flotation, or compaction, aim to reduce the available volume of voids, thus increasing the soil liquefaction *resistance*.

In the present Chapter the basics and definitions of liquefaction are firstly discussed; secondly, an in-depth review of liquefaction mitigation techniques is proposed, with particular attention to innovative proposals that have been (or are still being) developed.

Figure 2.1: *Tilted buildings as a consequence of liquefaction after Niigata Earthquake (from website: depts.washington.edu).*

Figure 2.2: *Lifted up pavement of a box auto after the Emilia Earthquake (property of DiCeA, University of Florence).*

2.2 The mechanism of liquefaction

2.2.1 Definitions

According to Castro (1975), "*the term liquefaction has been used to refer to a group of phenomena which have in common the development of high pore pressures in saturated sands due to static or cyclic loading under constant volume conditions*; the "Dictionary of Soil Mechanics and Foundation Engineering" defines liquefaction as "*the state existing when saturated sandy soil loses shearing strength and effective stresses are reduced as a result of increased pore water pressure*" (Japanese Geotechnical Society, 1998). Again, Castro and Poulos (1977) stated that, during liquefaction, "*a saturated sand loses a large percentage of its shear resistance (due to monotonic or to cyclic loading) and flows in a manner resembling a liquid until the shear stresses acting on the mass are as low as its reduced shear resistance*". From these definitions, it is clear that *liquefaction* is a phenomenon characterized by the excess of pore water pressure generation in saturated cohesionless soils subjected to undrained loading conditions. The pore water pressure generation "*is a hallmark*" of all liquefaction occurrences (Kramer, 1996).

In saturated soils, the tendency to volume changes under drained loading conditions corresponds to a variation of pore water pressure under undrained loading conditions[1]. If soil tends to contract, the increase of positive pore water pressure causes a reduction of effective stress, as expressed by Equation 2.1 (*Effective Stress Principle*, after Terzaghi, 1936), where σ and σ' denote the total and effective normal stress respectively, and u represents the initial pore water pressure. The generation of positive *extra* pore pressure (Δu), leads to a decrease in σ', which produces, in turn, a reduction of the soil shear strength; the latter, which represents the shear stress at failure, τ_f, can be described by a Mohr-Coulomb's failure criterion (Eq. 2.2, where ϕ' and c' represent internal effective friction angle and soil effective cohesion respectively), where c' is null for cohesionless soils. In a limit case, the developed Δu can be great enough to annul the effective stress, and consequently the soil shear strength. Equation 2.3, that is often referred to as *initial liquefaction*, is equivalent to the condition $\tau_f = 0$, which surely corresponds to a state of instability.

$$\sigma' = \sigma - u = \sigma - (u + \Delta u) \tag{2.1}$$

$$\tau_f = \sigma' \cdot tan\phi' + c' \tag{2.2}$$

$$\sigma = u + \Delta u \tag{2.3}$$

Liquefaction can be triggered either by monotonic or cyclic loading; the nature of the applied load can determine the way the soil achieves failure, but it is not specifically part of the liquefaction definition, which, in turn, has the development of pore water pressure in saturated soils as a common basis. Therefore, it is necessary to distinguish between different instability phenomena, related to the specific loading conditions, namely *static* and *seismic* liquefaction, that occur as a consequence of the increased pore water pressure under constant volume con-

[1] During earthquakes the loading rate is so fast that even cohesionless soils cannot drain fast enough.

ditions. There are numerous evidences that static and seismic liquefaction are strongly related, as discussed further on.

Equation 2.3 is not, however, the common denominator of all liquefaction phenomena, that can be distinguished into two main groups, named *flow liquefaction* and *cyclic mobility*. The way these occurrences are triggered, and the potential damages they can produce, are very different, and they can be clearly understood by referring to the overall theory of *steady* (*critical*) *state*, a valuable tool that can provide significant insight into the nature of these occurrences.

Liquefaction may occurs also under monotonic loading and under cyclic loading not due to the earthquake[2]. The present Thesis deals with the effects of cyclic loading on cohesionless saturated soils at high strain levels and at failure, with specific reference to *seismic* liquefaction.

Flow liquefaction, cyclic mobility, cyclic liquefaction

Despite being generally referred both to as *liquefaction*, *flow liquefaction* and *cyclic mobility* are two distinct phenomena. The main difference between them is represented by the amplitude of the existing static shear stress (*driving stress*) compared to the soil strength in the liquefied state. According to Kramer (1996), flow liquefaction "*can occur when the shear stress required for static equilibrium of a soil mass (the static shear stress) is greater than the shear strength of the soil in its liquefied state*", whereas cyclic mobility "*occurs when the static shear stress is less than the shear strength of the liquefied soil*".

Practically, in flow liquefaction the failure condition is governed by the initial static shear stresses: the pore pressure increase, produced by monotonic or cyclic stresses, decreases the soil shear strength allowing the static stresses to induce the soil mass failure. Differently, during cyclic mobility, that can only be triggered by cyclic loading, "*the deformations [...] are driven by both cyclic and static shear stresses*", and they "*develop incrementally during earthquake shaking*", so the failure condition is governed by the soil strain rate. *Cyclic liquefaction* or, equally, *level ground liquefaction*, indicates a particular case of cyclic mobility characterized by the absence of driving stresses. The major damages due to cyclic liquefaction are represented by the upward flow of pore water after pore water pressure dissipates (such as sand boils, settlements), since there are no existing shear stresses able to drive great lateral deformations, while the main failures connected to flow liquefaction and cyclic mobility are often referred to as *flow failures* and *lateral spreadings*, respectively. Flow failures, specifically, are one of the most disastrous occurrences of liquefaction.

2.2.2 Liquefaction susceptibility

The evaluation of liquefaction susceptibility represents the first step before any further liquefaction-related hazard estimation is made and several criteria can be applied to understand if a certain site is susceptible to liquefaction.

Table 2.1 illustrates the factors that influence the susceptibility of a soil deposit to liquefaction; among these, three conditions are essential for liquefaction to be triggered:

[2]For example, liquefaction-related problems have also been investigated for gravity structures in marine environments such as breakwaters, offshore platforms and offshore turbines foundations, due to the effect of repeated wave loads (e.g. Oumeraci (1994); De Groot et al. (2006)).

- the soil deposit is fully saturated;
- the soil is a sandy-silty soil with non plastic fines and contractive tendency;
- the amplitude and the duration of the cyclic stress is sufficiently high.

Table 2.1: *Factors affecting the liquefaction occurrence (from Japanese Geotechnical Society (1998)).*

Soil properties	Unit weight, grain size distribution, fines content, average grain size, clay content, plasticity index, relative density, structure of skeleton, shear modulus, damping ratio, coefficient of volume compressibility, degree of saturation, specific gravity of soil particle
Geological conditions	Water table, geological age, total stress, effective stress, overconsolidation ratio, earth pressure at rest, initial static shear stress, deformation constraint condition, boundary condition against seepage: drainage conditions
Earthquake motion	Horizontal acceleration, magnitude of earthquake, intensity of shear stress and number of cycles or duration, strain level, direction of shearing

If a soil deposit is prone to liquefaction there is the need to understand how it can be triggered and what kind of damages can be expected, i.e. to existing structures. Four different simplified criteria can be used for liquefaction susceptibility evaluation: historical, geological, compositional and state criteria (Kramer, 1996).

The historical criterion is based on the evidence that liquefaction often occurs in sites that have already experienced it in the past, if no changes in soil or groundwater have happened. The characteristics of liquefied sites can be used to evaluate the possibility of liquefaction. The geological criterion is based on the analysis of the geological aspects, such as the level of groundwater table, morphology, age of deposits, stratigraphy, etc.; the compositional criterion is based on the characteristics of soil, such as its grain distribution, grain size, the percentage of fines, the shape and mean dimensions of grains. All these factors have specific influence on the possibility of liquefaction.

Critical and steady state

The state criterion relates the soil *initial state* (the combination of soil density and effective stress at the time of an earthquake) to the liquefaction susceptibility. The concept of *critical state* (Roscoe et al., 1958) is particularly useful to understand this relationship.

Critical state can be described as the physical state in which no more changes in volume or stresses are occurring in the material when it is being continuously sheared[3]. Loose and dense sand specimens, isotropically consolidated to the same effective confining pressure and subjected to drained monotonic load, achieve the same void ratio at critical state, named *critical void ratio*, e_{cr}; the combination of confining stress and void ratio at critical state defines the so-called *critical state locus*. The critical state, with the additional requirement of steady rate of

[3]The Critical State Soil Mechanics has been essential to describe the soil behavior within a unique theoretical framework (e.g. Roscoe et al. (1958); Schofield and Wroth (1968); Wood (1990)).

deformation, is often referred to as *steady state* (Poulos, 1981). The combination of void ratio and effective confining stress at steady state defines the *steady state locus*, which is a helpful tool (despite being difficult to determine) to discern the possibility of liquefaction. Critical and steady state are practically synonymous when applied to sand, since the rate of deformation may be significant only for clay (Lupini et al., 1981; Castro et al., 1982); for such reason, it is often assumed, for practical purposes, that critical and steady state are coincident (e.g. Sladen et al. (1985); Idriss and Boulanger (2008)).

Been and Jefferies (1985) introduced the *state parameter*, ψ (Eq. 2.4), as the difference between current void ratio, e, and the void ratio at the steady state of deformation, e_{ss}, for the same effective confining pressure. In the stress-void ratio plane (logarithmic scale), the steady state locus is represented by a straight line (Fig. 2.3). If the soil initial state is plotted above the steady state line (SSL), flow liquefaction can happen *only if* the residual shear strength is lower than the initial static shear stress. Cyclic mobility, instead, can happen for *both* dense and loose soils (i.e. the initial state is plotted above or below the steady state line) (Kramer, 1996). When $\psi > 0$, a soil may undergo flow liquefaction or cyclic mobility, since it exhibits contractive behavior; for $\psi < 0$, on the contrary, the soil exhibits dilation (i.e. negative pore water pressure under undrained loading conditions), thus it is not prone to flow liquefaction, but it may be subjected to cyclic mobility.

$$\psi = e - e_{ss} \tag{2.4}$$

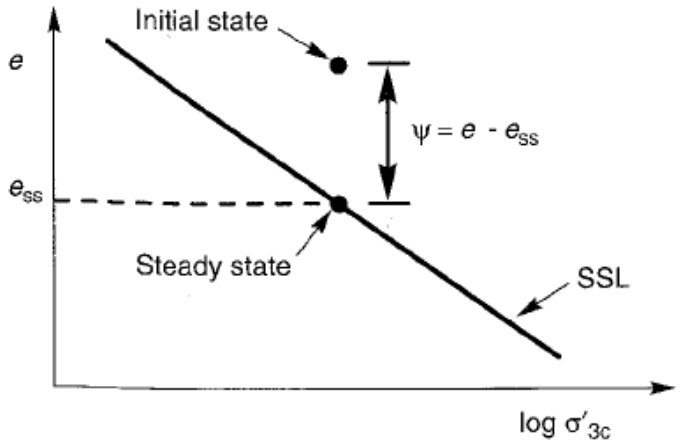

Figure 2.3: *State parameter and steady state line in the stress-void ratio plane (from Kramer, 1996).*

2.2.3 Undrained monotonic loading

It is known that an overall instability of cohesionless soils can be achieved due to undrained static, monotonically increasing, loading conditions. Liquefaction triggered by static loading is generally named *static* liquefaction. Flow liquefaction can be triggered by static loads. The main concern related to static liquefaction is represented by the movement of large soil masses, often referred to as *flow slides*.

Figure 2.4 presents the typical results of an undrained triaxial test on loose saturated sand

subjected to monotonically increasing load (stress-controlled test). The initial state is plotted above the SSL (Fig. 2.4d), therefore the specimen can be subjected to flow liquefaction (i.e. in drained test, it would exhibit contraction toward the SSL). As the stress increases, strain and positive pore pressure develop (Fig. 2.4a, c), while the mean effective stress is reduced (Fig. 2.4b). At point B, maximum stress is achieved; this point is followed by a rapid increase of pore water excess (B-C), which in turn produces the reduction of effective stress. At point C, the soil approaches the steady state line. Point B represents the beginning of the instability: the shear stress required for equilibrium is higher than the residual strength (point C, Fig. 2.4b), thus the specimen underwent monotonic flow liquefaction.

Flow liquefaction surface

Point B in Figure 2.4 represents the triggering of flow liquefaction; it belongs to the so-called *flow liquefaction surface*, FLS, the projection of which in the mean effective stress-deviatoric stress plane is a straight line toward the origin[4]. Since soils with initial shear stress lower than that at steady state can't undergo flow liquefaction, it follows that the steady state represents a boundary for the flow liquefaction surface, that is therefore broken off in correspondence of this point. The FLS differentiates stable and unstable behavior of saturated cohesionless soils subjected to undrained loading conditions. When the stress path reaches the FLS, the process is not reversible. A schematic representation of the FLS is provided in Figure 2.5.

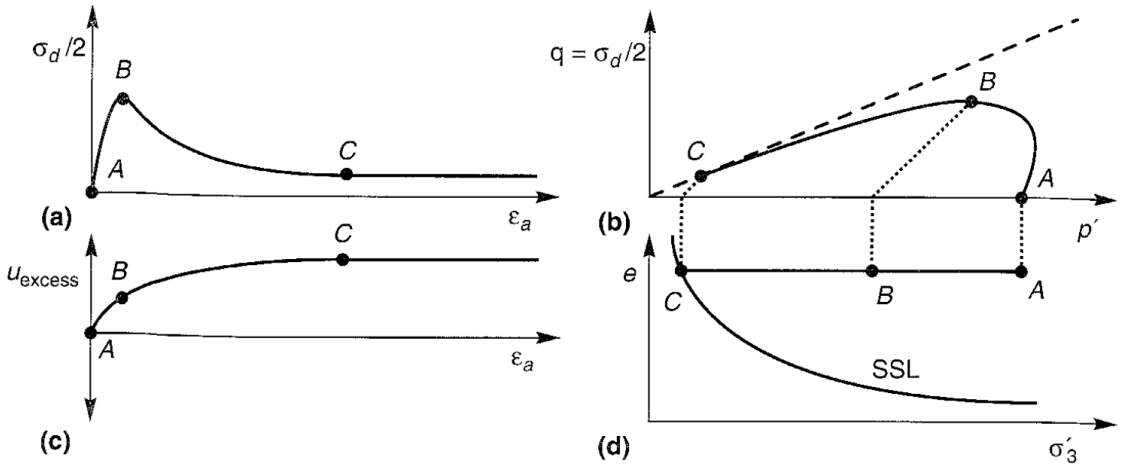

Figure 2.4: *Stress paths of loose saturated sand subjected to monotonic loading: axial strain again deviatoric stress (a), mean effective stress against deviatoric stress (b), axial strain against pore water pressure (c), and effective confining pressure against void ratio (d) (from Kramer, 1996).*

[4]Some Authors proposed the existence of a *collapse surface*, originating from the steady state point, e.g. Sladen et al. (1985); the concept of FLS as a surface coming from the origin of the stress-space has been generally more accepted, e.g. Lade (1993); Yang (2002).

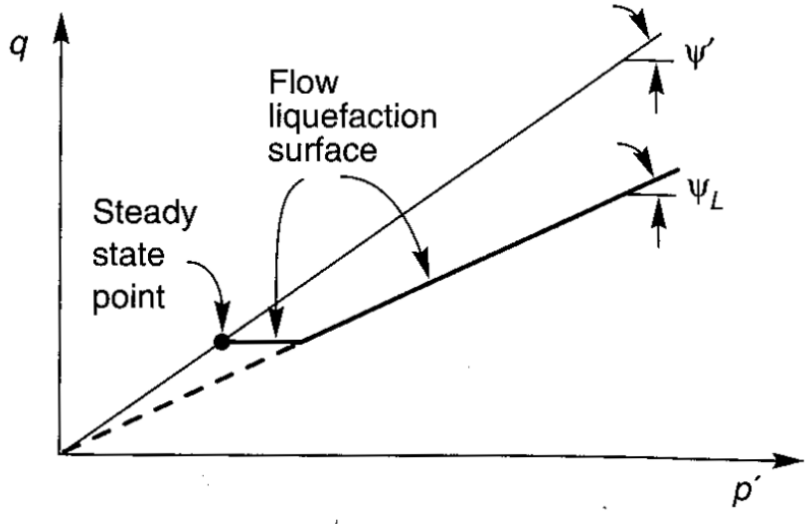

Figure 2.5: *Steady state and flow liquefaction surface lines in the mean effective-deviatoric stress plane (from Kramer, 1996).*

2.2.4 Undrained cyclic loading

FLS and cyclic loading

The importance of the *FLS* is due to the fact that it represents the boundary of a soil instability that can be achieved by *both* monotonically or cyclically undrained sheared material (Vaid and Chern, 1983): flow liquefaction is triggered when the stress path crosses the *FLS* during undrained shear, regardless of the nature of the applied load, despite the stress paths being different for soil cyclically or monotonically loaded. This aspect is clearly shown in Figure 2.6 for specimens anisotropically consolidated before shearing (point A). Points B and D belong to the *FLS* and represent the beginning of instability after monotonic or cyclic loading, respectively. Point C is the steady state, toward which the stress paths move.

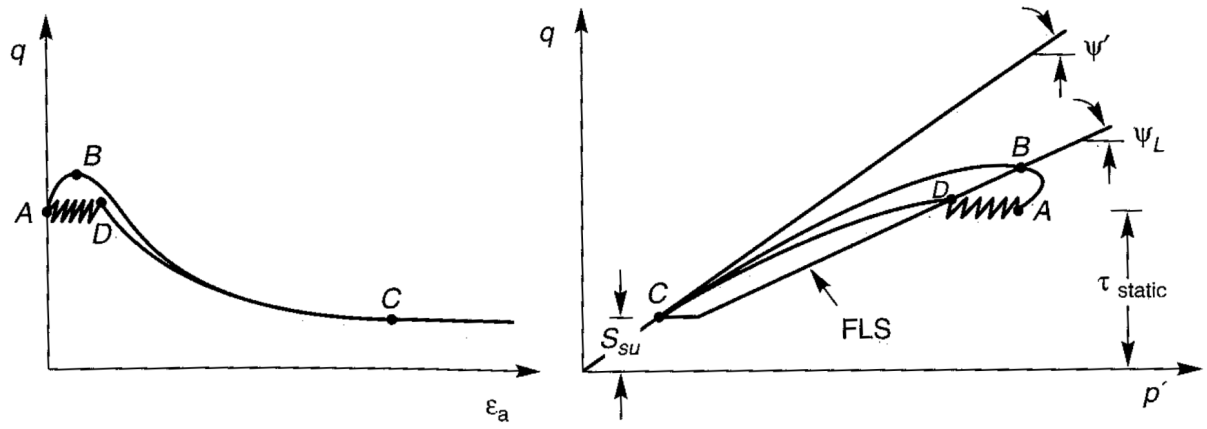

Figure 2.6: *Flow liquefaction triggered by either monotonic or cyclic loading in the stress-strain space (left) and in the stress space (right) (mod. from Kramer, 1996).*

Flow liquefaction and cyclic mobility

Figure 2.7 shows the regions of liquefaction susceptibility in the stress space in the case of cyclic loading. Two different regions, namely flow liquefaction and cyclic mobility, can be distinguished on the basis of the initial stress state.

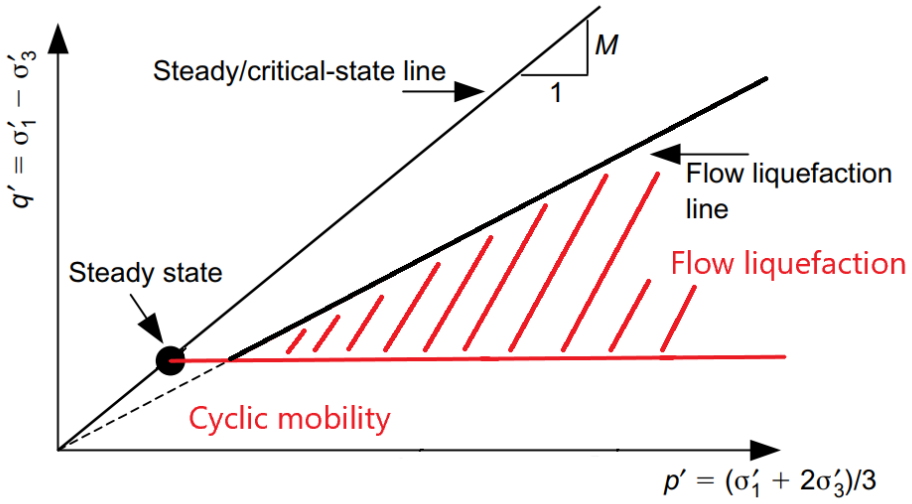

Figure 2.7: *Liquefaction regions in the stress plane: flow liquefaction, below the trace of the FLS and above the steady state, and cyclic mobility, below the steady state (mod. from Yang, 2002).*

Cyclic mobility is only triggered by cyclic loading conditions. Kramer (1996) distinguished among three different combinations of initial conditions and cyclic loads that can lead to cyclic mobility. These combinations can be observed from the results of cyclic triaxial tests, as shown in Figure 2.8. The stress condition requires that the initial shear stress is below the steady state (Fig. 2.7); when a cyclic load is applied, the relation between the stress amplitude, the possibility of stress reversal, and the steady state, becomes significant.

In particular, if there is no stress reversal (i.e. the soil is cyclically loaded in compression) and there is not crossing of the steady state, cyclic mobility is described by a stress path that moves to the left of the stress space, toward the stress state (Fig. 2.8a), where it fails; additional cycles of loading let the stress path moving along the SSL. Great deformations are expected within each cycle, as a consequence of the reduced effective stress. If there is a temporary crossing of the steady state and the stress path reaches the FLS, this corresponds to a certain degree of instability, with the accumulation of large permanent strain (Fig. 2.8b). In both cases, at the end of the cyclic loading, effective stresses are stable on a value that is lower than the initial one. If there is stress reversal ($\tau_{cyc} > \tau_{static}$) and no crossing of the steady state, the soil is loaded both in compression and in extension (Fig. 2.8c). The stress path moves toward the origin, and effective stresses eventually reach zero value. Further loading cycles let the stress path move along the compression and extension drained failure envelope: the condition $\sigma' = 0$ is achieved twice in a cycle, and significant deformations accumulate in this case. Even if $\sigma' = 0$, however, the soil would reach the steady state upon dilation if it is loaded monotonically after initial liquefaction.

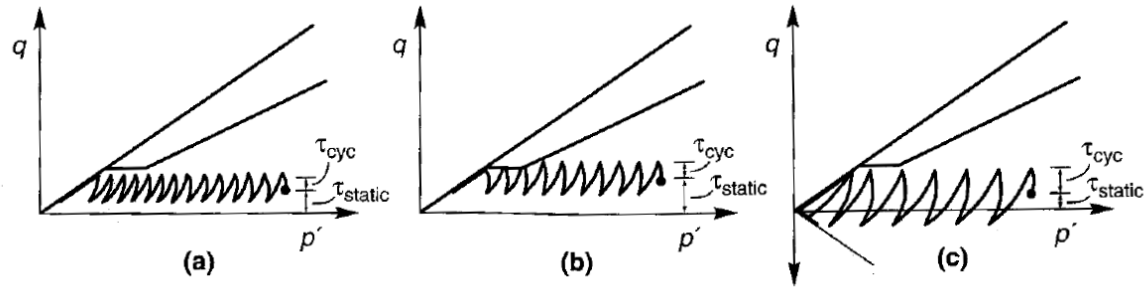

Figure 2.8: *Occurrences of cyclic mobility in cyclic triaxial tests. No shear stress reversal and no crossing of the steady state (a), no stress reversal and provisional crossing of the steady state (b), stress reversal without crossing of the steady state (c) (mod. from Kramer, 1996).*

The mechanism of Δu generation

The generation and accumulation of excess pore water pressure in saturated soils subjected to undrained loading conditions is the distinctive factor of liquefaction. Either flow liquefaction or cyclic mobility need the effective stress path to move toward the origin in the stress space: this implies that positive pore pressure increases during loading.

The way Δu develops is schematically represented in Figure 2.9. If the load was applied in *drained* conditions (volume changes allowed), the soil initial void ratio would decrease from point A to point B, reflecting a natural grain rearrangement due to cyclic shear; since pore pressure is constant during drained shear, no change in effective stress would take place. For undrained loading, instead, the prevented plastic volumetric change (A-B) is compensated with an expansion of the soil skeleton under reduced effective stresses (from point B to point C), with a reduction equal to Δu. For a limit case, "*the sand skeleton would be carrying zero normal stress [...] and the pore water would be carrying the entire normal stress [...]*" (Idriss and Boulanger, 2008). The contracting sand is therefore forced to keep constant volume by a stress change.

The development of pore pressure is mainly related to the amplitude and duration of the cyclic shear. If the induced cyclic stress is great enough, the pore pressure equals the initial confining stress, no interparticle forces act among sand grains any longer, and the solid particles are suspended into water. The excess pore pressure development, given the same effective confining stress and amplitude of shear, essentially depends on the amplitude of the prevented volumetric change under undrained cyclic loading (Fig. 2.9). Once the cyclic load ends, settlements occur upon water drainage. The sand attains a denser packaging, and the time needed to reach the new stable configuration depends on the rate of drainage and on the value of the excess pore water pressure attained, that is related to the initial state and both to the amplitude and duration of the cyclic load; the longer and stronger the stress application, the longer the liquefied state is maintained (Ishihara, 1985). Figure 2.10 illustrates the effects of positive pore pressure build-up on the stress state of a liquefiable soil (the case shown could be classified as an ideal case of cyclic liquefaction, since there are no static shear stresses needed for the equilibrium).

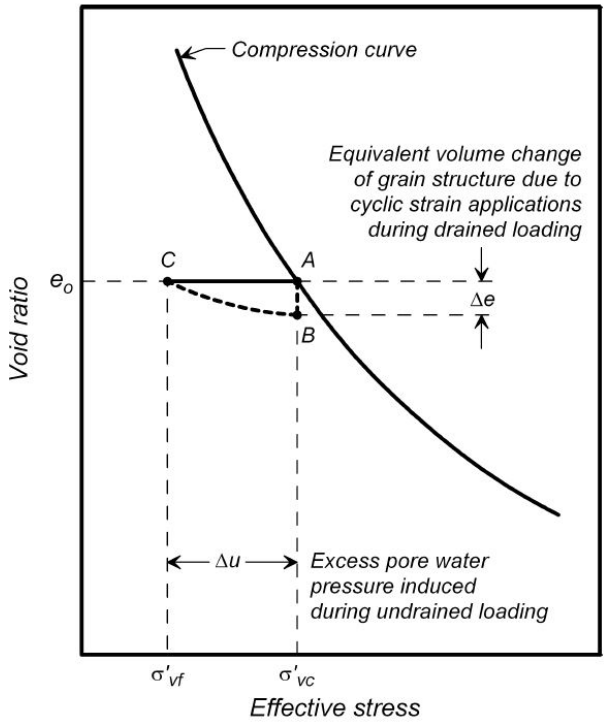

Figure 2.9: *Mechanism of pore water pressure generation during cyclic loading (from Idriss and Boulanger, 2008).*

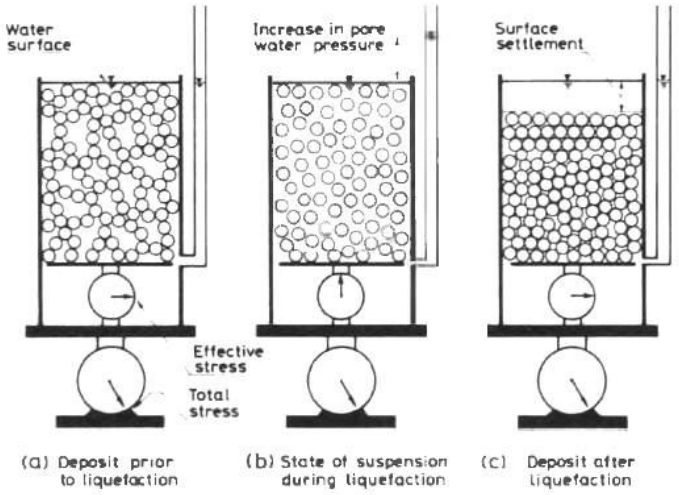

Figure 2.10: *The liquefaction mechanism in a saturated soil deposit (mod. from Ishihara, 1985).*

2.2.5 Initial liquefaction

Historically, most of the actual knowledge on seismic liquefaction phenomena was developed in the last century by means of laboratory investigations, such as cyclic triaxial or cyclic simple shear tests. The term *initial liquefaction*, that was used by Seed and Lee (1966) based on experimental testings, is defined as the point where the total pore water pressure equals the effective initial confining pressure (i.e. $\sigma' = 0$). Figure 2.11 shows the results of cyclic torsional shear tests performed on isotropically consolidated loose and dense sand specimens. As the cyclic load is applied, the pore water pressure increases and it accumulates for both samples; however, the behavior of loose and dense sand is different once the initial liquefaction is achieved. For loose sand (Fig. 2.11a) it corresponds to a full loss of shear strength (collapse), demonstrated by the development of sizable shear strain, while for denser sand (Fig. 2.11b) the alternation of load cycles (stress reversal) induces the development of high negative Δu that produces, in turn, a partial and temporary shear resistance recovery. However, after several cycles, the accumulated permanent strain becomes very large.

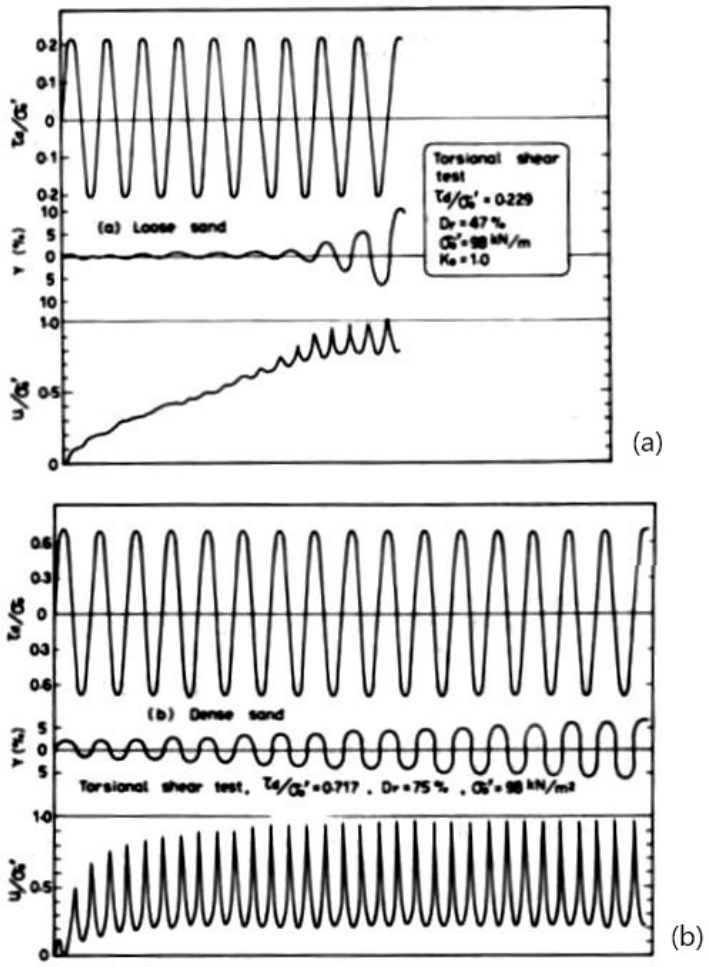

Figure 2.11: *Results of cyclic undrained torsional shear test on Fuji river (Japan) sand: a) loose sand, b) dense sand (mod. from Ishihara, 1985).*

Initial liquefaction can be quantitatively defined by introducing the excess pore water pressure ratio, r_u, as the ratio between the excess pore water pressure developed during loading

and the initial effective confining stress. In cyclic triaxial tests, it represents the ratio of the pore water pressure to the initial minor effective stress, that is the effective consolidation pressure (σ'_c)(Eq. 2.5), while in cyclic simple shear tests it represents the ratio of Δu to the vertical effective consolidation pressure (σ'_{vc})(Eq. 2.6).

The condition $r_u = 1.0(100\%)$ is generally assumed as initial liquefaction. As shown in Figure 2.11, however, if r_u is less than 1.0 (the pore pressure doesn't approach the initial confining effective stress), the failure condition is conventionally defined with reference to a yield value of the strain level: in particular, 5% double amplitude axial strain (ϵ_{DA}, or peak to peak) is assumed in cyclic triaxial tests[5]. According to Ishihara (1996) "*it has been customary to consider the state of 100% pore water pressure build-up or alternatively the development of 5% double-amplitude axial strain as a yardstick to recognize a state of cyclic instability covering a wide range of density of sand on a common basis*".

$$r_u = \frac{\Delta u}{\sigma'_c} \tag{2.5}$$

$$r_u = \frac{\Delta u}{\sigma'_{vc}} \tag{2.6}$$

2.3 Seismic liquefaction hazard evaluation

The evaluation of the seismic liquefaction hazard, at a given site for the earthquake expected in a given return period, needs the analysis of the seismic action and the estimation of the soil capacity to withstand the irregular earthquake-induced loading sequence (Youd and Idriss, 2001); once the seismic motion is defined, the liquefaction *resistance* can be defined on the basis of laboratory or *in situ* tests.

The most commonly employed methods to evaluate the potential for liquefaction are the cyclic stress approaches, that characterize both the earthquake loading and soil liquefaction resistance in terms of cyclic stresses.

2.3.1 Seismic motion assessment

Earthquakes are represented by random cyclic loading sequences over time, as shown by the acceleration time history recorded during the Christchurch Earthquake reported in Figure 2.12. A detailed ground response analysis is usually the best way to assess the time history of the induced random cyclic loading sequence with depth at a given site. Then, an effective value for the earthquake loading can be determined from the whole shear stress time history at each depth of interest. However, since many geotechnical data are required to perform a reliable ground response analysis, it is often not possible to follow this way. Thus, the value of the effective cyclic shear stress induced by the expected earthquake is frequently estimated by *simplified* procedures.

[5]Since the relation between axial strain, ϵ_a, and shear strain, γ, is $\gamma = \epsilon_a(1+\nu)$, being ν the Poisson's ratio, the corresponding yield value for the shear strain (peak to peak) is $\gamma_{DA} = 7.5\%$ ($\nu = 0.5$ under prevented volumetric changes).

The expected earthquake loading in terms of shear stress, τ, is usually normalized to the effective vertical overburden pressure , σ'_{v0}, defining the *Cyclic Stress Ratio*, CSR (Eq. 2.7).

$$CSR = \frac{\tau}{\sigma'_{vo}} \tag{2.7}$$

The most common simplified method used to calculate CSR was firstly proposed by Seed and Idriss (1971). The expression of CSR is given in Equation 2.8, where a_{max}, g, σ_{v0}, σ'_{v0}, r_d represent the peak acceleration at ground surface, the gravity acceleration, the total overburden stress, the effective overburden stress and a coefficient of stress reduction with depth, respectively.

$$CSR = \frac{\tau}{\sigma'_{v0}} = 0.65 \times \frac{a_{max}}{g} \times \frac{\sigma_{v0}}{\sigma'_{v0}} \times r_d \tag{2.8}$$

Once the amplitude of the expected earthquake loading (demand) is evaluated from ground response analysis or by a simplified procedure (like the one specified above), it is compared with the soil liquefaction resistance (capacity) obtained from laboratory (typically cyclic triaxial, cyclic simple shear and cyclic torsional tests) or *in situ* tests (typically Cone Penetration Test, Standard Penetration Test, or shear wave velocity, V_s, measurements). If laboratory test results are used, reference is made to curves which expresses the liquefaction resistance as a function of the number of loading cycles. Consequently, an equivalent number of cycles must be also defined for the expected earthquake loading and it can be obtained by using some relations from literature (e.g. Seed and Idriss (1982), among the others). Otherwise, the liquefaction resistance to compare to the expected earthquake loading can be determined according to some simplified liquefaction method (CPT-, SPT-, or V_s-based), as better described in the following Paragraph.

2.3.2 Liquefaction soil failure and resistance

It is not simple to use a univocal criterion to match soil failure for both flow liquefaction and cyclic mobility. In the first case, the failure condition is easily recognized by means of the FLS, and flow failures *in situ* are evident. Conversely, in case of cyclic mobility, the developed strain is used to identify the failure condition, since there is not a clear failure mechanism that can be detected. Sand boils are considered as evidence of cyclic liquefaction, but "*the definition of failure is imprecise*" (Kramer, 1996), because developed deformations may be acceptable or not depending on a particular in field condition. *In situ*, the distinction between liquefaction phenomena is often cumbersome, and no differentiation is usually made among all the pore pressure increase-related events, all simply referred to as *liquefaction*.

The liquefaction resistance quantitatively defines the ability of soil to face liquefaction occurrences. Liquefaction resistance can be determined from laboratory tests as well as from in field investigations.

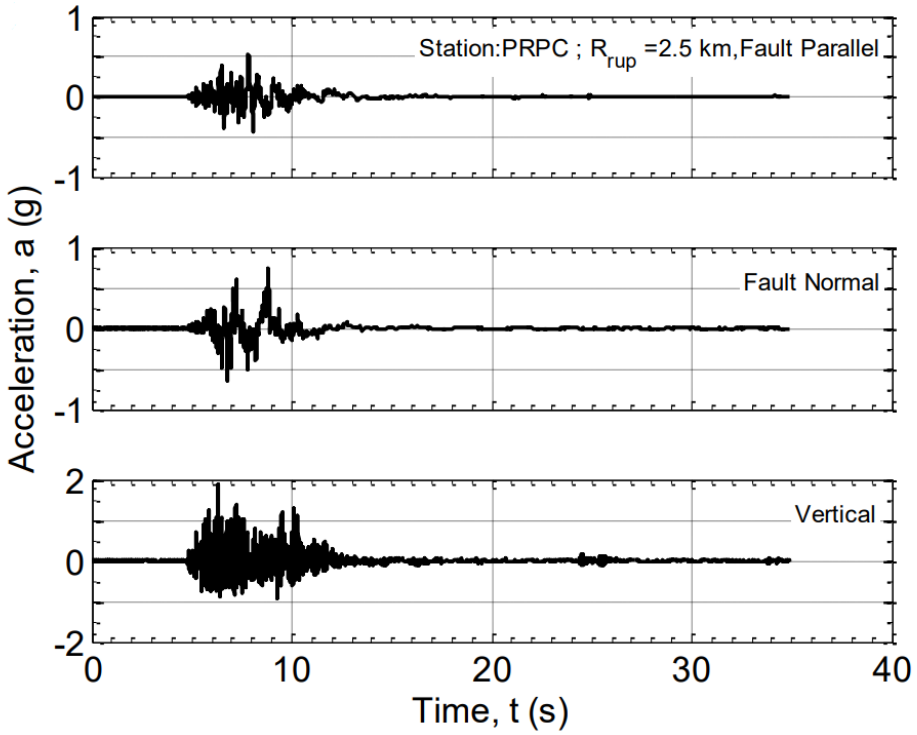

Figure 2.12: *Ground response in terms of acceleration time history at the Pages Road station during the Christchurch Earthquake (mod. from Bradley and Cubrinovski, 2011).*

Liquefaction resistance from laboratory tests

Cyclic triaxial, cyclic simple shear and cyclic torsional (undrained) shear tests have been commonly used to determine the liquefaction resistance of sands (Peacock and Seed, 1968; Finn et al., 1971; Castro, 1975; Silver et al., 1976; Iwasaki et al., 1978; Tatsuoka et al., 1982; Ishihara, 1985; Hyodo et al., 1991; Polito and Martin II, 2001; Ghionna and Porcino, 2006; Yamamuro et al., 2018). In cyclic triaxial tests, a cylindrical specimen is firstly consolidated (isotropically or anisotropically) to an effective confining pressure and then subjected to a constant-amplitude cyclic axial load (stress-controlled test) applied at a certain frequency. In cyclic simple shear tests, a cylindrical sample is firstly consolidated and secondly subjected to a horizontal shear stress applied at the top or at the bottom of the sample; when a cyclic torsional shear test is performed, a cyclic torsional stress is applied undrained to a cylindrical specimen that was previously consolidated. As discussed further on, the liquefaction resistance of a sand has been evaluated in this work by means of a cyclic triaxial device; thus, the main focus is put on such apparatus.

Figure 2.13 and Figure 2.14 show the results of stress-controlled cyclic triaxial undrained tests on isotropically consolidated Toyoura sand, in a loose and dense state, respectively. In the stress-path curve (Fig. 2.13b, 2.14b), the shear stress is plotted versus the effective mean principal stress. For the loose sample, it can be observed that the effective stresses decrease with the number of loading cycles as a consequence of the increasing in pore pressure; at the same time, the shear strain amplitude increases. However, a sizable amount of strain develops only during the eighth loading cycle, and effective stresses rapidly gets zero-value. Conversely, for the dense sand, the effective stresses also decrease as the pore water pressure increases, but

they don't reach zero-value. Moreover, shear strain increases much less than in loose sand, despite the higher initial superimposed shear stress amplitude.

Broadly speaking, it is customary to identify liquefaction failure from laboratory testings at the point of initial liquefaction ($r_u = 100\%$) or when a yield strain level is reached during loading cycles (commonly 5% peak to peak after cyclic triaxial tests) (Ishihara, 1996; Kramer, 1996).

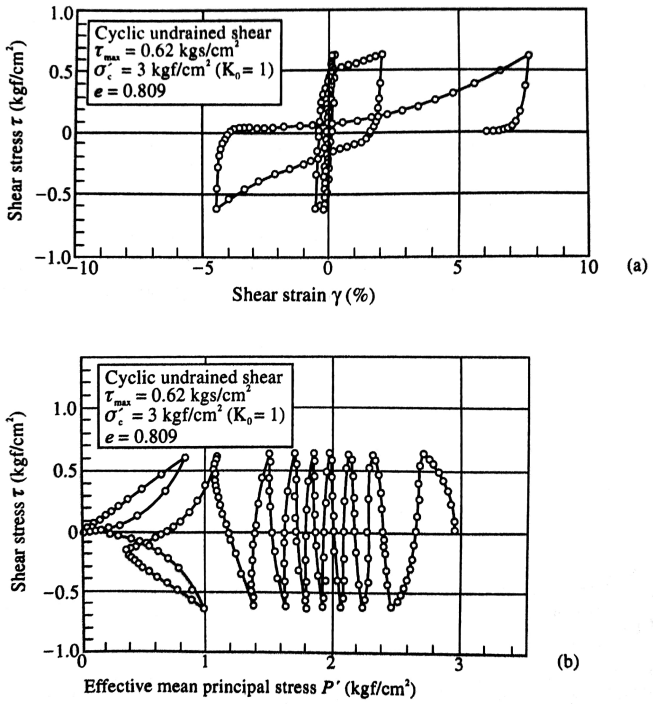

Figure 2.13: *Results of a cyclic undrained shear test on loose Toyoura sand: a) stress-strain curve, b) stress-path curve (mod. from Japanese Geotechnical Society, 1998).*

By analyzing the results from experimental tests it appears that the liquefaction resistance of a potentially liquefiable material must be a relation among the number of loading cycles, the amplitude of the induced cyclic shear stress, and the initial state of the material. Such a relation is usually given in the form of a *liquefaction resistance curve* in the number of cycles-shear stress plane. The applied shear stress in laboratory tests is usually normalized to the effective confining pressure, therefore, it is customary to define the *Cyclic Stress Ratio*, *CSR*, as the ratio of the shear stress to the initial effective confining stress. The expression of *CSR* is different depending on the kind of test, as reported in Equations 2.9 and 2.10 for cyclic triaxial and cyclic simple shear test, respectively. In these Equations, q_{cyc} and τ_{cyc} are the deviatoric stress and the shear stress acting on the horizontal plane, respectively.

$$CSR = \frac{q_{cyc}}{2\sigma'_c} \tag{2.9}$$

$$CSR = \frac{\tau_{cyc}}{\sigma'_{vc}} \tag{2.10}$$

By using the results from a series of cyclic tests, a liquefaction resistance curve can be drawn

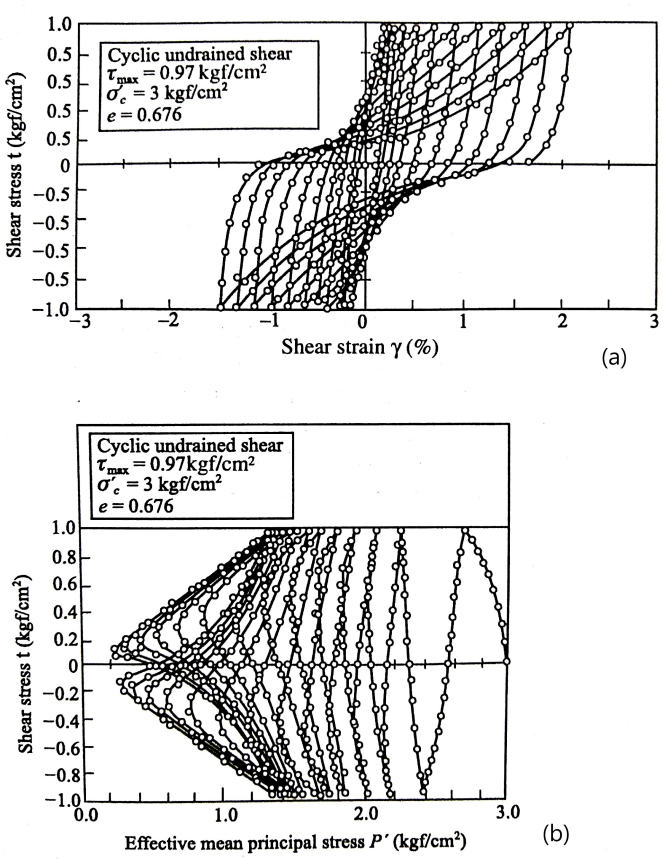

Figure 2.14: *Results of a cyclic undrained shear test on dense Toyoura sand: a) stress-strain curve, b) stress-path curve (mod. from Japanese Geotechnical Society, 1998).*

in the *N*-*CSR* plane, being *N* the number of loading cycles that induces failure. Examples of liquefaction resistance curves from cyclic triaxial tests are provided in Figure 2.15, in which the effects of specimens preparation methods on the cyclic strength of a medium-dense Monterey sand are shown for a given value of confining pressure. The number of cycles required to reach liquefaction increases as the *CSR* decreases; it is possible, in the specific case, to refer to a unique value of the liquefaction resistance, e.g. by defining it as the *CSR* required to trigger liquefaction in 20 loading cycles (Ishihara, 1996).

CSR value required to trigger liquefaction in a specified number of cycles is referred to as *Cyclic Resistance Ratio*, *CRR*. The experimental *CRR* values are generally well fitted by a power relation (Equation 2.11, where *a* and *b* are soil parameters to be determined from regression based on the experimental data).

CRR increases with relative density and decreases as the effective confining stress increases. These aspects reflect the behavior of the material, that tends to contract or dilate as a consequence of its initial state. The effects of initial state on the *CRR* are shown in Figure 2.16, in which data were collected from cyclic triaxial tests performed by Vaid and Sivathayalan (1996).

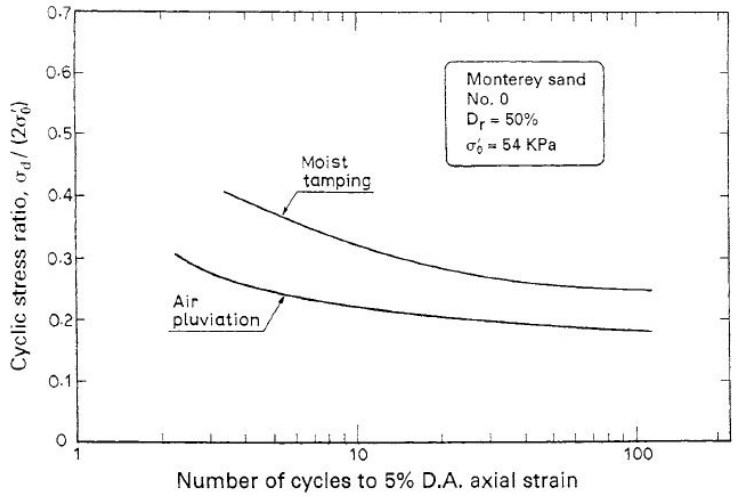

Figure 2.15: *Liquefaction resistance curves of specimens reconstituted with different techniques (from Ishihara, 1996).*

$$CRR = aN^{-b} \tag{2.11}$$

Liquefaction resistance from *in situ* tests

The *CRR* to be compared to the normalized earthquake loading *CSR* can be determined from laboratory test results on samples taken from the investigated site; however, high quality undisturbed samples are necessary for this purpose (e.g. collected by freezing), and granular soil specimens are often too disturbed to provide meaningful results from laboratory analysis. For these reasons, the soil liquefaction resistance is commonly assessed by using standard *in situ* test results, like those obtained e.g. from Standard Penetrometer Test (SPT), Cone Penetration Test (CPT) or shear wave velocity measurements. For this purpose, the used parameter (e.g. the

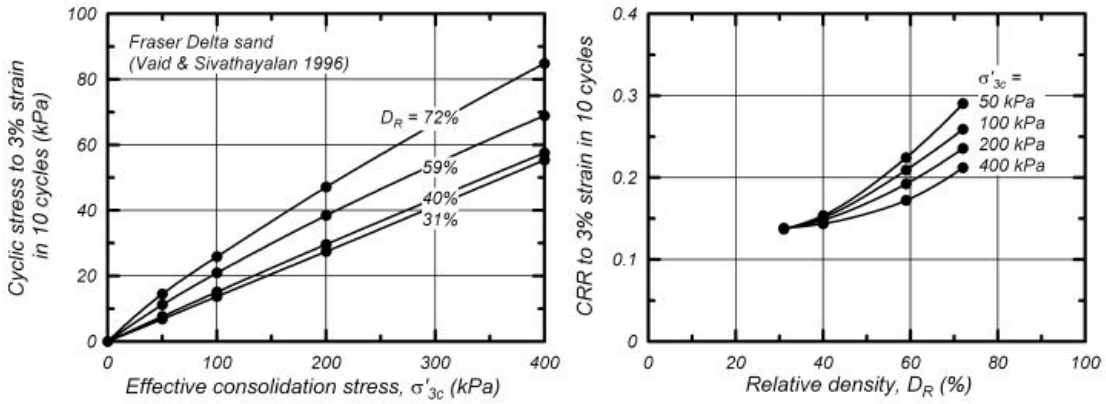

Figure 2.16: *Cyclic stress (left) and CRR (right) to 3% axial strain in 10 loading cycles after cyclic triaxial tests for different relative densities and effective confining stresses (from Idriss and Boulanger, 2008).*

number of blows from SPT or the penetration resistance from CPT) is normalized to the corresponding effective vertical overburden pressure and corrected to determine the equivalent parameter for clean sand, which is used as the reference material parameter. This parameter is then related to the in field Cyclic Resistance Ratio (CRR) as shown for example in Figure 2.17, where the normalized and corrected tip resistance obtained from CPT tests is related to the CRR evaluated with reference to earthquakes magnitude 7.5. For different magnitude values, magnitude scaling factors are available to take into account the appropriate characteristics of the expected action.

2.4 Liquefaction countermeasures

If a given site is prone to liquefaction, appropriate design of structures and/or suitable types of ground improvement must be chosen to face possible liquefaction phenomena; this Thesis deals with remedial measures against soil liquefaction, thus excluding those aspects related to any structural design to prevent liquefaction-induced damages. Figure 2.18 shows a schematic process for the assessment of liquefaction hazard at a certain site; large deformation is expected if no structural or soil improvement measures are taken to prevent liquefaction in a susceptible site.

A general review on standard liquefaction countermeasures is presented in this Paragraph, while the most appealing and recently developed techniques are described in Section 2.5.

2.4.1 Effectiveness and classification of liquefaction countermeasures

As explained in Section 2.2, liquefaction is essentially triggered by the development and accumulation of positive pore water pressure under undrained loading conditions in loose saturated soils which would exhibit contractive behavior under drained loading conditions. The techniques developed to mitigate liquefaction effects often focus on one of the key factors that may trigger liquefaction: some of them aim to reduce the development of Δu, others act on soil

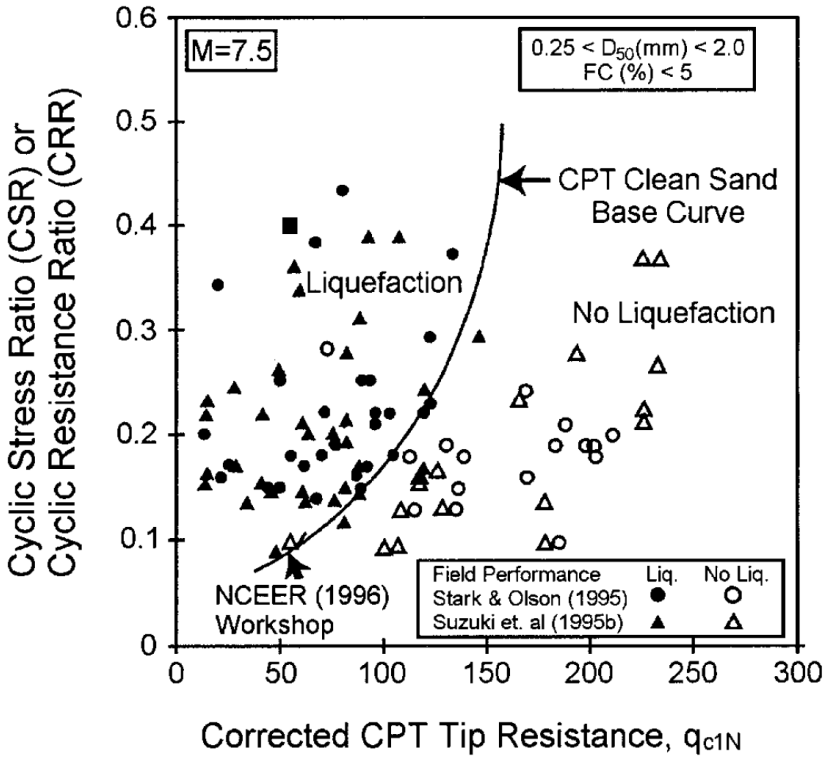

Figure 2.17: *Liquefaction chart from CPT tests (from Youd and Idriss, 2001).*

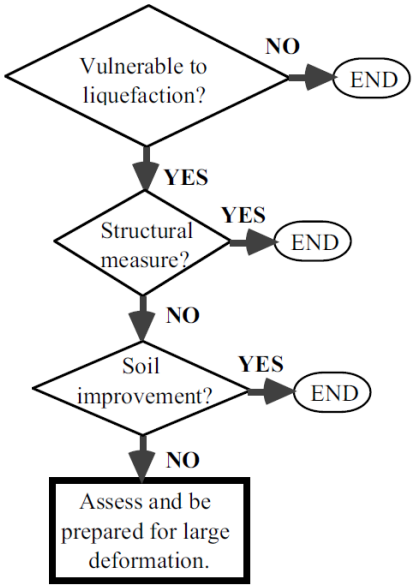

Figure 2.18: *Conceptual process for ground improvement against liquefaction (from Towhata, 2008).*

density, others on the mechanical interaction among soil grains.

The most traditionally worldwide used techniques are fundamentally based on the improvement of the mechanical properties of the soil mass by increasing the soil density (e.g. sand compaction pile, vibro-flotation, dynamic tamping), or by means of grain solidification (e.g. injection methods, deep mixing) or by the lowering of the ground water table or by facilitating the dissipation of the earthquake-induced pore water pressure (e.g. dewatering by trenches, drains, partial saturation), or by means of grain adjustment (e.g. soil replacement); a combination of different techniques, such as densification and drainage, or densification and reduction of soil saturation, could be required to face the liquefaction risk at a specific site. Andrus and Chung (1995) reported that areas improved by means of the above mentioned techniques showed good performances during earthquakes.

According to Towhata (2008), there are four principles of working on which the overall liquefaction mitigation techniques are based:

- soil densification;
- bonding of grains (solidification);
- lowering of ground water table;
- water drainage.

Huang and Wen (2015) recently proposed a new classification of liquefaction mitigation techniques, including the new proposals, like *biocementation* or *biogas*. Their classification is shown in Table 2.2: they pointed out that densification and bonding of grains lead to soil reinforcement, and they classified under the *saturation degree reduction* the methods which aim to inhibit the pore water pressure generation under undrained loading conditions.

In the following Paragraphs the remedial measures against liquefaction are presented and discussed, assuming of secondary importance, for the purposes of the present study, the detailed description of the technological aspects of each method. The classification given in Table 2.2 is assumed; an exhaustive discussion on innovative techniques is given apart, as previously stated.

Table 2.2: *Classification of liquefaction countermeasures (mod. from Huang and Wen, 2015).*

Soil reinforcement	Soil replacement
	Soil densification: sand compaction pile, vibration compaction, dynamic compaction, blast compaction, compaction grouting
	Bonding of grains: permeation grouting, splitting grouting, jet grouting, deep mixing, pile method, biocementation
Saturation degree reduction	Lowering of groundwater table, air injection, biogas
Drainage	Gravel pile method, dissipation using screen pipes

2.4.2 Soil reinforcement

Soil replacement

Soil replacement consists of replacing the liquefiable soil with a not liquefiable one; because of its grain size distribution, gravel is often used as replacement material. Furthermore, due to its high hydraulic conductivity, gravel provides the fast dissipation of pore water pressure as an additional benefit. One of the main drawbacks of soil replacement is represented by its high economic costs; moreover, this technique cannot be applied for treatments of soils beneath existing structures.

Densification methods

A loose saturated sand is more susceptible to liquefaction than a dense one, which develops negative pore water pressure due to its dilative behavior, and it also consequently develops a lower level of strain during cyclic loadings (Sec. 2.2); the decrease of the void spaces among grains inhibits the potential volume contraction of soil, thus preventing liquefaction. If the soil is artificially densified, an improvement of its liquefaction resistance can therefore be easily achieved. The techniques that provide the soil with a denser grain packaging are usually referred to as *densification* methods.

Densification, or compaction, is the most intuitive way of liquefaction mitigation, and it has been widely used worldwide; it is considered the standard for liquefaction mitigation (Andrus and Chung, 1995). Matso (1995) showed that during the Kobe Earthquake (1995, Japan) a site improved by densification performed better than the existing surrounding untreated sites. Examples of densification methods are: sand compaction piles, vibro-flotation, compaction by tamper, compaction by roller, compaction by explosion, vibro-rod flotation (e.g. Ohsaki, 1970; Tokimatsu et al., 1990; Aboshi et al., 1991; Akiyoshi et al., 1993; Okamura et al., 2003; Adalier and Elgamal, 2004; Nashed et al., 2004; Shenthan et al., 2004; Lu and Tan, 2012). In different ways, the treated soil is given a more stable configuration with a decrease of its initial voids volume. In the case of compaction, for instance, the deposit is compacted by the impact of heavy weight dropped from a certain height; for the case of sand compaction pile, instead, sand piles are produced within a deposit by means of pipes that are firstly inserted and then extracted from the soil.

The major drawback of densification methods is the generation of vibrations, that makes the use of these techniques unfeasible for improvements near existing structures. Compaction grouting is a low-vibratory technique that improves the soil primarily by densification and secondly by solidification and reinforcement. A low-mobility grout is injected into the soil without penetrating the voids: the adjacent soil mass is displaced and densified. Compaction grouting can be successfully used to treat soil around existing buildings (Boulanger and Hayden, 1995).

Bonding of grains

When a liquefiable soil is provided with an artificial cohesion its liquefaction resistance increases; grains movements are reduced, and the soil shear strength benefits from the provided bonds (Eq. 2.2). Typical effects of bonding of grains on sand are the increase in resistance to

cyclic as well as to monotonic loading (e.g. Saxena et al., 1988; Clough et al., 1989; Schnaid et al., 2001; Ismail et al., 2002; DeJong et al., 2006; Montoya et al., 2013), and the reduction of the hydraulic conductivity of soil (Nemati and Voordouw, 2003; Schwarz and Chirumalla, 2007). Porcino et al. (2015) found that the hydraulic conductivity of Ticino sand grouted with a sodium silicate-based grout was reduced from 4×10^{-4} m/s to $\approx 10^{-9}$ m/s. Mitchell and Wentz (1991) reported that liquefiable areas treated with solidification didn't experience severe damages during the Loma Prieta Earthquake (1989, USA).

Solidification of soil grains is generally achieved by means of different types of stabilizing grouts injected into the soil (Karol and Berardinelli, 2003). The use of chemicals is today widely diffused in engineering practice (Indraratna et al., 2015): grouts are usually suspensions or solutions made up of acrylamides, acrylates, polyurethanes, and sodium silicate. High injection pressure is often needed to perform these improvement methods; the treated soil volume is currently limited within 1-2 m from the grout injection point, and there is no way of measuring the effectiveness of the treatment during its performance, with the consequence of an overestimated design to overcome these uncertainties (DeJong et al., 2010). At the end of the grouting process, a stabilized soil skeleton is formed: the strength and stiffness properties of the treated soil are enhanced, and a decrease in water flow is expected.

Among the techniques based on the bonding of grains, injection methods and deep-mixing are the most used ones. In injection methods, stabilizing mixtures are injected into the soil, while in deep-mixing, stabilizing agents are mixed at depth with the original soil by means of rotating auger. Permeation grouting and jet grouting improve the soil mainly by solidification, but they also densify the sand skeleton. In permeation grouting, a grout is injected into the soil, filling the voids volume without significant disturbance to the existing grains pattern, while in jet grouting a high pressure fluid jet erodes the soil, that is mixed at the same time with grout. A grout made up of colloidal silica particles can also be used to stabilize a liquefiable soil deposit (Gallagher, 2000); colloidal silica grouting represents the main topic of this study, and it is described separately in the next Chapter.

2.4.3 Saturation degree reduction

It is well known that pore water is practically incompressible; for this reason, a change in total stress under undrained loading conditions corresponds to a change in pore water pressure of equal magnitude in the saturated soil element. However, if the soil is not fully saturated, the development of pore water pressure is prevented by the presence of gas entrapped within the pores, that is able to adsorb part of the applied stress due to its volume compressibility, higher than that of water. Thus, the liquefaction resistance of a partially saturated soil is greater than that of a completely saturated one (Yoshimi et al., 1989; Xia and Hu, 1991; Tsukamoto et al., 2002; Yang et al., 2004; Yegian et al., 2007; He and Chu, 2014).

The water table can be lowered by means of draining trenches, or by the installation of deep wells furnished with pumps. Dewatering is a very expensive and difficult technique, since it needs the installation of continuously working machines and seepage cutoffs (Andrus and Chung, 1995).

2.4.4 Drainage

The installation of drains (e.g. gravel pile drains, steel pile with drainage function, stone columns) allows to limit the development and build-up of water pore pressure, thus reducing the liquefaction susceptibility of a site. Drains provide a rapid dissipation of Δu, inhibiting their accumulation during earthquakes (Seed and Booker, 1977; Brennan and Madabhushi, 2002). The design of a drainage system is often based on design charts (Seed and Booker, 1977; Onoue, 1988).

Drains are installed in the ground by means of a casing; once the casing is at the desired depth, the material constituting the drains is put into the casing and the casing pipe is then lifted up. Gravel drains are often used because of their great hydraulic conductivity. The stiffness of the stone columns also plays a really significant role in increasing the liquefaction resistance of the soil (e.g. Pal and Deb, 2018).

2.5 Innovative remedial measures against liquefaction

The continuous development of knowledge and technology has led in recent years to the proposals of innovative techniques to face liquefaction hazard. Practical application in field of the techniques described in this Section is still limited: most of the results comes from laboratory investigations. These newly proposed methods originate from the need to reduce economic costs and increase the sustainability of ground improvement treatments (Bao et al., 2019). A safer use in urbanized areas (e.g. reduction of induced vibrations on buildings) and the possibility of large-scale homogeneous treatments are also desired. According to DeJong et al. (2010), there are over 40.000 ground improvement projects carried out every year all over the world, with a total cost exceeding 6 US billion $/year; the request of sustainable and effective alternatives is therefore today fundamental. The most promising innovative remedial measures against liquefaction are *air injection*, *bentonite suspension grouting*, *biocementation*, *biogas*, *colloidal silica grouting* and mitigation using tyre chips (Huang and Wen, 2015). These techniques, except for *colloidal silica grouting* that is discussed apart in Chapter 3, are presented together with a general review of the state of the art to date.

Air injection and biogas aim to reduce the degree of saturation of soil, biocementation and colloidal silica grouting aim to provide the soil with an artificial cohesion, the use of tire chips aims reduce the pore pressure build-up due to the deformable nature of tire scraps, while the use of bentonite suspensions aims to reduce the extra pore water pressure development due to a clay-gel formed within the pore spaces that increases the threshold above which Δu are generated.

2.5.1 Saturation degree reduction: induced partial saturation

The *induced partial saturation* consists of lowering the degree of saturation of a liquefiable soil deposit by introducing gas bubbles within the pores. If air is introduced at a desired depth, the method can be referred to as *air injection*; when a gas is instead produced into the soil, e.g. by means of the respiratory process of certain microorganisms, the method can be referred to as

biogas. In general, different gases, such as oxygen or nitrogen, could be injected or produced within the pore spaces.

To evaluate the effects of gas bubbles on soil, Grozic et al. (1999) studied the behavior of loose gassy sand by means of monotonic consolidated undrained triaxial tests; Grozic et al. (2000) performed cyclic triaxial tests on sandy specimens prepared with different degrees of saturation and relative density. The cyclic resistance ratio increased with increasing gas content and D_r; however, some gassy specimens could still undergo liquefaction if they were sufficiently loose. Carbon dioxide was used to induce partial saturation in the specimens. Okamura et al. (2003) evaluated the liquefaction resistance and degree of saturation of a partially saturated sand improved with sand compaction piles: in this case, air injection was a by-side benefit of the piles construction process. Okamura et al. (2006) showed that the presence of gas bubbles in the unsaturated soil lasted for more than 10 years, at least under hydrostatic conditions. Tamura et al. (2002) proposed theoretical formulations to derive the P-waves velocity, V_p, of a soil containing gas bubbles; Tsukamoto et al. (2002) showed that V_p is a powerful means to measure the degree of saturation of near-saturated specimens, stating that it can be successfully used as a saturation marker both in laboratory and *in situ*. Yang et al. (2004) provided several correlations to evaluate the liquefaction strength of a partially saturated sand by measuring the P-waves velocity. Some relations were proposed between CSR and the Skempton's pore pressure coefficient B and between CRR (at 20 loading cycles) and V_p. Okamura and Soga (2006) found a unique relation between the potential volumetric strain and the liquefaction resistance of partially saturated sands. Together with the initial fluid pressure and confining pressure, the degree of saturation, S_r, was used as a testing parameter in undrained triaxial tests. As a result of the experimental investigation, it was concluded that the effect of gas on liquefaction resistance is significant for soils with high confining pressure and low initial pore water pressure. According to Okamura and Soga (2006), the liquefaction resistance of a partially saturated sand can be estimated from that of fully saturated one by using the potential volumetric strain.

Yegian et al. (2007) introduced small amounts of gas into potentially liquefiable sandy soils; large scale samples were prepared and tested under dynamic loading (cyclic shear) in an opportune flexible box. Two techniques were used to induce partial saturation in the specimens, namely water electrolysis[6] and drainage-recharge[7].The results showed that liquefaction could be inhibited; furthermore, the presence of entrapped air within a 151 cm sand column, partially de-saturated by drainage-recharge technique, was evaluated after 442 days: only a small amount of air escaped from the specimen (S_r increased of about 1%). Eseller-Bayat et al. (2009) applied cyclic simple shear stresses on fully saturated and partially saturated samples and observed that a reduction in S_r from 99.7% to 86.2% had led to a considerable decrease of Δu; moreover, partially saturated specimens showed less settlements, if compared to those exhibited by fully saturated ones. An investigation on the water flow influence on the endurance of gas bubbles within the soil matrix was also conducted: two sand columns, horizontally and

[6]Two electrodes were employed for water electrolysis (anode and cathode); an electrical current of specific intensity produced oxygen and hydrogen, and a certain amount of water thrown out of the specimen indicated that induced partial saturation was completed.

[7]After a specimen was fully saturated, pore water was slowly drained from its bottom and then reintroduced from its top; at the end of the recharge phase, a certain volume of water remains above the surface of the sample, thus indicating that gas bubbles have been entrapped within the specimen.

vertically disposed, were tested under low and high hydraulic gradients, and it was proven that very little volume of air escaped during the water flow process without any significant diffusion.

A different technique used in laboratory to produce partially saturated soil samples was studied by Eseller-Bayat et al. (2012a,b): the addition of the chemical compound sodium perborate monohydrate[8] to the sand was used to achieve a more uniform distribution of oxygen gas bubbles within the samples. An empirical model for the prediction of the excess pore pressure ratio, based on the results of experimental testing, was also proposed. Furthermore, a plexiglass tube filled with partially saturated sand (drainage-recharge) was prepared to evaluate the long-term endurance of gas bubbles. After 115 weeks under hydrostatic conditions, a 2% increase in S_r was detected; a column was tested under vertical upward water flow, but the latter didn't significantly affect the S_r value. The stability of bubbles under hydrostatic and flow conditions was therefore confirmed. At the end, the effects of cyclic horizontal loads on the degree of saturation was analyzed by vibrating the tube basement in a small shaking table, up to excitation of 1**g**: it was proven that S_r didn't vary over 10000 loading cycles. Okamura et al. (2011) used a pressurized air injection technique to produce *in situ* de-saturation of a soil susceptible to liquefaction; an air injector was placed in a saturated layer, at a depth of 6 m, and a partially saturated area (S_r ranging from 98% to 68%) was observed within a radial distance of 4 m from the injection point.

A certain volume of gas can be generated into the pore water due to the biological activity of microorganisms (*biogas*). Several chemical processes that produce gases as a byproduct are known in nature, such as aerobic respiration, fermentation, denitrification and methanogenesis, that generate carbon dioxide (CO_2), hydrogen (H_2), nitrogen (N_2) and methane (CH_4), respectively. Nitrogen gas is particularly appealing to improve soils against liquefaction, since it has very low solubility in water, it is not greenhouse, not combustible, and it is chemically inert. A study conducted by Rebata-Landa and Santamarina (2012) proved that partial saturation can be induced in a soil due to biologically-mediated processes. The Authors evaluated the use of denitrification[9] to generate nitrogen gas into different soil types; anaerobic bacteria were chosen for this goal, and P-waves velocity was measured during gas generation and used as a soil saturation indicator. They demonstrated that bio-mediated gas generation led to a decrease of V_p as S_r decreased, and to an increase of liquefaction resistance. The Authors tested different soil types, from uniform-grained to mixed-grained ones, showing that grain size affects the early evolution of gas production: in particular, the fines content played a significant role in the measures of V_p. It was stated that gas bubbles could escape more easily from soil specimens with low fine content (partial recovery of V_p) and that a more uniform distribution of gas bubbles can be achieved by means of denitrification, if compared e.g. with the air injection method. However, monitoring the reaction intermediates is essential to ensure the development of N_2 without any accumulation of undesired compounds. Denitrification

[8]The sodium perborate monohydrate ($NaBO_3 \cdot H_2O$) reacts with water, generating hydrogen peroxide (H_2O_2), that is a direct source of oxygen gas.

[9]Denitrification is the biological process in which nitrate (NO_3^-) is reduced into nitrogen gas through intermediates, like nitrite (NO_2^-). It is worth noting that, if respiratory denitrification stops before N_2 is produced, being the efficiency of the chemical reaction less than 100%, undesired and harmful byproducts, like nitrite or nitrous oxide (N_2O), could accumulate.

is a temperature-related process: values between 15°C and 35°C are the optimal ones (Stanford et al., 1975), while low pH and temperature negatively influence the conversion rate from nitrate to nitrogen gas (Saleh-Lakha et al., 2009; Šimek and Cooper, 2002).

He et al. (2013) studied biogas as a remedial measure against liquefaction: biogas was generated by means of the denitrification process, and its effects on the cyclic behavior of a liquefiable sand were studied by conducting 1**g** shaking table tests with a fully equipped laminar box. Bacteria were isolated from anaerobic sludge of wastewater treatment plant; after supplying nutrients, the dominant species in the culture was identified in Acidovorax species, a very common denitrifying bacterium. The desired amount of gas could be controlled by adjusting the reagents concentrations according to the stoichiometry of chemical reactions. Sand samples (mean grain size 0.40 mm, round-shape, siliceous) were prepared for testing: after the laminar box was assembled, the sand was placed into the bacterial suspension at a relative density, D_r, of about 20% and it was then left for some days before shaking in order to allow sufficient gas generation. The target peak acceleration in the shaking table was $1.5 m/s^2$. The testing box was equipped with accelerometers, displacement and pore pressure transducers, being the latter at the bottom, at 1/3 and 2/3 depth. He et al. (2013) showed that, for the same D_r, the pore pressure generated in partially saturated samples was much smaller than that developed in the fully saturated one, even if S_r was only reduced of 5%. He and Chu (2014) carried out laboratory tests to evaluate the undrained response of loose sands, de-saturated by biogas, under monotonic loading conditions. A series of isotropically consolidated undrained compression and extension tests was performed; a microbial denitrification process was used to allow generation of nitrogen bubbles within the samples. The undrained shear strength could be increased and the pore water pressure. He et al. (2016) summarized previous experiences on sandy soils under cyclic and monotonic loads. They showed that the higher the initial nitrate content, the higher the decrease in S_r. Peng and Zhang (2017) performed shaking table tests on fully and partially saturated sand samples: they showed that the liquefaction resistance of de-saturated sand (biogas) increased as S_r decreased due to the reduced excess pore water pressure developed during shaking; surface settlements of partially saturated specimens were less than that of saturated sand.

Researchers have shown that reducing S_r of a liquefiable soil is effective in increasing its liquefaction resistance. Injecting air into the soil can be a real cost-effective remedial measure, and first attempts of a practical application of the method has already been performed (e.g. Okamura et al. (2011)); the study on biogas is still to date at laboratory scale. The major shortcomings of biogas-induced partial saturation can be summarized as follows: an incomplete denitrification process can lead to the production of undesired and harmful compounds; even if no specific species of bacteria are requested to reduce nitrate to N_2, it is necessary to understand if microorganisms can be injected in the soil, if they can live at desired depth, or if existing microorganisms can be used.

Gas bubbles durability over time *in situ* can also be a concern, even if some Authors demonstrated that they are sufficiently stable also under water flow (e.g. Eseller-Bayat et al., 2009).

2.5.2 Biocementation

Biocementation consists of using the biological processes of specific microorganisms to precipitate inorganic compounds that link the soil grains. These bio-products are by-side compounds of specific biochemical processes, and they provide the grains with cohesion (i.e. cementation). Types of microorganisms, products, percentage of products, chemical reactions, rate of chemical reactions, nutrients and reagents required to obtain a desired improvement are fundamental factors affecting the success of bio-mediated ground improvement. Specific kinds of bacteria, reactions and compounds that can be used to perform biocementation have already been identified and tested by several researchers; due to their works, the complexity of biocementation processes can be described with great accuracy.

The oldest, most investigated and replicated way to perform biocementation is commonly referred to as *Microbial Induced Calcium Carbonate Precipitation* (*MICCP*). In MICCP, bacteria are used to precipitate calcium carbonate ($CaCO_3$) among the grains. The first approaches to this technique can be found in Castanier et al. (1999); Stocks-Fischer et al. (1999); Fujita et al. (2000); Whiffin (2004). MICCP through urea hydrolysis (*ureolysis*) represents the standard biocementation process: dedicated bacteria, such as *Sporosarcina pasteurii* (*Bacillus pasteurii*), an aerobic microorganism containing the enzyme urease, are cultivated in laboratory and then injected into the soil via a urea-containing suspension; the sum of these suspensions are called *biogrout*, that can be defined as "*a dry matter or solution of one or several inorganic soluble salts and biomass of microorganism(s) or their enzyme(s), which are necessary to initiate transformation and precipitation of inorganic components*" (Stabnikov et al., 2015). Due to hydrolysis, catalyzed by the enzyme, urea is decomposed into ammonium (NH_4^+) and carbonate (CO_3^{2-}); as a result of bacterial metabolic activity, the pH of the proximal environment increases. In presence of calcium ions, the produced carbonate ions precipitate as calcium carbonate crystals (e.g. calcite, aragonite, vaterite). When enough calcium carbonate is precipitated, a durable soil stabilization is achieved (Van Paassen et al., 2009). The major drawbacks of this process are represented by high pH values and by the release of ammonium (dangerous for the environment at high concentrations) that needs to be extracted and removed.

Beyond MICCP with urease positive bacteria, other types of biogrouting techniques are known to date, and different compounds, such as iron oxides, silica, iron sulfides, can be precipitated to promote bonding of grains (Ehrlich et al., 2015). As examples, alternative calcium-based precipitation methods are denitrification (precipitation of calcium carbonate due to reduction of nitrate by denitrifying bacteria, using e.g. ethanol or acetate as electron donor), calcium phosphate precipitation from calcium phytate, calcium carbonate precipitation, removing CO_2 from a solution of calcium bicarbonate with the addition of urea to increase pH and produce carbonate ions (Stabnikov et al., 2015). Iron-based biogrout uses precipitation of iron materials as binding materials Ivanov and Chu (2008); Ivanov et al. (2010); Weaver et al. (2011).

The dynamic behavior of liquefiable sands treated with MICCP was studied by Montoya et al. (2013). Sand samples were improved with different amounts of cohesion (from lightly to heavily bio-cemented) and subjected to centrifuge and cyclic shear tests. Shear waves velocity measurements were used to assess the level of improvement (300 m/s, 650 m/s and 1200 m/s for lightly, moderately and heavily treated materials, respectively). Bacteria 'Sporosarcina

pasteurii' were used in the biological grout. As a result of the experimental investigations, an increase in liquefaction resistance of bio-grouted material was recorded: MICCP treatment improved the soil behavior under cyclic loading conditions by reducing the pore pressure excess and settlements for similar base input accelerations, if compared to the results obtained for untreated sand: however, ground surface peak accelerations also increased. This represents a great drawback of the method, due to the need of minimizing this undesirable effect while maintaining enough improvement at the same time.

Burbank et al. (2011) manipulated indigenous urease native bacteria and showed by means of laboratory and *in situ* tests that it is possible to enrich existing ureolytic bacterial communities to hydrolyze urea in presence of calcium ions, and then to precipitate sufficient calcium carbonate within the pore spaces of potentially liquefiable soils. Moreover, it was proven that enrichment of ureolytic microbes is possible in soils with different characteristics (mineralogy and grain distribution). Burbank et al. (2013) demonstrated that natural indigenous bacteria can be stimulated to produce precipitation of a significant amount of calcium carbonate, and that a significant increase of the cyclic resistance of treated soils can be achieved with moderate levels of improvement. Desired bacteria can be activated by using suitable nutrients. A microcosm experiment showed that indigenous bacteria can be successfully used to induce sufficient calcite precipitation and to modify the soil properties; a series of cyclic triaxial tests was also performed to demonstrate the feasibility of biocementation for liquefaction mitigation. Figure 2.19 shows the results of these tests in terms of liquefaction resistance curves for treated and untreated materials; the benefits for bio-treated samples are clear.

Denitrification can also be used to precipitate inorganic compounds mong the soil grains (Van Paassen et al., 2010). Kavazanjian et al. (2015) proposed the use of denitrification as a two-stage improvement process: a first step, in which improvement against liquefaction is offered by gas generation (saturation degree reduction) followed by a second step in which precipitated compounds provide the liquefiable sand with durable improvement (bonding of grains).

By summarizing, the main advantage of biocementation is the possibility of using widely-available bacteria species to stabilize soils by means of bio-produced inorganic compounds, but the major shortcomings are the difficulties in obtaining homogeneous treatments, how biocementation can be performed *in situ* and how to deal with the increased shear wave velocity and reduced damping properties of treated material, due to its increased stiffness.

2.5.3 Bentonite suspension grouting

The principle of working of bentonite suspension grouting is similar to that of colloidal silica grouting (Chapter 3): a bentonite suspension permeates through the sand pores and it substitutes the pore water, forming a bentonite-based gel and modifying the mechanical properties of the material. The presence of bentonite significantly increases the liquefaction resistance of sand, since it reduces the development of pore water pressure: the inhibition of Δu is due to the increased threshold above which extra pore pressure is generated (El Mohtar et al., 2008, 2014). In Figure 2.20 the results of cyclic triaxial tests on sand and sand-bentonite mixtures are presented for isotropically consolidated ($\sigma'_c = 100kPa$) specimens: given a certain CSR, the loss of

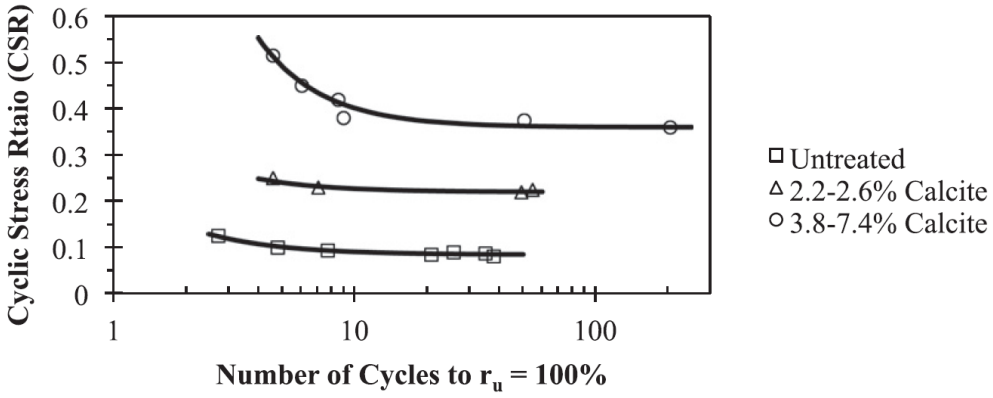

Figure 2.19: *Liquefaction resistance curves for untreated and bio-treated material with different calcite content (from Burbank et al., 2013).*

initial effective confining stress depends on the bentonite content and it increases as bentonite content decreases. El Mohtar et al. (2013) showed that bentonite content and hydration time of bentonite within the pore spaces are key factors affecting the cyclic resistance of sand-bentonite material. Furthermore, El Mohtar et al. (2014) showed that pre-shear age significantly improves the performances of the material under both undrained cyclic and monotonic loading conditions. As shown in Figure 2.21a, the number of cycles to liquefaction increases as bentonite content and age increase, while the development of extra pore pressure decreases (Fig. 2.21b). The Authors stated that "*the changes in material response [...] appear to be controlled by the properties of the pore fluid formed in the presence of bentonite: a concentrated clay gel [...]. The formation of this pore fluid is responsible for the increase in the critical strain at which excess pore pressure is generated*".

For practical application, however, the penetration of a bentonite suspension through a soil is prevented by its high viscosity; moreover, such a viscosity needs to be recovered within the pore spaces, to improve resistance against cyclic loading. For these reasons, the rheological properties of bentonite suspensions have also been investigated. Rugg et al. (2011) showed that adding Sodium Pyrophosphate facilitates the permeation of concentrated bentonite suspensions (bentonite contents > 10% by dry mass) through a sand matrix; similar modified bentonite suspensions are needed to increase their initial mobility and to maintain the thixotropic nature of the fluid (Yoon and El Mohtar, 2013). El Mohtar et al. (2013) showed that the addition of 0.5% Sodium Pyrophosphate by mass of clay is effective in reducing the initial viscosity of concentrated (10%) bentonite suspensions to allow permeation through sandy soils. The thixotropic nature of the suspension is recovered over time, thus ensuring its effectiveness in improving the soil performance.

The use of bentonite for liquefaction mitigation is particularly fascinating because bentonite is widely available and environmentally-friendly. However, despite the overall benefits to the mechanical behavior of treated material described by literature, it is thought that the main concern of this method is how to deliver the stabilizing grout to a target area; the use of additives to increase the initial mobility of the suspension represents a valid solution, but it complicates the design and it increases the economic costs of the remediation.

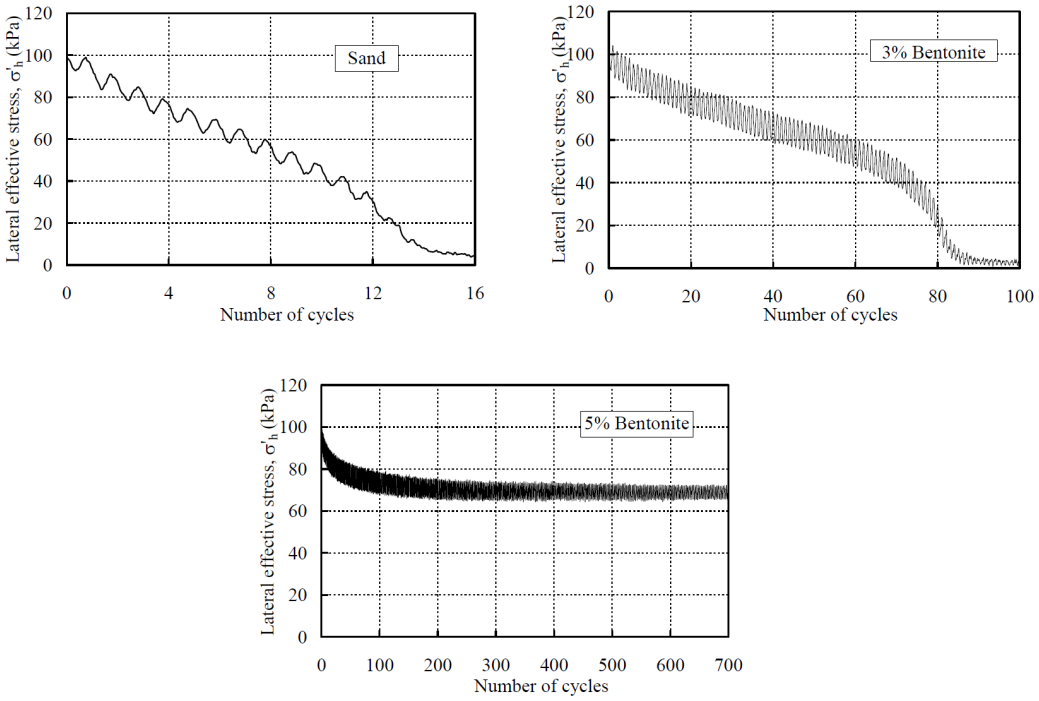

Figure 2.20: *Changes in effective stresses during cyclic triaxial tests for $CSR = 0.125$ (% of bentonite by dry mass) (from El Mohtar et al., 2008).*

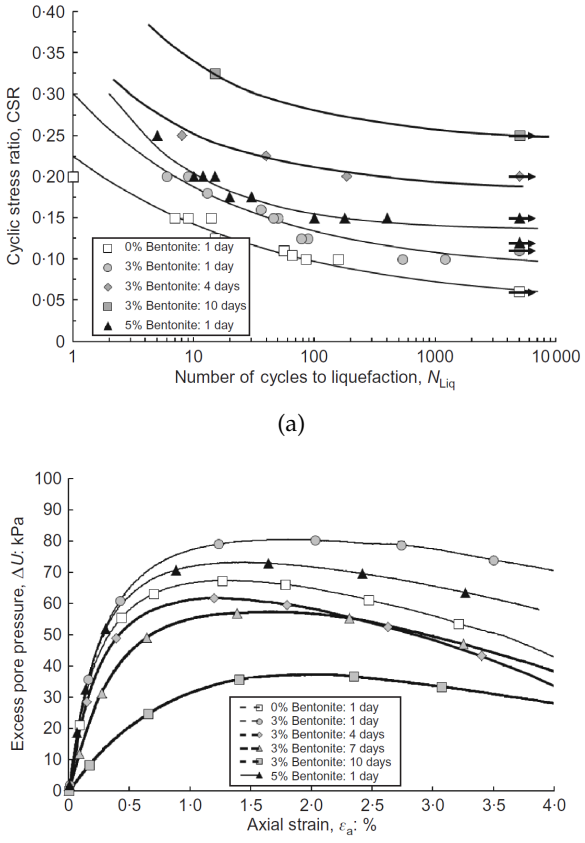

Figure 2.21: *Cyclic resistance curves (a) and pore pressure excess (b) for sand with different bentonite content and age from undrained cyclic (a) and monotonic (b) triaxial tests (from El Mohtar et al., 2014).*

2.5.4 Tire chips

Sand mixed with wasted tire chips can be successfully used as a backfill material with high liquefaction resistance: shaking table, undrained monotonic and cyclic triaxial tests on sand mixed with chips showed that the soil-chips mixture had a higher liquefaction resistance than that of neat sand (Zornberg et al., 2004; Hazarika et al., 2007; Hyodo et al., 2007; Uchimura et al., 2007; Hazarika et al., 2008; Okamoto et al., 2008; Hazarika et al., 2010); the rise up of pore water pressure was inhibited by the presence of tire chips, being this effect higher as the chips content increased. Towhata (2008) reported that "*the reason for the increased liquefaction resistance of tire chip mixture is probably that the rigidity of tire chip particles is lower than that of sand grains, allowing some volume compression under developed excess pore water pressure. Thus, the volume compression of tire chip produces a situation similar to drainage or dewatering which decrease the extent of excess pore water pressure.*". Conversely, Promputthangkoon and Hyde (2007) found that undrained cyclic behavior of sand-tire chips mixture was worse than that of untreated sand: according to Mashiri et al. (2015), however, this discrepancy with other literature data may be ascribed to the relatively high constant void ratio used by the Authors.

The compressibility of sand-chips mixture has also been evaluated: pure sand exhibited significant lower strain than that of mixtures (Rao and Dutta, 2006; Promputthangkoon and Hyde, 2007). For instance, Figure 2.22 shows the results obtained from 1D normal compression tests on sand-tire chips mixtures: vertical strain increased with tire chips content over the whole range of the tested vertical stress. In the plot, the mixtures are expressed in terms of ratio (by solid volume) of sand to tire chips. The Authors suggested that 20% chips content may be the limiting percentage to be mixed with sand to avoid unacceptable settlements.

Kaneko et al. (2012) showed that better performances in liquefaction mitigation can be obtained by putting pure tire chips in layers beneath the sand instead of mixing them with it; they also confirmed that tire chips developed less pore pressure due to their high deformation characteristics, and that they are able to filter seismic waves due to the low stiffness of tire crumbs. By the analysis of 1D shaking table tests, Bahadori and Manafi (2013) stated that the mean damping ratio of soil increased as tire chips content increased. Mashiri et al. (2015) performed strain controlled undrained cyclic tests on sand-tire chips mixtures, showing that their liquefaction potential was lower than that of clean sand. In Figure 2.23 the number of cycles to liquefaction of sand-tire chips mixtures (STCh) increases, for a given strain, with the gravimetric proportion of tire chips, therein expressed in percentage. Moreover, the shear modulus decreased with increasing the amplitude of shear strain and the number of cycles, while the damping ratio increased with single amplitude shear strain and decreased as the number of cycles increased.

Mixing tire chips with sand enhances its liquefaction resistance, but the increased compressibility of the material requires a specific attention; furthermore, it may be questionable if the method is environmentally sustainable.

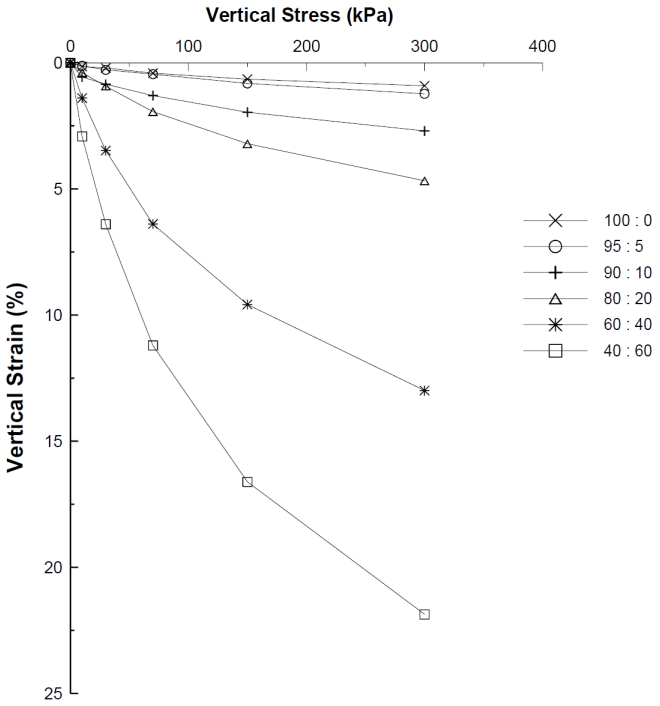

Figure 2.22: *Vertical stress against vertical strain from oedometer tests on sand-tire chips mixtures with different chips content (from Promputthangkoon and Hyde, 2007).*

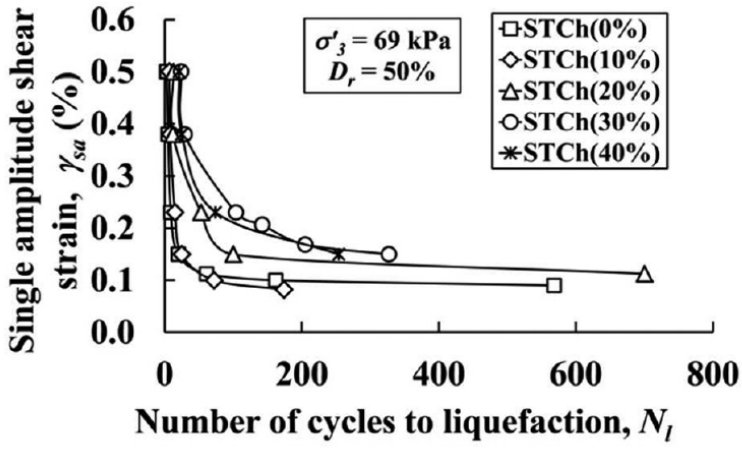

Figure 2.23: *Results of undrained stain controlled cyclic triaxial tests on sand-tire chips mixtures (from Mashiri et al., 2015).*

Chapter 3

Colloidal silica

3.1 Introduction

The use of nanotechnology in Geotechnical Engineering has known a great impulse in the recent decades; nanoparticles can be added to the soil to modify and to improve some mechanical characteristics of the material. For example, adding nanoclay to a cohesive soil significantly changes its plasticity properties and its hydraulic conductivity (Kananizadeh et al., 2011; Nikookar et al., 2013).

In the field of Geotechnical Earthquake Engineering, a stabilizing *grout* made of colloidal silica particles has been successfully used to increase the liquefaction resistance of a liquefiable sand (Gallagher, 2000; Gallagher et al., 2007a; Porcino et al., 2011). If properly mixed with a reactant, the colloidal silica grout changes its initial liquid-like physical state into a solid-like one by increasing the mixture viscosity over time; as the latter increases, the colloidal silica grout forms a *gel*, a continuous, random-packaged network of bonded silica clusters. The increase in viscosity is related to the chemical structure of the grout, and it can be controlled by managing several factors, like the percentage of solids diluted in the mixture and the reactant concentration, among others. A colloidal silica gel formed within the pore spaces links the soil grains, thus providing the treated material with a sort of artificial cohesion (Vranna and Tika, 2015).

Although different uses of colloidal silica have been proposed for engineering practice over the years (in tunnelling industry, it has been chosen to prevent water flow (e.g. Butrón et al., 2010); in the petroleum industry, to reduce the permeability of rocks to water and gases (e.g. Seright, 1995); in the environmental practice, to form barriers against fluid flow to protect groundwater from contaminants (e.g. Moridis et al., 1996; Noll et al., 1992)), this PhD Thesis deals with colloidal silica grouting for liquefaction mitigation. This Chapter presents a comprehensive review of scientific publications concerning this topic: the most significant results are described and discussed in detail, and benefits and drawbacks of colloidal silica grouting are outlined.

3.2 Colloidal silica properties

3.2.1 Colloidal silica: a chemical grout

Colloidal silica (thereafter indicated as *CS*) can be defined as a stable *sol*[1] of silica particles with size ranging from 5 up to 100 nm. It is obtained from saturated solutions of silicic acid, $Si(OH)_4$, (Iler, 1979; Karol and Berardinelli, 2003), and it results as a clear, harmless, and low viscosity mixture (Iler, 1979; Moridis et al., 1995; Gallagher, 2000) that is commercially available with different concentrations of silica particles, the size of which is fairly constant in such products. If diluted to 5% CS particles by weight, its cost could be comparable to that of microfine cement and its viscosity can initially be comparable to that of water (Gallagher et al., 2007b; Agapoulaki and Papadimitriou, 2015, 2018). Furthermore, it is a durable product over time: Whang (1995) expected that the longevity of colloidal silica is over 25 years.

The stability of the sol (which is mainly made up of water (*hydrosol*)) is governed by the interparticle forces acting among the solids (Iler, 1979; Bergna and Roberts, 2005), and it indicates that particles can't settle or coalesce at a significant rate. In particular, repulsive forces acting on silica particles' surface prevent their agglomeration. If the sol is destabilized, a *gel* state takes place; the latter can be described as a system "*made of a continuous solid skeleton made of colloidal particles or polymers enclosing a continuous liquid phase*" (Bergna and Roberts, 2005).

A colloidal silica sol can be become a gel by essentially reducing the repulsive forces acting among silica particles, that can be therefore linked together and agglomerate. *Gelling* of the colloidal silica sol indicates the development of silica networks that follows a viscosity increase; "*when a sol is gelled, it first becomes viscous and then develops rigidity and fills the volume originally occupied by the sol*" (Bergna and Roberts, 2005). The concentration of silica throughout the gel is constant, "*and the overall medium becomes viscous and then is solidified by a coherent network of particles that, by capillary action, retains the liquid*" (Iler, 1979).

The fundamental unit of colloidal silica particles is the SiO_4 tetrahedron; amorphous silica (not crystalline, like e.g. quartz) is composed of a pattern of random packaged $[SiO_4]^{4-}$ tetrahedra. In the structure, each oxygen ion can be linked to no more than two cations; the Si-O bond is the stable bond that acts among the molecules. Two distinct groups of SiO_4 can share only one oxygen, but each oxygen can be shared with adjacent groups. A sketch of a colloidal silica particle is reported in Figure 3.1, in which the fourth oxygen of the tetrahedra is above or below the plane. It can be observed that the Si-O-Si bonds represent the mutual connection among each SiO_4 group.

Some properties of colloidal silica are of significant interest for engineering practice and they encourage the analysis and development of further studies on the use of CS grouting for ground improvement. In particular:

- It is a non toxic, inert and durable product;
- Its viscosity can be adjusted and can be kept as low as that of water over a wide range of times, allowing easier permeation of soils;

[1] A sol is a dispersion of solids of colloidal size into a liquid phase.

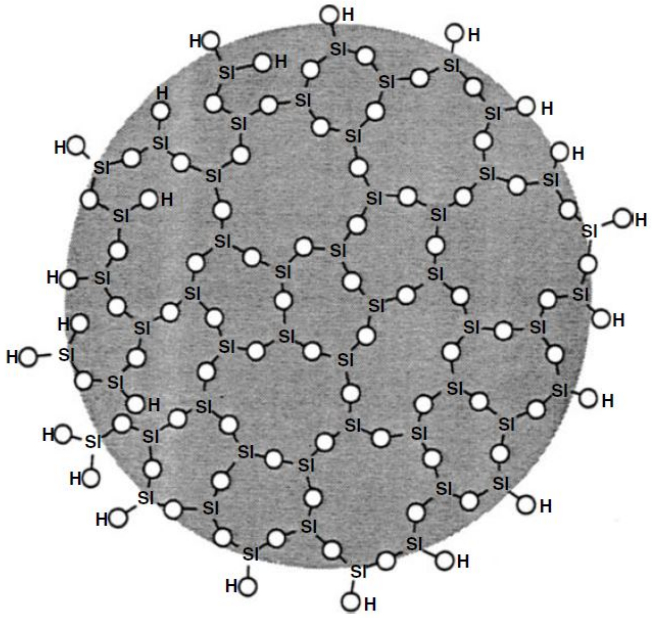

Figure 3.1: *Scheme of a colloidal silica particle with hydroxyl groups (from Bergna and Roberts, 2005).*

- After a certain time it can form a colloidal silica gel that can provide the soil grains with an artificial cohesion, thus modifying the mechanical properties of treated soil.

Colloidal silica could potentially be injected into soils to treat liquefiable layers by means of low injection pressures (Gallagher et al., 2007a); theoretically, CS grouting would be particularly favorable to improve soils under foundations of existing structures, where other standard techniques (e.g. densification, drains installation, etc.) could not be safely used (Towhata and Kabashima, 2001). Initial high mobility of grout facilitates its transportation through porous media (e.g. Noll et al., 1993; Moridis et al., 1996; Gallagher and Lin, 2005; Gallagher et al., 2007a; Bolisetti et al., 2009; Hamderi and Gallagher, 2015); some Authors proposed the use of natural or augmented groundwater flow as a suitable mechanism of grout delivery (e.g. by means of low-head injection and extraction boreholes) (Gallagher and Finsterle, 2004). The treatment by colloidal silica is defined as *passive site stabilization*, or *passive site remediation*, and indicates the non-disruptive way CS can be delivered to improve soil deposits (Gallagher et al., 2002; Gallagher and Koch, 2003). The artificial cohesion that soil grains are provide with as a result of CS grouting is effective in reducing the liquefaction potential of treated sand (Gallagher and Mitchell, 2002; Liao et al., 2003; Díaz-Rodríguez and Antonio-Izarraras, 2004; Kodaka et al., 2005; Díaz-Rodríguez et al., 2008; Towhata, 2008; Porcino et al., 2011; Conlee et al., 2012; Porcino et al., 2012; Vranna and Tika, 2015; Andrianopoulos et al., 2016).

Colloidal silica grouting can be classified as a remedial measure against liquefaction based on the grains solidification principle. The main advantages of this method compared to other conventional techniques can be summarized as follows: high initial mobility of the grout, environmentally-friendly product, low injection pressure required, reduced economic costs, especially if the grout could be very diluted. Conversely, great hydraulic conductivity reduction is expected for the treated material.

3.2.2 The gelation process

A colloidal silica sol is stabilized when manufactured by adding to it alkaline solutions, like sodium hydroxide, to prevent gelation, that can subsequently be activated by properly mixing CS with a reactant, like an electrolyte; sodium chloride ($NaCl$) is commonly used for this purpose. The particles agglomeration essentially takes place due to the decrease of the repulsive forces acting on silica particles, and it is characterized by the formation of Si-O-Si bonds resulting in an increase of viscosity and in the development of a gelled matrix. In Figure 3.2 a schematic representation of the gelation process is given.

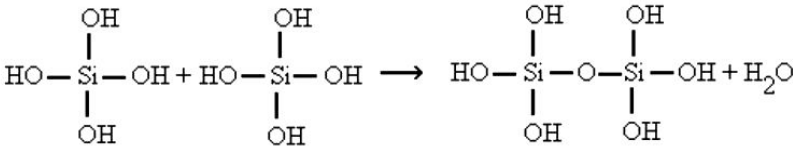

Figure 3.2: *Representation of colloidal silica gelation process (from Spencer et al., 2008).*

The electrolyte acts as a catalyst, but it is not the only factor that affects the *gel time*, that is the time that passes between the start of the colloidal dispersion destabilization and the end of the agglomeration process. The gel time depends not only on the amount of the electrolyte added to the sol, but also on particles' size, pH, temperature, and silica content (Iler, 1979). It is worth noting that the electrolyte concentration in the grout only affects the gel time, and not the strength of the resulting gel pattern (Gallagher et al., 2007a; Cao et al., 2010). In this work, the CS grout indicates the mixture of CS sol with other components, as described further on.

The knowledge of the rheological properties of the material is essential to address the gelation process for a proper site design (Agapoulaki and Papadimitriou, 2015; Pedrotti et al., 2017; Agapoulaki and Papadimitriou, 2018). The rate of grout viscosity increase can be adjusted by managing the parameters that govern the silica particles interaction at the micro-scale. The parameters of colloidal silica grout that influence the gel time can be summarized as follows (Iler, 1979):

- Silica content
- Ionic strength[2]
- Temperature
- pH
- Silica particles' size

If solids' size within the CS sol (products are commercially available with a given mean particles' size) and temperature (for potential grouting treatments soil temperature is slightly constant at shallow depths, where liquefiable deposits lay (Baggs, 1983; Popiel et al., 2001)) can be reasonably assumed as a datum, silica content, ionic strength and pH most significantly affect the gel time. Figure 3.3 shows the effect of pH on the gelation process of a 5% by weight

[2]The ionic strength of a solution can be defined as a measure of the ions concentration of the solution itself.

colloidal silica content mixture at 0.1 NaCl normality. It is observed that the solution has a viscosity initially comparable to that of water ($\approx$ 1.1 cP at 20°C), and that, after a certain time, a strong and sudden viscosity increase is measured. Keeping the initial viscosity almost as low as that of fresh water implies great initial mobility and easy soil penetration of the stabilizing grout (Gallagher et al., 2007b). However, the adjustment of pH, at least for *in situ* application, seems cumbersome.

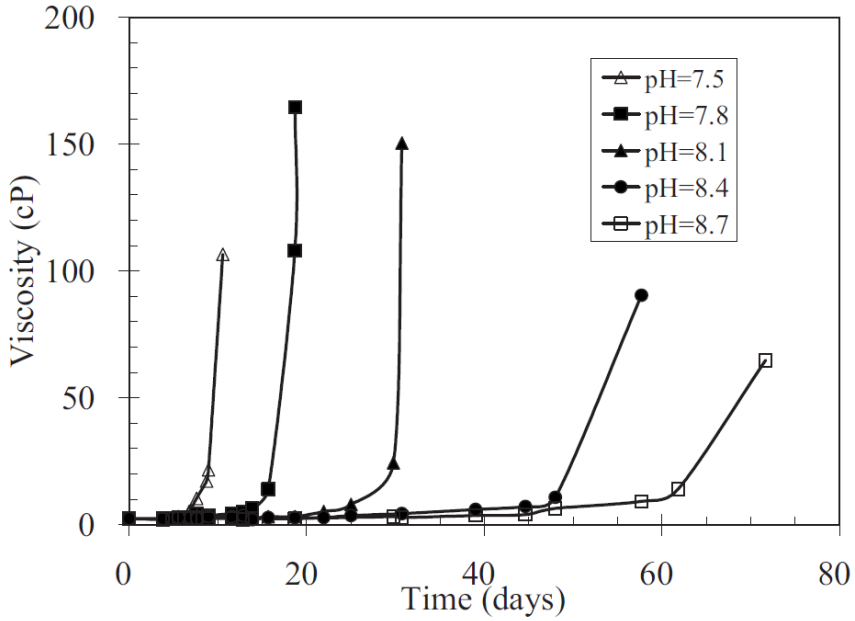

Figure 3.3: *Viscosity measurements on a 5% by weight colloidal silica mixture at 0.1 N NaCl (from Gallagher and Lin, 2009).*

Agapoulaki and Papadimitriou (2015, 2018) studied in detail the rheological properties of colloidal silica grout; the influence of the aforementioned factors was investigated, and a clear understanding of the interaction among them was provided. A set of charts and equations were provided to predict the rate of viscosity increase for a given CS product. The results are in agreement with previous data from literature (e.g. Persoff et al., 1994, 1999; Gallagher, 2000). In particular, Agapoulaki and Papadimitriou (2018) pointed out that, for practical in field application, a specific site design (e.g. specific viscosity measurements) is anyway required. In Figure 3.4a the results of viscosity measurements on pure colloidal silica are reported as a function of colloidal silica content, for a given pH, temperature and reactant concentration, while in Figure 3.4b the results show the viscosity as a function of the reactant concentration, for a given colloidal silica content, temperature and pH. As can be observed in Figure 3.4, the viscosity can be controlled by means of these parameters, and for a given pH and temperature of the grout, the gelation process is faster as silica and electrolyte content increase.

The design of a proper gel time for in field application is one of the main reason why its use *in situ* has to date been very limited (Gallagher et al., 2007a), despite the potential improvement that colloidal silica grouting could offer. If the gel time would be too short, in fact, the grout couldn't permeate homogeneously the liquefiable layer, and if it would be too long, the gel formation wouldn't occur where it was required. Moreover, some contaminants that could be

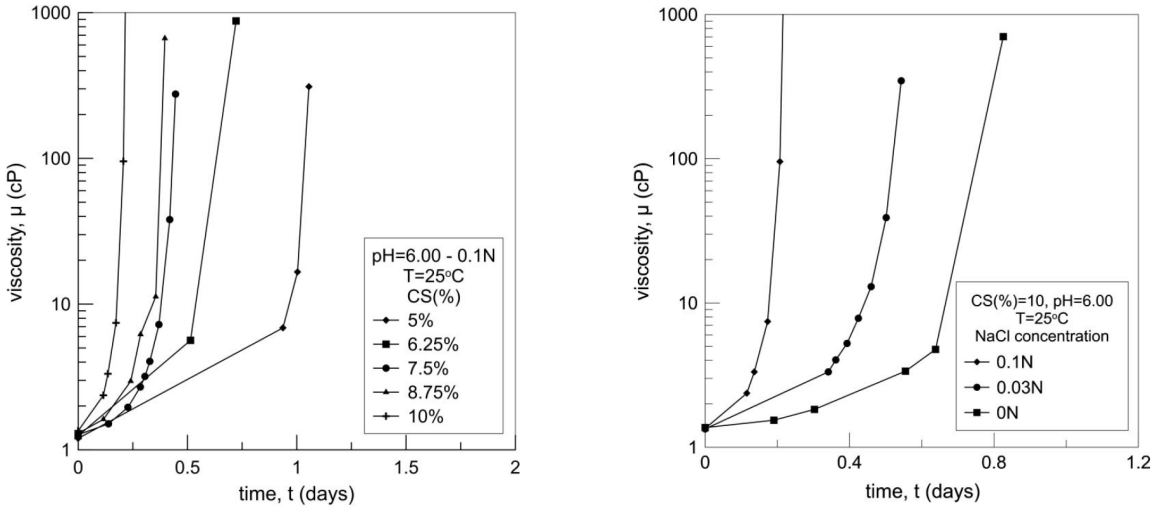

(a) (b)

Figure 3.4: *Results of viscosity measurements on pure colloidal silica grout for different silica contents (a) and different reactant concentrations (b) (from Agapoulaki and Papadimitriou, 2018).*

present in groundwater can chemically interact with colloidal silica (Persoff et al., 1994).

Several efforts to face such problems have already been made (e.g. Gallagher and Finsterle, 2004; Hamderi and Gallagher, 2013). In particular, Pedrotti et al. (2017) developed and validated an electro-chemically inferred model aimed to predict the CS gel time with varying pH, CS concentration, silica particles' size and electrolyte concentration, thus providing a useful tool for taking into account the existing *in situ* groundwater characteristics. On the basis of the existing literature, the influence of each factor on gel time is summarized in Table 3.1.

Table 3.1: *Gel time as a function of colloidal silica properties.*

		Gel time
Silica content	increase	decrease
Ionic strength	increase	decrease
Temperature	increase	decrease
Particles' size	increase	increase
pH	between 5-6	minimum

3.2.3 Silica gel properties

Very few data have been reported in literature regarding the properties of pure colloidal silica gel. Liao et al. (2003) showed that the shear vane resistance of pure CS gelled samples was very low, and that it was not possible to prepare e.g. cylindrical specimens for testing. Towhata (2008) reported the results of unconfined compression test on a pure CS gelled sample in which vertical and lateral strains were measured, the latter by means of laser transducers put at 1/3 and 2/3 depth of a 7 cm height specimen. The results are shown in Figure 3.5: it is worth noting that the material shows a strain softening behavior, but the main interesting aspect is that the ratio of lateral to axial strain (the Poisson's ratio ν) is $\approx$0.3, while incompressible materials

require ν to be 0.5.

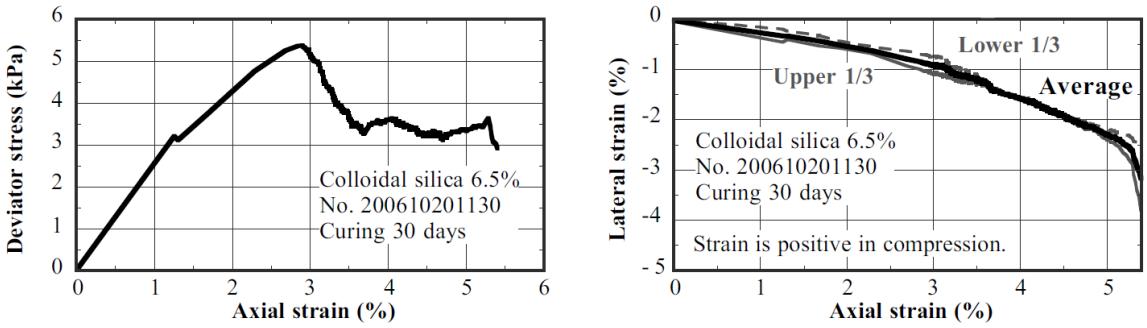

Figure 3.5: *Unconfined compression test results on pure colloidal silica sample (mod. from Towhata, 2008).*

Andrianopoulos et al. (2016) evidenced that the compressibility of the CS gel can be responsible for the increased liquefaction resistance of sand, together with bonding of grains. Thanks to the compressibility of silica gel the pore pressure build-up would be reduced. Wong et al. (2018) reported the results of oedometer tests on pure colloidal silica samples. Their results confirmed that CS gel is compressible, as illustrated in Figure 3.6, where the 1D-compression curves are reported for silica samples tested after different curing times (1-8 weeks).

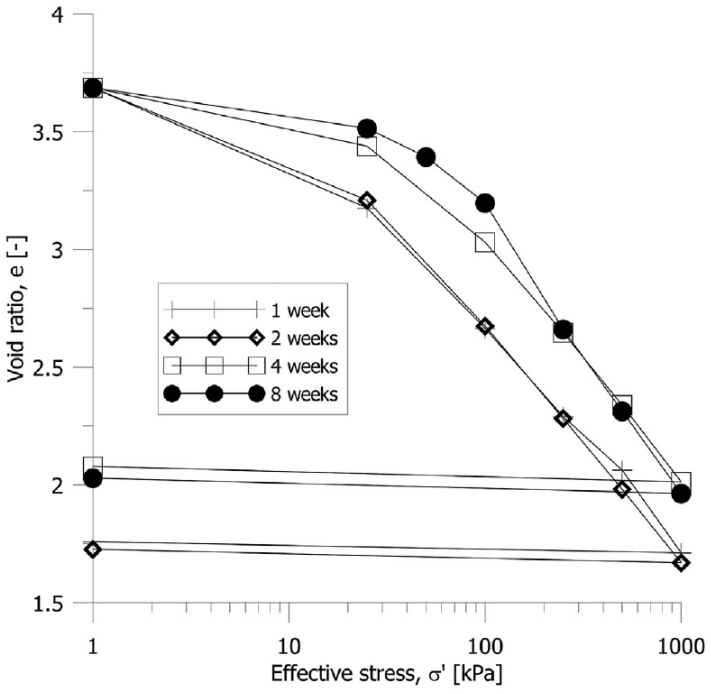

Figure 3.6: *Oedometer test results on pure colloidal silica samples after different aging time (mod. from Wong et al., 2018).*

3.3 Colloidal silica treated sand properties

3.3.1 Mechanical behavior under cyclic loading conditions

Colloidal silica stabilized soil has been tested under cyclic loading conditions to understand the effectiveness of such a stabilization method for liquefaction mitigation purposes. Historically, the analysis on the mechanical behavior of treated sand under cyclic loading condition has been followed by those under the static loading one; for this reason, the literature review is herein presented in this order.

Gallagher and Mitchell (2002) performed cyclic triaxial tests on treated and untreated Monterey n°0/30 liquefiable sand. Treated loose samples (relative density, D_r, equal to ≈22%) were prepared by pluviating dry sand into molds containing the colloidal silica grout. In this way, the specimens were fully saturated by gel. Silica contents were varied between 5 and 20% by weight of the grout, whereas gel time was set between 4h and 1d. Different curing times were waited before each sample was tested. A number of samples were cyclically tested, while the remaining part was subjected to unconfined compressive strength tests. The major objective of the study was to investigate the different response to cyclic loading of treated and untreated samples; then, the effects of curing time on deformation properties of the specimens and the optimum colloidal silica content for liquefaction mitigation were also evaluated. A commercial colloidal silica, named DuPont Ludox-SM, was used; as a neat product, it contains 30% silica by weight. Sodium chloride and hydrochloric acid were employed for adjusting the gel time, by adjusting ionic strength and pH of the grout respectively. No back pressurization phase was performed to saturate the samples for triaxial testing, to not destroy the gel bonds within the pores. Consequently, it was not possible to measure the pore pressure response during the shear phase, and the peak to peak axial strain was used to quantify the failure condition. The specimens were tested at a confining stress of 100 kPa. It was found that, the higher the silica content, the smaller the strain experienced by treated specimens during cyclic loading (Fig. 3.7). Furthermore, no samples failed during the tests, thus a part of those could be subjected to additional unconfined compression tests after cyclic loading, showing strength values that varied with the amount of strain previously developed: the higher was the experienced strain, the lower was the measured unconfined compression strength. Treated samples exhibited small strain during cyclic loading, that was homogeneously distributed during the loading sequence; furthermore, they didn't collapse, while untreated specimens showed small strains that increased rapidly as liquefaction was initiated, causing the soil to fail within a few number of cycles. It was observed that samples treated with lower CS contents experienced more strain than samples treated with higher CS contents, for a given CSR (Fig. 3.8). Axial strain of treated sand was found not to be symmetric about the zero strain; this result also agreed with the data from Saxena et al. (1988); the same tendency will also be shown by Porcino et al. (2011). The Authors indicated that CS content ranging from 5 up to 10% CS (by weight) can be considered a good compromise between effectiveness and economic advantage to improve the sand liquefaction resistance.

Liao et al. (2003) demonstrated that liquefaction resistance of a sand collected from a hydraulic fill on the west Taiwanese coast can be improved by colloidal silica grouting. Cylin-

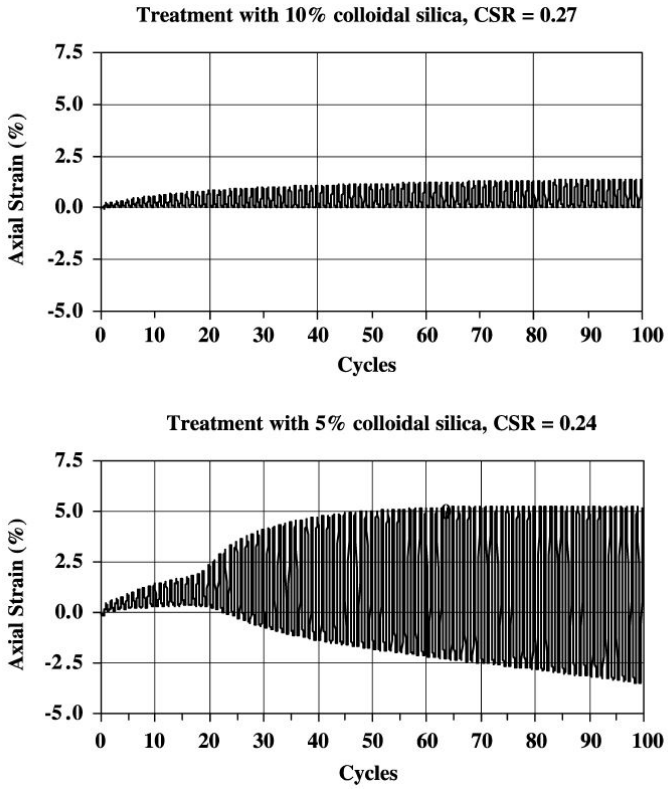

Figure 3.7: *Axial deformation during cyclic loading for treated sand (from Gallagher and Mitchell, 2002).*

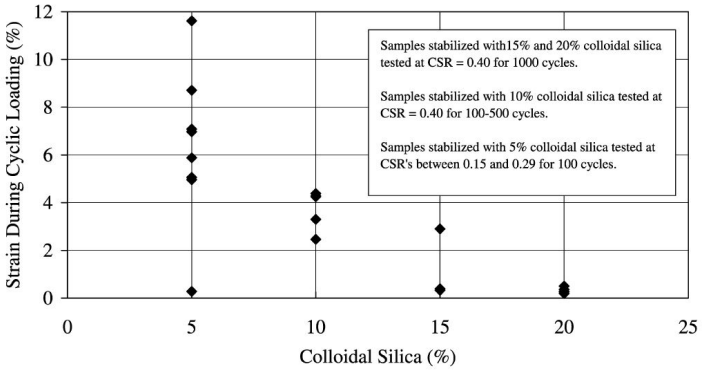

Figure 3.8: *CS content versus strain during cyclic loading for different stress levels (from Gallagher and Mitchell, 2002).*

drical sand specimens for undrained cyclic triaxial testings were prepared at a relative density of 50%±3% and dry tamped in layers into a split mold; a colloidal silica solution was permeated through the samples from the bottom to the top, by letting about 3 times the volume of voids pass throughout the soil. Very short gel time (about 8 minutes) was chosen for specimens preparation, while different curing times (up to 28d) were waited, after the mold was dismantled, before testing. After curing, carbon dioxide flushing followed by deaired water permeation was performed before a back pressure was used to saturate the samples (B>0.95); however, a little amount of water could flow inside the specimens, since their volume of voids was almost completely occupied by grout. Before cyclic loading, the samples were isotropically consolidated at a constant effective consolidation pressure of 98 kPa. Because of colloidal silica treatment, a strong improvement in liquefaction resistance of grouted sand (4 to 7 folds increase) was detected if compared to that of untreated sand. Moreover, for a given number of loading cycles, the increase in liquefaction strength was also directly proportional to the curing time each sample had been experienced. Axial strain for treated sand showed a gradual increase with the number of cycles until initial liquefaction occurred, while untreated ones showed sudden large deformation as initial liquefaction was initiated. Pore pressures were measured during triaxial tests: it was revealed that very high stress ratios were required to activate the mechanism of pore pressure build-up, since almost all voids were filled with silica gel; these high stresses caused a rapid increase in pore pressure at initial loading stage, even if many more cycles could be withstood by grouted sand before reaching initial liquefaction.

Díaz-Rodríguez and Antonio-Izarraras (2004) performed a series of cyclic simple shear tests on a natural liquefiable sand before and after several colloidal silica grout treatments were applied; the samples were prepared by pluviating dry sand, collected from the port of Lazaro Cardenas (Mexico), into molds containing colloidal silica grout. All tests were conducted at a fixed frequency of 1 Hz, and the initial liquefaction condition (defined in the paper as $\Delta u = \sigma'_{vc}$) was selected as the criterion to analyze and compare test results. Curing time was set in 3d for all specimens; parameters such as colloidal silica content and relative density were used to investigate the behavior (in terms of shear strain and pore pressure response) of treated and untreated sand. Treated samples were prepared with colloidal silica contents ranging from 10 up to 20% by weight. In agreement with data from previous studies, an increase in liquefaction resistance for the investigated sand was recognized as CS content increased. Figure 3.9 shows that the rate of pore pressure ratio rise-up with number of cycles was faster as CS content decreased, being the maximum for untreated sand. The axial strain was found not to be symmetric about the zero-strain axis, but a bit shifted toward extension zone for CS content equal to 20%, while peak-to-peak shear strain rate with cycles number decreased as the CS content increased, showing a trend similar to that of pore pressure ratio response. It was concluded that large benefits, in terms of liquefaction resistance increase, could be obtained for the studied sand by means of colloidal silica grouting.

Kodaka et al. (2005) performed monotonic as well as cyclic torsional shear tests on Toyoura sand treated with 4% by weight colloidal silica grout. Specimens were prepared by dry pluviation and were reconstituted at a D_r=40%; they were saturated with the help of carbon dioxide, followed by flushing of deaired water and of colloidal silica solution, from the bottom to the

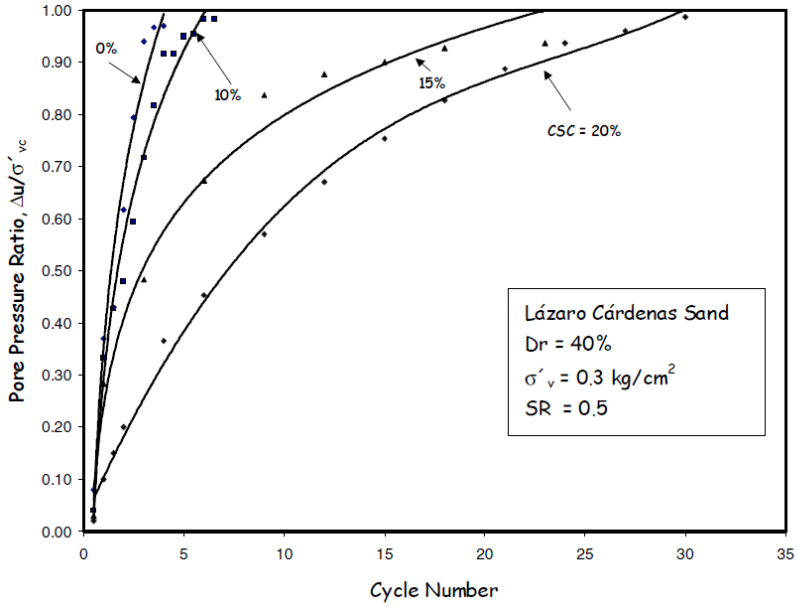

Figure 3.9: *Pore pressure ratio against number of cycles for colloidal silica treated and untreated materials after cyclic simple shear tests (from Díaz-Rodríguez and Antonio-Izarraras, 2004).*

top of the samples. Four weeks curing time was waited before tests were carried out. Both drained and undrained torsional shear tests under monotonic loading conditions were performed; undrained torsional shear tests were also carried out under cyclic loading conditions. They showed that treated specimens had a higher liquefaction resistance than untreated ones, as shown in Figure 3.10a (on the x-axis, the number of cycles needed for DA=1% shear strain was required to account for the reduced development of strain in grouted sand). Figure 3.10b shows the stress path followed by a treated sample in the mean effective-shear stress plane: the instability condition (i.e. zero effective stress) was not achieved (i.e. no collapse).

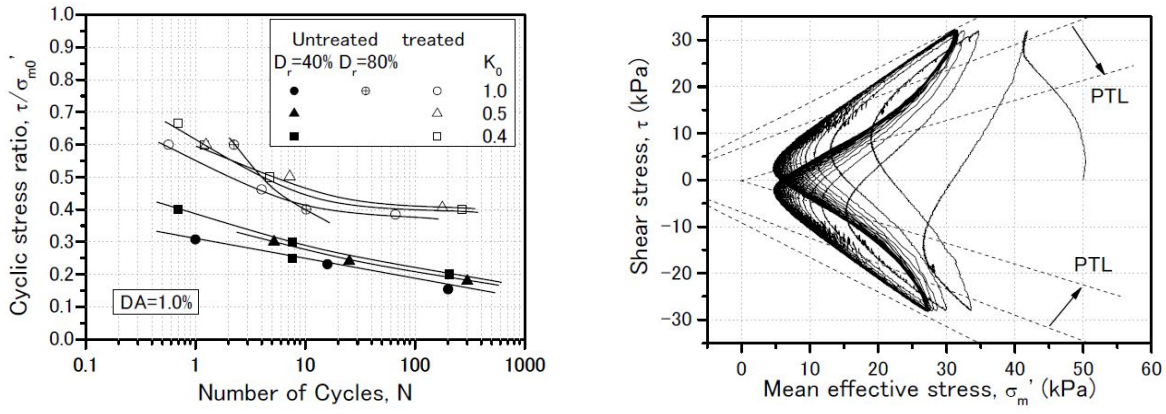

(a) (b)

Figure 3.10: *Cyclic resistance curves for CS treated and untreated materials (a); stress path exhibited by a treated sample (b) (from Kodaka et al., 2005).*

A centrifuge model test was used by Gallagher et al. (2007b) to evaluate the liquefaction resistance and deformation characteristics of liquefiable loose Nevada No. 120 sand treated with

6% by weight CS solution; gel time was set in 56h. Two shaking events were applied (uniform peak acceleration of 0.20 and 0.25**g**), but liquefaction did not occur during either shaking; 0.3% and less than 0.1% vertical strain were measured at the center of the model during the first and second test, respectively. These values are about up to 25 times less than those recorded by Taboada (1995) for untreated sand in a similar centrifuge test. Conlee et al. (2012) also performed centrifuge tests to evaluate the dynamic response of sands treated with 4, 5 and 9% CS by weight; a significant reduction of induced deformation for colloidal silica grouted sand was shown if compared to that of the untreated material. Pamuk et al. (2007) showed that the deformation of a loose liquefiable sand compared to that of a CS treated one (5% by weight) was significantly higher after centrifuge model of end-bearing piles in saturated sand.

Díaz-Rodríguez et al. (2008) performed cyclic simple shear tests on a natural silty sand treated with colloidal silica mixture to evaluate the liquefaction resistance of the grouted material. CS contents up to 14.5% by weight were used for the treatments. Firstly, the Authors evaluated the effects of initial relative density and effective vertical stress on cyclic shear resistance of the untreated sand. Then, cyclic simple shear tests were carried on treated material after a 7d curing time. A calcium chloride solution was added to the CS diluted solution to speed up gelling of the grout. A sinusoidal load was applied with a frequency of 1 Hz. Pore pressure response was not measured directly during the tests, but it was inferred from the measurements of vertical stresses changes needed to keep constant the specimens' height, and liquefaction was defined in terms of double amplitude shear strain achieved during the tests. Treated and untreated samples were reconstituted at two different D_r (40 and 60%); the liquefaction resistance curves of the treated and untreated material were determined and compared. Figure 3.11 shows the results from tests performed at $D_r = 40\%$. It can be observed that, for a given value of initial vertical effective stress, D_r, and cyclic shear stress, liquefaction was triggered after more loading cycles for treated than for untreated material.

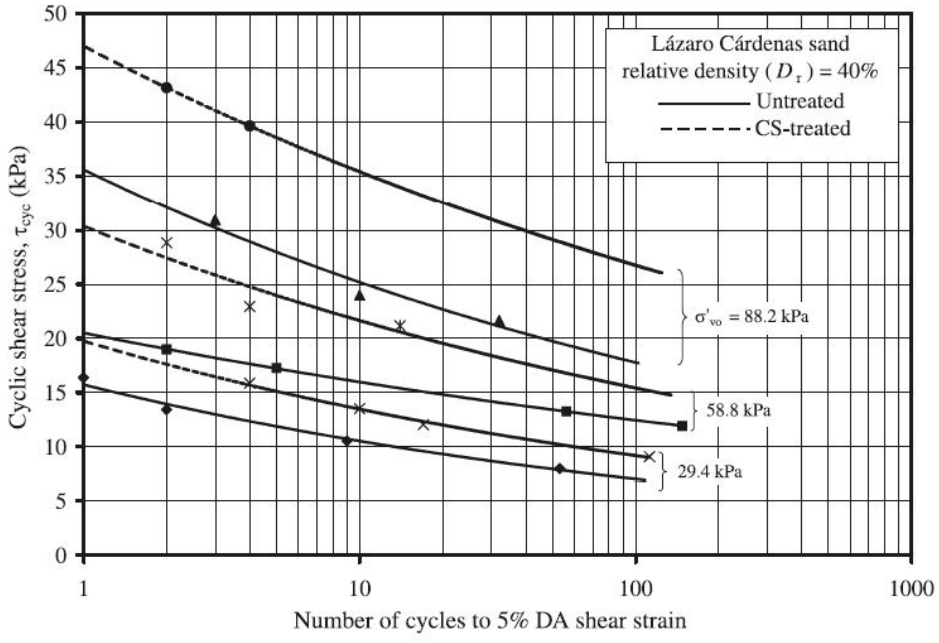

Figure 3.11: *Cyclic resistance curves for treated and untreated sand at $D_r = 40\%$ (from Díaz-Rodríguez et al., 2008).*

Fig. 3.12a shows the results reported by the same Authors in terms of pore pressure response of the treated material for different initial CS contents. A significant increase in the number of cycles required to initiate liquefaction is detected for contents higher than 7.25%, while for the latter value this effect was less evident; the same tendency was recognized for shear strain, that was significantly reduced for CS increasing from 7.25% to 10.8% (Fig. 3.12b). A clear improve in liquefaction resistance of the treated material was anyway shown. The benefits of the CS silica treatment were mainly imputed to an artificial cohesion the gel provided the sand particles with, for a given initial state. CS gel acts as a binder among grains, and it also helps in developing less pore pressure excess.

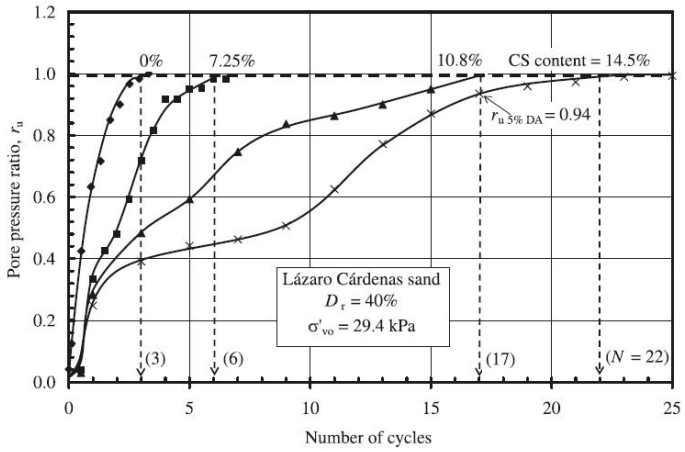

(a)

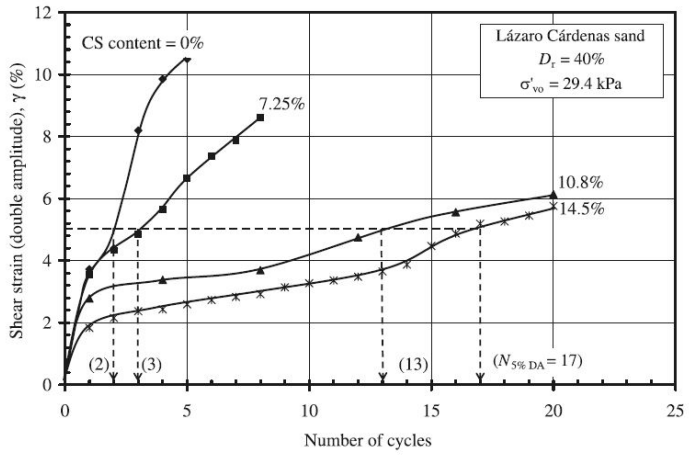

(b)

Figure 3.12: *Pore pressure (a) and shear strain (b) response for treated and untreated material (from Díaz-Rodríguez et al., 2008).*

The effects of colloidal silica grouting were also studied for sands subjected to low up to medium cyclic shear strain by means of resonant column tests (Spencer et al., 2007, 2008); the behavior of untreated sand was taken as the reference for comparison. In particular, the effects of silica content, age and cyclic shear were studied for treated loose Nevada No. 120 sand. Sand specimens (71 mm diameter and 142 mm height) were air pluviated directly into the resonant column device and manufactured at a target of 50% relative density. The resonant column ap-

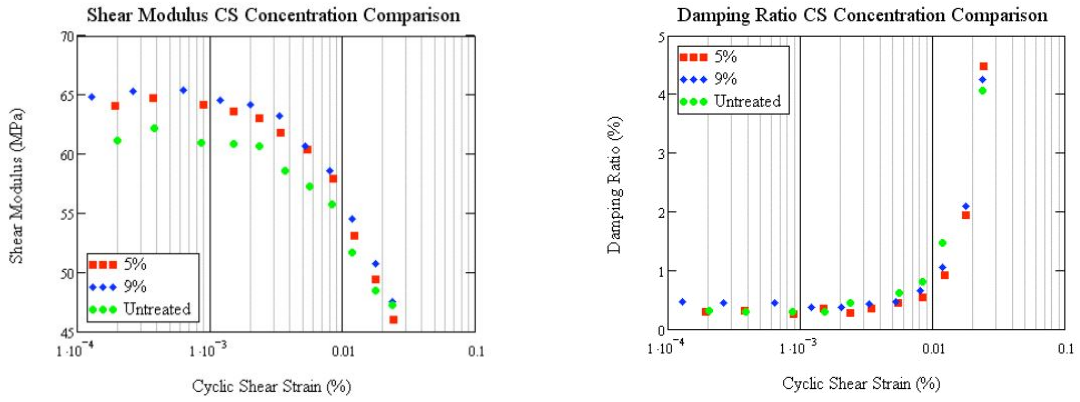

(a) (b)

Figure 3.13: *Shear modulus (a) and damping ratio (b) for treated and untreated sand from resonant column tests (from Spencer et al., 2008).*

paratus was modified to allow samples manufacturing and permeation of colloidal silica grout directly inside the device chamber. Different CS contents were chosen for tests, 5, 7 and 9% by weight. Only the results for 5 and 9% CS treated sand are shown in the paper. A salt solution was used to adjust gel time in 2-3h; 10 times the gel time was chosen as curing time before testing. At small strain levels, only a slight increase in shear modulus was recognized for treated samples if compared to that of untreated ones; besides, the effect of silica treatment on damping ratio was negligible over the whole strain range. These results are shown in Figure 3.13a and 3.13b, respectively, where data represent the average of multiple tests for each CS content used. Similar results were obtained by Conlee et al. (2012), which revealed a slightly increase of shear modulus, measured by means of the shear wave velocity, V_s, by means of bender elements test. Therefore, it could be concluded that the major effects of colloidal silica treatment can be evidenced if large cyclic shear strains (e.g. liquefaction) are expected. Batilas et al. (2018) performed resonant column tests on clean and silty sands treated with colloidal silica grouts (6 and 10% CS by w.). Figure 3.14 shows the results of resonant column tests on clean sand treated with 10% CS solution at different confining pressures. The tests revealed that, for a given density, confining pressure and low strain level, colloidal silica grouting increased the shear modulus of the material and its damping ratio.

Porcino et al. (2011, 2012) carried out an experimental campaign on a silicate-grouted sand. An overall analysis of the mechanical properties of treated and untreated sand was made. 10% by weight silica content grouts were used in these studies. Unconfined compression strength tests, undrained monotonic simple shear tests, undrained cyclic simple shear and triaxial tests, permeability tests, and drained triaxial monotonic compression tests were performed. For triaxial testing, specimens were prepared outside the triaxial chamber by using a dedicated device, and they were then saturated by applying a back pressure equal to 300 kPa.

The microscopic investigations performed by these Authors showed that the colloidal silica treatment provides the soil with an artificial cohesion (Fig. 3.15). The undrained cyclic response of treated material under triaxial loading conditions was significantly different from that of the untreated one: given a similar CSR, the treated specimens experienced low strain

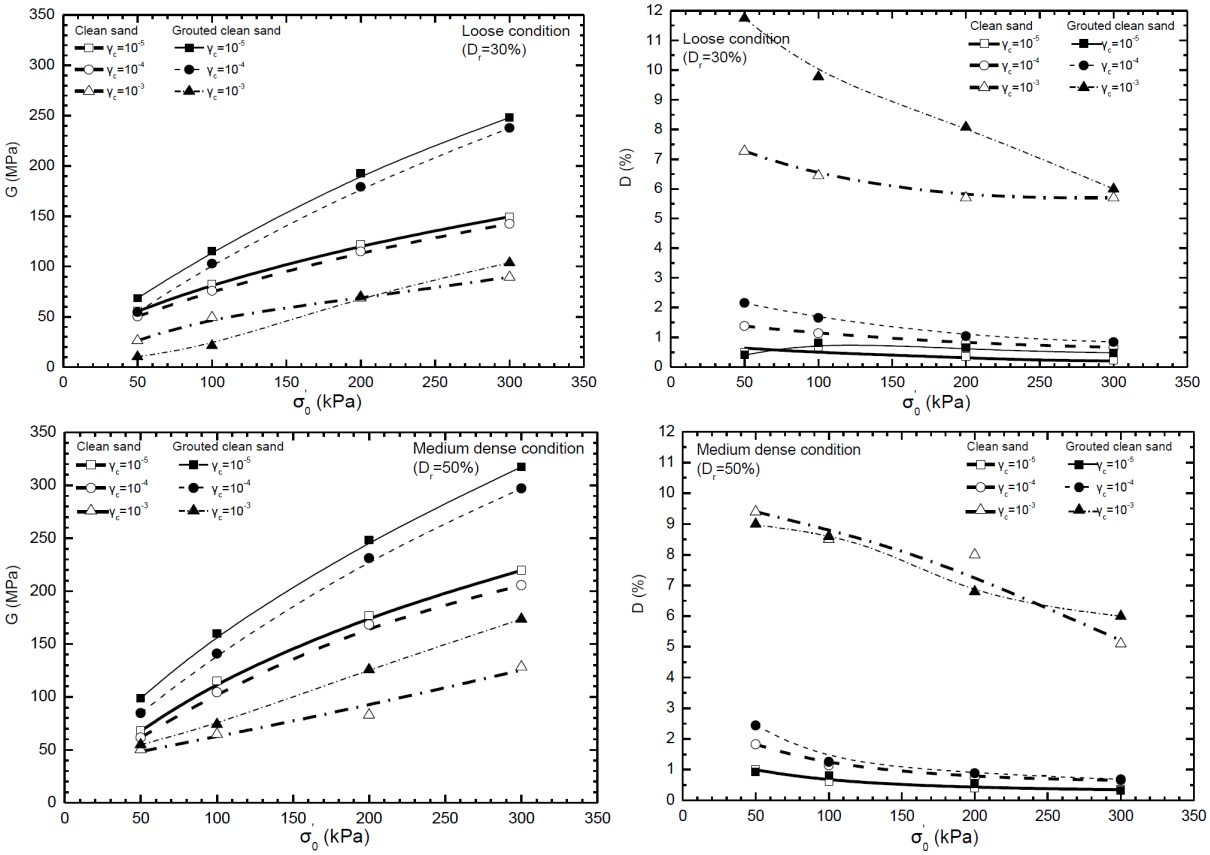

Figure 3.14: *Results of resonant column tests on a 10% CS grouted clean sand. Clockwise: shear modulus, damping ratio for loose sand, and damping ratio, shear modulus for dense sand (from Batilas et al., 2018).*

during loading, and the pore pressure ratio r_u didn't reach 1.0 value. Similar results were obtained from undrained simple shear tests. Figure 3.16 shows the liquefaction resistance curves of treated and untreated material; the liquefaction resistance of treated material was significantly higher than that of untreated one. Regarding the pore pressure response, the Authors concluded that the prediction models commonly used for cohesionless soils didn't work satisfactory with weakly cemented materials. The effect of CS treatment was equivalent to the effect of densification: dense untreated samples had liquefaction resistance similar to that of loose treated ones. According to Porcino et al. (2012), the liquefaction resistance in cyclic simple shear tests of a D_r=45% sand was similar to that of a dense sand (D_r=75%).

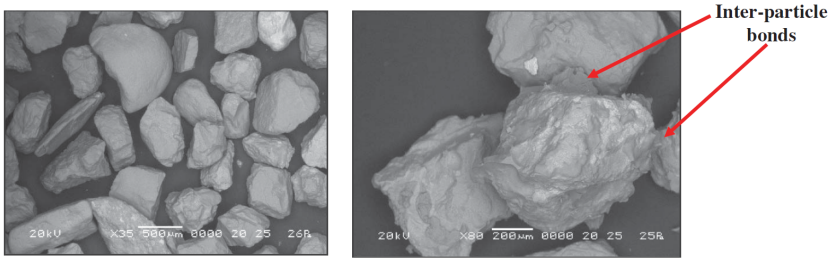

Figure 3.15: *E-SEM pictures of untreated (left) and CS treated sand (right) (from Porcino et al., 2011).*

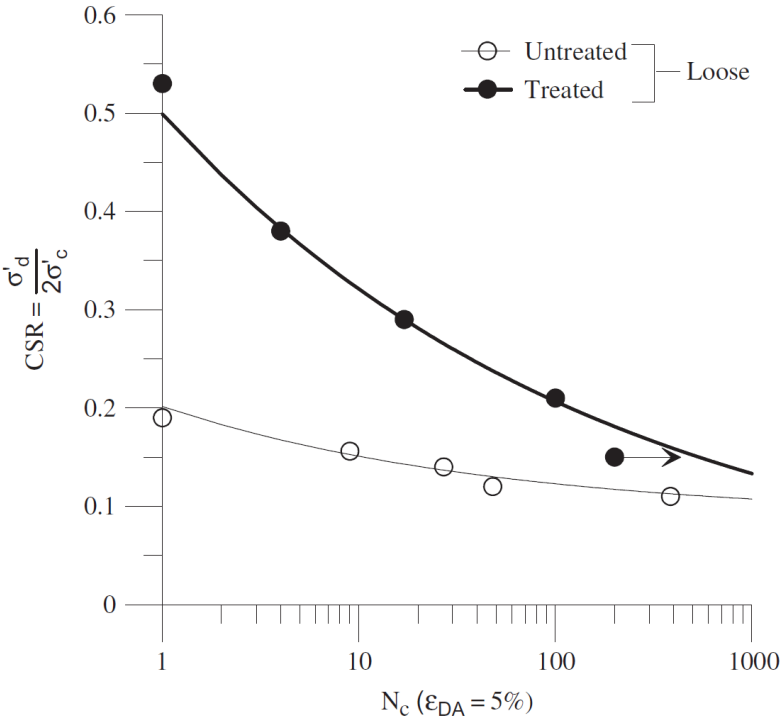

Figure 3.16: *Liquefaction resistance curves of loose treated and untreated material after cyclic triaxial tests (from Porcino et al., 2011).*

Vranna and Tika (2015) presented the results of an experimental laboratory campaign on a silty-sand (with non-plastic fines content) treated with colloidal silica. Monotonic undrained triaxial tests were performed on samples treated with 6% and 10% CS content grouts. Specimens were prepared by using the undercompaction method (Ladd, 1978), and a procedure

was set up to let the treatment solution permeate the material from the bottom to the top of the samples. The complete refill of voids by the grout was assumed once four times the volume of the specimens was collected from the upper outlet. Similarly to Porcino et al. (2012), the results pointed out that the main improvement was in terms of cohesion, due to the presence of gel bonds between the sand grains. Cyclic triaxial tests results showed that the higher the CS content, the higher the liquefaction resistance (herein defined in terms of double amplitude axial strain)(Fig. 3.17). After cyclic loading, monotonic tests were carried out by the Authors to investigate the possible occurrence of bonds breakage. The initial stiffness of the cyclically tested sand was lower than that of the treated sand under monotonic loading condition, but the peak shear resistance was still comparable; therefore, no degradation of shear resistance was observed after cyclic loading. Therefore, no significant deterioration of the attained improvement resulted. Mollamahmutoglu and Yilmaz (2010) found that the loss of unconfined compression strength in CS treated sand samples that were previously cyclically sheared was only ≈10%.

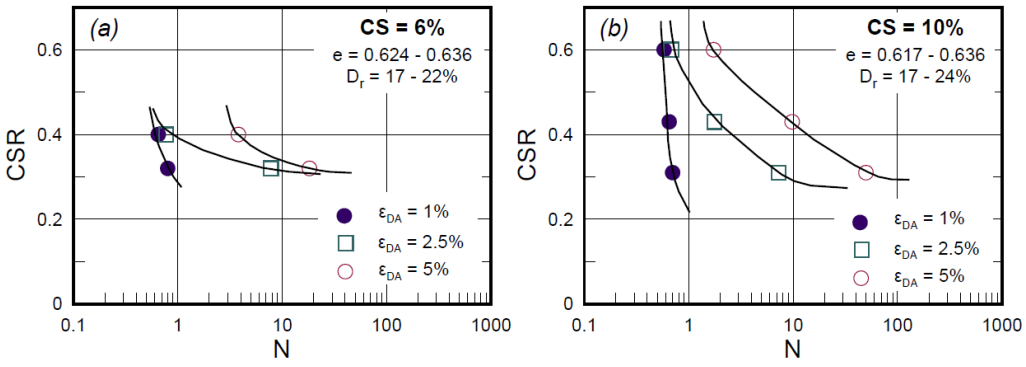

Figure 3.17: *Cyclic resistance curves of loose silty-sand (fines content = 10%) treated with 6% (a) and 10% (b) colloidal silica solutions after cyclic triaxial tests (from Vranna and Tika, 2015).*

3.3.2 Mechanical behavior under static loading conditions

The mechanical properties of colloidal silica treated sands under static loading conditions have been investigated by some Researchers by using different laboratory tests. Defining the curing time, or age, as the time between the formation of the gel and the time when a given laboratory test is performed, it has been observed that the *strength* of the gelled sand matrix increases as curing time increases.

Unconfined compression tests have been performed on CS treated and untreated material over the past years. Yonekura and Miwa (1993) discovered that the unconfined compression strength (UCS) of treated samples was still increasing after 3 years. Persoff et al. (1999); Gallagher and Mitchell (2002); Mollamahmutoglu and Yilmaz (2010) pointed out that UCS increased as CS content and curing time increased. Recently, Georgiannou et al. (2017) found that unconfined shear strength of colloidal silica treated samples with 10% silica concentration slightly increased (about 15% more) with increasing curing time (Fig. 3.18).

According to Persoff et al. (1999), the unconfined compression strength of material treated

with 10-20% CS increased proportionally with the concentration of silica particles. Gallagher and Mitchell (2002) confirmed that UCS of treated samples increased with increasing the percentage of CS (5 up to 20%); moreover, they performed unconfined compression tests on treated samples that were previously tested under cyclic loading condition, showing that the residual UCS was a function of the strain developed during cyclic tests; the higher the experienced strain, the higher the UCS degradation. This suggested that cyclic loading weakened the specimens by breaking only some of the bonds among sand grains. Moradi and Seyedi (2015) found that the UCS of a stabilized silty sand developed with samples age. By summarizing, literature data agree that bonds among the grains are stronger as CS content and/or curing time increase, and that they can be subjected to repeated load without significant strength degradation.

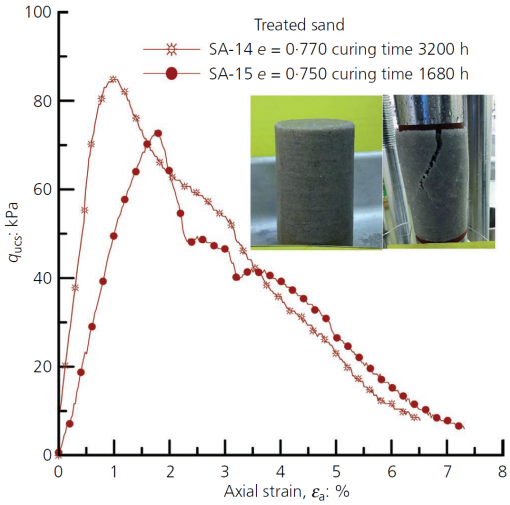

Figure 3.18: *Unconfined compression tests on grouted sand (from Georgiannou et al., 2017).*

Porcino et al. (2011, 2012) found that treated specimens showed more dilation and higher peak stress ratio than untreated ones, both from undrained monotonic simple shear and drained triaxial compression tests. Figure 3.19 illustrates the results obtained from drained triaxial compression tests: dilation of treated samples was significantly enhanced. Moreover, the treatment was found to provide the sand with cohesion, since the failure envelope for treated material, detected from drained triaxial tests and defined in terms of the maximum mobilized stress ratio with a Mohr-Coulomb strength criterion, was parallel to that of the untreated sand, but upward shifted (Fig. 3.20). Thus, the peak friction angle seemed less affected by the presence of gel.

Georgiannou et al. (2017) conducted a large experimental laboratory campaign on CS treated and untreated sand subjected to direct shear, triaxial and unconfined compression strength tests. Only triaxial drained tests are presented in their paper for comparison with the results from direct shear tests. Hydrochloric acid and a salt solution were used to adjust the gel time of a 10% CS by weight grout used for the treatment; gel time was set in 10h. Samples were then cured for several hours before they were tested. Treated specimens were reconstituted by wet deposition of dry sand into the grout solution: D_r of untreated sand ranged from ≈37% to ≈93% and for treated sand from ≈22% to ≈68%. The behavior of treated loose sand under direct shear was comparable to that of untreated dense sand. It was moreover observed that

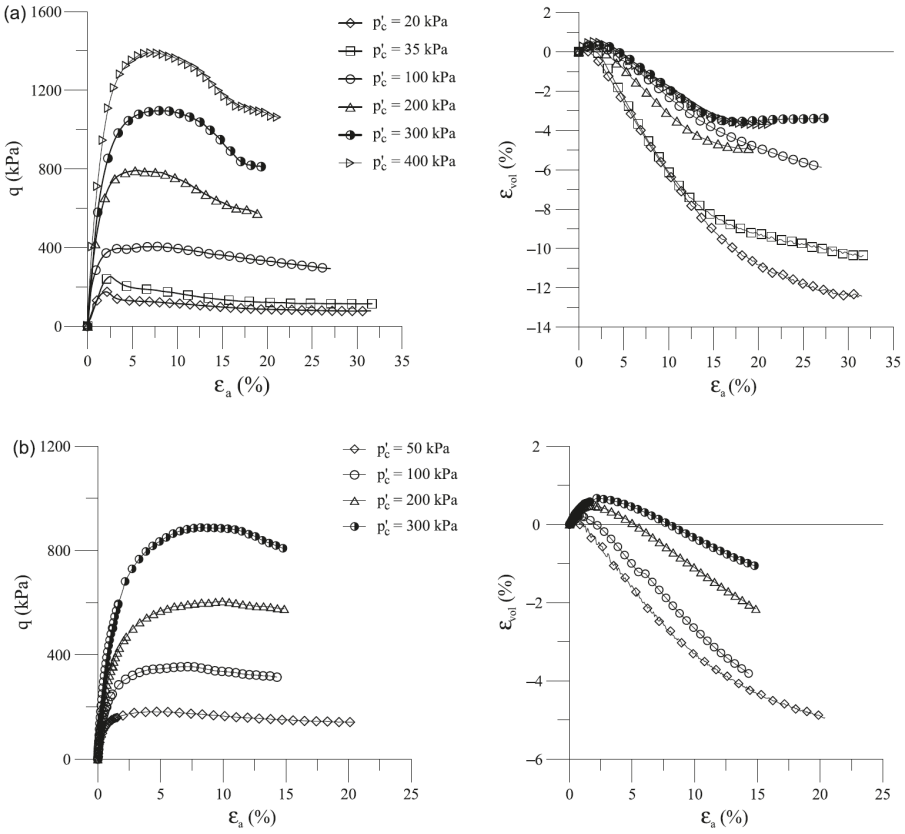

Figure 3.19: *Results of drained triaxial tests on treated (a) and untreated material (b) (from Porcino et al., 2012).*

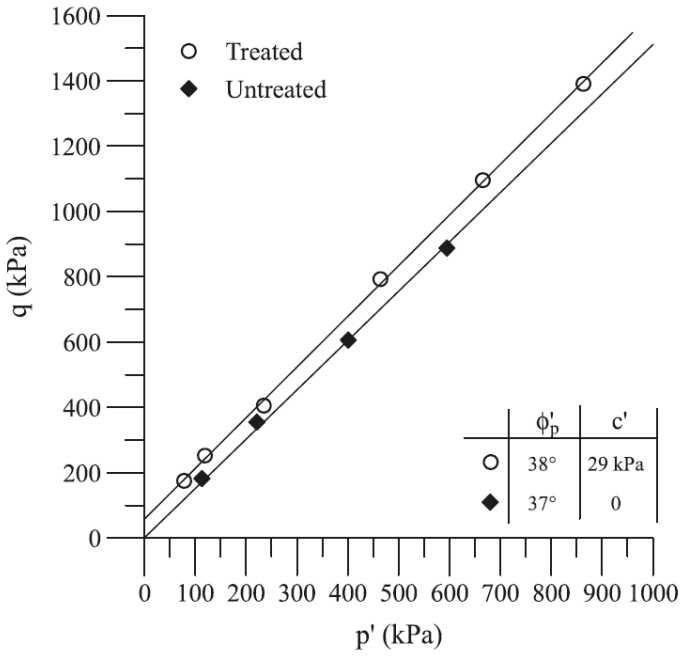

Figure 3.20: *Shear strength envelopes for treated and untreated sand in the deviatoric-mean effective stress plane after drained triaxial compression tests (from Porcino et al., 2012).*

under anisotropic loading, stabilized sample showed enhanced compressibility if compared to that of the untreated one under 1D-compression tests, as shown in Figure 3.21, where normal compression tests on treated and untreated material subjected to isotropic and 1D loading are reported. Therefore, it seems that CS gel can facilitate the grains rearrangement under anisotropic loading condition.

Nouri Delavar and Noorzad (2017) performed drained monotonic triaxial tests on a silty sand grouted (as low) with 5% CS by weight. Medium dense treated samples ($D_r = 40\%$) were tested after three days of curing under monotonic loading condition; saturation of the specimens was not performed via back-pressurization, but they were kept under water under a suction of 800 kPa for two days to remove entrapped air. The specimen preparation method (tamping), in fact, did not ensure that all voids were filled with gel. The Authors found that the soil cohesion increased as CS content increased for all the fine contents investigated, thus revealing that the main improvement could be ascribed to the cohesion.

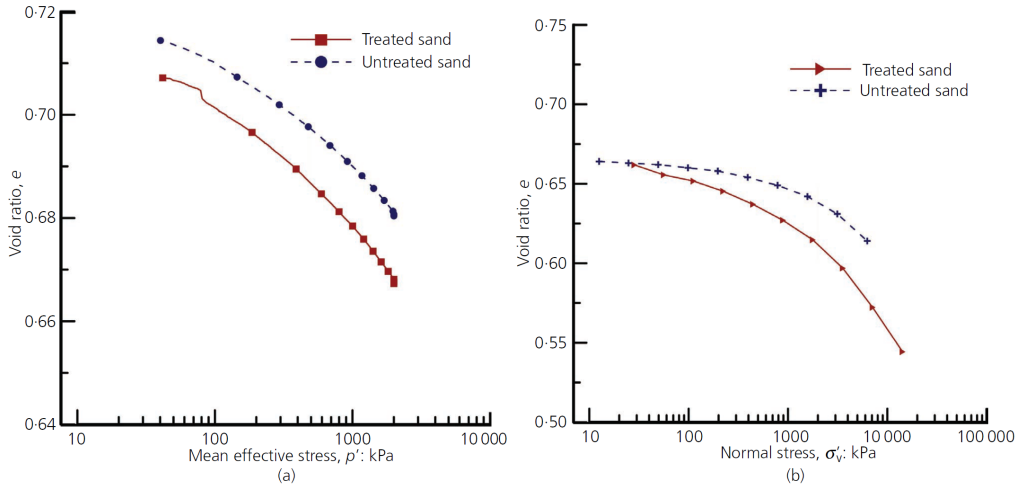

Figure 3.21: *Normal compression tests: isotropic (left) and mono-dimensional (right) compression (from Georgiannou et al., 2017).*

Wong et al. (2018) showed that the the drained peak shear strength of CS treated samples was higher than that of untreated one. Figure 3.22 shows the results of drained direct shear tests on treated and untreated sand. Treated specimens showed more dilation than that of the untreated one; furthermore, peak resistance and dilation increased as curing time increased. Very high colloidal silica content (34% by weight) was used for samples treatment.

3.3.3 Colloidal silica transport through porous media

Once the potential use of CS grout for liquefaction mitigation was demonstrated, a key issue for practical application is the permeation mechanism of such mixtures to liquefaction-prone areas. Some Authors focused on this aspect, performing laboratory experiments on physical models. Gallagher and Finsterle (2004) developed a box model to investigate the transportation of colloidal silica grout through a potentially liquefiable soil layer by means of injection and extraction wells using a low hydraulic head (0.02) (Fig. 3.23). The model consisted of a 20 cm thick layer of loose sand pluviated into a box (76x30 cm, 26.5 cm height) to obtain a

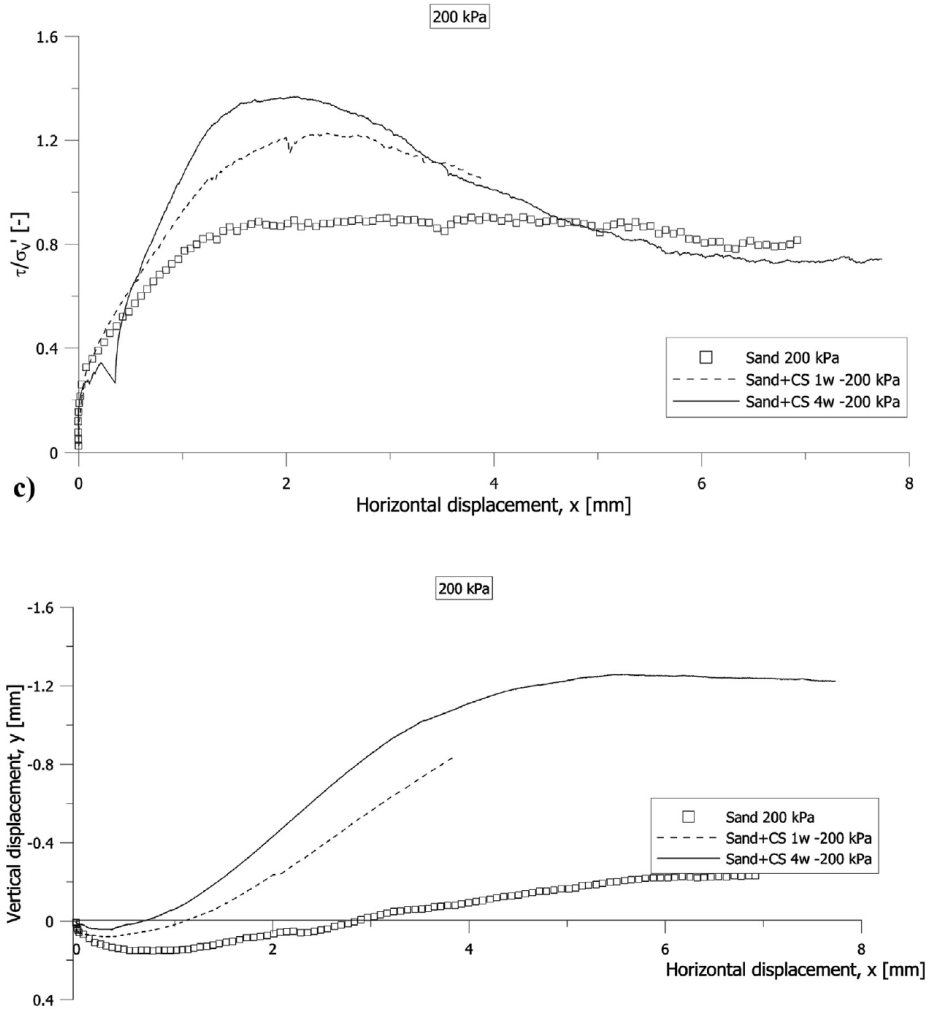

Figure 3.22: *Results of drained direct shear tests on treated and untreated sand at effective vertical confining stress of 200 kPa; 1-4w indicates 1-4week curing time (from Wong et al., 2018).*

$D_r = 40\%$; after saturation with water, a low gradient was established between injection and extraction points. Five PVC pipes were used to deliver a colloidal silica solution (5% CS by weight) within the soil layer for about 10h, while two additional pipes were used as extraction wells at the opposite side of the box. Curing time was set in 14d once the stabilizer delivery was completed. After the box was dismantled, several specimens were collected for unconfined compression strength testings: the results of these tests were consistent with other data from literature (e.g. Persoff et al., 1999; Gallagher and Mitchell, 2002). Cl^- concentration in pore water was continuously monitored during CS transportation; from this concentration, it was possible to determine the relative concentration of CS in the pore fluid, therefore it was chosen as an indicator of soil permeability and of rheological properties of the injected material. The Authors concluded that low-gradient injection and extraction wells could be successfully used for colloidal silica delivery, at least at the investigated laboratory scale. Finally, an overall reasonable agreement between experimental results and a numerical simulation on grout transportation was recognized, even if discrete aspects of the model were not always matched.

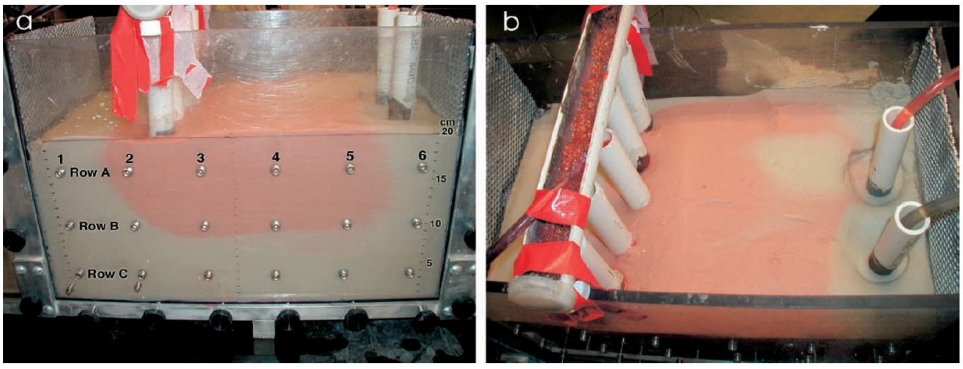

Figure 3.23: *Box model experiment for colloidal silica delivery study. (a) Side view; (b) plan view. Colloidal silica progression after 3 h; the flow is from left to right (from Gallagher and Finsterle, 2004).*

Gallagher and Lin (2005) aimed to evaluate the colloidal silica transport mechanism by means of four column tests; these tests were used to analyze the factors affecting the stabilizer delivery through the porous medium. They also performed UCS tests on treated material, revealing that the CS content they used (5% CS by weight) could sufficiently enhance the liquefaction resistance of Nevada No. 120 sand. Sand samples ($D_r = 40\%$) were prepared within each column, which was equipped with a series of sampling ports to extract fluid samples to monitor its characteristics (including Cl^- concentration and pH) along the stabilizer delivery path. Colloidal silica was supplied from the bottom to the top of the column; a good correspondence between Cl^- and CS concentrations was found, so that the former were used to estimate the silica concentration in the solution. It was noticed that the viscosity of the mixture had the greatest influence on travel time of grout through the columns; once the viscosity approached a certain value (3.6 cP in that case) the flow rate of grout delivery was greatly reduced. In a further study, Gallagher and Lin (2009) analyzed the colloidal silica grout transport mechanism in loose sand or graded silty sand specimens (0.9 m columns) tested under low hydraulic gradients (0.04, 0.09, 0.18). They showed that a 5% CS content solution can successfully permeate

the soil columns; Nevada and Ottawa sands (at a relative density of ≈40%) used in the study had initial permeability equal to 7.6×10^{-5} and 2.2×10^{-3} m/s, respectively. Furthermore, the effects of pH, ionic strength, viscosity, hydraulic gradient and hydraulic conductivity were also taken into account; UCS tests were also performed. For a viscosity value ≈4 cP, the grout movement inside the columns essentially stopped. They concluded that, for practical in field design, hydraulic gradients (i.e. injection pressures) must be chosen appropriately in accordance with the distance the grout has to cover, and by considering that the initial hydraulic conductivity of the medium decreases as the grout starts gelling within the pores. Bolisetti et al. (2009) also focused their study on the grout injection processes, confirming that the increase of viscosity highly affects the grout transportation.

Hamderi and Gallagher (2013) evaluated the injection and extraction rates and optimum wells disposal for *in situ* colloidal silica treatment by means of numerical analysis. The Authors evidenced the importance of the extraction flow rate (which depends on the initial conductivity of the target layer) for horizontal colloidal silica delivery; moreover, they found that a distance from the inlet to the outlet well between 2 and 4 m can provide a sufficient amount of improvement to the soil for the maximum simulated injection-extraction rates available. Conversely, when low injection or extraction rates were used, the problem of grout sinking could occur, suggesting the need of a proper estimation of the minimum flow rate when designing the treatment for a specific site.

More recently, Hamderi and Gallagher (2015) developed a pilot-scale facility to further investigate the transport mechanism of colloidal silica grout. Liquefiable sand was put into a large box facility and a colloidal silica grout was injected by means of several injection and extraction wells. Both low and high injection rate tests were performed. Two low rate and six high rate tests were carried out. For low rate tests, a 6% CS by weight solution was used, and it was injected and extracted at a flow rate of 65 ml/min/well (total flow rate equal to 260 ml/min) for the first test; due to sinking problems during the grout delivery, the flow rate was doubled for the second test and the relative density of the sand was increased from 22% up to 48%. During the tests, electrical conductivity cells placed into the box was used to assess the grout distribution throughout the model. For high rate tests, instead, a 9% CS by weight solution was used for one test, while for the remaining five a tracer NaCl solution was employed. At the end of the sixth high rate test with CS grout, the treated sand was left 25 days to cure before it was excavated. The injection rate for this test was set in 6800 ml/min/well (approximately 50 kPa per well). A 0.3 m deep horizontal surface was used for several pocket penetrometer tests. At last, 24 cylindrical samples were trimmed and subjected to unconfined shear strength tests. The final CS concentration, due to CS grout transport, was estimated from the measurements of electrical conductivity, and by relating pocket penetrometer and UCS measures on treated sand samples. If Gallagher and Lin (2009) confirmed that UCS could be used to indicate if sufficient improvement had been achieved in the sand, the Authors also revealed that pocket penetrometer measures can be used for the same purpose. In particular, they also evidenced that concentration of CS as low as 1% by weight may provide enough cohesion to mitigate liquefaction effects. This aspect, they said, needed further investigations. The physical model was also accompanied by a numerical simulation of each high rate test performed.

3.3.4 In field colloidal silica grouting

Groutability of soils by means of colloidal silica grout Groutability of soils is generally estimated based on grain size distribution and initial hydraulic conductivity. The grain size distribution criterion is illustrated in Figure 3.24, where the boundaries for most liquefiable soils (according to the Italian Standard NTC 2018-DM 17/01/18, for soils with uniformity coefficient lower than 3.5) are also indicated, while the hydraulic conductivity values for soil groutability are shown in Table 3.2. As can be seen, except for sandy silt, liquefiable soils can be treated with all commonly used grouts, thus with colloidal silica solutions. For instance, Gallagher and Lin (2009) showed that sand and silty-sand characterized by initial permeability in the range 2.2×10^{-3} - 4.6×10^{-5} m/s could be easily treated with a 5% CS grout.

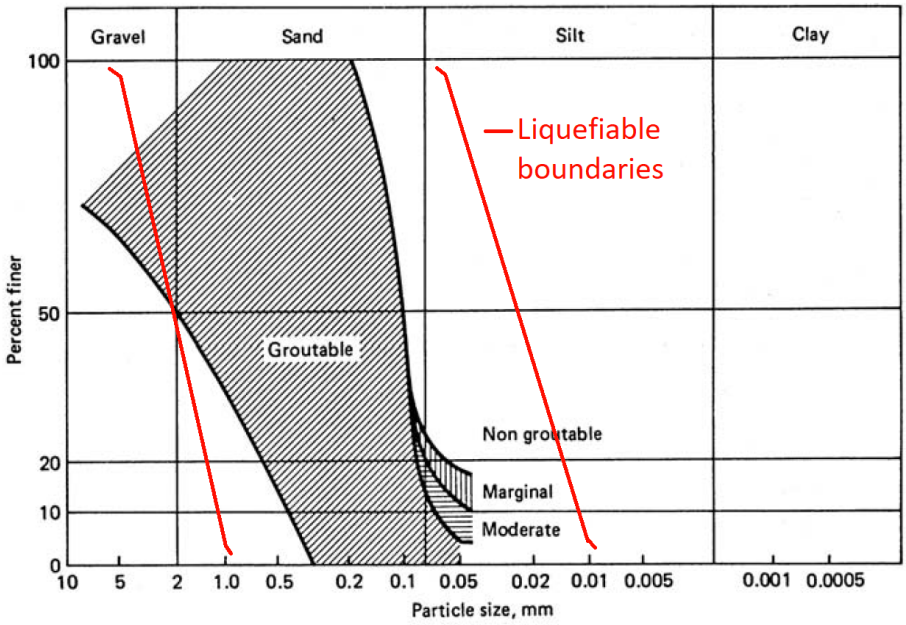

Figure 3.24: *Groutability of soils (mod. from Karol and Berardinelli, 2003).*

Table 3.2: *Ranges of hydraulic conductivity for soils groutability (mod. from Karol and Berardinelli, 2003).*

k (m/s)	Groutability of soils
10^{-8} or lower	ungroutable
$10^{-7} - 10^{-8}$	groutable with difficulty by grouts with under 5cP viscosity and ungroutable at higher viscosities
$10^{-5} - 10^{-7}$	groutable by low-viscosity grouts but with difficulty when viscosity is more than 10 cP
$10^{-3} - 10^{-5}$	groutable with all commonly used chemical grouts
10^{-3} or higher	use suspended solids grout or chemical grout with a filler

***In situ* tests** The site test performed by Gallagher et al. (2007a) and described below represents the first full-scale application of the passive site stabilization concepts for liquefaction mitigation by colloidal silica grouting. More recently, Rasouli et al. (2016) demonstrated that a

controlled permeation grouting method can be used to inject colloidal silica grout under existing infrastructures, improving the liquefiable resistance of sand deposits. Few other applications are reported in scientific literature, which are mainly related to the use of colloidal silica to form impervious barrier to prevent the flow of contaminants. For instance, Moridis et al. (1996) aimed to reduce the grouted soil permeability to impede contaminants flow and to have control on groundwater flow; a 30% by weight colloidal silica solution was injected into a heterogeneous gravel-sand-silt deposit by means of two injection wells at depths of 3.0, 3.6 and 4.2 m. Upon excavation, it was revealed that soil was uniformly grouted and that a ≈3 m height grouted sand column could be excavated. Noll et al. (1993) was able to treat a 5 m diameter zone (≈3 m thick) with a 5% CS solution by means of a central injection well and radially disposed extraction wells, to demonstrate the ability of CS grout to prevent contaminant flow.

Concerning the use of colloidal silica grouting to reduce the seismic liquefaction hazard, Gallagher et al. (2007a) performed a field test on a 2 m thick sand layer treated with 7% CS solution; grouting was followed by a blast-test to evaluate the improvement at the target site by comparing the pore pressure response and settlements in treated area with those recorded in an adjacent untreated one. The setup of full-scale field test is illustrated in Figure 3.25. Eight injection wells, disposed radially on a circular zone of 9 m diameter, were used to pump the grout into the subsoil, and one extraction well was equipped with a submersible pump in the center of the improved area to direct the grout flow toward the inner of the circle. The characteristics of the improved site and of the grout injection are summarized in Table 3.3; low injection pressures were used for grout delivery, according to the concept of a non-disruptive mitigation technique. After grouting, the injection wells were equipped with explosive charges at depth to induce liquefaction in the treated area and in the adjacent untreated one. Based on the pore pressure analysis, the treated area liquefied ($\Delta u / \sigma'_0$ recordings, being σ'_0 the vertical effective stress at the depth of the installed pressure transducers, ranged from 0.93 to 1.04 immediately after blasting); in terms of induced settlements, instead, no large deformations were exhibited in the treated zone, suggesting that the CS treatment had significantly improved the deformation resistance of the sand layer. Moreover, typical deformations connected to flow liquefaction (e.g. sand boils) were not observed throughout the whole treated area. In an adjacent untreated test pile area (Fig. 3.26) maximum settlements of 0.5 m were recorded, while maximum values in the treated area were ≈0.3 m. Further field investigations by means of Cone Penetration Test and V_s profiles did not reveal these tests to be good indicators of the effectiveness of the *in situ* treatment, suggesting the need of other kinds of measurements to monitor the success of the treatment. The Authors concluded that, even if liquefaction occurred in the treated layer according to the pore water pressure criterion, the minor settlements clearly indicated the increased stiffness of the grouted site.

Rasouli et al. (2016) presented a detailed report on the application of *controlled permeation grouting* used to improve by colloidal silica grouting liquefiable areas under the Fukuoka Airport (JP). In their study, a controlled curve drilling machine was developed and used to inject the stabilizing grout point by point by an injection hose inserted in the borehole, as schematically shown in Figure 3.27. Two different areas of the Fukuoka Airport, named A and B, needed to be improved, where underground structures already existed (i.e. a drainage pipe

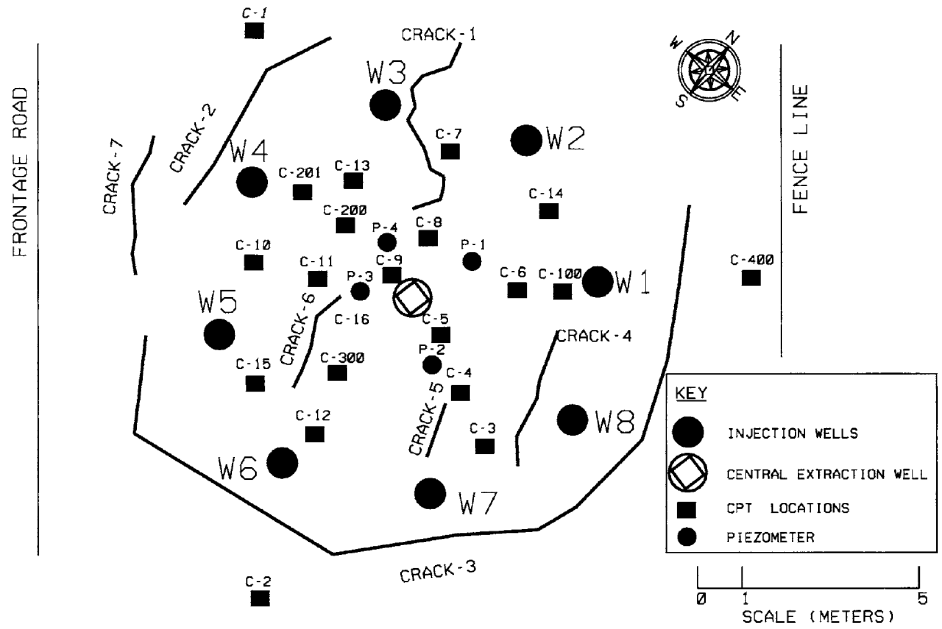

Figure 3.25: *Setup of treated area in the full-scale CS grouting field test (from Gallagher et al., 2007a).*

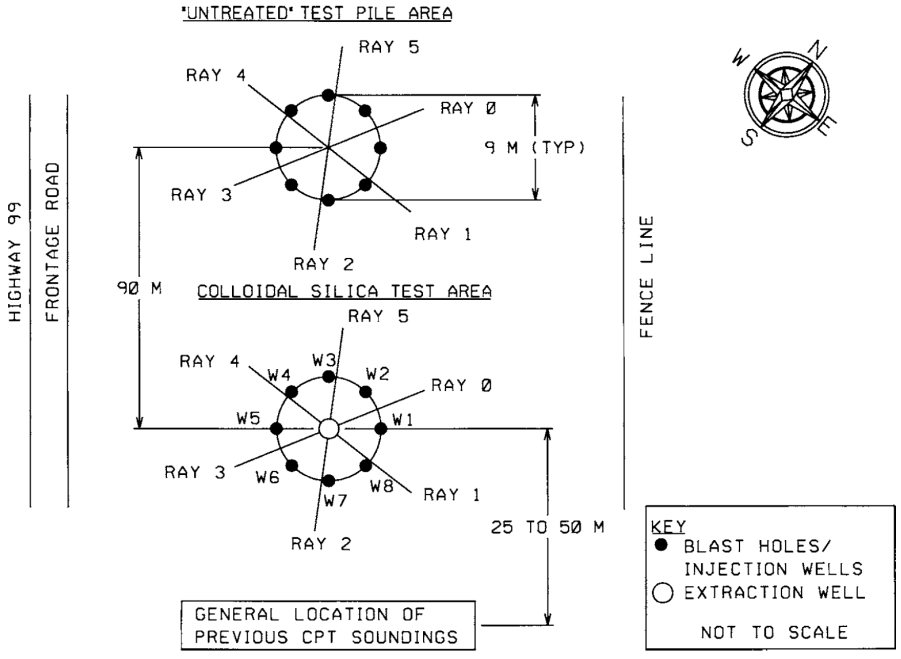

Figure 3.26: *Setup of the testing area in the full-scale CS grouting field experiment (from Gallagher et al., 2007a).*

Table 3.3: *Characteristics of full-scale colloidal silica grouting test (from Gallagher et al., 2007a).*

Liquefiable untreated layer characteristics	
Thickness (m)	≈10
Position (m below ground surface)	≈5
Soil classification (USCS)	SP or SP-SM
Groundwater level (m below ground surface)	≈2.5 (2.8-3.4 due to tidal fluctuations)
Relative density (%)	40-45
Hydraulic conductivity (m/s)	8×10^{-5} (4 m depth)-5×10^{-4} (11.5 m depth)
V_s (top/bottom) (m/s)	130/180
Liquefiable treated layer characteristics	
Thickness (m)	2
Position (m below ground surface)	≈6.5
Grouting method characteristics	
Grout composition	CS, fresh water, NaCl
Grout CS content (% by weight)	7
Grout gel time (min)	90
Grouting method	injections from boreholes
Grout injection method	Tube-a-manchette (7.6 cm diameter); 2 stage bottom-up process (from 8.5-7.5, 7.5-6.5 m)
Target injection rate (L/min)	13
Grouting pressures (kPa)	75-150 (175 spikes occasionally)
Number of injection boreholes	8
Drilling depth of injection boreholes (m)	10
Number of extraction boreholes	1
Drilling depth of extraction borehole (m)	11
Boreholes disposition	Radially around extraction borehole
Radius between injection and extraction boreholes (m)	4.5
Blast test characteristics	
Blast holes	corresponding to injection boreholes
Explosives depth (m below ground surface)	6.4, 8.5
Detonations	from bottom to top, 1 s delayed

and common ducts susceptible of lifting during earthquakes). These two areas are illustrated in Figure 3.28; in particular, zone A (Fig. 3.28) corresponds to the runway, so that vertical boring could not be possible to maintain its full operation during the treatment. The controlled curved drilling machine was used for this reason in zone A. Both zones A and B consist of shallow liquefiable sands with 10.5% (zone A) and 9.9% (zone B) fine contents; based on SPT results, the sand layers were very loose. A colloidal silica grout was used for the improvement of both areas: 8% by weight silica was used in the stabilizing mixture. The results of an experimental campaign performed on reconstituted sand samples were used to select the proper silica content. Finally, the success of the treatment was evaluated and it was proven that the proposed controlled permeation grouting technique could be satisfactory used to improve the liquefiable soil under existing infrastructures. An injection hose was used to deliver the grout and to produce point by point improvement (Fig. 3.29); technical details of the grouting procedure are listed in Table 3.4. The most innovative aspect emerging from the study of Rasouli et al. (2016) is the use of the curve drilling machine that allowed ground improvement while the airport was continuously operating (zone A, Fig. 3.28). Controlled permeation grouting therefore is an effective method to deliver silica grout under existing structures and it can solve some of the main problems (e.g. treatment homogeneity, need of long gel times to ensure grout transportation, grout dilution and sinking during its delivery) indicated in previous studies (e.g. Gallagher et al., 2007a; Hamderi and Gallagher, 2015).

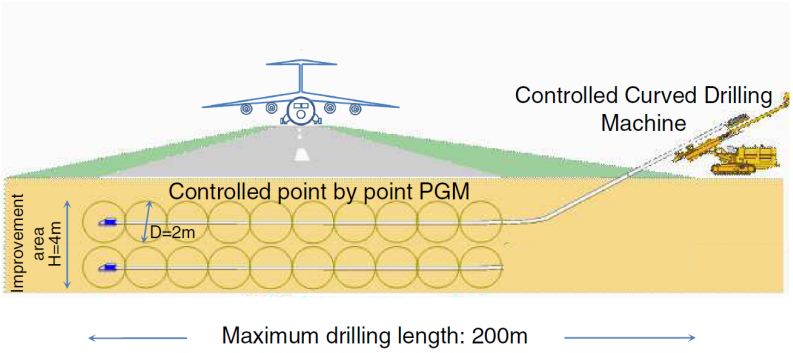

Figure 3.27: *Schematic concept of controlled point by point permeation grouting to improve a target area under existing facilities (from Rasouli et al., 2016).*

Table 3.4: *Characteristics of controlled permeation grouting at Fukuoka Airport (from Rasouli et al., 2016).*

Grouting method characteristics	
Grout CS content (% by weight)	8
Grout gel time (min)	240
Grouting method	controlled permeation grouting
Grout injection method	injection hose within the hollow drilling case
Injection rate (L/min)	12
Grouting pressures (kPa)	300-500
Diameter of improved area at injection point (m)	≈2.4

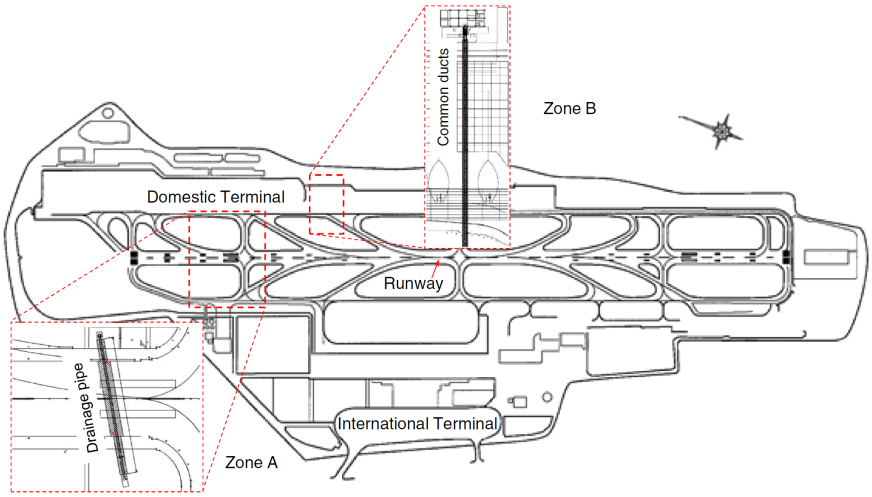

Figure 3.28: *Improved areas at Fukuoka Airport (from Rasouli et al., 2016).*

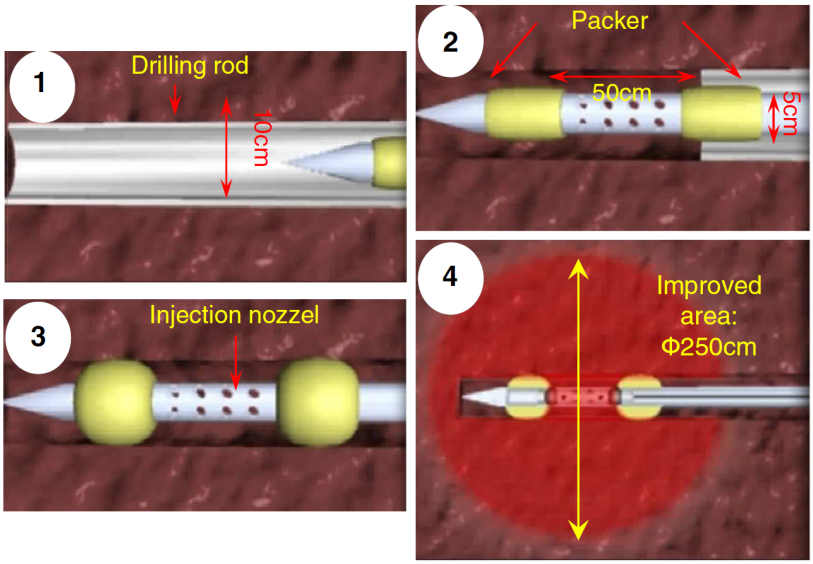

Figure 3.29: *Chronological sequence of the injection procedure by means of an injection nozzle in controlled permeation grouting (from Rasouli et al., 2016).*

3.3.5 Hydraulic conductivity

Due to colloidal silica grouting, the hydraulic conductivity of treated soil is expected to decrease. Persoff et al. (1999) evaluated the hydraulic conductivity of grouted samples by means of a falling head permeameter, under a confining pressure of 207 kPa and with hydraulic gradients varying between 23 and 37 and between 4 and 5, depending on the samples hydraulic conductivity. The specimens were prepared by mixing soil mass and grout in a mold: thus, grout completely filled the pore spaces and, despite being this preparation method unable to simulate an injection, it was properly chosen to maximize specimens reconstitution technique for laboratory testings. The permeability values therefore represent the minimum ones, in the (practically unattainable) case of a perfect grout injection. The results are reported in Figure 3.30 for two different tested treated material. It is shown that the hydraulic conductivity of treated samples decreases as silica content and UCS increase. A great reduction of permeability for treated samples was revealed, up to a minimum of 2×10^{-11} m/s for 27% CS treated Monterey sand.

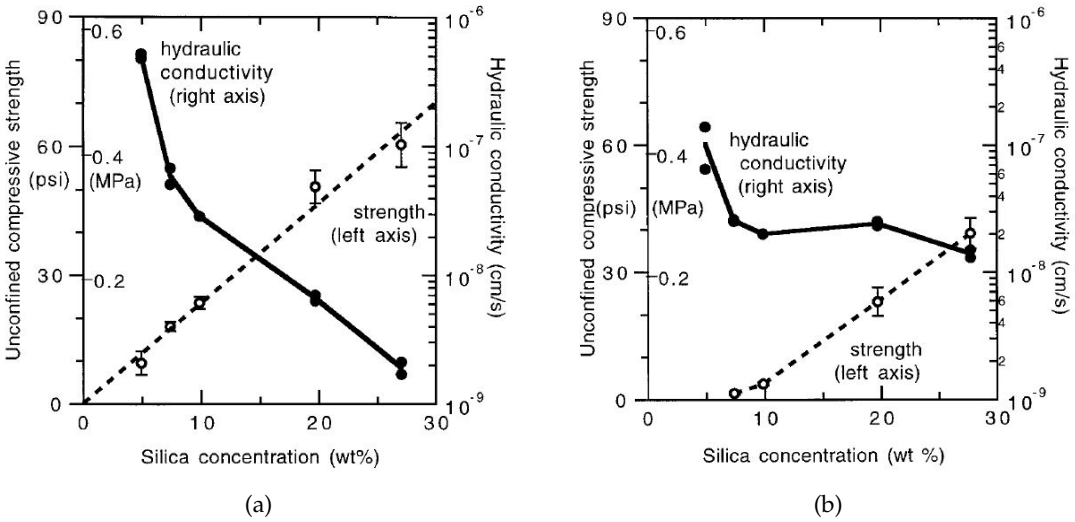

Figure 3.30: *Hydraulic conductivity and UCS for: Monterey sand (a), Trevino soil (b) (from Persoff et al., 1999).*

Porcino et al. (2012) obtained permeability values of the order of 10^{-9} m/s for samples stabilized with a silicate-based grout. Permeability was measured by means of a flow pump system; a grout flushing procedure was developed for samples treatment: low grouting pressures (≈10 kPa) were used for this purpose. Wong et al. (2018) performed a series of oedometer tests on pure colloidal silica and on colloidal silica treated sand samples. On the basis of the consolidation times during oedometer tests on treated material they estimated a hydraulic conductivity of treated samples similar to that of clay (of the order of 10^{-10} m/s).

By summarizing, the magnitude of the treated material hydraulic conductivity depends on the CS content and it is significantly lower than that of the untreated one. The reduced permeability is ascribed to the nature of the gel: the latter consists of silica chains that form a micro-porous network through which water can flow (Iler, 1979). The magnitude of gel microporosity (pore amount and size) is related to the amount and spatial distribution of silica chains,

thus, to the silica content. Table 3.5 summarizes the effects of colloidal silica treatment on the permeability of soil as reported in the aforementioned studies.

Table 3.5: *Effects of CS treatment on soil hydraulic conductivity.*

Reference	Type of material	CS (%)	k untreated (m/s)	k treated (m/s)
Persoff et al. (1999)	Monterey sand, Trevino soil	5-27	Not indicated	up to $\approx 10^{-11}$
Porcino et al. (2012)	Ticino sand	10	Not indicated	$\approx 10^{-9}$
Wong et al. (2018)	Leighton buzzard sand	34	$\approx 10^{-2}$	$\approx 10^{-9} - 10^{-10}$

3.4 Summary and conclusions from literature review

The state of the art related to the experimental studies carried out on colloidal silica in view of its application for liquefaction hazard mitigation, described in the previous Sections, is summarized in Tables 3.6 and 3.7. By means of an in-depth analysis of the scientific literature on this topic, some conclusions and shortcomings on colloidal silica grouting can be drawn as follows.

- CS is effective in improving the liquefaction resistance of liquefiable sand.
- The main contribution to the improvement is due to an artificial cohesion provided by the silica gel to the soil grains.
- The CS transportation through porous media is significantly affected by the rate of viscosity increase.
- The shear strength of the treated soil increases over time and as CS content increases.
- CS *in situ* applications are still limited, due to the need for a specific design for the site.
- CS treatment greatly reduces the hydraulic conductivity of the natural material.
- CS treated material seems to be more compressible than untreated one under anisotropic loading conditions, due to the compressibility of silica gel.
- It seems possible to further reduce the CS content in the grout, while retaining the effectiveness in improving soil liquefaction resistance.

This Thesis aims to in-depth investigate the latter point, that is if very low CS contents are effective in mitigating the liquefaction resistance of a clean sand (Hamderi and Gallagher, 2015). To this purpose, the mechanical behavior of a liquefiable material treated with low-content CS grouts is analyzed. The main characteristics and mechanical properties of soil treated with weak gel are determined both under static and cyclic loading conditions.

Table 3.6: *Summary of information regarding significant scientific contributions on colloidal silica grouting. Symbol of test types: Cf centrifuge, CSS cyclic simple shear, DS direct shear, Od oedometer, Pp pocket penetrometer, RC resonant column, SHt shaking table, SS simple shear, TS torsional shear, Tx triaxial, UCS unconfined compression strength, (U)CTx (undrained) cyclic triaxial.*

Reference	Test types	CS (% by weight)
Yonekura and Miwa (1993)	UCS	32
Persoff et al. (1999)	UCS; permeability tests; specific tests to evaluate the effects of contaminants	5-27
Towhata and Kabashima (2001)	Tx (compression and estension), cyclic Tx; SHt	4.5-6.5
Gallagher and Mitchell (2002)	UCTx; UCS	5-20
Díaz-Rodríguez and Antonio-Izarraras (2004)	CSS	10-20
Gallagher and Finsterle (2004)	Box model; UCS	5
Gallagher and Lin (2005)	Column tests (grout transport mechanism); UCS	5
Kodaka et al. (2005)	Monotonic and cyclic TS	4
Spencer et al. (2007, 2008)	RC	5-9
Gallagher et al. (2007a)	Full-scale field testing; grouting and blast-testing	7
Gallagher et al. (2007b)	Cf; box model	5-6
Pamuk et al. (2007)	Cf	5
Díaz-Rodríguez et al. (2008)	CSS	7.25-14.5

Table 3.7: *Continues from Table 3.6.*

Reference	Test types	CS (% by weight)
Gallagher and Lin (2009)	Column tests (grout transport mechanism)	5
Bolisetti et al. (2009)	Column tests (grout injection mechanism)	32
Porcino et al. (2011)	UCS; Undrained monotonic SS; CSS; UCTx	10
Conlee et al. (2012)	Cf	4-9
Porcino et al. (2012)	UCS; Drained monotonic Tx; CSS	10
Hamderi and Gallagher (2013)	10 m^3 pilot-scale facility for grout delivery study; Pp; UCS	6-9
Agapoulaki and Papadimitriou (2015)	Rheological tests (*CS only*)	5-10
Vranna and Tika (2015)	Undrained monotonic Tx; UCTx	6-10
Rasouli et al. (2016)	Application at Fukuoka Airport	8
Georgiannou et al. (2017)	DS; UCS; Drained monotonic Tx; Od	10
Nouri Delavar and Noorzad (2017)	Drained monotonic Tx	5-30
Agapoulaki and Papadimitriou (2018)	Rheological tests (*CS only*)	5-10
Batilas et al. (2018)	RC	6-10
Wong et al. (2018)	Od; DS	34

Chapter 4

Experimental testing

The laboratory experimental tests carried out within the framework of this PhD Thesis are illustrated in the present Chapter. Firstly, a description of the used materials is provided; secondly, each of the testing procedures is described in detail. Tests were performed on untreated sand and on sand treated with colloidal silica grout to show how low-content silica gel can affect properties and mechanical behavior of the soil. Cyclic and monotonic triaxial tests, direct shear tests, oedometer tests and X-ray micro-tomography tests were carried out; the results obtained from untreated material were taken as the reference for comparison of the results, which are shown and discussed in the following Chapter. The grout permeation and the hydraulic conductivity of treated and untreated sand were also evaluated. Results are compared with literature data, to provide deeper knowledge on colloidal silica grouting.

4.1 Materials

Sand The tested soil consisted of a clean, uniform, mainly siliceous sand, named *S*3 sand, which has previously been used by researchers as a reference material for laboratory testings (Modoni and Gazzellone, 2011; Chiaro et al., 2014; Salvatore et al., 2017, 2018). It was obtained by sieving a commercial sand, extracted from the Fossanova quarry (LT, Italy) and named FO-25 sand, between the sieves ♯40 (0.425 mm) and ♯80 (0.180 mm) (ASTM D422-63 and ASTM E11-09 series). Fossanova FO-25 sand mainly consists of quartz ($SiO_2 > 90\%$ by volume), with additional traces of metals. It was sieved to reduce the influence of the fine fraction and to obtain a sand with a narrow grain size distribution like those of other 'standard' liquefiable literature sands.

S3 sand can be described as a sub-rounded, low-sphericity grains sand (Fig. 4.1a); its properties are summarized in Table 4.1, where G_s is the specific gravity and U represents the uniformity coefficient. Its grain distribution is shown in Figure 4.1b, where it is compared with the boundary distributions of most liquefiable soils for $U < 3.5$, according to the Italian Standard NTC 2018-DM 17/01/2018. S3 sand is classified as SP (Unified Soil Classification System). Maximum and minimum void ratio, named e_{max} and e_{min} respectively, were calculated according to the German standard DIN 18126-71.

Table 4.1: *S3 sand characteristics.*

G_s (-)	e_{max} (-)	e_{min} (-)	D_{50} (mm)	$U = \frac{D_{60}}{D_{10}}$ (-)	USCS Classification
2.65	0.839	0.559	0.30	$\frac{0.32}{0.20}$ =1.6	SP

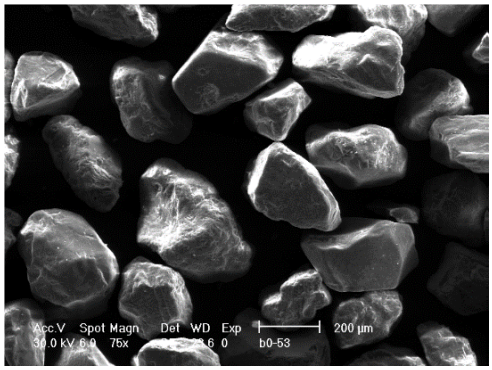

(a)

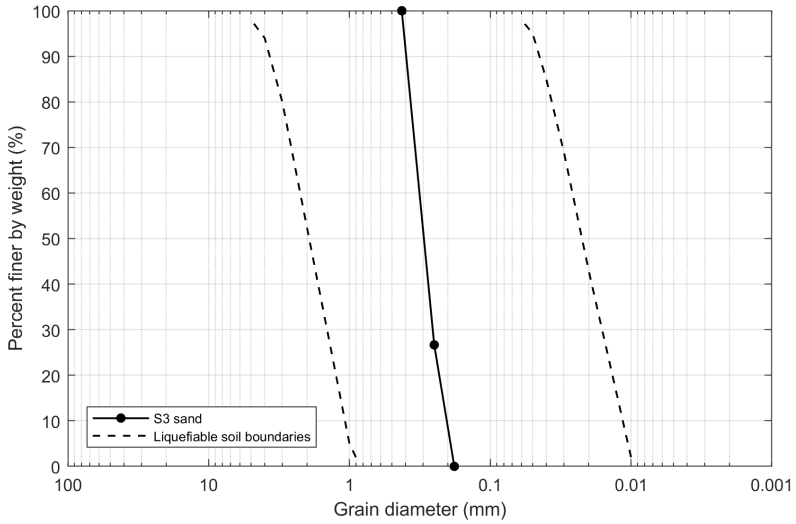

(b)

Figure 4.1: *SEM image of S3 sand (a) and grain distribution (b).*

Representativeness of S3 sand The representativeness of S3 sand to study the effects of CS grouting in reducing soil liquefaction hazard is referred to its grain size distribution and its hydraulic conductivity: the former influences its liquefaction susceptibility, while the latter essentially defines if it is groutable.

The hydraulic conductivity of S3 sand was measured by means of laboratory constant head permeability tests; dry sand layers were put into a permeameter cell (70 mm diameter, ≈180 mm height) and tamped by means of a steel tamper to obtain different initial void ratios. Saturation of the samples was achieved by flushing fresh water within the samples at least for one hour; three tubes connected to sampling ports disposed along the permeameter cell were used to measure the hydraulic gradients, i, which ranged between 2 and 3.

Test results are listed in Table 4.2 and plotted in Figure 4.2, where the hydraulic conductivity $k_{T=10°C}$, referred to a temperature of 10°C according to the standard UNI CEN ISO/TS 17892-11, is plotted against void ratio, e. For comparison, $k_{T=10°C}$ of S3 ($D_{50} = 0.30$ mm), for the void ratios used in this work, is within the range $10^{-3} - 10^{-5}$ m/s, that is the hydraulic conductivity range of a medium-fine sand with void ratio between 0.6-0.8 (generally corresponding to loose up to medium-dense sand, that is, prone to liquefaction) and grain size of 0.1-0.5 mm (Karol and Berardinelli, 2003).

Therefore, on the basis of grain distribution and hydraulic conductivity criteria, the used S3 sand can be classified as a liquefiable material (Fig. 4.1b) and easily groutable soil by means of the most commonly used chemical grouts (Tab. 3.2 and Fig. 3.24).

Table 4.2: *Constant head permeability tests on S3 sand.*

e (-)	$k_{T=10°C} \times 10^{-4}$ (m/s)
0.576	2.44
0.577	2.55
0.598	2.59
0.599	2.58
0.608	2.66
0.625	3.00
0.662	3.20
0.672	3.37
0.699	3.79
0.707	3.68
0.730	4.21
0.731	4.60

Colloidal silica grout *MasterRoc®MP 325* (BASF SE) colloidal silica was selected as the stabilizing agent in this Thesis. The product properties are summarized in Table 4.3. To date, the cost of MasterRoc MP 325 was ≈4 Euro/L, while, for instance, one of the most used colloidal silica product, named Ludox-SM 30 (Sigma-Aldrich), provided as a 30% by weight colloidal silica content solution, was ≈38 Euro/L. Therefore, if the effectiveness of diluted MasterRoc MP 325 in liquefaction mitigation is verified, great savings can be achieved for potential *in situ* treatments.

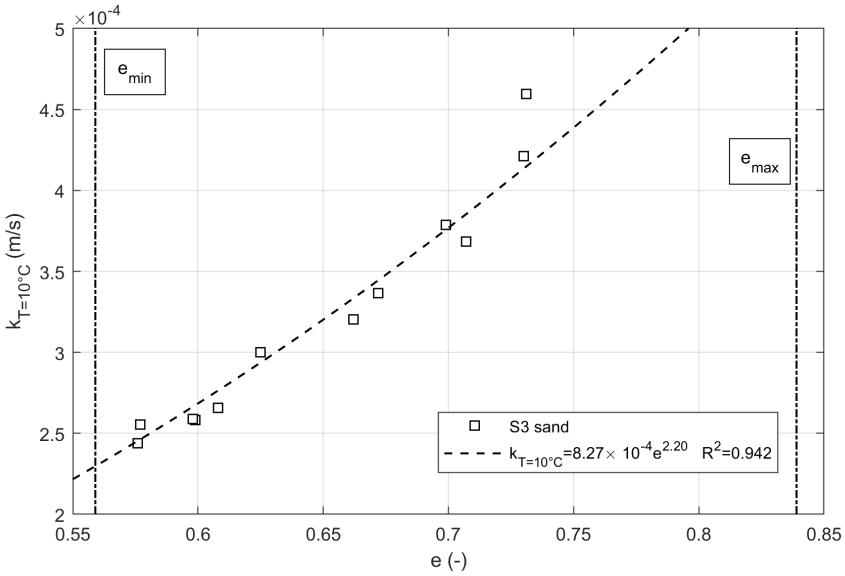

Figure 4.2: *Results of constant head permeability tests on S3 sand.*

Table 4.3: *MasterRoc®MP 325 properties.*

Color	clear
Viscosity (20°C) (mPa·s)	≈10
Density (20°C) (kg/L)	1.1
pH (20°C)	10±1
SiO_2 content (% by weight)	15±1

Gelling of the CS sol was induced by adding to it a certain amount of a reactant, that is herein referred to as the 'accelerant[1]', which consisted of a saline solution made of distilled water and sodium chloride (10% by weight NaCl solution). The colloidal silica grout solution used in this study was finally made up of CS solution, accelerant and distilled water. The CS content is intended as the amount of silica solids in the grout solution, by weight, and indicated by CS_W.

To obtain the different fractions of the grout, calculations were made in terms of volumes, and then converted by using the fraction densities, assuming those of distilled water and of the accelerant equal to 1.0 and 1.1 kg/L at 20°C, respectively (the influence of temperature on testings was neglected, since room temperature was fairly constant during the experimental investigations). Therefore, named V_{MR}, V_{acc} and V_{H_2O} the volume of colloidal silica sol, of the accelerant and of distilled water respectively, and being ρ_{MR}, ρ_{acc} and ρ_{H_2O} the corresponding densities, the concentration MR_{Vol} of MasterRoc MP 325 (by volume of the grout) is expressed by Equation 4.1, being V_{tot} the total volume, while the concentration MR_W of MasterRoc MP 325 (by weight of the grout) is expressed by Equation 4.2; the silica solids content CS_W (by weight) is obtained by means of Equation 4.3, since MasterRoc MP 325 is provided as a 15% silica content product (Tab. 4.3). The concentration of accelerant (by volume of the grout), α, is defined by Equation 4.4; the utility of this parameter is described further on. Practically, the fractions V_{MR}, V_{acc} and V_{H_2O} were obtained by fixing CS_W, V_{tot} and α.

[1]The term is actually improper, since without adding the accelerant the gelation process wouldn't take place.

$$MR_{Vol} = \frac{V_{MR}}{V_{MR} + V_{acc} + V_{H_2O}} = \frac{V_{MR}}{V_{tot}} \tag{4.1}$$

$$MR_W = \frac{V_{MR} \cdot \rho_{MR}}{V_{MR} \cdot \rho_{MR} + V_{acc} \cdot \rho_{acc} + V_{H_2O} \cdot \rho_{H_2O}} \tag{4.2}$$

$$CS_W = 0.15 \cdot MR_W \tag{4.3}$$

$$\alpha = \frac{V_{acc}}{V_{tot}} \tag{4.4}$$

4.2 Preliminary tests

A set of preliminary tests on pure colloidal silica grout and on colloidal silica treated sand was performed to analyze the gelation process and the development of gel strength over time.

4.2.1 Gelation process: glass test

To evaluate the gelation process (i.e. the rate of viscosity increase) several tests on pure colloidal silica grout were carried out. The gel time, t_g, is a fundamental parameter and it must be carefully chosen: in field, for the correct grout delivery and stabilization of the target soil, while for laboratory investigations, to allow specimen preparation for experimental testings: if gelation is too fast, there could not be enough time to complete the procedure, while if the process is too slow, testing times may become unpractical.

Gel time was evaluated empirically by preparing several grout solutions of equal V_{tot} with different α and CS_W. Distilled water, accelerant and MasterRoc MP 325 were poured in this order into glasses, mixed, gelling at constant room temperature. A plastic film was put on the top of the glasses to avoid any evaporation. The t_g was determined as the time between the addition of colloidal silica and the time at which less than ≈10-15% of the mixture flew along the glass walls after its rotation of 90° on the horizontal plane. Different silica concentrations were used: 1%, 2%, 3% and 5% by weight. No gel was detected for $CS_W = 1\%$ and $\alpha = 0.80$ after 21 days; it is considered that such low CS content may be unfeasible for in field practical applications, and for this reason it was not further tested. The results of the experiments are shown in Figure 4.3, where gel time is plotted against the percentage of accelerant by volume of grout. As it was expected, t_g increased as α decreased for a given CS_W, while to obtain a given t_g, α decreased as CS_W increased. The decrease of t_g with increasing α, for a given CS_W, follows an exponential law; this confirms that the increase of grout viscosity with time is non linear (e.g. Fig. 3.3).

For $CS_W = 2\%$, the gelled matrix was not as firm as for higher CS concentrations: the solidity of the gel pattern depends on the silica content, and 2% could represent the lower boundary between liquid and gel. The gel formed by means of $CS_W = 2\%$ can be described as a *weak* gel.

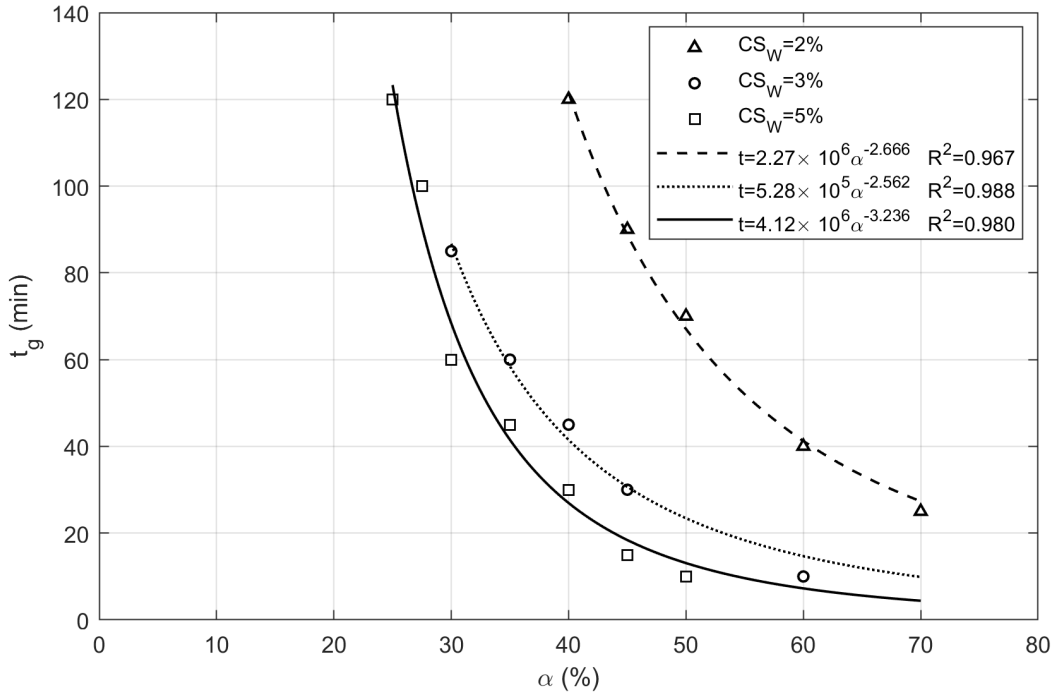

Figure 4.3: *Results of glass tests on pure colloidal silica grout.*

4.2.2 Gelation process: volume changes

It is questionable if grout changes in volume during solidification. To verify that there are no volume changes during gelling, as it is hypothesized due to the nature of the gelation chemical process[2], a simple test was carried out on pure silica grout. The latter was poured into two burettes (with a different size, 5 ml and 25 ml, and precision of 1/10 ml and 1/20 ml, respectively) at constant room temperature (20°C); the height of the meniscus was recorded in every burette before and after gelation. Volume changes would produce the meniscus to move up inside the burettes, and it could be visually observed and recorded. The top of the burettes was sealed with a plastic film to avoid evaporation. To ensure gelation, an amount of grout was also collected in glasses, and glass tests were repeated for each concentration tested. Two tests were performed: in each test, firstly 2% and secondly 10% silica contents were used in the two burettes, assuming $\alpha = 0.4$ and $\alpha = 0.2$, respectively. 10% CS was chosen because it is hypothesized that greater volume changes, if happened, would be more detectable as the silica concentration increases. Both the tests indicated that there were no volume changes during gelation; for $CS_W = 2\%, 10\%$ there was no movement of the meniscus inside both the burettes. As an example of these test results, Figure 4.4 shows the meniscus height in the 25 ml burette for $CS_W = 10\%$ before and after gelation.

[2]The increase in grout viscosity is a consequence of silica particles aggregation: there are no apparent reasons how this process could be related to a volume change.

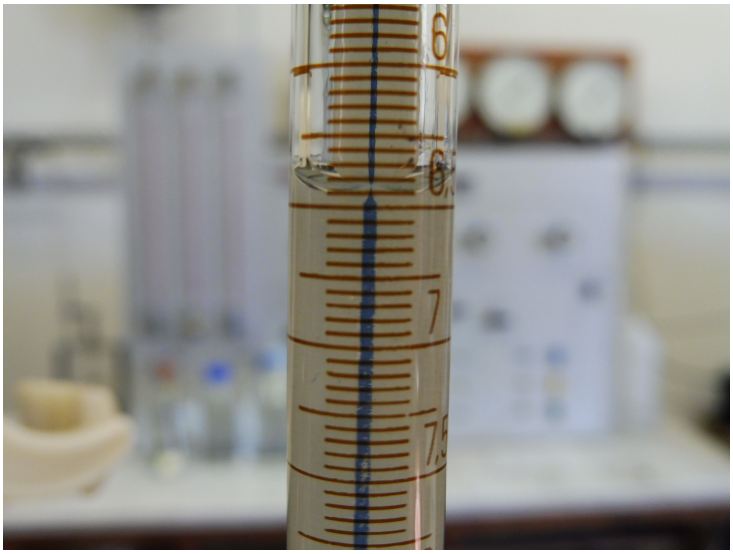

(a)

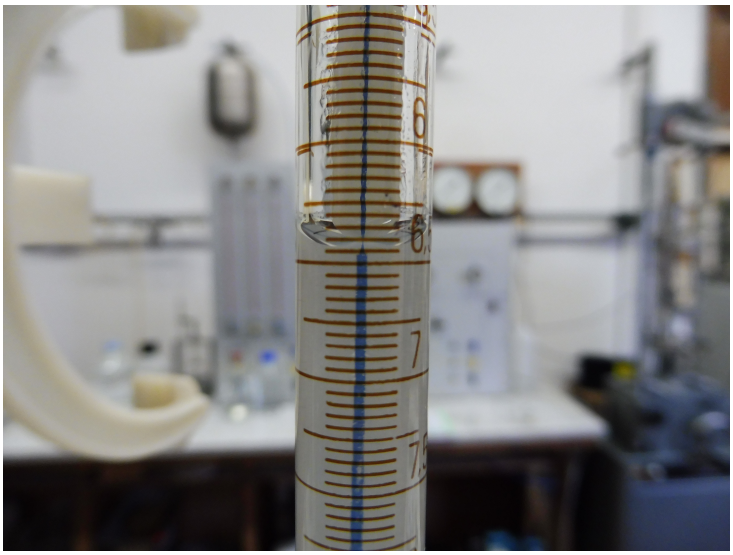

(b)

Figure 4.4: *CS_W=10% test on 1/20 ml precision burette: before (a) and after gelation (b).*

4.2.3 Silica gel compressibility

The silica gel compressibility (Towhata, 2008) was analyzed by preparing two pure colloidal silica specimens (CS_W = 5%, 10%) inside a dedicated plexiglass box (71 mm diameter, 18 mm height) with impervious bottom and side wall. Tests were performed the day after gelation and they were kept under water before placing an impervious platen on the top, fitting snugly into the sample ring. The vertical compressive load was applied to the soil by means of a steel rigid cap placed above the upper platen. Consequently, *undrained* confined 1D-compression tests on pure gel were performed and the observed strain was ascribed to the compressibility of the gel skeleton, being the water flow prevented by the impervious disc. It was not possible to apply any loading sequence during these tests, since both samples started to subside under the weight of the cap distributing the load that transmitted a pressure of ≈1.4 kPa. Results of these tests are shown in Figure 4.5. Therefore, even if a proper measurement of the silica gel compressibility was not possible, a clear evidence of it was observed.

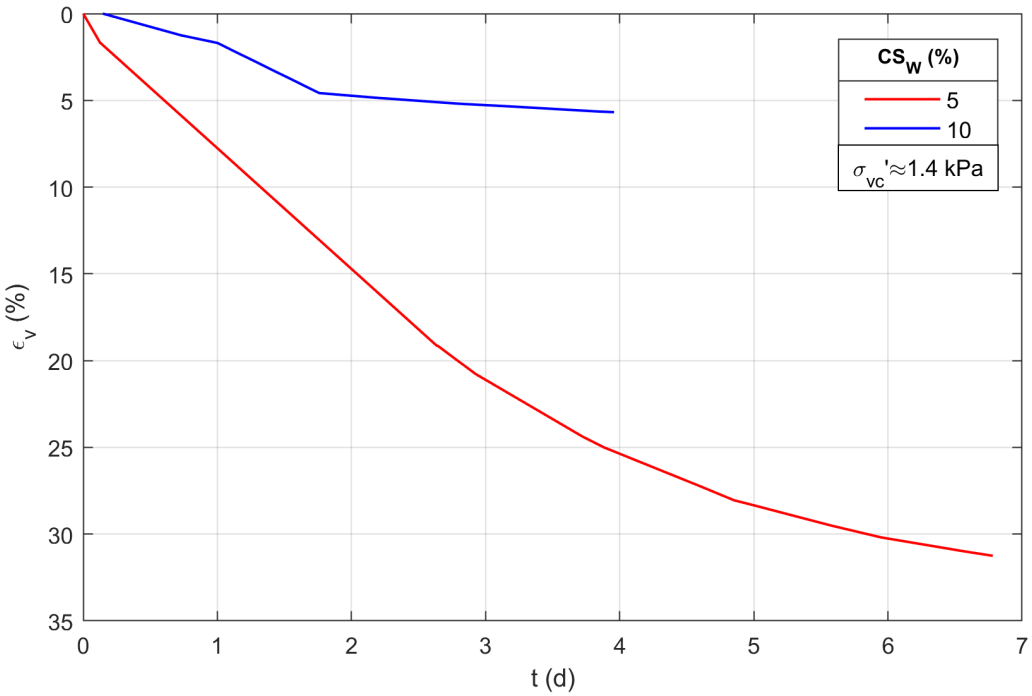

Figure 4.5: *Undrained oedometer tests on pure colloidal silica samples.*

4.2.4 Gel strength: pocket penetrometer tests

The 'strength' of colloidal silica treated sand increases with time (Chapter 3). *Curing time* (t_c) is here defined as the time between the end of gelation (t_g), as determined by means of glass tests, and the beginning of any other laboratory test. In order to choose a proper t_c for laboratory testing, a set of grouted sand specimens was prepared, for each tested value of CS_W (2, 3 and 5%), by pluviating a fixed weight of dry sand into glasses containing the same V_{tot}; α was chosen to obtain $t_g = 120$ min for the whole set of specimens. After pluviation, the top of the glasses was carefully sealed by means of a plastic film, to avoid evaporation. In this way,

loose specimens of equal density were prepared; since t_g was the same for all samples, it was therefore possible to investigate the effects of t_c on the maximum undrained strength of treated material. Pocket penetrometer tests were used for this purpose. These tests were performed to define the standard t_c to adopt in experimental testings: for practical purposes, in fact, the main part of the available strength needs to be developed before any test (e.g. triaxial, oedometer, etc.) was run, but it was also necessary to optimize the testing times.

For each sample, three determination of pocket penetrometer shear resistance were done, eventually assuming the mean value. The undrained maximum strength, PPR, against t_c, expressed in days, is plotted in Figure 4.6. It is shown that PPR increased over time, as it was expected from literature data. It was confirmed that, given a certain t_c, PPR increases as CS_W increases.

Based on the results of these preliminary investigations, the standard t_c used in all further tests, if not differently stated, was set in 5 days, since most of the PPR was available after that time: for instance, the difference between $PPR(t_c = 14d)$ and $PPR(t_c = 5d)$ for $CS_W = 5\%$ is $\approx$7%.

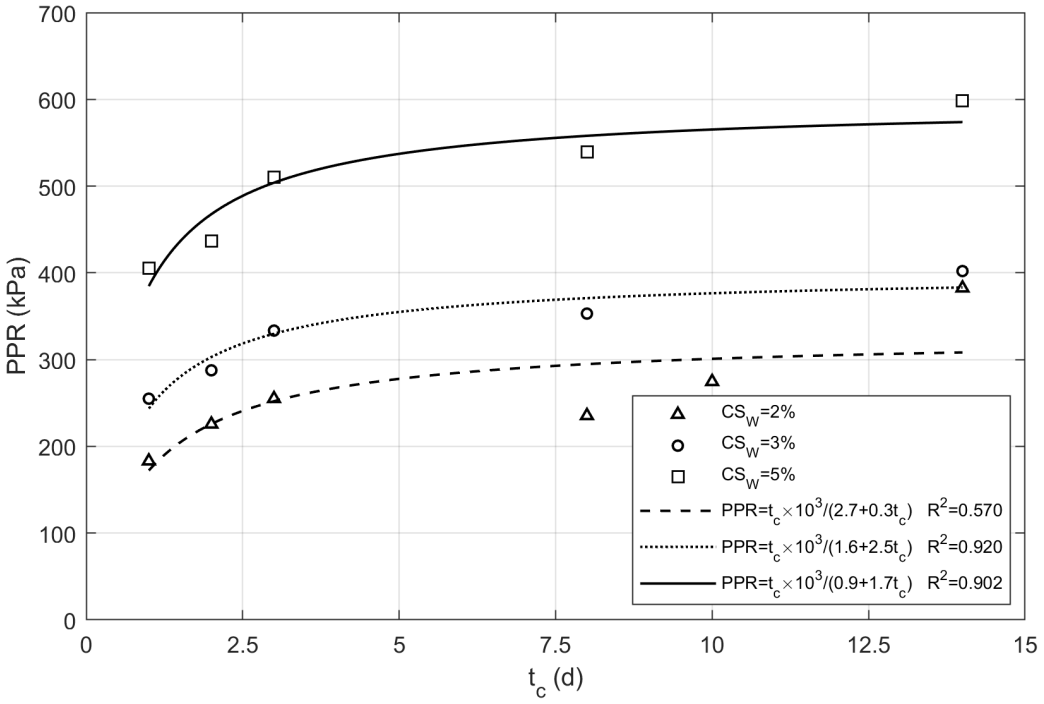

Figure 4.6: *Results of pocket penetrometer tests on treated sand.*

4.2.5 Permeation tests

Simple grouting tests were performed to verify that MasterRoc MP 325 CS grout can permeate S3 sand without the need of high injection pressures, as it is for other colloidal silica products (e.g. Gallagher and Lin, 2009). A triaxial permeameter cell, belonging to the geotechnical laboratory of Braunschweig University of Technology (Germany), was used to this aim; at the end of each test, the treated material hydraulic conductivity was also measured.

Cylindrical sandy specimens (D=50 mm, H=100 mm) were firstly prepared in the triaxial chamber[3] by pouring dry sand into a latex membrane, stretched along the walls of a split mold. A plastic top cap was put above the sample, the membrane was then stretched over it and fixed with o-rings; with the aid of vacuum, the split mold was removed and the specimens dimensions were recorded. The triaxial cell was filled with deaired water, and a small confining pressure (20 kPa) was applied to sustain the samples. CO_2 flushing was performed for about a hour after vacuum was removed. Distilled and deaired water was flushed from the bottom to the top of the specimens by means of low hydraulic gradients (up to a maximum of 3), to promote saturation. Specimens were not consolidated. After saturation, the hydraulic conductivity of untreated S3 sand was measured. Details of the tests are listed in Table 4.4, where ID indicates the test identification code. The hydraulic conductivity of natural sand, measured by means of the triaxial apparatus, was about the same for all specimens and very well in agreement with the results obtained from the constant head permeameter (i.e. samples without any confining pressure) (Fig. 4.2).

After the measurements of $k_{T=10°C}$, 500 ml grout solutions (2% CS by weight, $\alpha = 0.30 - 0.40$, and 5% CS, $\alpha = 0.25 - 0.15$) were prepared and they permeated into the water-saturated samples, in falling head mode, by assuming $i \leq 1.5$. The arrangement of a permeation test setup is shown in Figure 4.7.

Figure 4.7: *Setup of grout permeation test on untreated sand; after treatment, the permeameter cell was adopted to measure the hydraulic conductivity of treated material.*

Once the injection was finished, one day was waited before measuring the hydraulic conductivity of treated material. The triaxial cell was dismantled before each record, to clean the drainage lines from the gelled matrix and to saturate them with deaired water; the samples were then put in place again and the $k_{T=10°C}$ values were registered after the cell was reassembled.

To ensure gel saturation, it was assumed that at least three pore volumes of grout should pass within the samples. This condition was verified for all the performed tests. However,

[3]The triaxial apparatus used for the grouting test was not the device used for shear tests, but a self-constructed one only used for these analysis.

during the first effort with $CS_W = 2\%$ (test $1P$), the grout flow stopped for $i = 1$ and $\alpha = 0.40$, due to the increased viscosity of the solution, once ≈ 250 ml of CS mixture were delivered. The process took about 11 minutes to be completed, while the time expected, based on the measured hydraulic conductivity of natural sand, was about 7 minutes. This delay was imputed to the increasing reduced mobility of grout during the permeation. Therefore, the percentage of accelerant to the total volume of grout was reduced and the following tests ($2P$, $3P$) were performed by using the same maximum i and $\alpha = 0.30$ (i.e. t_g increased); in this way, almost the total volume of grout (≈ 480 ml) was successfully delivered into the specimens. The flow continued without interruption under a minimum $i = 0.5$, and it was manually stopped.

The first permeation test with $CS_W = 5\%$ ($4P$) was performed with $\alpha = 0.25$; as it happened for test $1P$, the grout flow stopped after a certain time, probably because of the too fast increase of grout viscosity. Therefore, test $5P$ was performed assuming $\alpha = 0.15$: in this case, the treatment solution could be successfully delivered without interruption. However, the flow was much slower in this case than in tests $2P - 3P$; this was due to the increased silica content in the grout.

These tests demonstrated that:

- low CS content grout ($CS_W = 2\%$) can successfully permeate medium-dense S3 sand;
- permeation was completed by means of low hydraulic gradients, confirming that high injection pressures are not required for potential *in situ* treatments;
- the groutability of the material decreases as grout viscosity increases (e.g. Bolisetti et al., 2009; Gallagher and Lin, 2009);
- grout initial viscosity increases with increasing CS_W;
- the rate of viscosity increase can be adjusted by changing t_g;
- appropriate measure of grout rheology is essential to predict how the mixture is delivered for practical applications.

Once the permeation process was completed, the hydraulic conductivity of treated sand was measured in falling head mode. As shown in Table 4.4, a 10^4 (10^5) fold decrease was recorded for 2% (5%) CS grouted material. The hydraulic conductivity of high-diluted CS grouted sand ($CS_W = 2\%$) has not been previously reported by any research; its magnitude seems very well in agreement with literature data on $CS_W \geq 5\%$ treated sand (e.g. Fig. 3.30a, where Monterey No. 0/30 sand, a poorly graded medium to fine sand with sub-angular grains, has $D_{50} = 0.49$ mm); furthermore, data results from tests $4P$ and $5P$ agree with those obtained by Persoff et al. (1999) (Fig. 3.30a). Test results are graphically represented in Figure 4.8, that shows the drastic $k_{T=10°C}$ reduction.

4.2.6 X-ray micro-tomography tests

X-ray micro-tomography tests were performed on treated sand to investigate the effects of colloidal silica grouting at the micro-scale. Loose samples were prepared by grout pluviation

Table 4.4: *Summary of permeation tests and hydraulic conductivity measurements (*=after CS treatment).*

ID (-)	e (-)	CS_W (%)	α (-)	$k_{T=10°C}$ (m/s)	$k_{T=10°C}$* (m/s)
1P	0.680	2	0.40	3.29×10^{-4}	3.45×10^{-8}
2P	0.695	2	0.30	1.68×10^{-4}	5.75×10^{-8}
3P	0.680	2	0.30	2.48×10^{-4}	2.19×10^{-8}
4P	0.659	5	0.25	2.41×10^{-4}	3.82×10^{-9}
5P	0.666	5	0.15	2.55×10^{-4}	1.50×10^{-9}

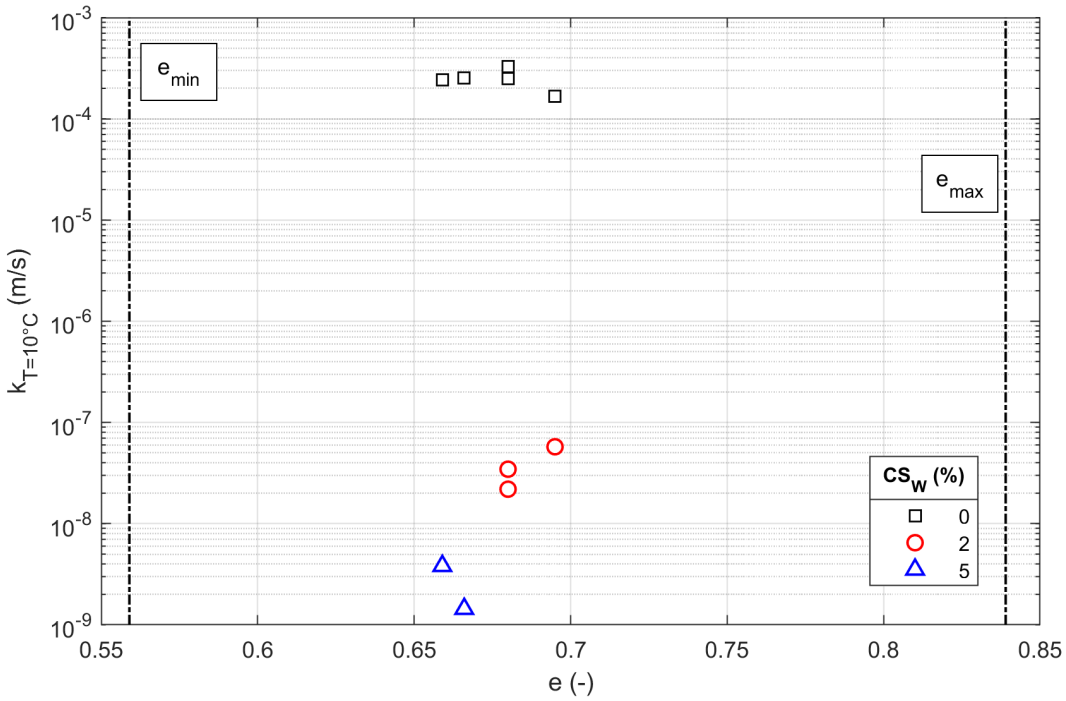

Figure 4.8: *Hydraulic conductivity of treated and untreated material ($t_c = 1$ day).*

into glasses; the same amounts of sand and grout were used to prepare specimens with the same initial void ratio. The specimens were trimmed after curing to obtain small cubic samples (≈1x1x1 cm) that were finally put into the scanning machine. Lower and upper grey thresholds were assumed equal for the visual analysis of all tests; it was therefore possible to interpret the results in terms of (relative) 'visual' porosity change. Visual porosity indicates the sample porosity calculated on the basis of the visual interpretation of the scanned image. It is expected that the presence of CS gel within the pores can be viewed as a decrease in visual porosity depending on CS content.

Tests were performed by means of a Skyscan 1172 high resolution micro-CT. This system has a sealed, micro-focus tungsten X-ray tube with a 5mm focal spot size. X-rays were produced by exposing the anode to an electron beam at 100 kV and 100 mA; the beam was filtered by Aluminum and Copper filter. Each sample was placed on the pedestal between the X-ray source and the CCD detector. 2D X-ray images were captured over 180° by rotating the sample with a slice-to-slice rotation angle of 0.2°, each 2D image representing one slice. Spatial resolution time was kept in the range 10-12 mm (pixel size).

3D images of the objects were reconstructed by using a modified Feldkamp algorithm for cone-beam acquisition geometry realized in Nrecon 1.6.9.4 software. The alignment, beam hardening and ring artifacts were corrected before starting the reconstruction process. CTan and CVol or CVox software were used for the image clean up and for 3D visualization, respectively.

The list of tests is shown in Table 4.5. Three different CS contents were tested.

Table 4.5: *X-ray computer tomography tests on treated material.*

ID (-)	CS_W (%)
1X	2
2X	4
3X	5

Table 4.6 summarizes the results obtained from X-ray micro-tomography tests. Computer calculations revealed that total visual porosity increased as CS_W decreased and, in detail, the recorded difference between 2% and 5% CS treated specimens was 17.31%. These tests confirmed that gelation process was successfully completed and that silica solids are enclosed within the pore spaces. The tendency in porosity decrease is visually shown in Figure 4.9, where two images of samples treated with CS_W=2, 5% are reported.

Table 4.6: *Results of X-ray computer tomography tests.*

ID (-)	Total visual porosity (%)
1X	37.93
2X	28.22
3X	20.62

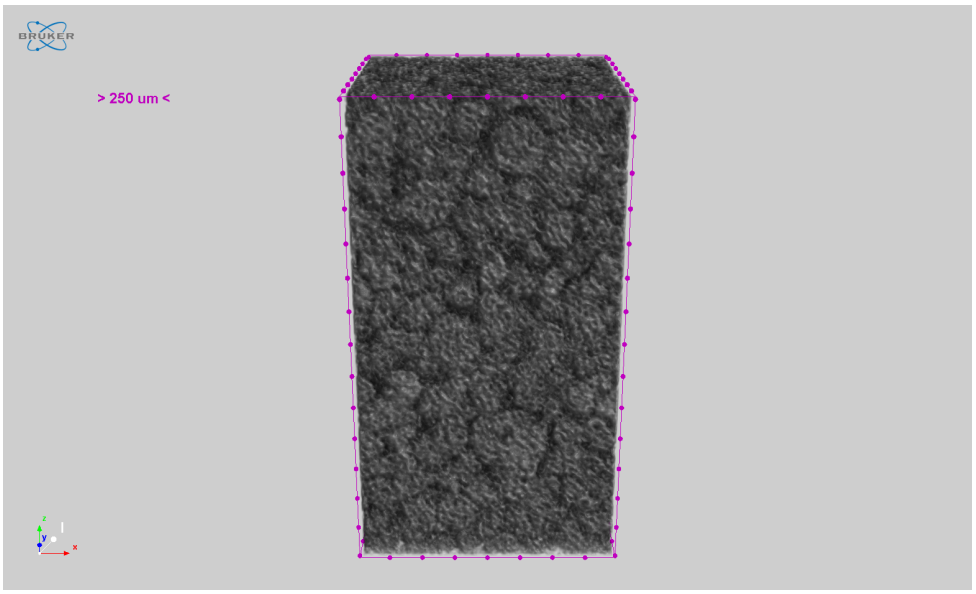

(a)

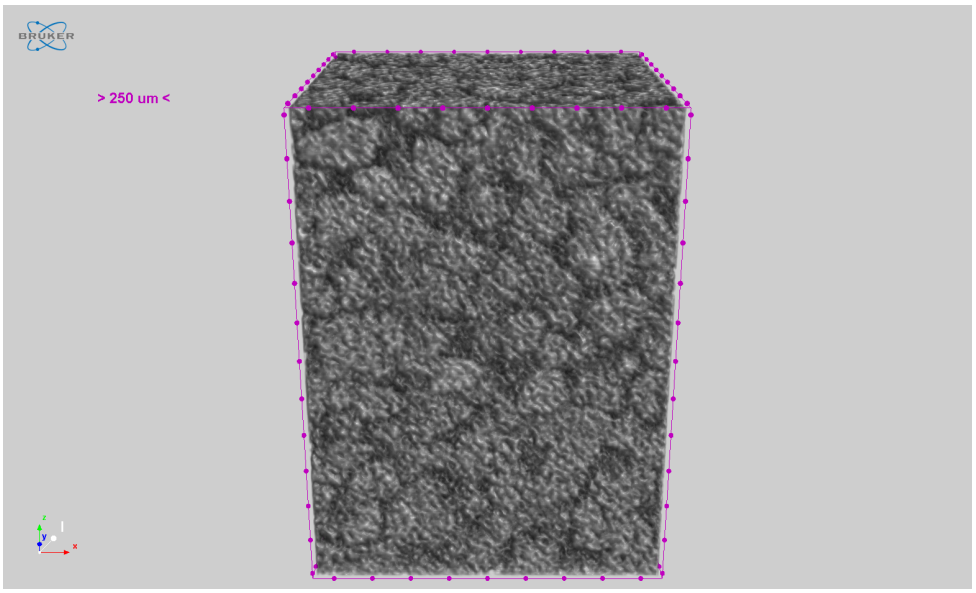

(b)

Figure 4.9: *Test results from X-ray computer tomography: scanned images of samples 1X ($CS_W = 2\%$) (a) and 3X ($CS_W = 5\%$) (b).*

4.2.7 Final remarks from preliminary tests

Significant information is obtained from the analysis of the preliminary tests described in the previous Sections. Firstly, it was possible to define t_g and t_c to standardize the samples preparation procedures: because treated specimens need to be prepared at the same initial conditions, to be representative of a certain state, it was required that the strength of the gel pattern (compressible material) developed in the same time for different CS_W. Therefore, if not differently stated, t_g and t_c were assumed equal to 120 minutes (by varying α and CS_W according to Fig. 4.3) and 5 days, respectively.

Secondly, it was shown that MasterRoc MP 325 can permeate medium-dense sand specimens by means of low hydraulic gradients; moreover, it was proven that the hydraulic conductivity of treated soil is greatly reduced by the presence of gel within the pore spaces; a weak $CS_W = 2\%$ gel produces a remarkable decrease of $k_{T=10°C}$.

4.3 Mechanical behavior analysis

Test procedures (and results in Chapter 5) are presented and discussed in this order: firstly, cyclic triaxial tests, used to assess the liquefaction resistance of untreated and treated materials, then direct shear and monotonic triaxial tests performed to better understand their stress-strain behavior, and finally, oedometer tests, to investigate the effects on settlements of CS treatment.

4.3.1 Preliminary mechanical tests on grouted material

Some preliminary mechanical tests on untreated and colloidal silica treated material were performed at the geotechnical laboratory of the University of Cassino and Southern Lazio (Italy), including cyclic as well as monotonic triaxial tests. They are described in this Section because they represented the first approach to treated material and they were used to correctly setup the experimental investigations described in the following Sections. A stress-controlled triaxial device (Megaris S.r.l) was used for this purpose (Fig. 4.10). These tests allowed a preliminary understanding of grouted sand properties and pointed out some limits of the adopted experimental procedure; as a consequence, the latter was modified as described further on. The results from these tests are described and discussed in the interest of completeness in a dedicated Section in Chapter 5.

Cylindrical specimens (70x110 mm) were prepared in loose and dense states. A grout permeation technique was used to let silica grout pass through the samples: silica grout was put into a reservoir, and it permeated the sand from the bottom to the top due to a difference in hydraulic head. Samples were not confined and a small seating load was put on the top to avoid any lifting during grouting. Test details are listed in Table 4.7. Loose samples were prepared by pouring dry sand in a split mold, with the aid of a funnel and without any tamping; dense sand ones were prepared by tamping dry sand with the aid of a steel plate. Before the shearing phase (cyclic and monotonic), both treated and untreated samples were saturated with deaired water; thus, during these tests there was a continuous measurement of the pore water pressure, even for gelled samples. Damages to the pore water pressure transducer, as reported in Fig.

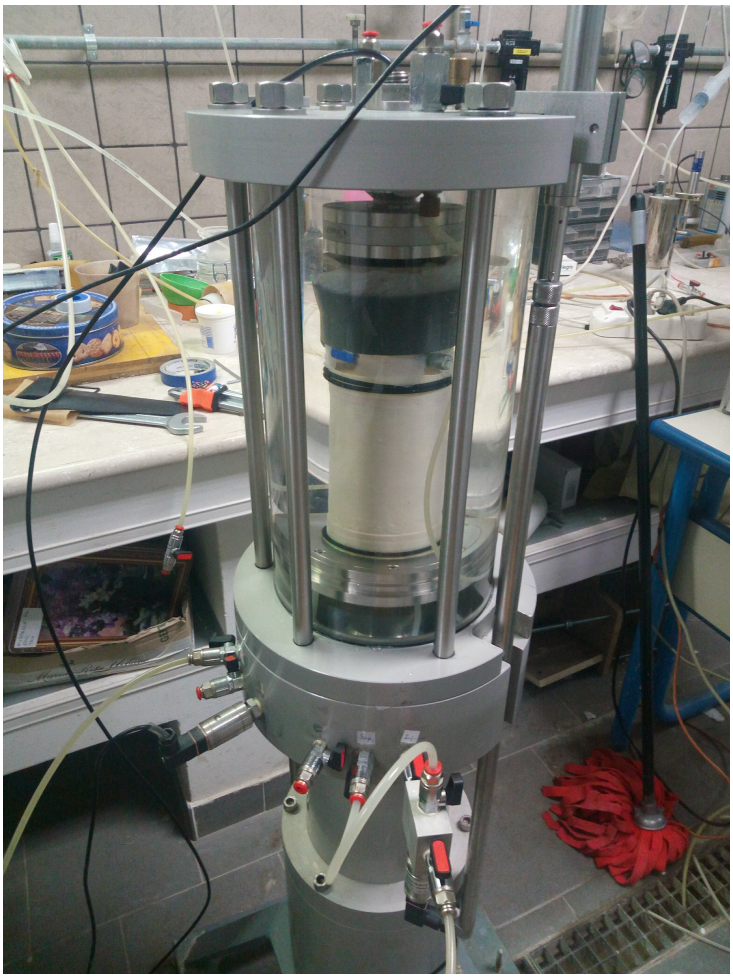

Figure 4.10: *The triaxial apparatus used for preliminary mechanical tests on treated and untreated sand.*

4.12, were not visually detected in this phase. However, it was often not possible to have a satisfactory saturation for gelled samples, although very high back pressure values were used ($B < 0.95$[4] for back pressure of 700 kPa). Back pressurization phase could destroy silica bonds formed within the grains; moreover, a not complete saturation affects the reliability of test results, especially those obtained from undrained tests. As discussed in Chapter 2, the presence of air in pore spaces increases the sand liquefaction resistance, and even a small reduction of S_r causes a great improvement of soil behavior under cyclic loading conditions. Furthermore, the procedure used to treat the samples does not guarantee a good reproducibility of treated specimens: for instance, samples 03-CA and 0.6-CA liquefied after 9 and 10 loading cycles, respectively, under the same normalized stress ratio and CS_W, but they were very different in void ratio after consolidation and in B value. As indicated e.g. by tests 12-CA and 18-CA, two samples prepared with similar void ratio gave a very different void ratio after isotropic consolidation and, despite having the same B value and CS_W, both the specimens didn't fail under very different CSR values. The observed disagreement is due to the technique used to prepare grouted specimens, that is proven not to reproduce specimens with enough accuracy. This evidence, together with the need of ensuring saturation and avoiding bonds' breakage by applying a back pressure, is at the basis of the choice of the wet pluviation technique for the preparation of gelled samples tested and discussed in this study.

Table 4.7: *Monotonic and cyclic triaxial preliminary tests (MD=monotonic drained, CU=cyclic undrained, e_c=void ratio after isotropic consolidation, BP=back pressure).*

ID (-)	Test type (-)	e_c (-)	BP (kPa)	B (-)	σ'_c (kPa)	CS_W (%)	CSR (-)	N (-)
13-CA	MD	0.65	700	0.85	50	0	-	-
07-CA	MD	0.64	700	0.90	100	0	-	-
09-CA	MD	0.61	700	0.96	200	0	-	-
16-CA	MD	0.60	700	0.95	300	0	-	-
15-CA	MD	0.59	700	0.99	400	0	-	-
10-CA	MD	0.63	700	0.96	200	2	-	-
14-CA	MD	0.60	700	0.84	200	5	-	-
04-CA	CU	0.64	700	0.93	100	0	0.15	No liq.
05-CA	CU	0.61	700	0.95	100	0	0.20	20
11-CA	CU	0.63	700	0.99	100	0	0.25	19
16-CycA	CU	0.62	700	0.95	100	0	0.35	5
03-CA	CU	0.76	700	0.85	100	2	0.15	9
06-CA	CU	0.62	700	0.94	100	2	0.15	10
12-CA	CU	0.70	700	0.89	100	5	0.25	No liq.
18-CA	CU	0.63	700	0.89	100	5	0.35	No liq.

[4]Since silica gel is compressible (Chapter 3), it is however questionable which B limit-value is considered enough for saturation of gelled samples. In common practice, in fact, $B \geq 0.95$ is the standard to check saturation in triaxial water-saturated specimens, assuming the compressibility of water much higher than that of the soil skeleton. Porcino et al. (2011, 2012) measured B values greater than 0.96 for $CS_W = 10\%$; Georgiannou et al. (2017) obtained $B > 0.97$ for the same tested concentration. Therefore, it is reasonable that, for the CS contents used in this study, $B \geq 0.95$ should have been achieved. Definitely, the B values reported in Table 4.7 for treated sand are considered as a consequence of ineffective saturation.

4.3.2 Cyclic triaxial tests

Undrained cyclic triaxial tests were performed on treated and untreated reconstituted sand samples to evaluate the mechanical behavior of the materials under cyclic loading conditions; loose and medium-dense sand specimens were tested. A dynamic electro-mechanical triaxial apparatus (*Dynatriax EmS*, Controls Group, Figure 4.11), belonging to the geotechnical laboratory of Florence University (Italy) was used to this aim. This device is able to perform cyclic as well as monotonic triaxial tests by means of an electro-mechanical servoactuation. Cell and back pressures are applied by two independent air-water systems; an electronic, computer-controlled valve regulates the back pressure inside the samples.

In this Section, the experimental procedures, included the specimens preparation techniques and failure criteria, are illustrated.

Figure 4.11: *The Dynatriax EmS system used for the purposes of this study.*

Specimens preparation for untreated sand

Cylindrical sandy specimens (50 mm diameter, 100 mm height) were used in the experiments. Samples were reconstituted to obtain two different D_r: loose samples were prepared with the wet pluviation technique, while medium-dense samples were prepared by means of the dry tamping method. For both techniques, a latex membrane was firstly put on the pedestal of the

triaxial device, fixed with o-rings, and it was then stretched along a split mold by applying a vacuum between the mold and the membrane; specimens dimensions were carefully recorded after the mold was removed. At last, the triaxial cell was put in place.

For the wet pluviation technique, once the membrane was stretched along the mold walls, the mold was partly filled with distilled and deaired water; then, with the aid of a funnel, dry sand was poured into it. Deposition of sand grains into water reproduces the natural growth condition of alluvial liquefiable deposits, like those present e.g. in the Emilia region (Vannucchi et al., 2012; Fioravante et al., 2013; Facciorusso et al., 2015, 2016); saturated loose specimens can be prepared by the wet pluviation method (Vaid and Negussey, 1988). Saturated porous stones had been previously placed at the the top and at the bottom of the specimens. The amount of water was equal to the samples volume of voids. A vacuum top cap was placed above the samples, the membrane was stretched over it and fixed with o-rings. Then, a vacuum was applied to the specimens before the mold was dismantled. Once the samples dimensions were measured, the loading ram was attached to the top cap: a vacuum line ensured the contact between these parts. The triaxial cell was finally filled with distilled and deaired water.

For medium-dense sand, once the membrane was stretched along the mold walls, one dry porous stone was put at the bottom of the sample and a fixed layer of dry weighted sand was put inside the mold; once the layer was leveled, it was tamped (one blow) by using a steel tamper, that consisted of a weight falling from fixed heights. Several sand layers of equal height and mass were posed and tamped; one dry porous stone was put above the samples, and the vacuum top cap was then put in place. The following cell installation procedure was identical to that described above.

Specimens preparation for treated sand

Cylindrical sandy loose specimens (50 mm diameter, 100 mm height) were used in the experiments. Special Plexiglass bottom and top caps were designed and manufactured to allow specimen preparation outside of the triaxial pedestal, in a way identical to that of untreated samples, avoiding at the same time any possible risk from the contact between the pore fluid and the electronic devices, such as the back pressure transducer and the back pressure valve; any contact between the grout and the drainage lines was also prevented. Electronic equipment may in fact suffer from the contact with colloidal silica grout; as an example, Figure 4.12 shows the deairing block, connected to the pore pressure transducer, that was damaged by silica scales after an effort in measuring the pore gel pressure of a treated sample, and that needed to be substituted after that.

Loose samples were prepared by using a modified wet pluviation technique: dry sand was poured into a split mold that was previously partly filled with the grout solution in its liquid state; the amount of grout was equal to the calculated volume of voids. This method has been previously used by several Researchers (e.g. Gallagher and Mitchell, 2002; Díaz-Rodríguez et al., 2008; Georgiannou et al., 2017) and it was chosen because it maximizes samples reproducibility and it ensures the preparation of very loose, saturated, homogeneous samples (Vaid and Negussey, 1988). Gel saturation was guaranteed by using this reconstitution technique. Specimens were not water-saturated before testing, because the application of a back pressure

may break the weak gel bonds formed within the soil grains, thus producing undesired effects. Avoiding the back-pressurization procedure is considered the safer way to eliminate any specimen disturbance, as previously discussed by some Authors (e.g. Gallagher and Mitchell, 2002; Mollamahmutoglu and Yilmaz, 2010; Vranna and Tika, 2015); furthermore, any contact between the gel and the pressure transducers of the triaxial machine was prevented.

Even if a permeation technique could have been used to reproduce *in situ* formation of treated material, the adoption of such a technique was not chosen because of the reasons discussed in paragraph 4.3.1. Moreover, using a permeation technique introduces several additional variables in the reconstitution procedure, like e.g. how much grout should pass throughout the specimen, the grout permeation rate, or the confining pressure needed to sustain the sample during grouting. As new variables are introduced, it becomes progressively cumbersome to prepare uniform treated sand specimens and to setup an easy reproducible method. Dealing with material treated with a chemical stabilizer, it has been fundamental to ensure the samples uniformity.

After the top cap was put in place in the same way as for untreated sand, the samples were sealed by means of valves and left to cure at constant room temperature. It is worth noting that the mold could be dismantled without applying any vacuum, since the gel matrix could sustain the specimen. Particular care was needed when handling the low-content CS grouted material. After t_c, the mold was removed and the sample was carefully transferred to the triaxial pedestal, with an impervious plexiglass disc at the bottom (to avoid contact between gelled samples and the bottom drainage lines connected to the pore pressure transducer) and one porous water-saturated stone at the top. Figure 4.13 shows a treated sample on the triaxial pedestal; at its top, the plexiglass top cap can be seen. Once the latter was removed, the vacuum top cap was put in place, the triaxial cell was assembled and the loading ram was connected to the sample. The cell was finally filled with distilled and deaired water.

Grouts were prepared to obtain $CS_W = 2\%, 5\%$. No medium-dense sand specimens were treated with colloidal silica grouting.

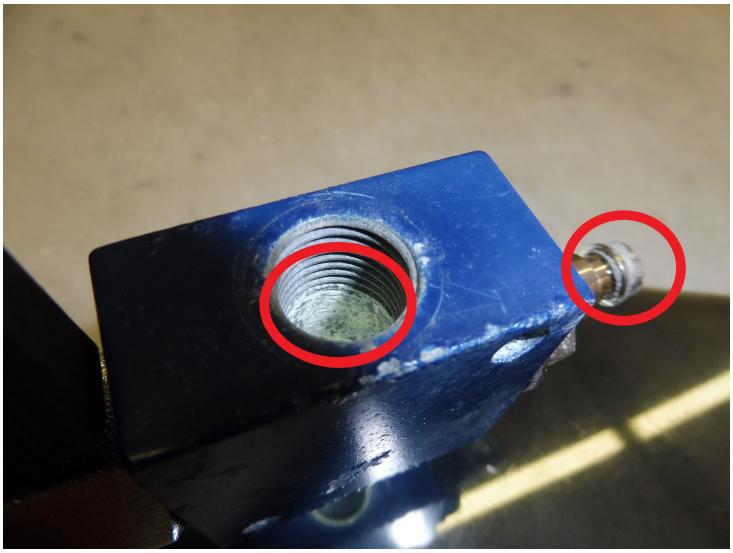

Figure 4.12: *Inner part and connection of the deairing block damaged from the contact with pore gel in a preliminary triaxial test.*

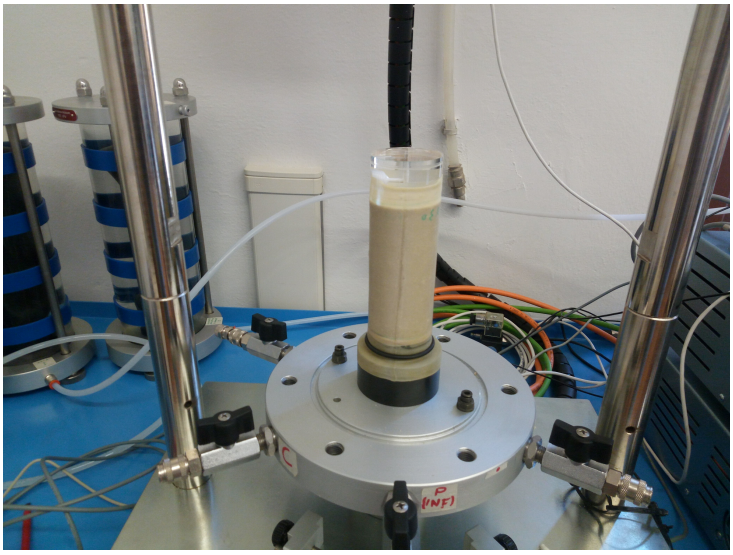

Figure 4.13: *Treated sand sample on the triaxial pedestal before dismantling the plexiglass top cap.*

Experimental procedure

Undrained cyclic triaxial tests were run on treated and untreated specimens in accordance with ASTM D5311 by applying a sinusoidal load of constant amplitude at a frequency of 0.1 Hz. All specimens were isotropically consolidated at $\sigma'_c = 100$ kPa before they were cyclically sheared; the upper drainage line was opened during consolidation, and it was subsequently closed during shearing, for both treated and untreated samples. Displacements, which meant compression of the specimen, were assumed positive. No failure was assumed for $N > 100$.

Untreated sand: liquefaction criterion Before testing, untreated sand specimens (both loose and medium-dense ones) were saturated by flushing of distilled and deaired water followed by back-pressure increments. For loose sand samples, the procedure was quite easy, since, due to their preparation method, a certain degree of saturation was already achieved during the specimens reconstitution; for dense dry samples, CO_2 flushing was performed to facilitate air removal. Full saturation was ensured by measuring the Skempton's coefficient B; the saturation phase was considered complete if $B \geq 0.95$.

Liquefaction was assumed to occur when $r_u = 1.0$ (Eq. 2.5) or $\epsilon_{DA} = 5\%$.

Treated sand: liquefaction criterion Measurements of pore pressure during the tests (including B check) were not possible. Other researchers, like e.g. Porcino et al. (2011); Georgiannou et al. (2017), saturated the triaxial specimens via a back-pressurization phase, and they were then able to measure the pore fluid pressure. This method, however, was not chosen because of the reasons discussed above.

Since r_u was not measured during the tests, failure of treated sand was achieved at $\epsilon_{DA} = 5\%$.

Tests setup A summary of the experimental procedures for treated and untreated material is presented in Table 4.8. The list of tests is shown in Table 4.9.

Table 4.8: *Cyclic triaxial tests characteristics.*

	Untreated sand	Treated sand
Loose samples	Yes	Yes
Medium-dense samples	Yes	No
CS_W (%)	0	2, 5
Wave load form	Sinusoidal	Sinusoidal
Load frequency (Hz)	0.1	0.1
Back pressurization before shearing	Yes	No
σ'_c (kPa)	100	100
Failure criterion	$r_u = 1.0$ or $\epsilon_{DA} = 5\%$	$\epsilon_{DA} = 5\%$

Table 4.9: *Undrained cyclic triaxial tests on treated and untreated material.*

ID (-)	CS_W (%)	e_c (-)	CSR (-)	N (-)
1C	0	0.657	0.20	37.5
2C	0	0.673	0.20	55.5
3C	0	0.670	0.27	6
4C	0	0.667	0.27	8
5C	0	0.668	0.32	3.5
6C	0	0.654	0.26	10
7C	0	0.745	0.16	6
8C	0	0.765	0.11	>100
9C	0	0.776	0.13	77
10C	0	0.772	0.15	22
11C	0	0.721	0.18	5
12C	5	0.779	0.26	1.5
13C	5	0.779	0.20	>100
14C	5	0.763	0.29	3.5
15C	5	0.760	0.38	0.7
16C	5	0.760	0.28	6.5
17C	5	0.787	0.37	0.7
18C	2	0.783	0.175	>100
19C	2	0.754	0.28	1.7
20C	2	0.782	0.26	3.5
21C	2	0.755	0.23	6.5
22C	2	0.788	0.22	4.5
23C	2	0.776	0.27	1.7

S3 samples representativeness of real liquefaction cases As shown in Table 4.9, loose and medium-dense S3 sand samples were tested ($e_{max} = 0.839$, $e_{min} = 0.559$). The initial state of sand was chosen to mimic real liquefaction cases. Figures 4.14 and 4.15 show some in-field investigations at the site of S. Carlo (FE, Italy) which experienced several liquefaction phenomena during the 2012 Emilia Earthquake (Fioravante et al., 2013). Figure 4.14 shows that S. Carlo village, as many others of that area, is founded on alluvial deposits (sand, silty-sand layers), while Figure 4.15 indicates that these deposits are characterized by low up to medium values of D_r. The shallow liquefiable sand layer, specifically, has natural D_r ranging from ≈30 to ≈60%. Facciorusso et al. (2015) showed that soils which liquefied during the 2012 Emilia Earthquake were characterized by D_r ranging from ≈24 to ≈40%. It is worth noting that the occurrence of liquefaction depends on the combination of initial void ratio and effective confining stress, as discussed in Chapter 2.

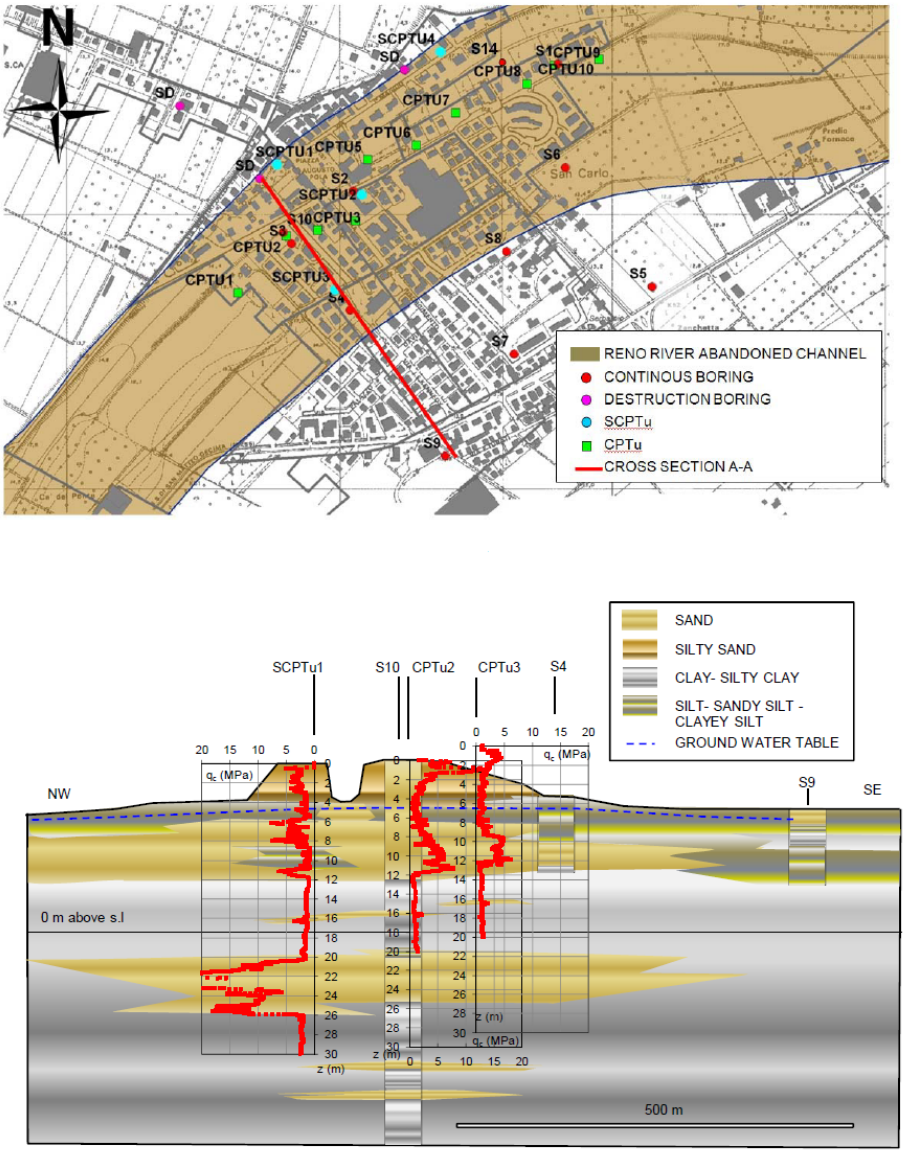

Figure 4.14: *Cross-section and soil profile at S. Carlo (mod. from Fioravante et al., 2013).*

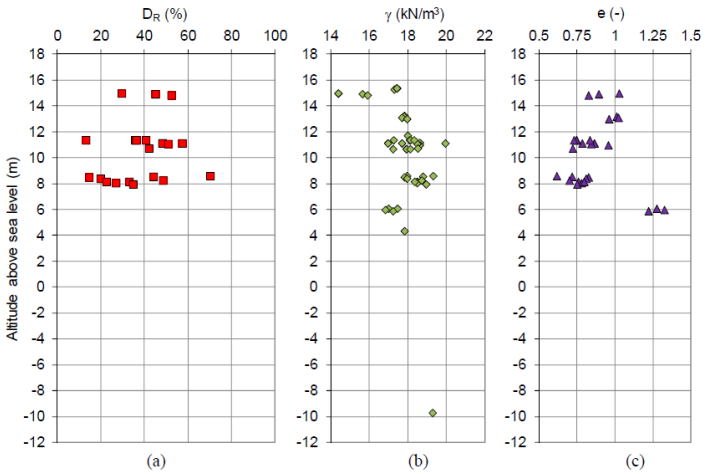

Figure 4.15: *Relative density (a), unit weight (b) and natural void ratio (c) of the alluvial soils of S. Carlo (from Fioravante et al., 2013).*

4.3.3 Direct shear tests

Direct shear tests were performed on treated and untreated material to obtain the effective shear stress parameters of untreated and treated soil, since they couldn't be get from triaxial testings on treated sand (Sec. 4.3.4) (there was no pore pressure measurement during undrained monotonic triaxial tests on treated samples). To allow drainage, a slow displacement rate was adopted, as discussed further on. Only loose sand samples were tested.

Specimens preparation for untreated sand

Untreated sand specimens were prepared by pluviating oven-dried weighted sand directly into the direct shear chamber; a funnel was used for this purpose and it was kept as close as possible to the specimens surface, to obtain loose samples of similar initial void ratio. Direct shear tests on untreated sand were performed at the geotechnical laboratory of Braunschweig University of Technology.

Specimens preparation for treated sand

For treated sand, the wet pluviation technique was used. The amount of grout needed to saturate the specimen was calculated on the basis of the total and void volumes available and it was then poured into the steel square mold. The latter was put on a glass plate outside the direct shear chamber, and its borders were sealed with silicon grease, to prevent seepage. Dry sand was poured into the mold to obtain the desired D_r; once the grout had gelled, the specimens were tested after t_c. Samples were put from the square mold into the direct shear box by extrusion with a wood tamper.

Experimental procedure

Displacement-controlled tests were performed on square specimens (10x10 cm for untreated sand, 6x6 cm for treated sand), 2 cm height. The displacement rate was sufficiently low to

prevent Δu generation: it was set in 0.03 mm/min for untreated sand, while a testing velocity of 0.0015 mm/min was used for treated material. For comparison, e.g. Georgiannou et al. (2017); Wong et al. (2018) used displacement velocities of 0.005 and 0.001 mm/m for 10% and 34% CS treated samples, respectively.

The shear chamber was filled with water, to facilitate specimens saturation. Samples were kept under water during t_c. Before shearing, samples were consolidated by applying different effective vertical consolidation stresses, σ'_{vc}; the consolidation phase was considered complete after 24h. During the test, horizontal and vertical displacements, as well as the contrast force, were measured. The failure condition was assumed at the maximum shear stress, τ_{max}, achieved during the test. Figure 4.16 shows the consolidation phase of a specimen into the direct shear apparatus used for testing of treated material.

Tests setup Tests details are presented in Table 4.10, while a tests list is shown in Table 4.11.

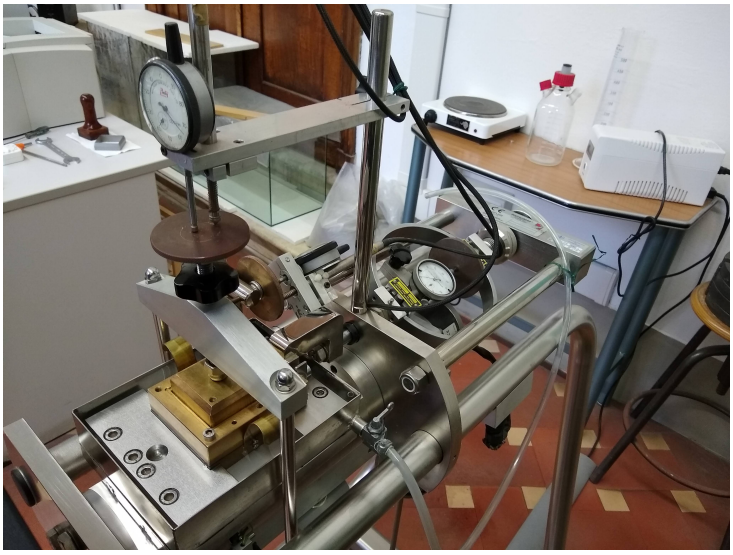

Figure 4.16: *Consolidation phase of a treated sand sample into the direct shear device.*

Table 4.10: *Direct shear tests characteristics.*

	Untreated sand	Treated sand
Loose samples	Yes	Yes
Medium-dense samples	No	No
CS_W (%)	0	2
Strain rate (mm/min)	0.03	0.0015
σ'_{vc} (kPa)	48, 98, 196, 294	49, 98, 147, 196, 294
Failure criterion	τ_{max}	τ_{max}

4.3.4 Monotonic triaxial tests

Monotonic triaxial compression tests were performed on treated and untreated material to investigate its behavior under static loading conditions. The specimens preparation methods for treated and untreated samples were identical to those described in Section 4.3.2; for monotonic

Table 4.11: *Direct shear tests on treated and untreated material.*

ID (-)	CS_W (%)	σ'_{vc} (kPa)	e_c (-)
1T	0	98	0.778
2T	0	196	0.778
3T	0	294	0.770
4T	2	98	0.778
5T	2	196	0.775
6T	2	294	0.744
7T	0	48	0.778
8T	2	49	0.776
9T	2	147	0.774

tests, however, only loose samples were tested. Silica solids contents were assumed in the range between 2 and 10%.

Experimental procedure

Before testing, all specimens were isotropically consolidated at different effective confining stresses. Drained tests were performed on untreated sand, while undrained tests without measurements of pore water pressure were performed on treated samples, since treated specimens were entirely gel-saturated, and back pressure saturation was not performed before testing, as for the case of cyclic triaxial tests. In this way, test results on treated sand can be only interpreted in terms of total stress (undrained shear resistance). Therefore, the upper drainage line was opened during consolidation and shear phases of untreated samples, while it was opened for consolidation and closed during shearing of treated material.

Strain-controlled tests were performed at an axial strain rate of 5.0%/h. The failure criterion was assumed for all specimens at the maximum deviatoric stress, q_{max}, achieved during the test. Figure 4.17a shows an example of a treated specimen during a monotonic triaxial compression test; the failure plane is clearly visible. Figure 4.17b shows the failed sample once the membrane was removed: the two parts have been divided along the shear plane to facilitate the observation.

Tests setup Tests details are presented in Table 4.12, while a tests list is shown in Table 4.13. One test (ID 8M-L) was performed after $t_c = 90$ days.

4.3.5 Oedometer tests

Oedometer tests were performed on treated and untreated sand to evaluate the compressibility of the materials. To date, the latter has not been enough investigated for treated material, therefore this aspect needs to be carefully analyzed to provide useful knowledge for future research.

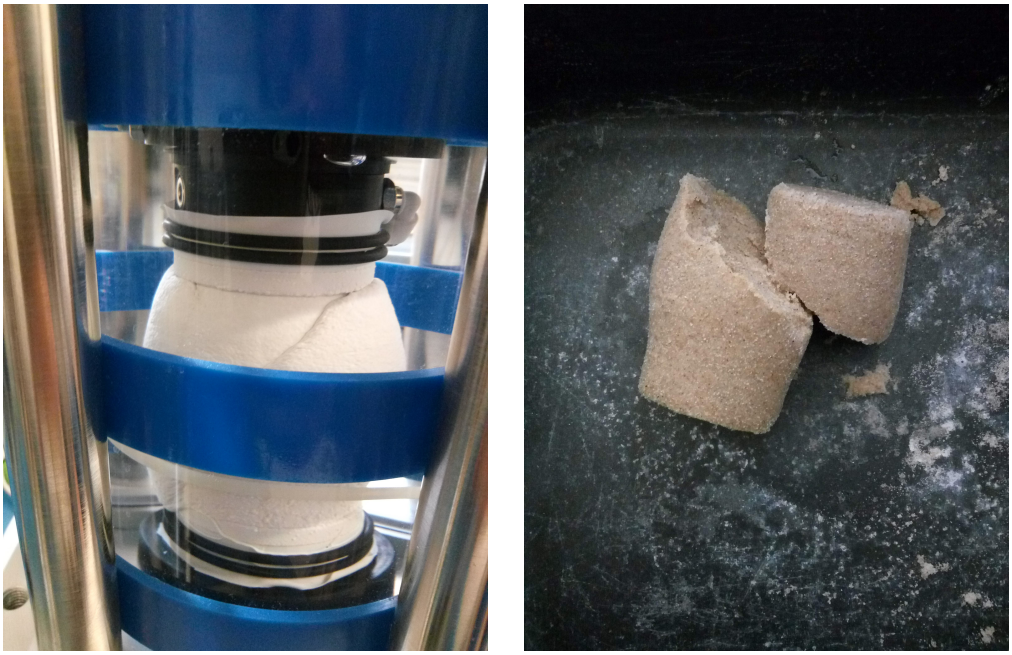

(a) (b)

Figure 4.17: *5% CS treated triaxial specimen during monotonic compression test (a) and after the test was dismantled (b).*

Table 4.12: *Monotonic triaxial tests characteristics (*=referred to $CS_W = 10\%$).*

	Untreated sand	Treated sand
Loose samples	Yes	Yes
Medium-dense samples	No	No
CS_W (%)	0	2, 3, 5, 10
Drained tests	Yes	No
Axial strain rate (%/h)	5.0	5.0
Back pressurization before shearing	Yes	No
σ'_c (kPa)	50, 100, 200, 300	50, (96*) 100, (200*) 200, (282*) 300
Failure criterion	q_{max}	q_{max}

Table 4.13: *Monotonic triaxial tests on treated and untreated material.*

ID (-)	CS_W (%)	σ'_c (kPa)	e_c (-)
1M	0	50	0.765
2M	0	100	0.763
3M	0	200	0.775
4M	0	300	0.790
5M	2	50	0.734
6M	2	100	0.774
7M	2	200	0.752
8M	2	300	0.783
8M-L	2	287	0.777
9M	3	50	0.737
10M	3	100	0.759
11M	3	200	0.767
12M	3	300	0.766
13M	5	50	0.760
14M	5	100	0.756
15M	5	200	0.778
16M	5	300	0.740
17M	10	96	0.770
18M	10	200	0.749
19M	10	282	0.759

Specimens preparation for untreated sand

Untreated sand specimens were prepared by pouring dry weighted sand into the oedometer mold to achieve a prefixed initial void ratio. Dry porous stones were put at the top and at the bottom of the samples; the oedometer cell was then filled with distilled and deaired water. Saturation was considered completed after one day.

Specimens preparation for treated sand

Treated sand samples were prepared in two different ways. In the first method (referred to as method A), dry sand was poured into the oedometer steel ring that was previously partly filled with colloidal silica grout. The amount of grout required to saturate the specimens was equal to the calculated volume of voids. In the second method (permeation, referred to as method B), dry sand was used to form the samples directly into the ring, as it was for untreated sand, and they were subsequently treated with CS grout poured by means of a syringe (not embedded) from the top of the specimens. The amount of grout was equal to the volume of voids.

These different methods for treated sand were chosen to replicate those proposed by Researchers who showed 1D-compression test results on silica treated material, for comparison of the results. In their studies, Georgiannou et al. (2017) and Wong et al. (2018) adopted method A and B, respectively. Method A was used more extensively in the present work, since it allowed full gel-saturation and a better replication of treated samples.

Treated specimens were always prepared outside the oedometer cell: the steel ring was

firstly put above a glass plate and sealed with silicon grease to prevent leaks from the bottom; once the specimen was formed and gelled, the ring was removed and put into the oedometer cell, with saturated porous stones at the top and at the bottom. The oedometer cell was filled with distilled and deaired water, and the specimen was left to cure for t_c. Saturation of untreated samples was considered completed after the same t_c under water.

Several CS contents were tested: beyond high-diluted grouted sand (i.e. $CS_W < 5\%$), few tests were performed on samples treated with $CS_W = 10\%$ and 13%, as a consequence of the results obtained from the first set of analysis, as discussed in the following Chapter.

Experimental procedure

After t_c was reached, the load sequence started; each loading step was applied conventionally for 24h. Both loading and unloading sequences were used. Two different sets of oedometer cells were used: one set, named Oedometer 1, has oedometer rings with diameter of 71.00 mm, while the other one (Oedometer 2) has rings with diameter of 50.47 mm. The height of the rings was the same for oedometer 1 and 2 and equal to 20 mm. Both the sets consist of three cells: the first apparatus is made of back-loading machines, while the second one is made of front-loading devices; oedometer 1 and 2 are shown in Figure 4.18a, b, respectively.

(a) (b)

Figure 4.18: *Different oedometer devices used in this work: oedometer 1 (a) and 2 (b).*

Tests setup Tests details are presented in Table 4.14 and the applied loading/unloading sequences are reported in Table 4.15. The initial height of the specimens was 20 mm for all samples. During tests 14E, 15E and 16E, several loading and unloading sequences were applied to the samples, with the aim of evaluating the effects of reloading after first compression. Tests 17E-18E were only subjected to two loading steps and they were used to assess the good quality

of samples prepared according to method A and the settlements viscous component exhibited by treated material.

Table 4.14: *1D confined compression tests on treated and untreated material.*

ID (-)	CS_W (%)	Method (-)	Oedometer (-)	e_0 (-)
1E	0	-	1	0.777
2E	5	A	1	0.795
3E	2	A	1	0.789
4E	3	A	1	0.745
5E	2	A	1	0.800
6E	5	A	1	0.805
7E	10	A	1	0.784
8E	10	A	1	0.784
9E	13	A	1	0.798
10E	0	-	2	0.795
11E	2	A	2	0.795
12E	5	A	2	0.795
13E	0	-	2	0.795
14E	2	B	2	0.780
15E	5	B	2	0.780
16E	10	B	2	0.780
17E	5	A	1	0.780
18E	5	A	1	0.779

Table 4.15: *Loading sequences for confined 1D compression tests. In brackets: loading/unloading step not performed for all tests.*

ID (-)	Loading sequence (kPa)	Unloading sequence (kPa)
1E-9E	10, 25,, 50, 99, 198, 396, 793, 1586	1586, 396, (25), 10
10E-16E	12, 25, 50, 100, 200, 400, 800, 1600	1600, 400, (25), (12)
17E-18E	248, 496	-

Chapter 5

Results and discussion

5.1 Introduction

In this Section, the main results of the experimental laboratory testings are presented and discussed by introducing the following quantities: the deviatoric stress $q = \sigma_1 - \sigma_3 = \sigma'_1 - \sigma'_3$, where σ_1 (σ'_1) and σ_3 (σ'_3) are the major and minor principal total (effective) stresses, and the mean effective stress, $p' = \frac{\sigma'_1 + 2\sigma'_3}{3}$. The axial strain is $\epsilon_a = \frac{H_0 - H}{H_0}$, being H_0 and H the height of the specimen at the initial state and at the state at which ϵ_a is calculated in triaxial tests, respectively. The deviatoric strain $\epsilon_q = \frac{2}{3} \cdot (\epsilon_a - \epsilon_r)$, being $\epsilon_r = \frac{D - D_0}{D_0}$ the radial strain, is also used. The volumetric strain is $\epsilon_{vol} = \epsilon_a + 2\epsilon_r$. According to the assumed sign convention, positive strain means compression of the sample. Vertical strain in 1D compression tests is defined as $\epsilon_v = \frac{H_0 - H}{H_0}$. Other relevant quantities are introduced and described further on. The complete list of test results is shown in the Appendix.

5.2 Cyclic triaxial tests

5.2.1 Untreated sand

Figure 5.1 shows the typical output of a cyclic triaxial test on untreated sand; in this case, the test 4C (medium-dense sand) is presented. The increase of r_u over N reflects the pore pressure development during the loading cycles; at the same time, effective stresses (p') are reduced, and the soil strain (ϵ_a, ϵ_q) develops; this sample liquefied after 8 cycles, being verified the condition $r_u = 1$.

Figure 5.2 shows the results of test 2C (medium-dense sand). In this case, the condition $\epsilon_{DA} = 5\%$ indicated liquefaction after N=55.5. The pore pressure ratio (i.e. the mean effective stress) never reaches zero value; the axial strain fluctuates around zero for many cycles before it gets greater, inadmissible values.

Liquefaction resistance curves The liquefaction resistance curves for untreated sand were obtained by putting the failure points obtained from tests in the N-CSR plane, and subsequently by means of a power regression of experimental data. The curves are reported in Figure 5.3 for both loose and medium-dense sand. As it was expected, the liquefaction resis-

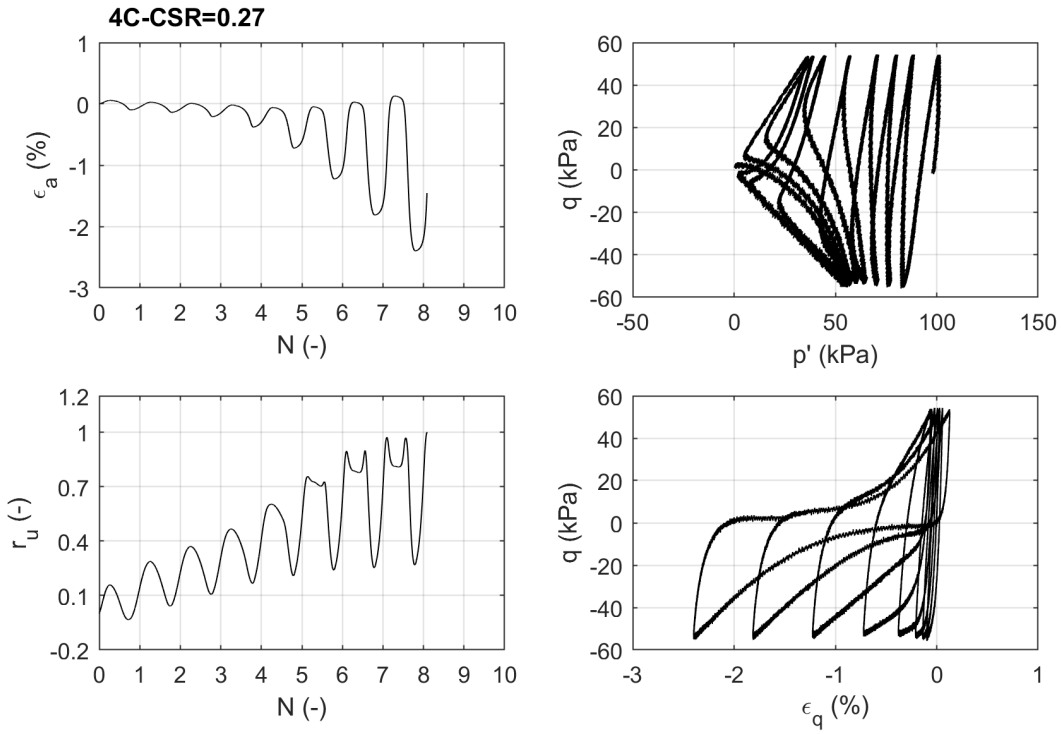

Figure 5.1: *Results of a cyclic triaxial test (liquefaction test, $r_u = 1$) on medium-dense untreated sand (ID=4C). Clockwise from top left: number of cycles versus axial strain, mean effective stress versus deviatoric stress, deviatoric strain versus deviatoric stress and number of cycles versus excess pore water pressure ratio.*

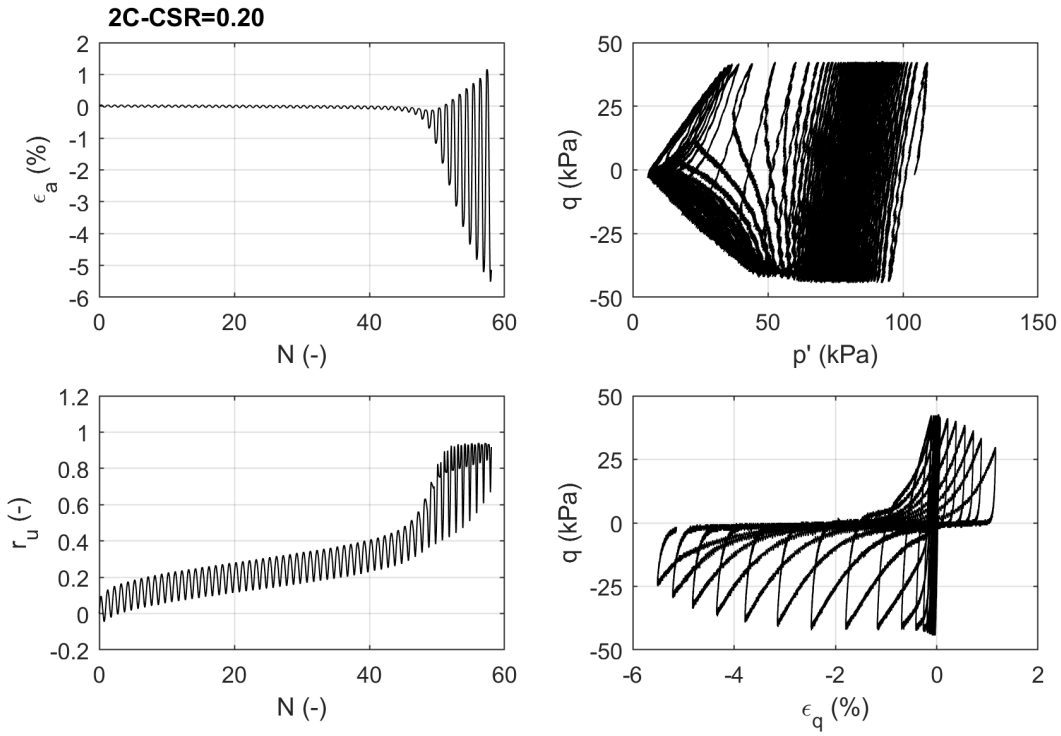

Figure 5.2: *Results of test 2C on medium-dense untreated sand.*

tance of medium-dense sand is higher than that of the looser one, confirming that the increase in relative density improves the soil performances under cyclic loading conditions. The black arrow close to the $CSR = 0.11$ point, on the right side of the graph, indicates that no failure was achieved during that test (number of loading cycles $N > 100$).

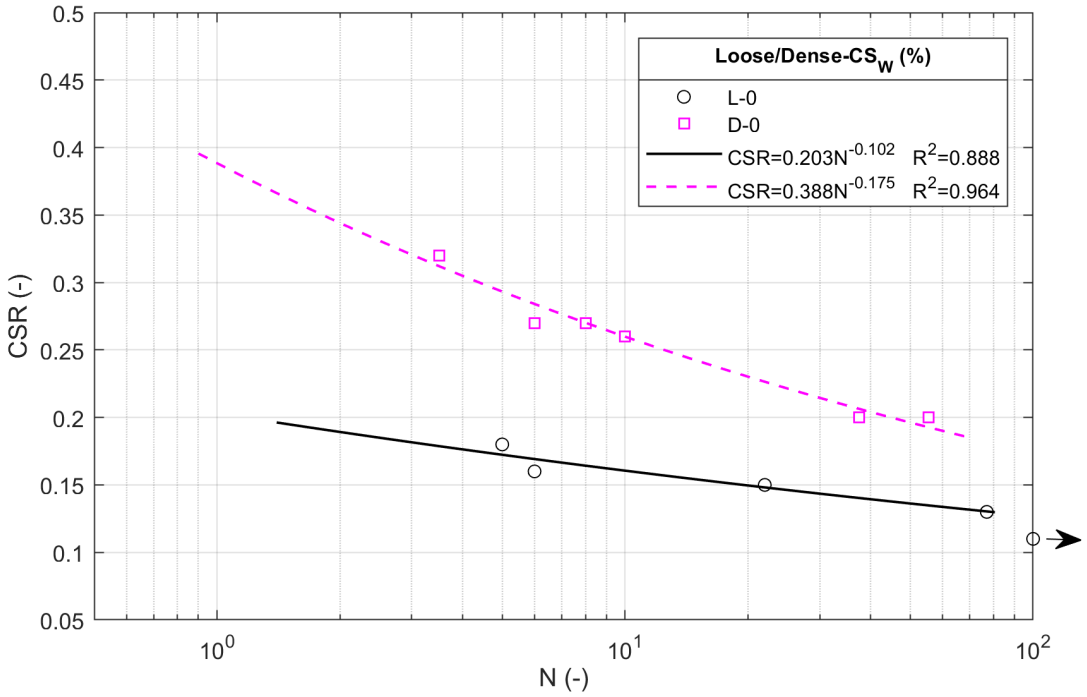

Figure 5.3: *Liquefaction resistance curves for untreated loose and medium-dense sand obtained from undrained cyclic triaxial tests.*

5.2.2 Treated sand

As stated in Chapter 4, back pressure was not applied to treated sand specimens and the pore pressure was not recorded during cyclic undrained tests. It followed that the liquefaction criterion was expressed in terms of axial strain, as previously discussed.

Figure 5.4 and 5.5 show the results obtained from cyclic triaxial tests on 5 and 2% CS treated sand, respectively; the former indicates that failure didn't occur ($\epsilon_{DA} < 5\%$ for $N > 100$), while the latter sample underwent liquefaction after 6.5 cycles. The axial strain was found not to be symmetric about the zero value, but it developed toward the extension zone: this result is consistent with other literature data (e.g. Gallagher and Mitchell, 2002; Porcino et al., 2011). It is thought that this is due to a sort of 'fatigue' phenomenon of the treated material.

Figure 5.6 shows the results for 5% CS treated sand; in this case, the specimen reached failure after 6.5 cycles.

Liquefaction resistance curves Figure 5.7 shows the liquefaction resistance curves of treated and untreated materials (loose state). It is confirmed that CS_W=5% improves the liquefaction resistance of loose sand, according to literature data (Chapter 3); in addition, however, it is shown that even high-diluted 2% CS grout is enough to improve the soil behavior under cyclic

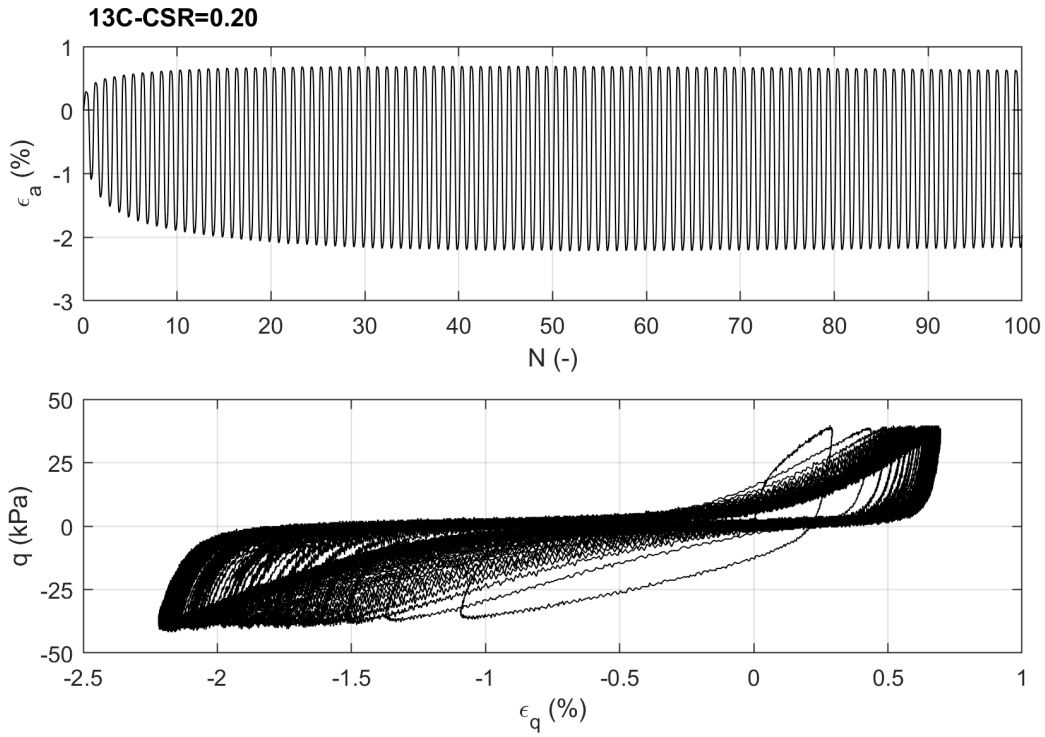

Figure 5.4: *Results of liquefaction test on loose treated sand (ID=13C, $CS_W = 5\%$).*

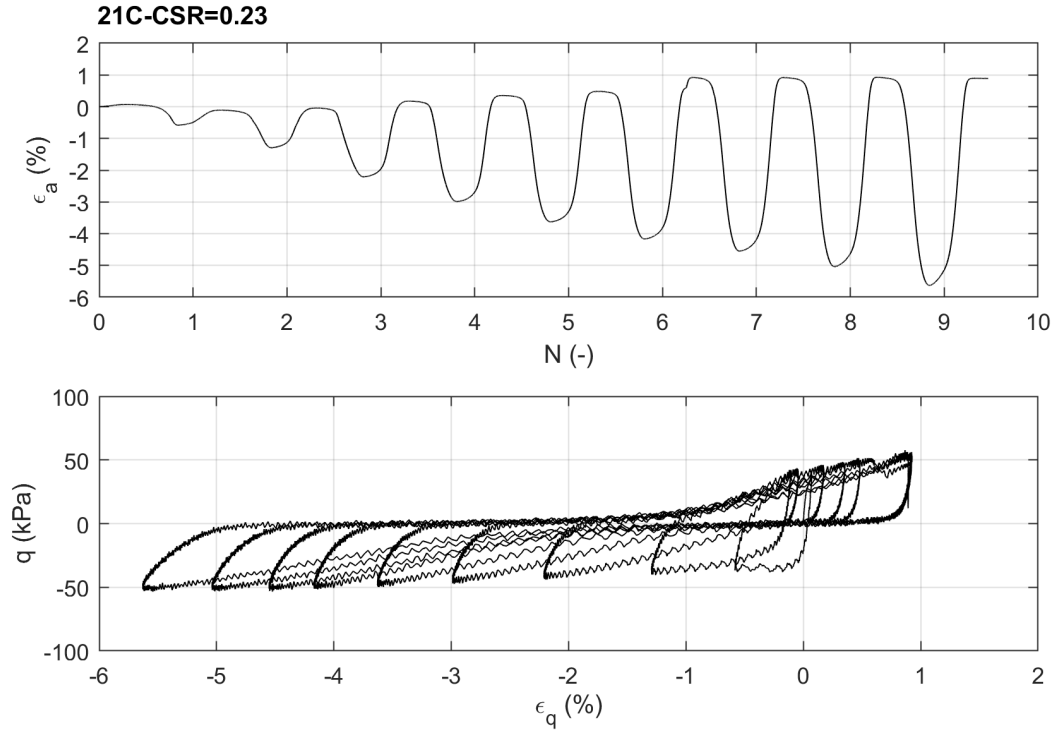

Figure 5.5: *Results of liquefaction test on loose treated sand (ID=21C, $CS_W = 2\%$).*

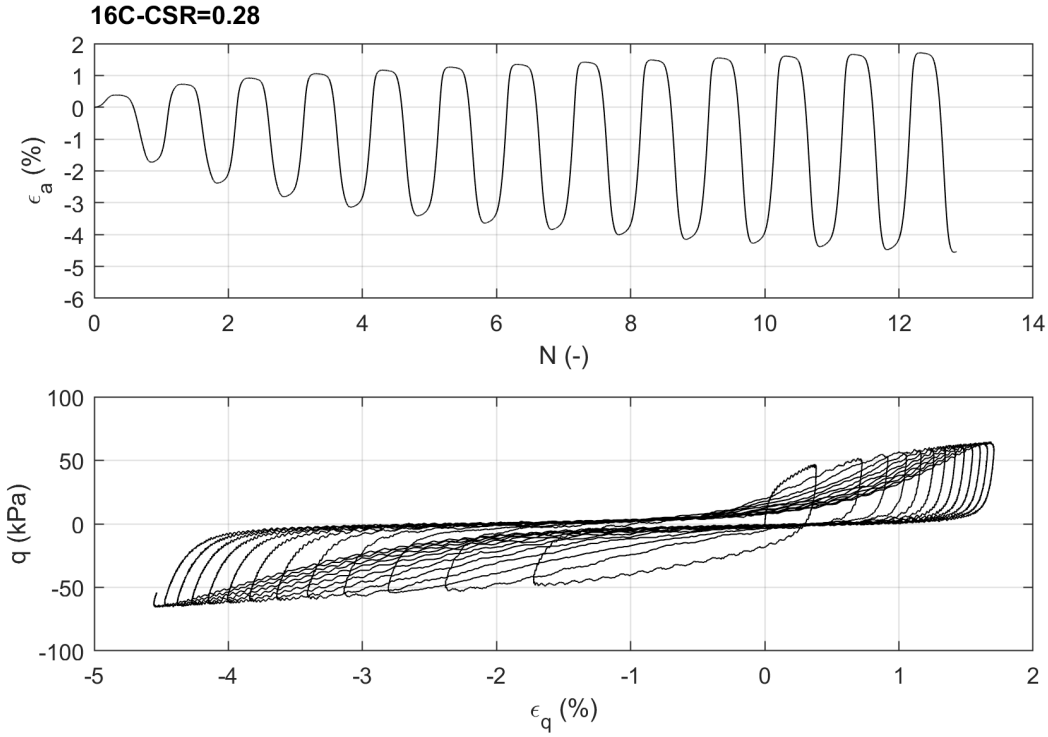

Figure 5.6: *Results of liquefaction test on loose treated sand (ID=16C, $CS_W = 5\%$).*

loading conditions, since the CRR curve is higher than the corresponding one for untreated sand. It means that the normalized cyclic stress required to induce liquefaction increases with increasing CS_W. This clearly indicates that low CS contents (i.e. 2% CS 'weak' gel) can be successfully adopted to mitigate the liquefaction risk of a potentially liquefiable sand.

It is useful to define an improvement factor, I_f, as the ratio between the normalized stress ratio of treated sand and that of the untreated one (Eq. 5.1). Figure 5.8 shows how I_f varies with N. The effect of the improvement is clearly represented by the increase of I_f as CS_W increases. The curves are almost parallel in the N-I_f plane, suggesting that, given a similar initial state, the increase in liquefaction resistance is entirely related to the amount of silica diluted in the stabilizing grout. By calculating I_f from literature data (Porcino et al., 2011) ($CS_W = 10\%$) and plotting its curve in the same Figure, it can be seen that the variation trend is comparable to that obtained in this study; furthermore, it is shown that, although the test conditions are slightly different from the two sets of experiments, the increase of I_f does not seem to be linearly related with CS_W (i.e. the 'amount' of improvement is not linear with silica content): it is likely that the properties of treated material are markedly different as CS_W increases. I_f decreases with N: the gel matrix degrades with loading cycles; for $N = 15$, I_f for $CS_W = 2\%$ is ≈30% greater than the corresponding reference value for untreated sand.

$$I_f = CSR_{Treated}/CSR_{Untreated} \tag{5.1}$$

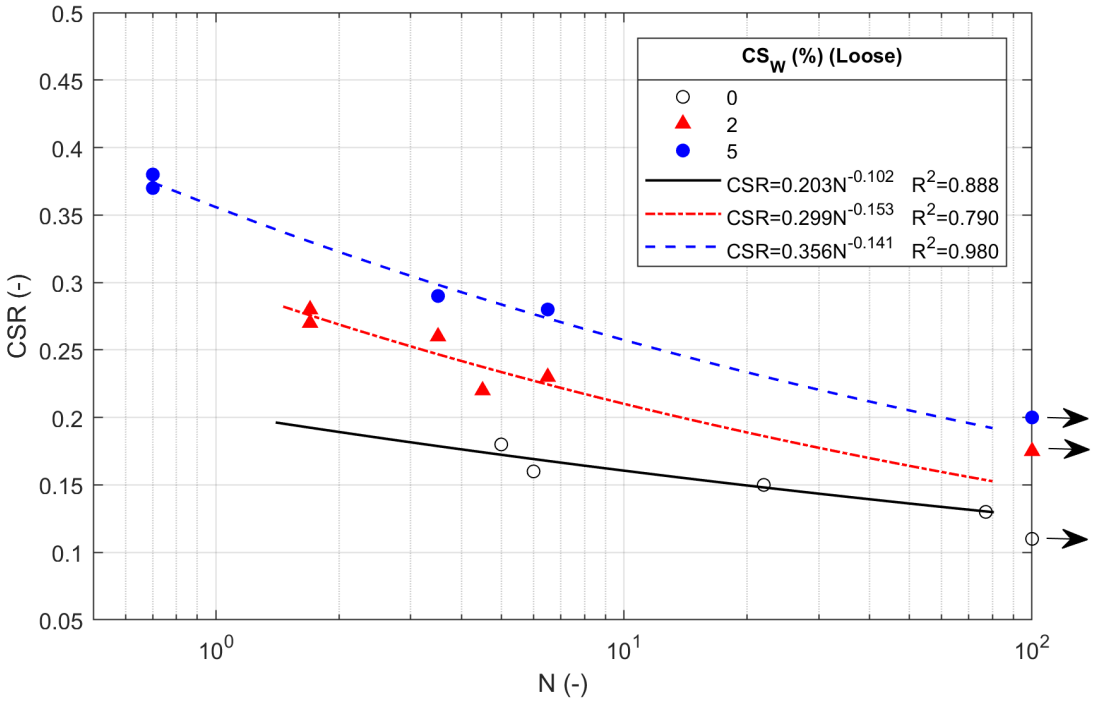

Figure 5.7: *Liquefaction resistance curves for treated (CS_W=2, 5%) and untreated material from undrained cyclic triaxial tests.*

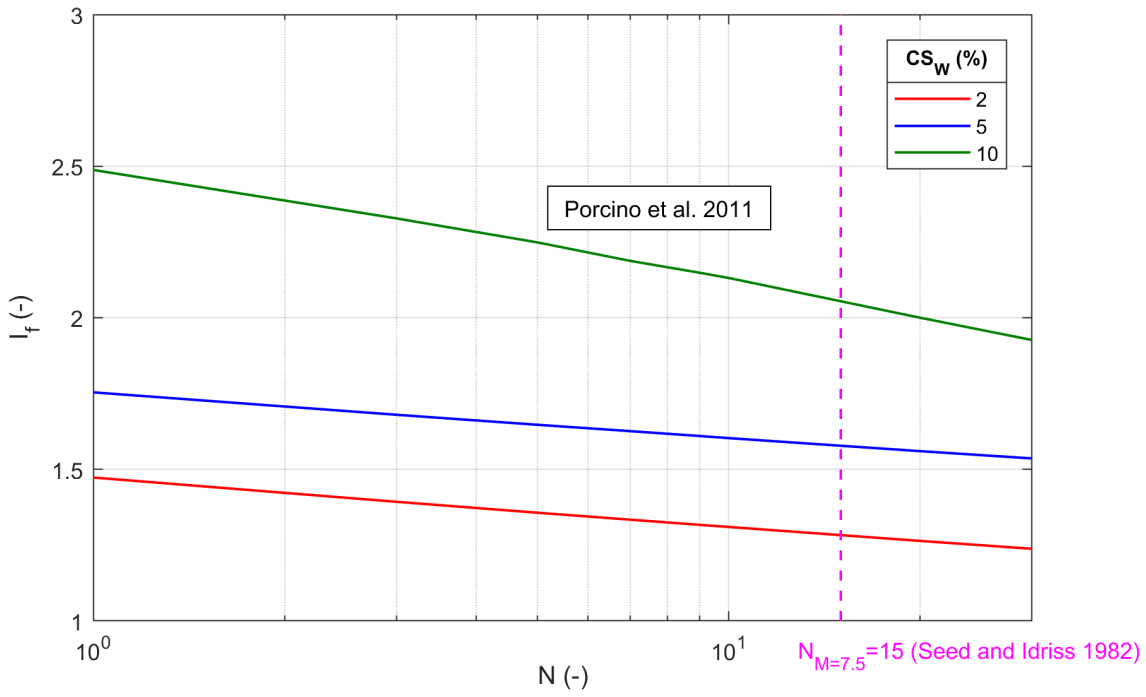

Figure 5.8: *Improvement factor I_f versus number of cycles N and comparison with data from Porcino et al. (2011).*

5.3 Direct shear tests

5.3.1 Untreated sand

The results of direct shear tests are shown for untreated sand in Figure 5.9a, b, where τ, S_h and S_v are the shear stress, the horizontal and vertical displacements, respectively. The maximum vertical strains corresponding to the measured values of S_v are ≈0.5% and ≈-1.5%. It is worth noting that, after an initial contraction, the sand exhibited a dilative behavior, despite being the specimens loose. This aspect is ascribed to the characteristics of S3 sand, which has a quasi-uniform grain size distribution of round or sub-rounded particles: the grain shape and uniformity facilitate the grain sliding and rolling over each other, thus forcing the volume to increase during shearing even if D_r is low.

5.3.2 Comparison between treated and untreated sand

Figure 5.10a, b, shows the test results on treated sand compared with those obtained for the untreated material. It can be observed that the presence of gel affects the soil shear resistance; in particular, the drained peak shear strength increases over the whole range of investigated consolidation stresses. Volumetric changes of treated and untreated S3 sand confirm a dilative behavior also for treated sand; however, according to literature data, some more dilation were expected compared to that exhibited by the untreated sand. This could be due to the initial low D_r of specimens used in this study, if compared to data reported by e.g. Porcino et al. (2012).

Figure 5.11 shows the failure envelopes drawn in the shear plane; ϕ' and c' (internal friction angle and cohesion) were calculated from experimental data by means of a linear regression and by assuming a Mohr-Coulomb failure criterion for soil (Eq. 2.2). Their values for treated and untreated sand are listed in Table 5.1. It can be stated that CS gel provides the material with an artificial cohesion, and that this latter is essentially responsible for the improved soil behavior, being the values of ϕ' practically unaffected by the presence of pore gel. Thus, failure envelopes of treated and untreated material are found to be almost parallel. This result is in agreement with those reported in previous studies (Porcino et al., 2012; Nouri Delavar and Noorzad, 2017; Kakavand and Dabiri, 2018), but it is herein shown that a 'weak' 2% CS gel improves the shear resistance of treated soil, at least over the investigated range of vertical consolidation stresses. The small increase in ϕ' is probably because of the increased roughness of grains after CS treatment.

Direct shear tests showed that treated sand is provided by a small amount of cohesion. Bonding of grains by means of siloxane bonds is the mechanism of soil improvement, as claimed in literature by several Authors (Persoff et al., 1999; Gallagher and Mitchell, 2002; Gallagher and Lin, 2005; Gallagher et al., 2007a).

The curves plotted in Figure 5.10b for treated material seems in disagreement with the values of σ'_{vc} they refer to. This is ascribed to the specimens' disturbance, a consequence of the extrusion process from the mold into the shear box. This procedure was necessarily followed for all treated sand specimens tested in direct shear, while, for instance, it was not necessary for oedometer samples. It is worth noting that, after applying the vertical load, the shear stress can be considered practically unaffected by the initial disturbance due to the extrusion of the spec-

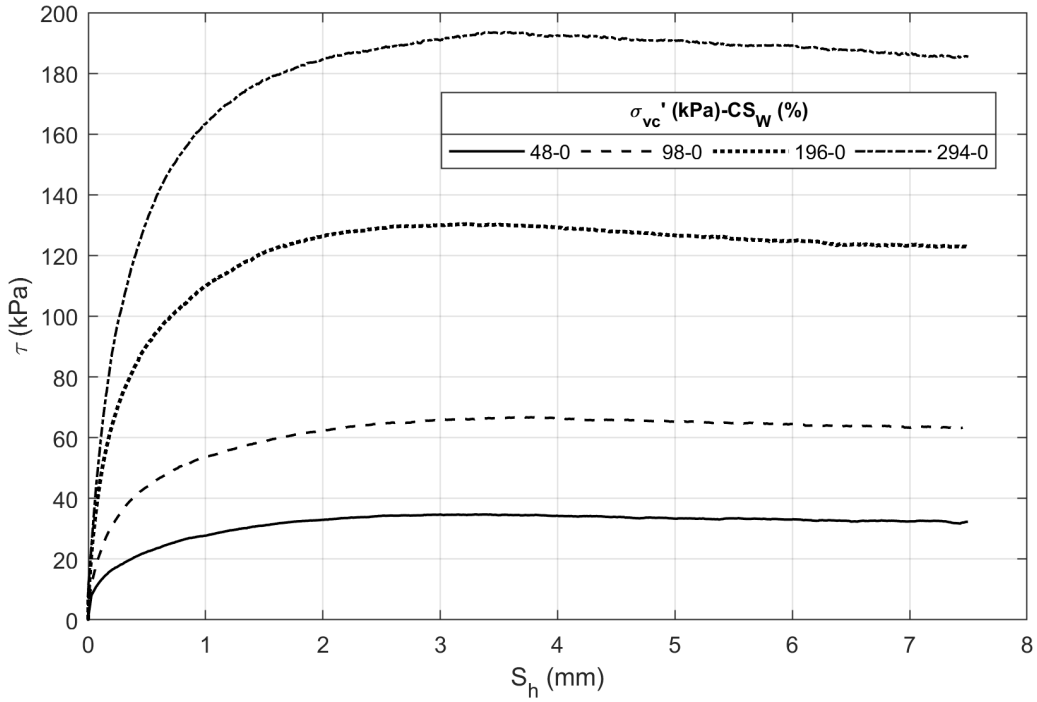

(a)

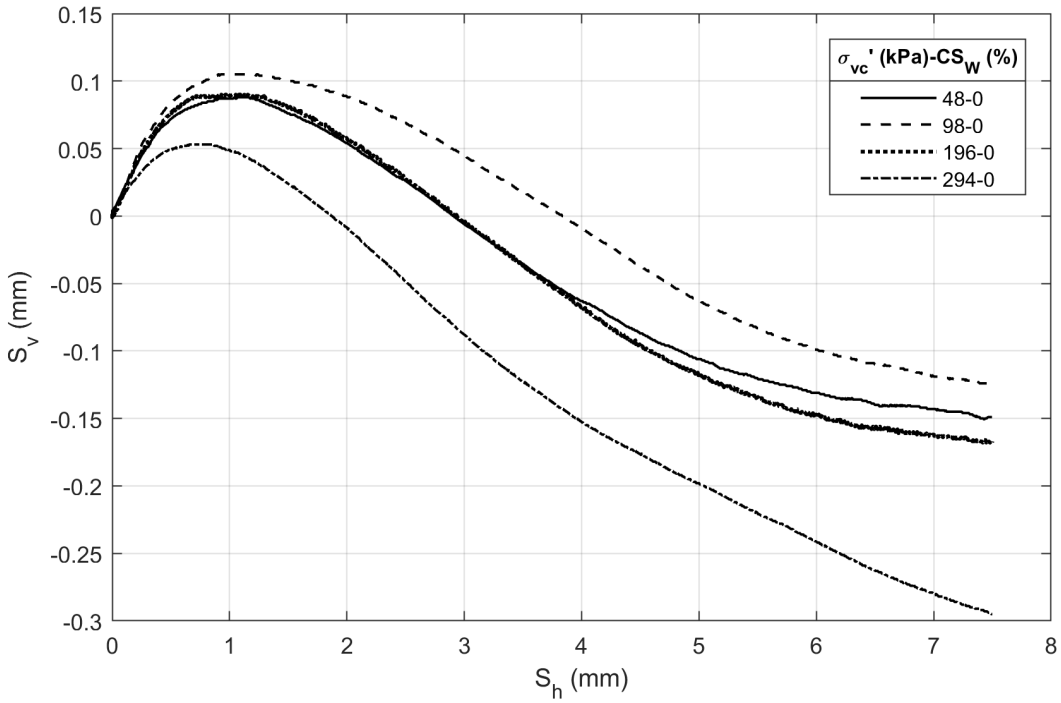

(b)

Figure 5.9: *Shear stress versus horizontal displacement (a) and vertical against horizontal displacement (b) from direct shear tests on untreated sand.*

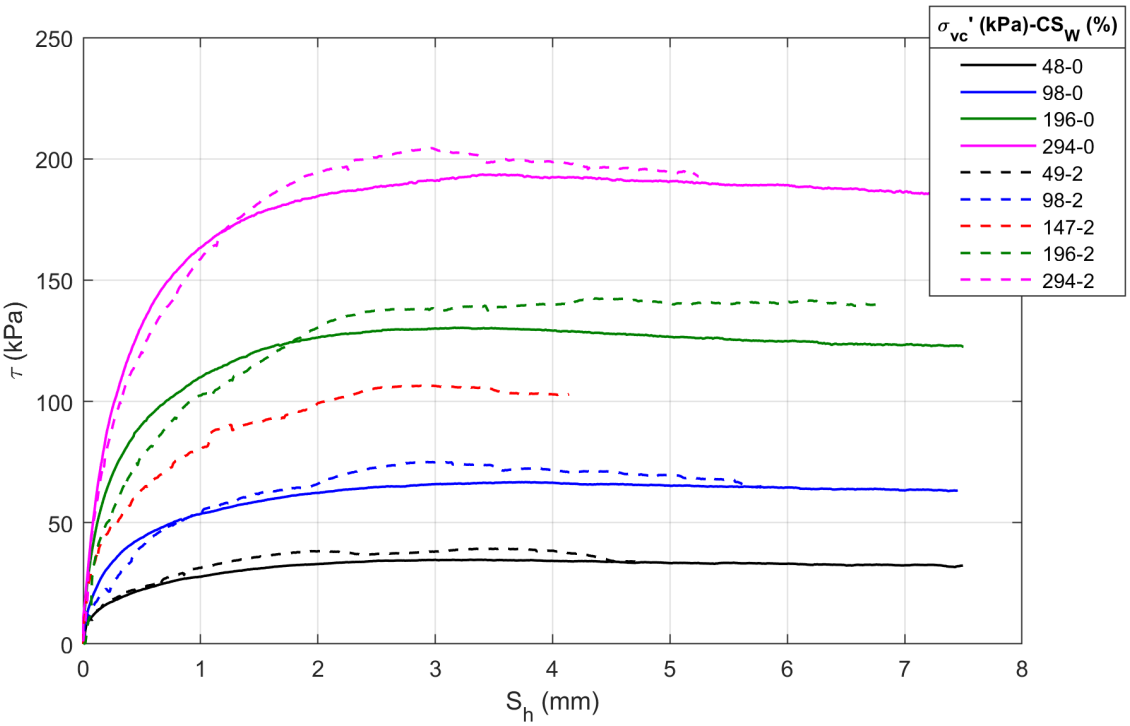

(a)

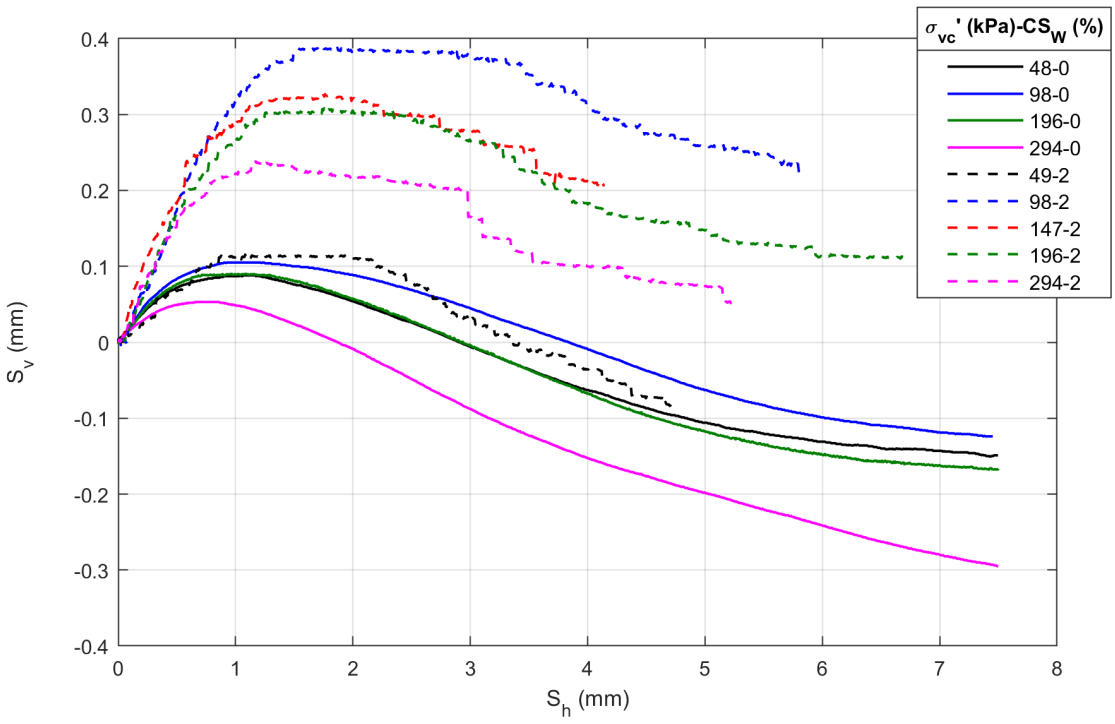

(b)

Figure 5.10: *Shear stress versus horizontal displacement (a) and vertical against horizontal displacement (b) from direct shear tests on treated and untreated sand.*

imen. To confirm this statement, in Figure 5.10a all the plotted curves are consistent with their σ'_{vc} value and with data for untreated sand. For this reason, in this study, the compressibility of treated as well as untreated sand was investigated by means of oedometer tests; a simple test on treated sand, described in detail in Section 5.6, was carried out to show the minimal disturbance of samples tested in the oedometer cell compared to that exhibited by a specimen tested in the direct shear box and to show the very good quality of oedometer specimens.

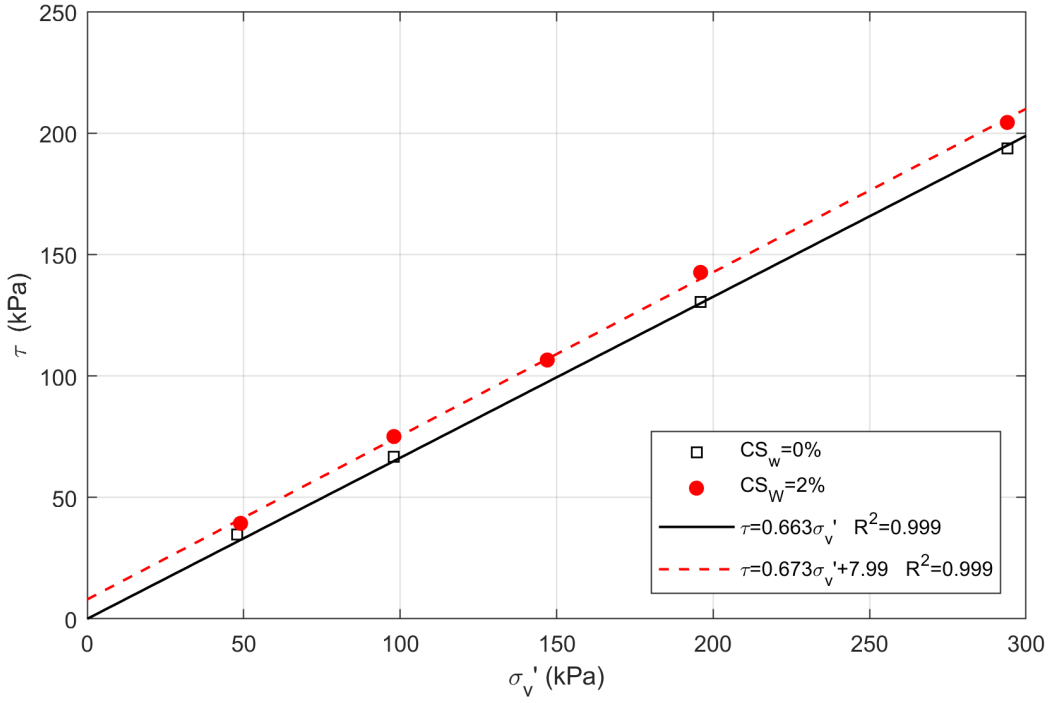

Figure 5.11: *Failure envelopes for treated and untreated sand from direct shear tests.*

Table 5.1: *Drained shear strength parameters for S3 treated and untreated sand from direct shear tests.*

ϕ' (°)	c' (kPa)	CS_W (%)
33.5	0	0
33.9	7.99	2

5.4 Monotonic triaxial tests

5.4.1 Untreated sand

The results of drained monotonic tests on untreated sand are reported in Figure 5.12a in terms of axial strain against deviatoric stress, while Figure 5.12b shows the specimens dilative behavior, over the whole investigated range of σ'_c. S3 sand shows a slightly volume increase after initial contraction, as it has happened in direct shear tests. Grains mutual sliding is enhanced by the proper characteristics of S3 sand. As σ'_c increases, q and ϵ_{vol} increases and decreases, respectively, given a certain value of ϵ_a.

The shear strength parameters were obtained by means of linear regression of failure points; the s'-t' plane, being $s' = \frac{\sigma'_1+\sigma'_3}{2}$ and $t' = \frac{\sigma'_1-\sigma'_3}{2}$, was adopted for this purpose, as shown in Figure 5.13. The values of ϕ' and $c'$are reported in Table 5.2; they are comparable with those ones obtained from direct shear tests on untreated sand (Tab. 5.1) and they are consistent for loose sand.

Table 5.2: *Drained shear strength parameters for S3 sand from monotonic triaxial tests.*

ϕ' (°)	c' (kPa)
33.7	0

5.4.2 Treated sand versus untreated sand

As illustrated in Table 4.12, several CS contents were tested under monotonic loading conditions. A comparison among the results obtained from triaxial tests on treated and untreated sand is provided, pointing out how the CS treatment modifies the monotonic behavior of treated material.

The comparison is shown in Figure 5.14 in terms of axial strain and deviatoric stress. Over the whole range of σ'_c and CS_W, treated sand exhibited higher peak stress; q_{max} increased as CS_W increased. Higher peak stress, if compared to that of untreated sand, was detected also for CS_W=2%. Therefore, the higher the CS content, the higher q_{max}, given an effective confining stress. These results confirm that CS treatment improves the soil behavior under static loading conditions, being the soil performances related to CS_W. The behavior of treated sand becomes significantly different from that of untreated sand as CS_W increases, as it is shown in Figure 5.15, where the stress-strain curves for treated and untreated material consolidated at $\sigma'_c = 200$ kPa are reported; for $CS_W = 10\%$, q_{max} is strongly higher than for untreated material.

As can be seen from Figure 5.14, the stress-strain curve of treated material is slightly under that of untreated S3 sand in the small strain region. In particular, the tangent modulus at small strain levels (i.e. $\epsilon_a \leq 2\%$), calculated as the slope of the stress-strain curves for each 0.1% interval of axial strain up to 2%, is much lower for 5% treated sand than for the untreated one. In Figure 5.16 the ratio between the tangent modulus for samples treated with a x% CS grout solution, E_x, and that of the untreated one, E_0, is plotted versus ϵ_a for different effective confining pressures. For 5% CS treated sand, the modulus is significantly lower than for 2% and 3% CS, for which it is much closer to E_0. Negligible variation respect to the unity is revealed, in the whole range of the considered ϵ_a, for the ratios $\frac{E_2}{E_0}$ and $\frac{E_3}{E_0}$, while the values of $\frac{E_5}{E_0}$ increase with axial strain, thus indicating that the development of peak shear resistance is delayed and slower than for untreated sand. This fact can be ascribed to the presence of gel, that facilitates grain rearrangement under triaxial loading conditions: in particular, such an effect becomes significant only for $CS_W > 3\%$ and it is less significant as σ'_c increases (e.g. Fig. 5.15). Similar conclusions can be inferred from Figure 5.10a where the results of direct shear tests are shown.

Since pore water pressure was not recorded during tests on treated sand, data analysis was only possible in terms of total stresses. Figure 5.17 shows that an increase in CS content induces an increase in the maximum shear stress at failure (i.e. the undrained shear strength), for all

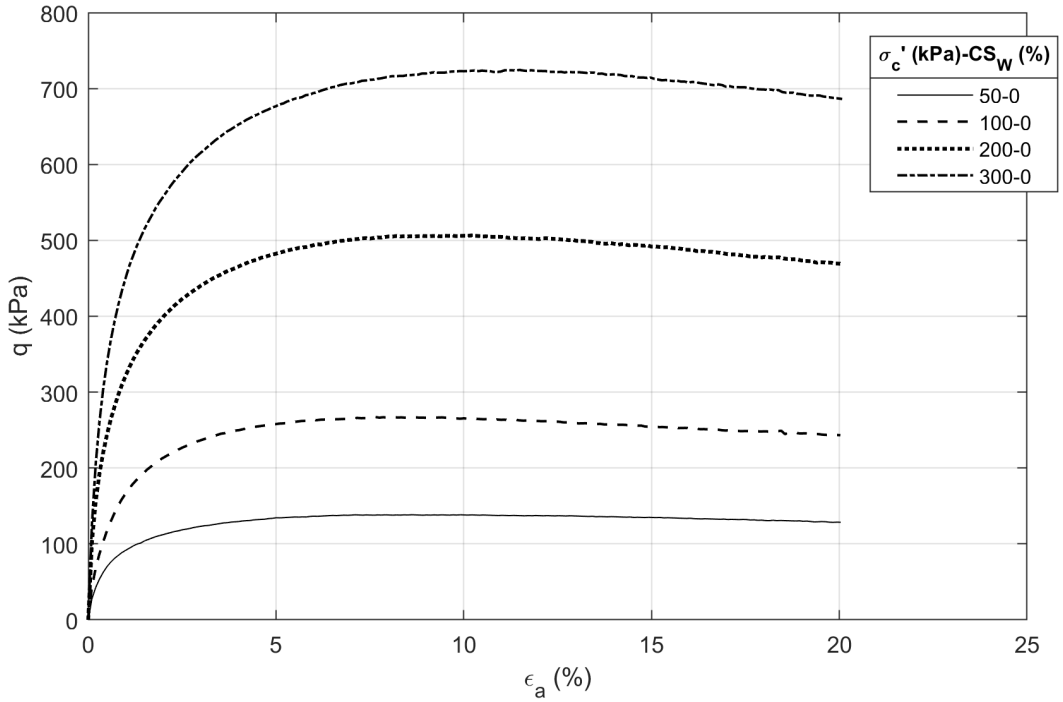

(a)

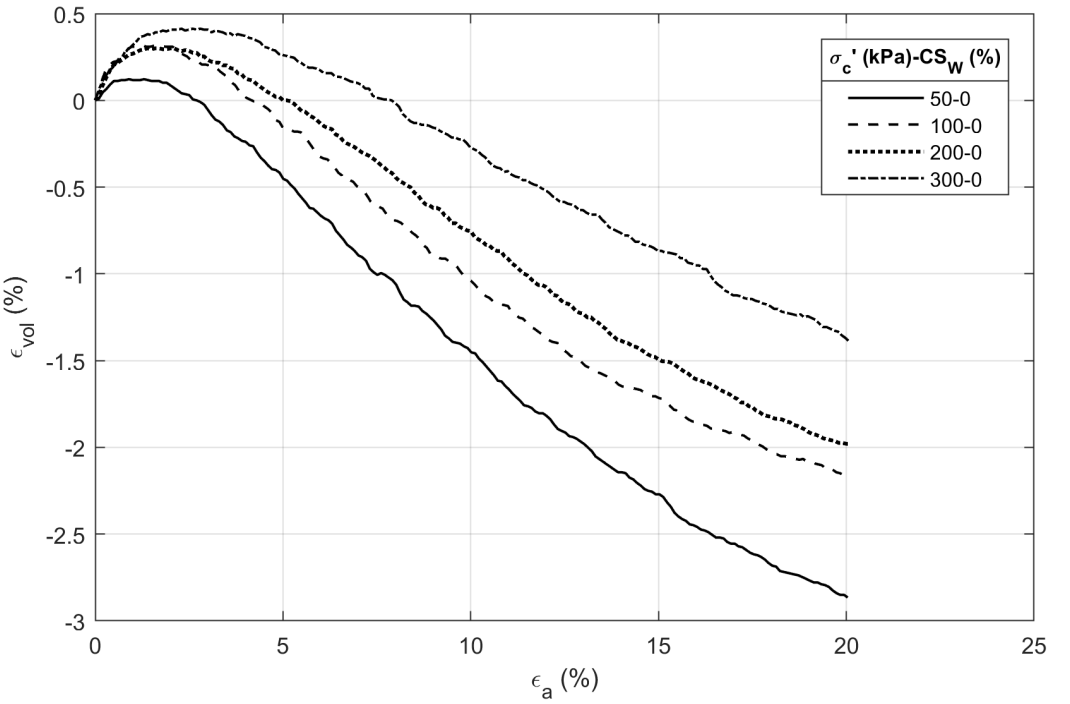

(b)

Figure 5.12: *Deviatoric stress versus axial strain (a) and volumetric strain against axial strain (b) from triaxial tests on untreated sand.*

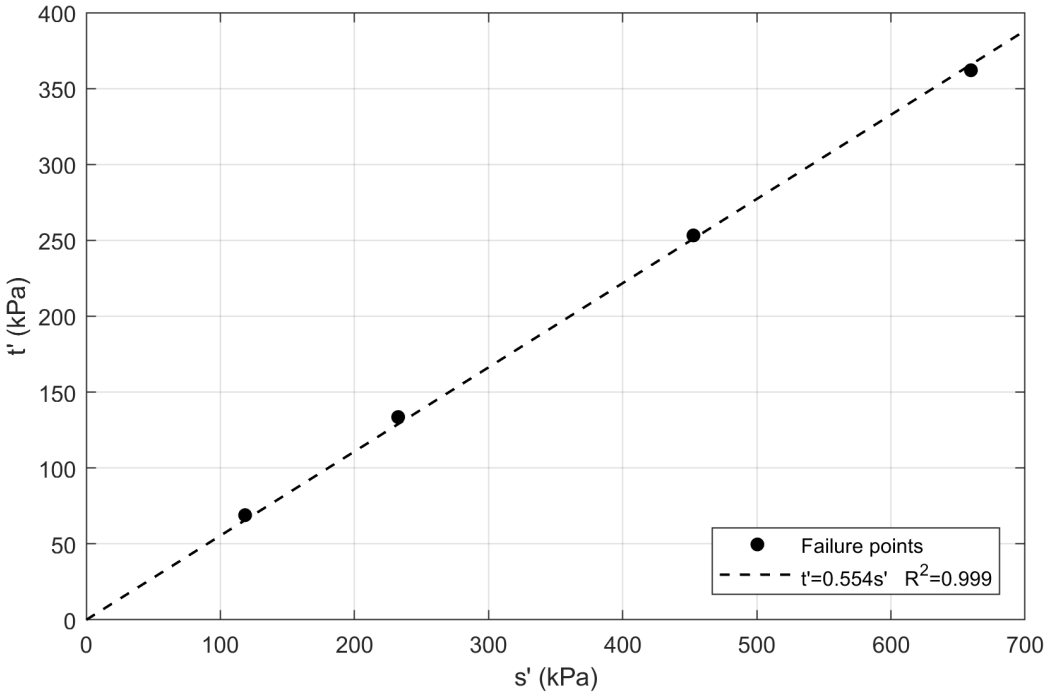

Figure 5.13: *Failure envelope for untreated sand in the s'-t' plane from drained monotonic triaxial tests.*

the given values of σ'_c. It is reasonably hypothesized that failure envelopes would be almost parallel in the $s' - t'$ plane, as they are in Figure 5.11, suggesting that cohesion, given by CS treatment, is mainly responsible for the improved soil performances under monotonic loading.

5.4.3 Effects of t_c on the mechanical response of treated sand

Several researchers have shown that the improvement of mechanical properties of soil treated with CS are affected by (curing) time. As described in Chapter 3, e.g., the unconfined compression strength of grouted samples increases as curing time increases. In this study, the effects of curing time on 2% CS grouted specimen was investigated by performing a monotonic triaxial test, according to the procedures described in Chapter 4, to verify the performances of treated material. Figure 5.18 shows the comparison of a triaxial test conducted on a 2% CS grouted sample performed after $t_c = 90$ days with data from treated and untreated samples. During curing, this sample was kept inside the latex membrane sustained by the mold, being the top and bottom caps sealed with valves, avoiding evaporation. As can be seen, the peak deviatoric stress increases with t_c, for a given CS_W; the difference between peaks, however, is quite small (approximately 22 kPa between the q peaks for treated sand tested after 5 days and 90 days) and it was not expected to be much greater if σ'_c was exactly the same value for both tests (300 kPa for $CS_W = 0\%, 2\%$ and $t_c = 5$ days, 287 kPa for $CS_W = 2\%$ and $t_c = 90$ days). Together with the results obtained from pocket penetrometer tests (preliminary tests), this result validates the choice of using $t_c = 5$ days as the standard curing time in this study (i.e. the most of the available shear resistance is developed within 5 days from t_g).

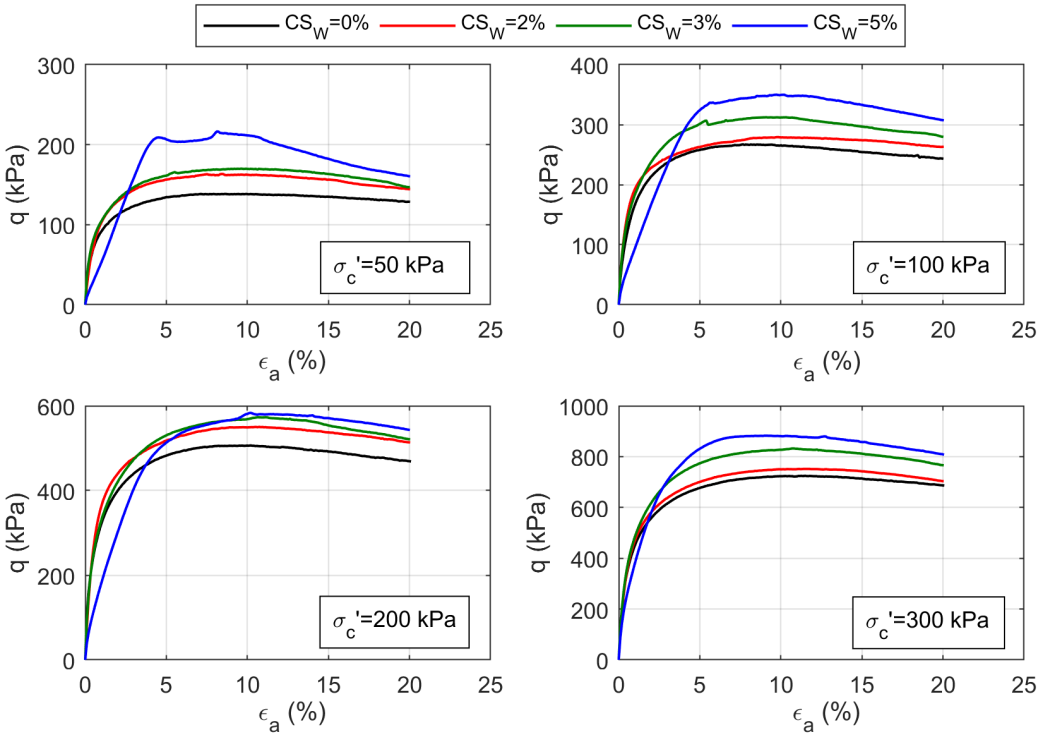

Figure 5.14: *Summary plot of experimental data from monotonic triaxial tests on treated and untreated S3 sand (results for 10% CS treated sand tests are not reported due to different σ'_c).*

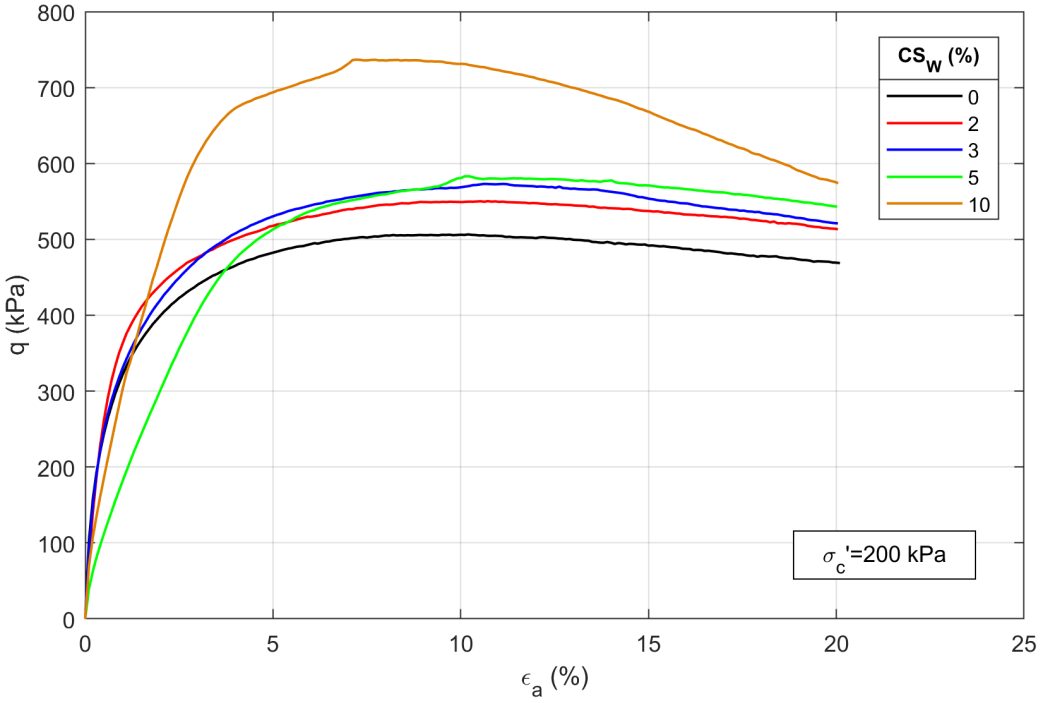

Figure 5.15: *Results of monotonic triaxial tests on treated and untreated sand for $\sigma'_c = 200$ kPa.*

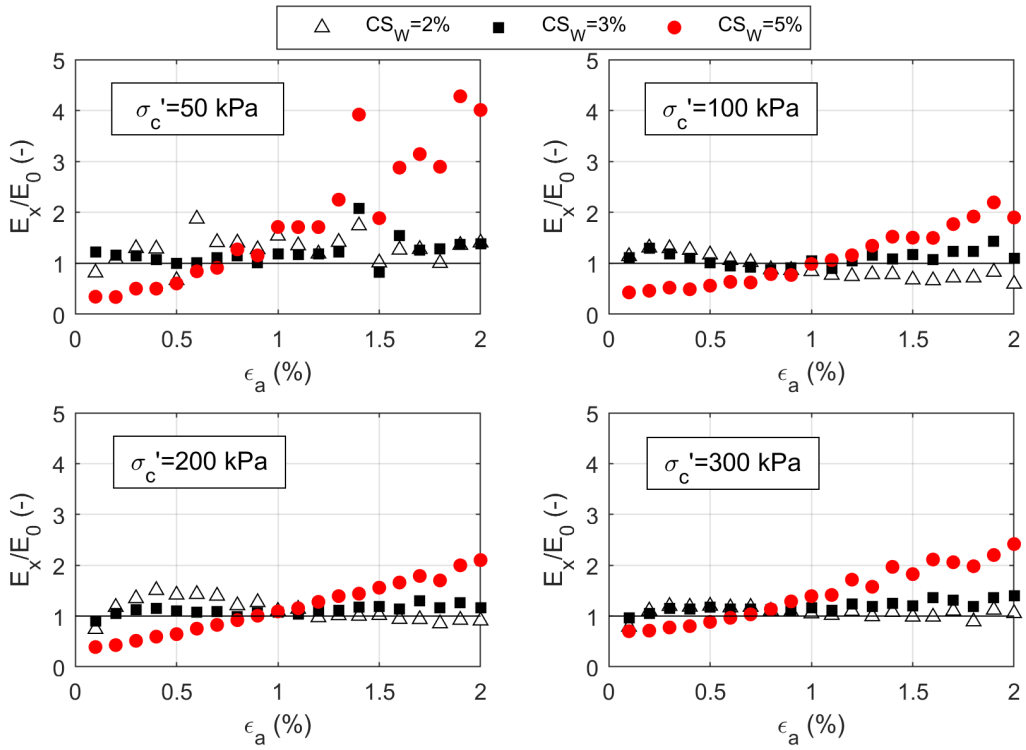

Figure 5.16: *Ratio between the tangent modulus of x% CS treated sand (E_x) and that of untreated sand (E_0) over the investigated range of σ'_c.*

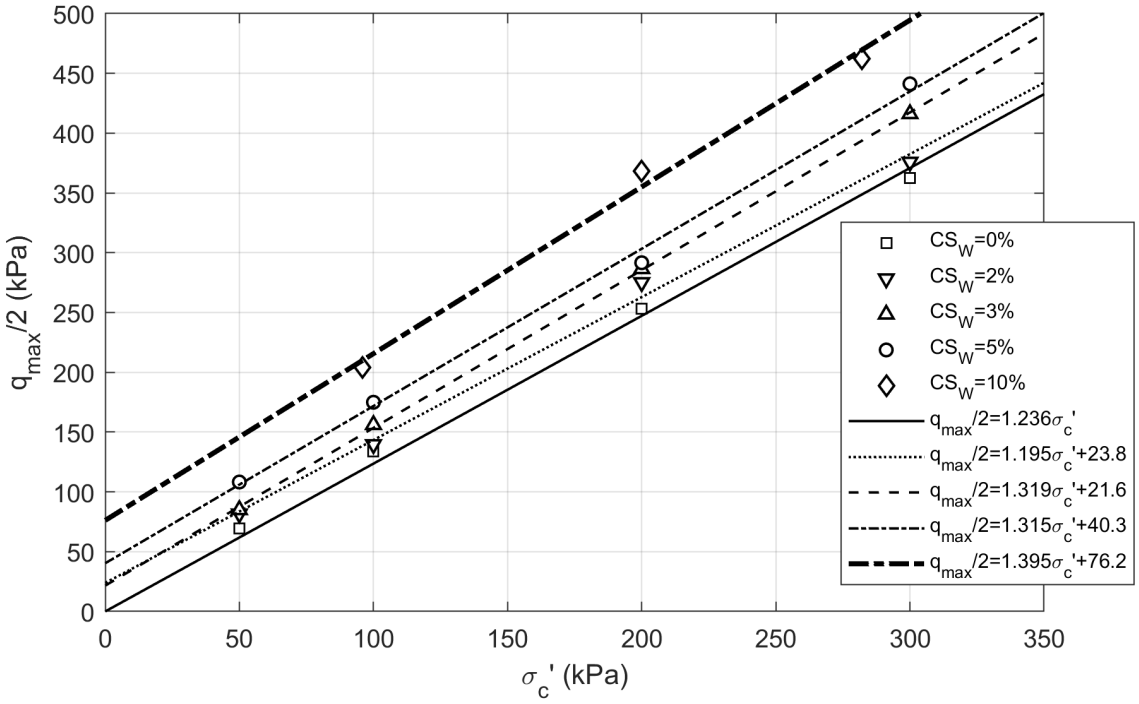

Figure 5.17: *Maximum shear stress at failure against effective consolidation stress for treated and untreated sand from monotonic triaxial tests.*

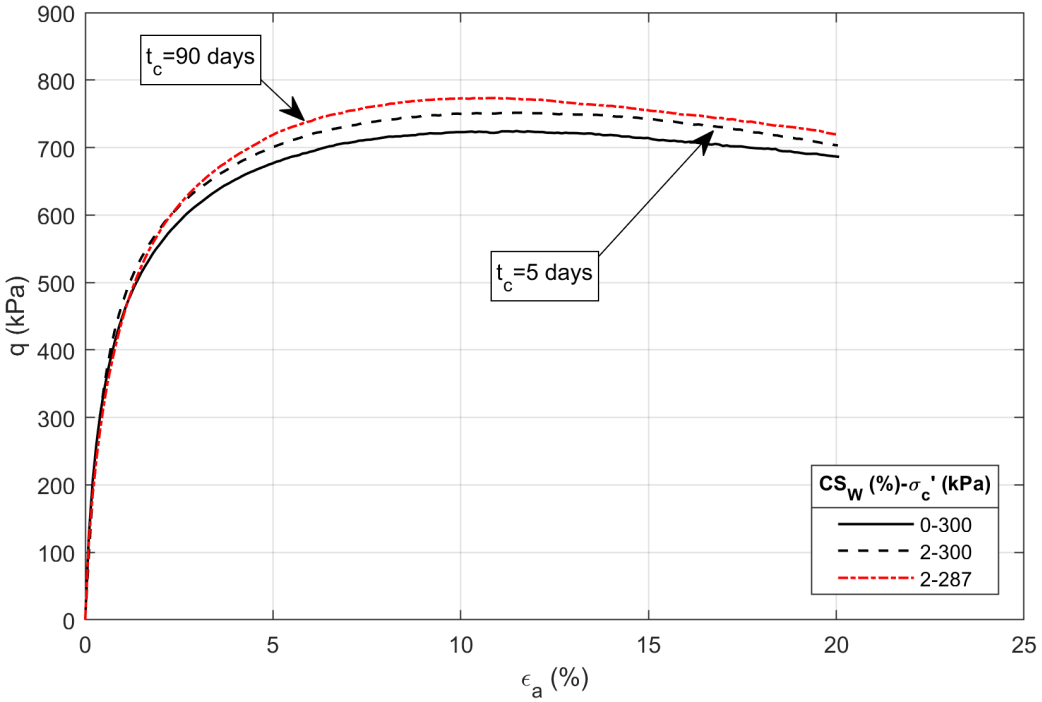

Figure 5.18: *Variation of ϵ_a-q curves with t_c for treated sand and comparison with untreated material.*

5.5 Preliminary mechanical tests: comparison with previous results

The results of tests listed in Table 4.7 are here briefly presented and discussed. Figure 5.19 shows the stress-strain and volumetric-axial strain relationships for untreated sand after monotonic drained tests. Dense sand exhibited peak deviatoric stress increasing with increasing σ'_c, and a significant dilation during the shearing phase. A linear regression through failure points in the $s' - t'$ plane provides the values of $c' = 0$ kPa and $\phi' = 39.3°$ ($c' = 0$ kPa and $\phi' = 33.7°$ obtained for loose sand, 50x100 mm cylindrical specimens). Figure 5.20 shows the comparison between linear regressions for untreated loose (Fig. 5.13) and dense sand.

Figure 5.21 shows the stress-strain and volumetric-axial strain relationships for dense treated and untreated sand consolidated at $\sigma'_c = 200$ kPa (for $CS_W = 5\%$, $B = 0.84$). As can be seen, the peak deviatoric stress for treated sand is higher than that of the untreated one, and it increases with CS_W. This result is consistent with data provided in the previous Sections; furthermore, tangent stiffness at small strain is lower for 5% CS treated sand than for 2% CS treated and untreated material (it is worth noting that similar results are obtained for specimens prepared with the wet pluviation technique and without water saturation). Some more dilation for treated sand is shown in the axial-volumetric strain plane, but volume change is not much as expected from other literature data (Porcino et al., 2011; Georgiannou et al., 2017). Enhanced dilation could be a consequence of bonds breakage: silica clusters, much smaller than sand particles, bind the grains any longer but fill the pore spaces, inducing more dilation during the shearing phase.

A comparison of these results with those from monotonic tests ($\sigma'_c = 200$ kPa) on treated and untreated sand shown in Section 5.4.2 is presented in Figure 5.22. Both for loose and dense

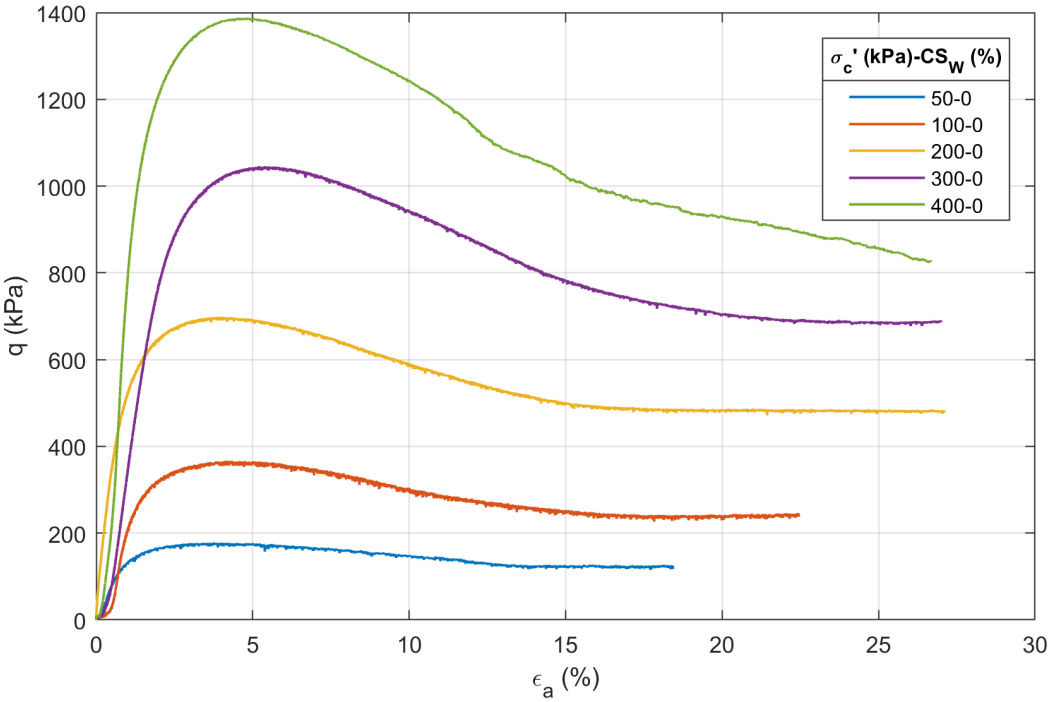

(a)

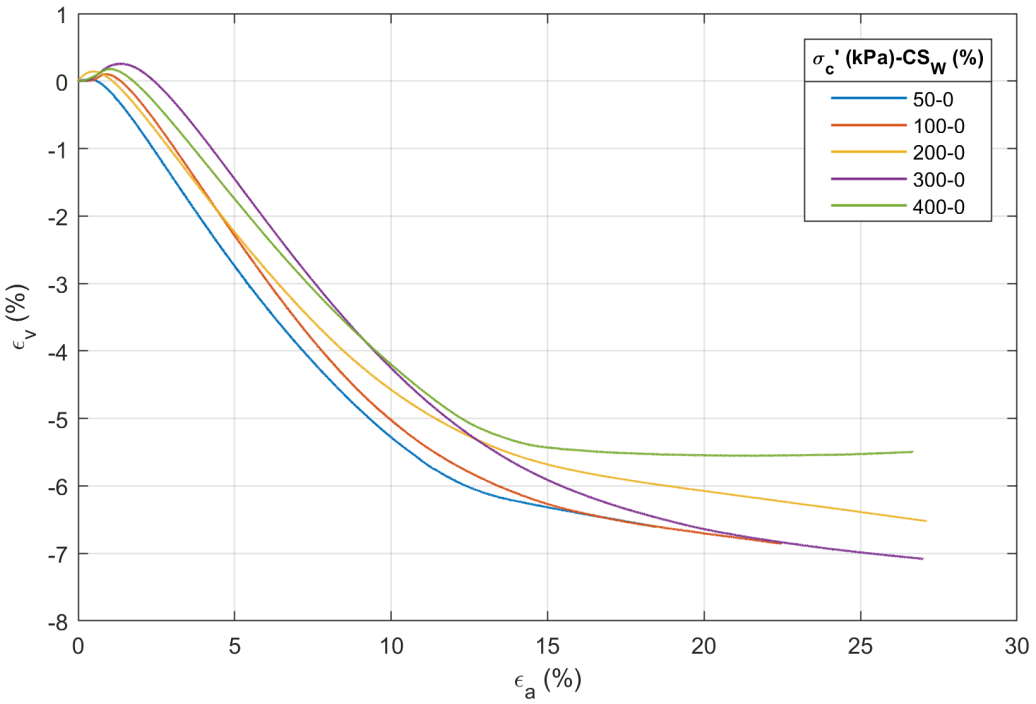

(b)

Figure 5.19: *Stress-strain (a) and ϵ_a against ϵ_v (b) curves for dense sand after monotonic drained triaxial tests.*

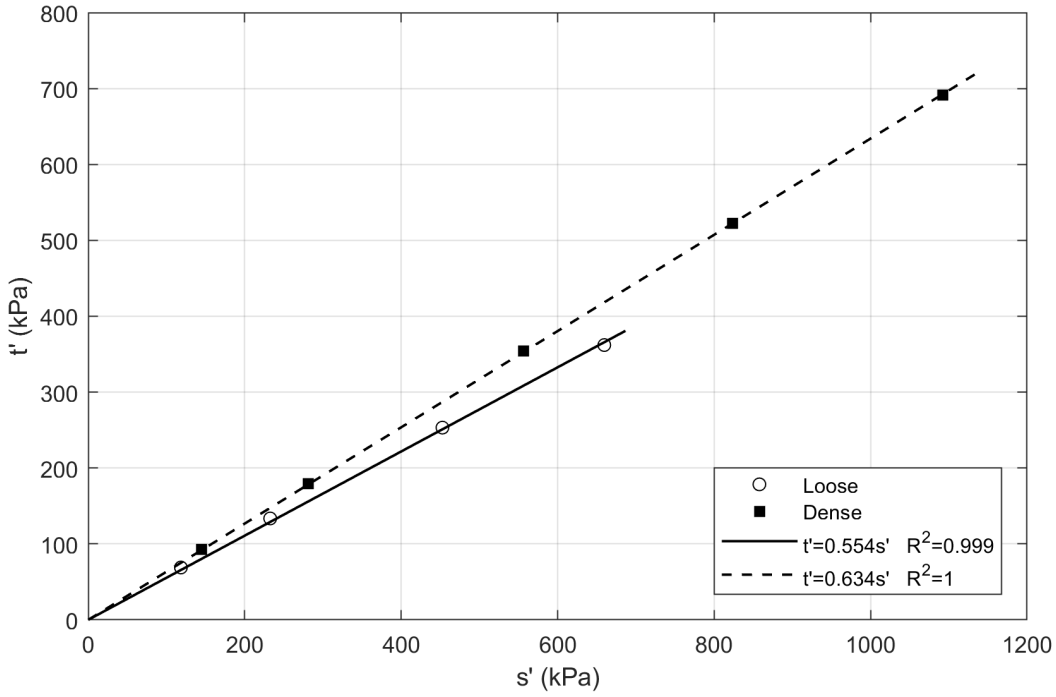

Figure 5.20: *Failure envelopes for loose and dense sand in the s′-t′ plane from drained monotonic tests.*

sand, the peak deviatoric stress increases with increasing CS_W; for 5% CS, tangent stiffness at small strain is significantly lower for loose sand than for dense sand. This can be because an improper gel distribution was achieved for dense sand, which behaves much similar to untreated sand. Moreover, it is worth noting that loose untreated sand and dense untreated as well as treated sand reach approximately the same stress at high strain levels ($\epsilon_a > 15\%$), while the deviatoric stress for loose treated sand is higher in the same conditions for both CS contents. It can be supposed that, after the stress peak is achieved (failure), a progressive breakage of silica bonds (or silica clusters) makes the treatment no more effective. This aspect, however, was not detected in loose sand, and it would need further analysis. It could be supposed that, when a back pressure is applied (dense sand), the breakage of silica bonds among the grains causes the improved soil to be made of sand grains and distinguished silica particles (i.e. the effect of the improvement is similar to densification, without cohesion), while if a back pressure is not applied (loose sand) the improved soil can be viewed as a continuous matrix of grains bonded by silica clusters (i.e. the effect of the improvement is equivalent to solidification). The role of back pressure in specimens preparation needs to be clarified and it may be possible to understand the different interpretations of the improvement nature, either in terms of densification (e.g. Georgiannou et al. (2017), who found results independent from the back pressure applied) or of bonding of grains (e.g. Porcino et al. (2011) and this study). It is more likely that a combination of both phenomena occurs in practice.

Concerning cyclic triaxial tests, results on treated sand are not fully convincing for the reasons discussed in Chapter 4. As a further proof, untreated sand in test 11-CA reached failure after 19 loading cycles ($e_c = 0.63$, $B = 0.99$, $CSR = 0.25$) but treated sand from test 06-CA

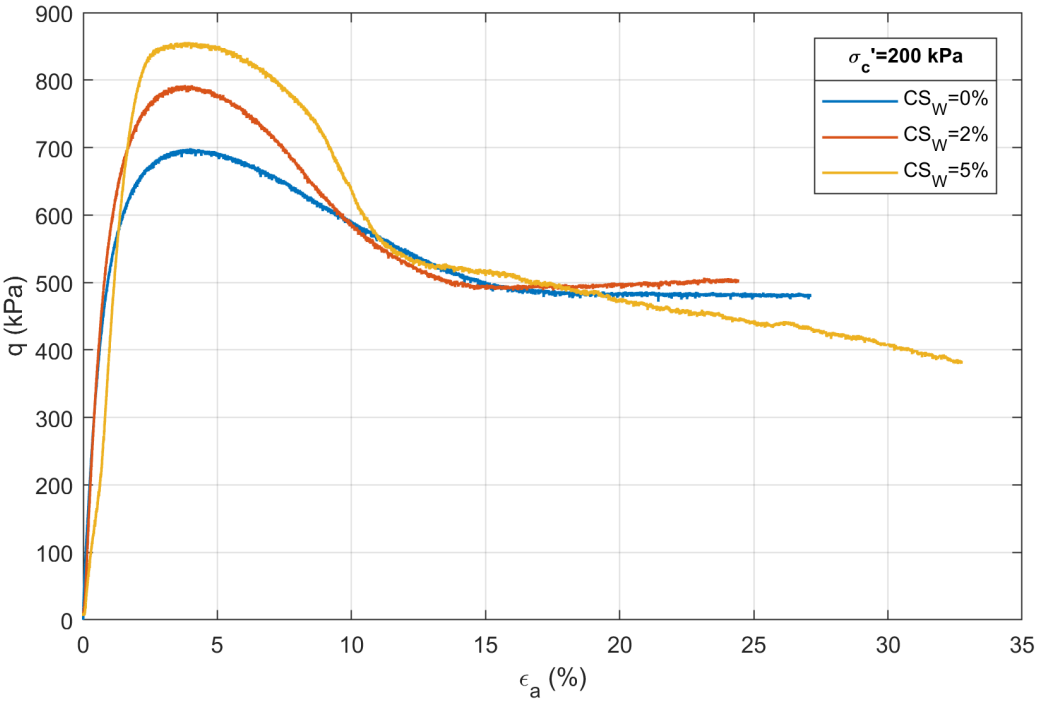

(a)

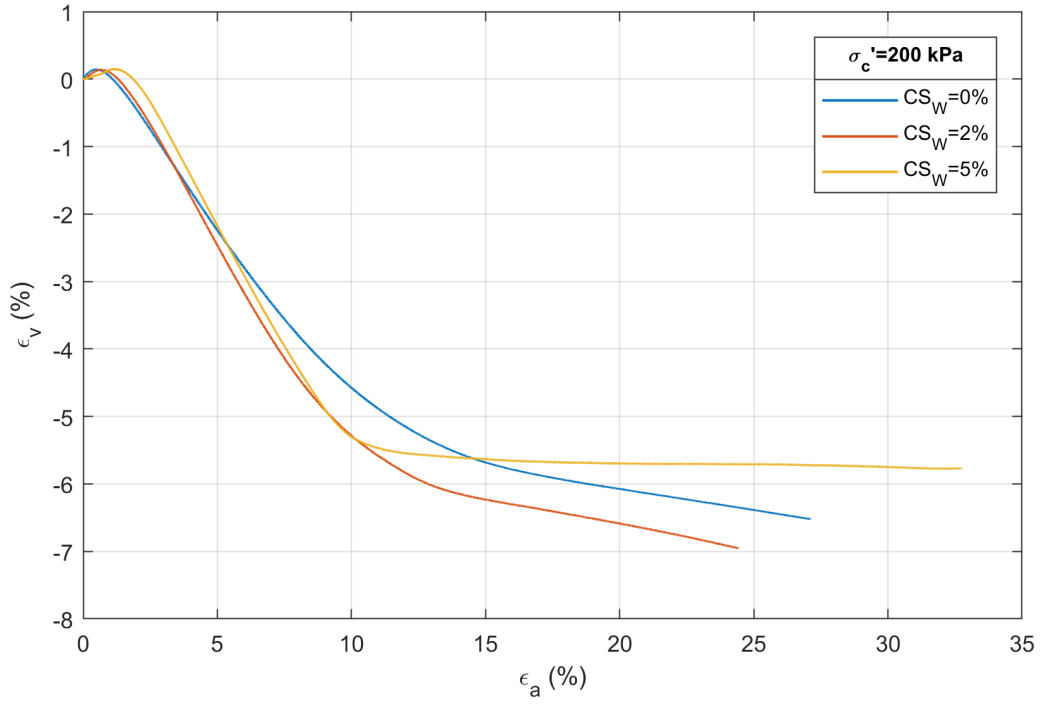

(b)

Figure 5.21: *Stress-strain (a) and ϵ_a against ϵ_v (b) curves for treated and untreated sand ($\sigma_c' = 200kPa$) after monotonic drained triaxial tests.*

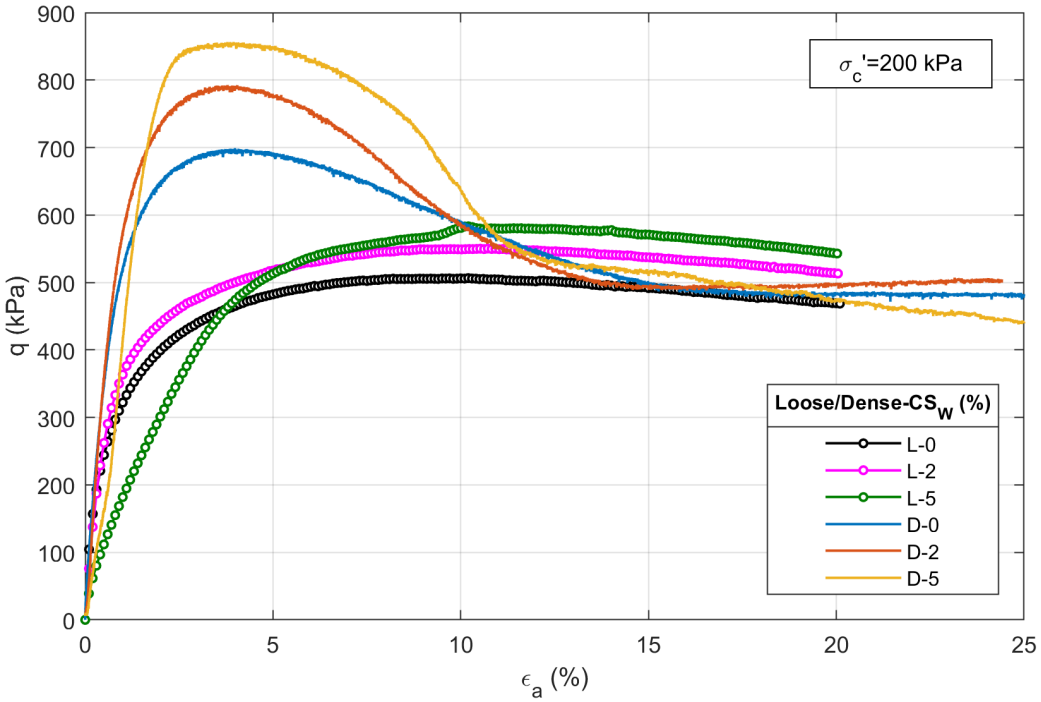

Figure 5.22: *Comparison among triaxial tests on loose and dense treated sand ($\sigma'_c = 200kPa$).*

($e_c = 0.62$, $B = 0.94$, $CS_W = 2\%$) failed after 10 cycles for $CSR = 0.15$ (Tab. 4.7). Treated sand reached failure before the untreated one, in contrast with all current experimental investigations on silica treated material. A summary plot of test 11-CA and 06-CA is provided as examples of test outputs in Figure 5.23. Tests were too few and results are too dispersed, thus it was not possible to detect a liquefaction resistance curve.

5.6 Oedometer tests

5.6.1 Samples disturbance and viscous effects

To ensure the quality of samples, pointing out the absence of disturbance that may lead to wrong interpretation of test results, three identical samples were prepared, using the method A, for testing in oedometer 1 (two samples) and shear box (one sample, by extrusion). All three samples were prepared with $CS_W = 5\%$ and with initial void ratio of ≈0.780. They were put in testing devices after 1 day from t_g, the chambers were filled with distilled water, and tests were run after the standard t_c of 5 days. In oedometer and direct shear test the vertical effective normal stresses were equal to 248 kPa and 245 kPa, respectively. Tests were used to compare differences in 1D settlements, under the applied load kept constant for 24h. Results are compared in Figure 5.24, where the recorded vertical displacement (ΔH) is plotted against time. As can be seen, settlements from the specimens tested in the oedometer are almost coincident, while they are significantly higher for the sample in direct shear box. Since all three specimens were under the same initial conditions, this highlights that oedometer samples don't suffer from some disturbance, that on the contrary affects samples in direct shear; furthermore, the

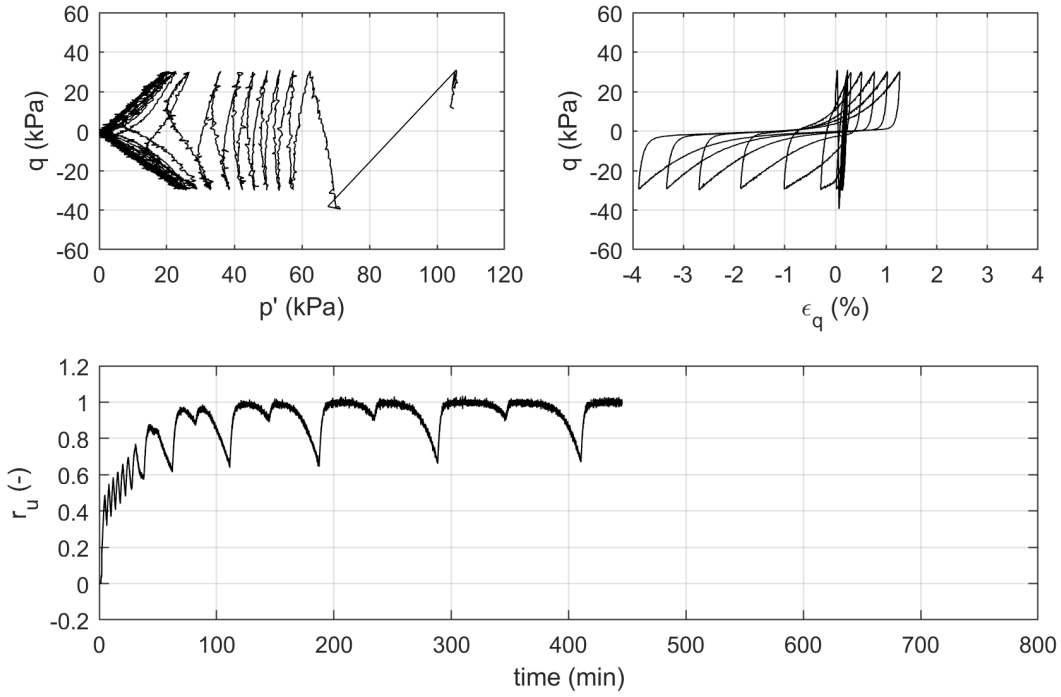

(a)

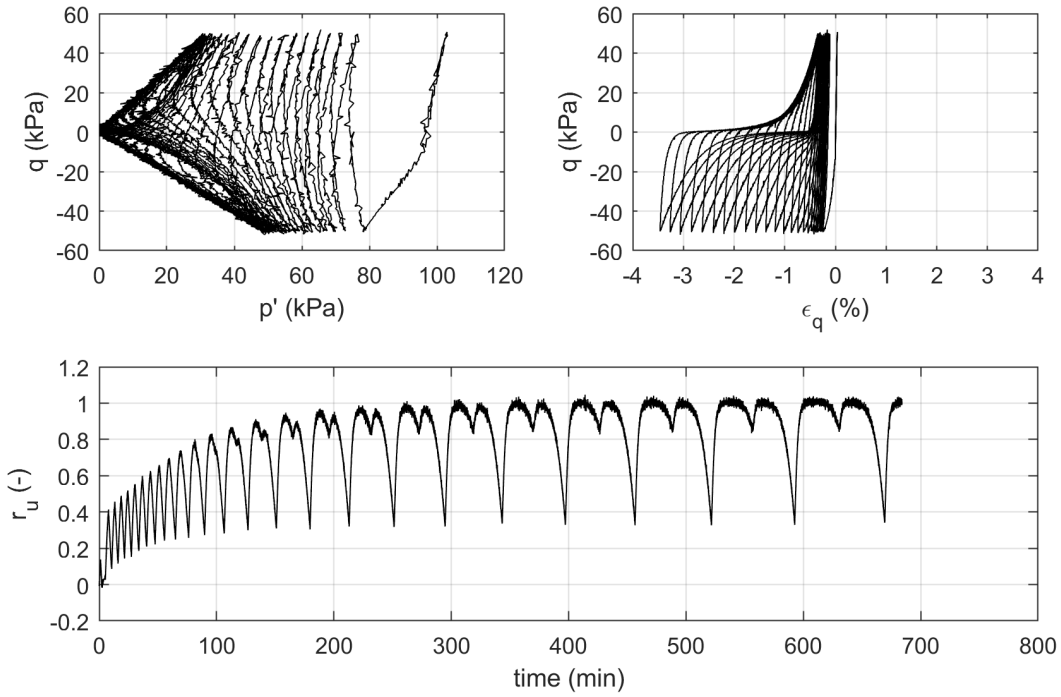

(b)

Figure 5.23: *Summary plots from cyclic undrained triaxial tests on samples 06-CA (a) and 11-CA (b).*

method adopted for specimen preparation guarantees very good samples' reproducibility. As a further proof of disturbance in direct shear, a slip in ΔH is observed during the loading phase. The results also show that settlements are practically instantaneous for the treated material, as it is confirmed by the additional data shown in Figure 5.28. The differences between the maximum settlements shown in Figure 5.24 for oedometer samples and in Figure 5.28b for a similar value of the normal stress is due to the progressive bonds breakage during subsequent loading (i.e. in Figure 5.24 samples are loaded once with the full load, while sample shown in Figure 5.28b, as well as samples tested under standard oedometer tests, is loaded by steps).

The two samples tested in the oedometer 1 ($\sigma'_{vc} = 248$ kPa) were also used to assess the viscous component of settlements. The first loading step was maintained for 7 days; then, an additional load ($\sigma'_{vc} = 496$ kPa) was applied and maintained for 30 days. During this time, settlements were monitored continuously. Figure 5.25 shows the development of vertical strain over time (immediate strain is removed for clarity); as can be seen, its viscous component is minimal: for instance, vertical strain increases of ≈0.15% over one month for both samples at $\sigma'_{vc} = 496$ kPa.

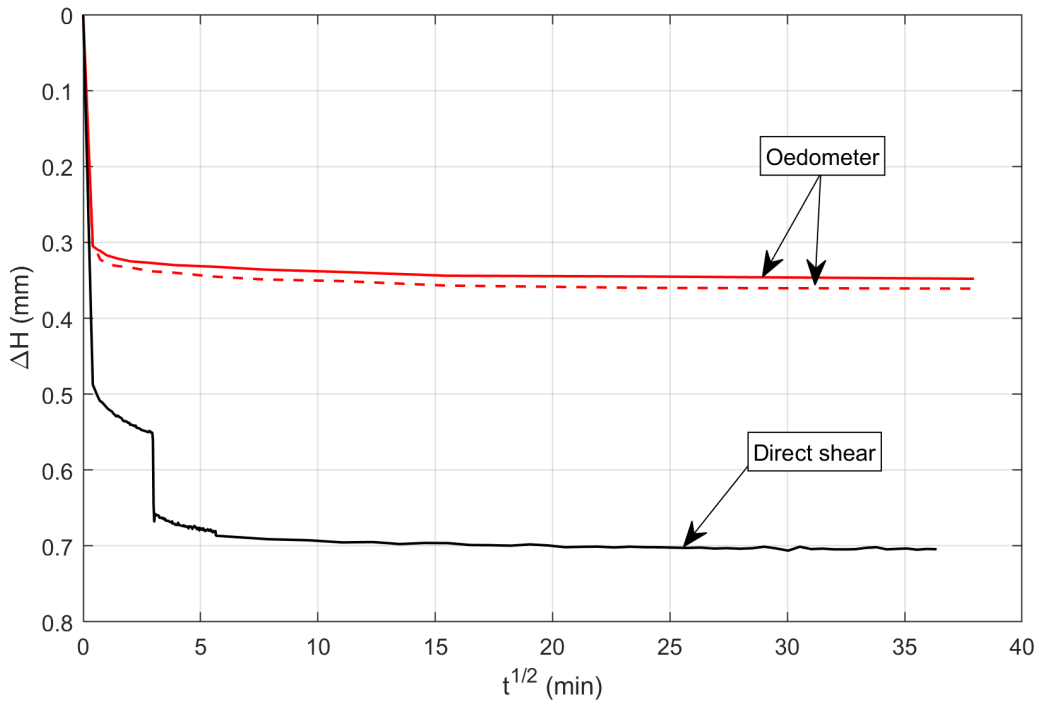

Figure 5.24: *Comparison among 1D settlements in oedometer and direct shear under the same initial conditions.*

5.6.2 Treated sand versus untreated sand

Method A

The results of oedometer tests are shown separately for oedometer 1 and 2, since their characteristics and the loading/unloading sequences were different between the two sets. Test results on untreated and treated sand specimens prepared according to method A described

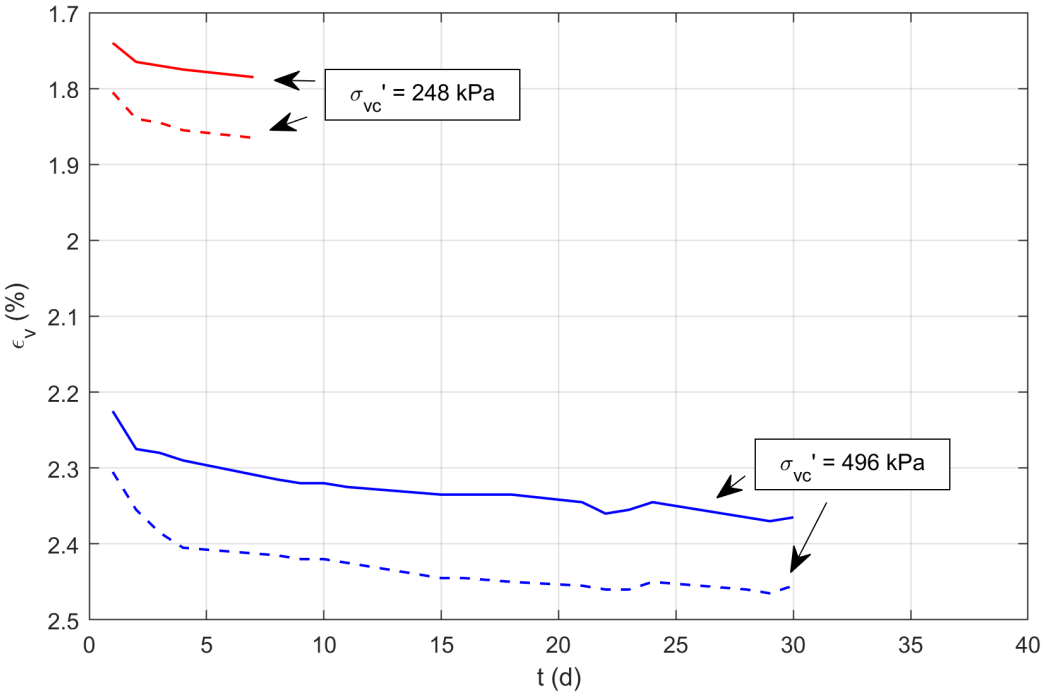

Figure 5.25: *Vertical strain over time for 5% CS treated specimens (method A, oedometer 1).*

in Section 4.3.5 are shown in Figure 5.26a for oedometer 1 (except for tests with $CS_W > 5\%$), while those obtained from oedometer 2 are presented in Figure 5.26b. Positive strain were associated to reduction in volume. It can be seen that the treated soil is *more* compressible than the untreated one. Swelling of samples is anyway excluded, since there are not volume changes during gelling, as demonstrated by preliminary analysis. According to Georgiannou et al. (2017), it can be argued that the grains rearrangement may be facilitated by the presence of the pore gel, which acts as a sort of buffer among sand particles. It is worth noting that this could be somehow observed from Figures 5.14 and 5.16. The difference between volumetric strain of treated and untreated material, $\Delta\epsilon_v$, increased with increasing CS_W for a given stress range, $\Delta\sigma'_v$.

Settlements were practically instantaneous both for treated and untreated material, as shown in Figure 5.27 for $CS_W = 0\%$ and in Figure 5.28a, b, for $CS_W = 2\%, 5\%$, respectively (oedometer 2). For treated material, settlements development occurs over time regardless of colloidal silica content (Fig. 5.28).

The obtained results are consistent with literature data (Fig. 3.21). However, silica gel is more compressible than water (Towhata, 2008) and this appears to be a critical issue for practical application of CS grouting. The minor strain of treated material was recorded for $CS_W = 2\%$, therefore it can be stated that low-contens grouts are generally preferable, since higher CS contents may lead to inadmissible strain.

In contrast with the experimental results shown in Figure 5.26, Wong et al. (2018) found that the compressibility of a silica-treated sand was significantly lower than that of the untreated sand (Fig. 5.29). Several factors can contribute to the observed discrepancy: the CS content they used, the characteristics of their natural sand and the specimen preparation method. In

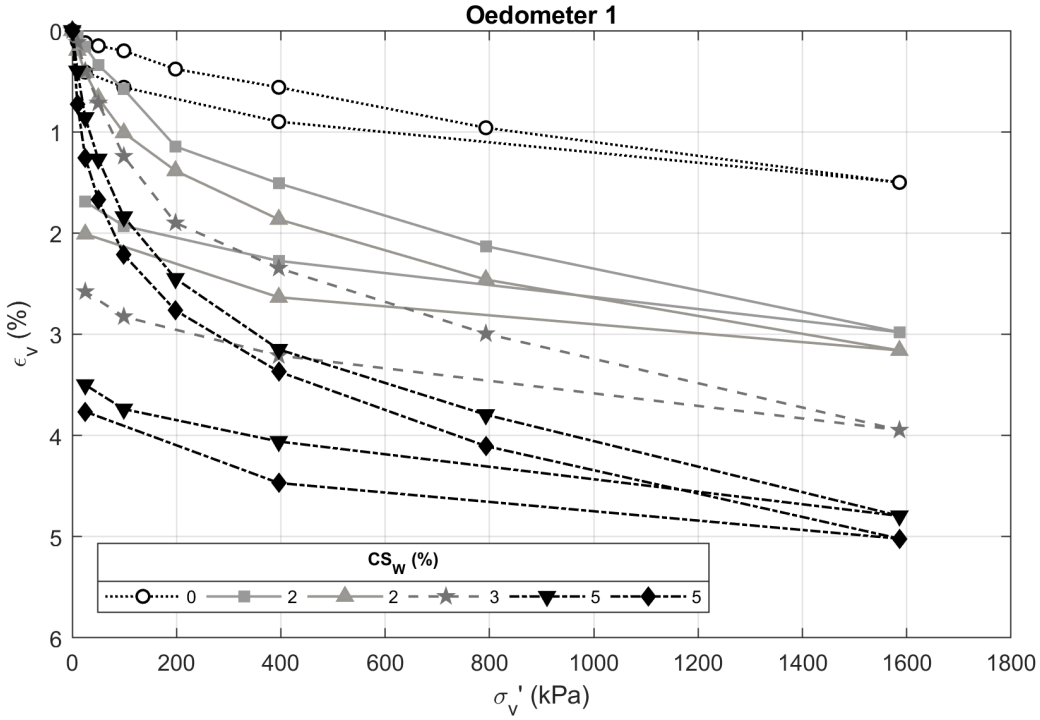

(a)

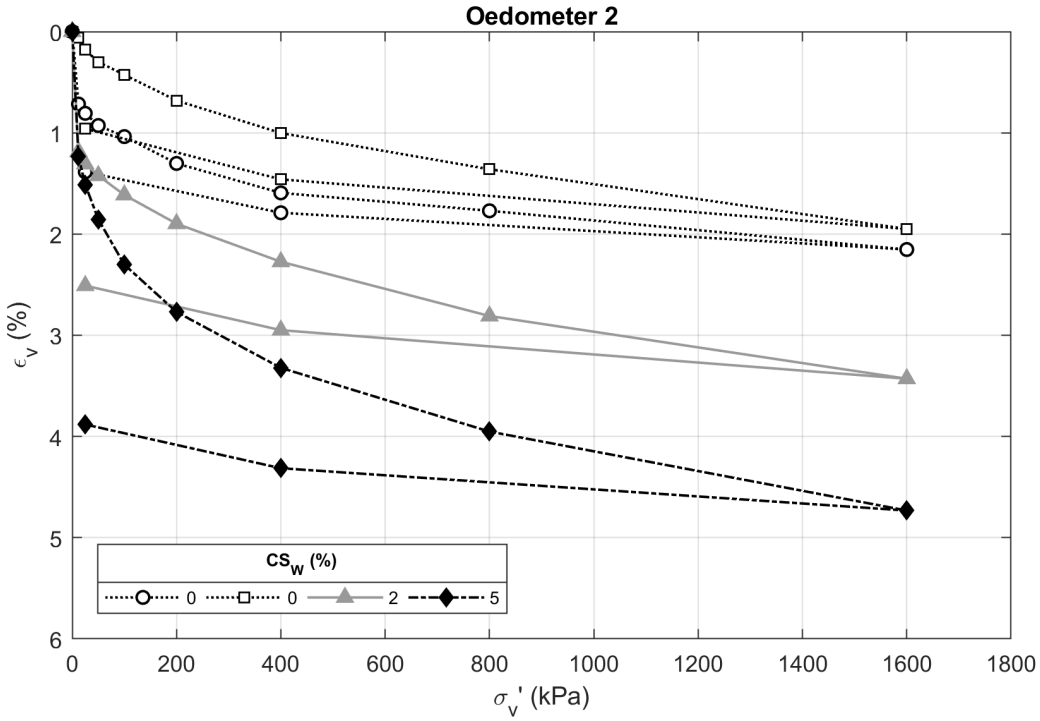

(b)

Figure 5.26: *Oedometer 1 (a) and oedometer 2 (b) test results (method A) ($CS_W \leq 5\%$).*

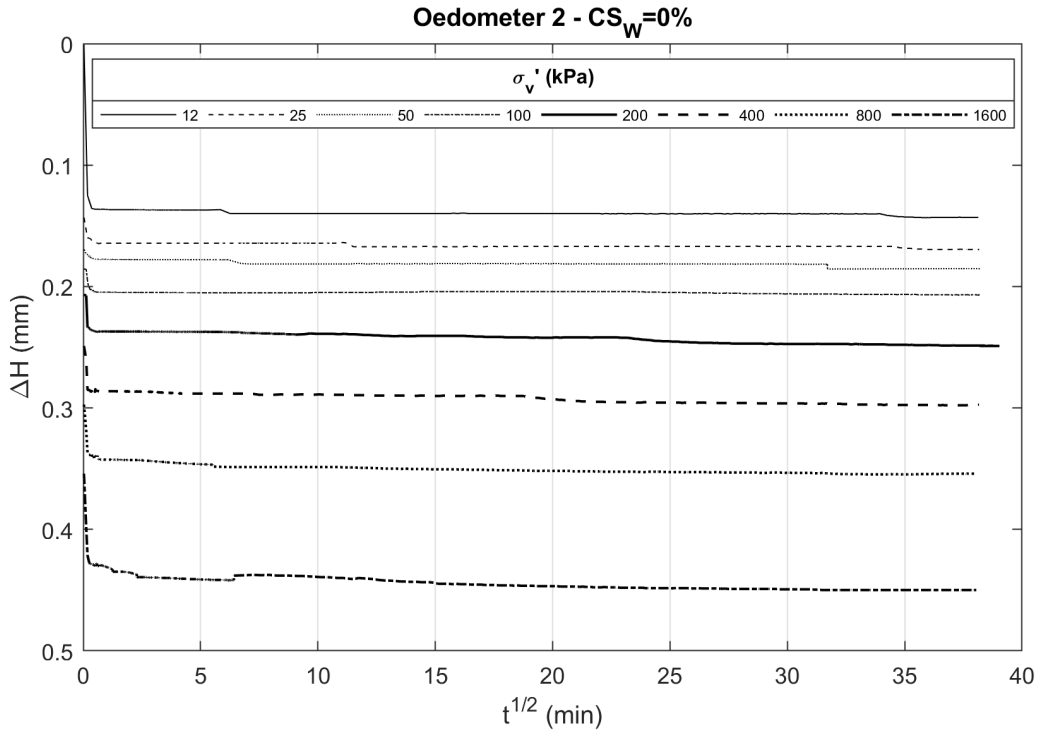

Figure 5.27: *Vertical displacement versus consolidation time for ID=13E (method A).*

particular, they used a sand with very different values of U (1.26) and D_{50} (1.20 mm) ($U = 1.6$ and $D_{50} = 0.30$ mm for S3 sand) treated with very high CS content (34% by weight). The colloidal silica product they used was Meyco MP 320 (BASF SE), a 40% by weight CS solution. To better investigate this aspect, by simulating in the best way the boundary conditions proposed by Wong et al. (2018), further tests were firstly performed increasing CS_W, and secondly using method B for the preparation of specimens with high CS contents ($CS_W > 5\%$).

In Figure 5.30, the results obtained from tests on 10% and 13% CS treated samples are plotted together with those previously reported in Figure 5.26a. For clarity, the new graphs are colored in red ($CS_W = 10\%$) and in blue ($CS_W = 13\%$). Differently from what was expected, vertical strain for $CS_W > 5\%$ was comparable to that of 5% CS: it is like there is a sort of threshold in CS content above which ϵ_v doesn't increase. Unfortunately, it was not possible to verify this hypothesis for CS content higher than 13% by weight, since the product used in this study is provided as a 15% by weight CS solution, and the addition of the accelerant necessarily dilutes the product 'as delivered'. Anyway, for this study, in no case the compressibility of treated sand was found lower than that of the untreated one.

Method B

Additional tests (oedometer 2) on samples prepared by means of method B, as it was firstly used by Wong et al. (2018), were also subjected to multiple loading and unloading sequences to evaluate the effects of reloading after the first compression phase.

The test results are presented in Figure 5.31, where they are compared with tests performed on untreated sand in oedometer 2. It can be seen that the relation between ϵ_v and CS_W is similar to those previously observed: $\Delta\epsilon_v$ increased as CS_W increased, but the curve for $CS_W = 10\%$

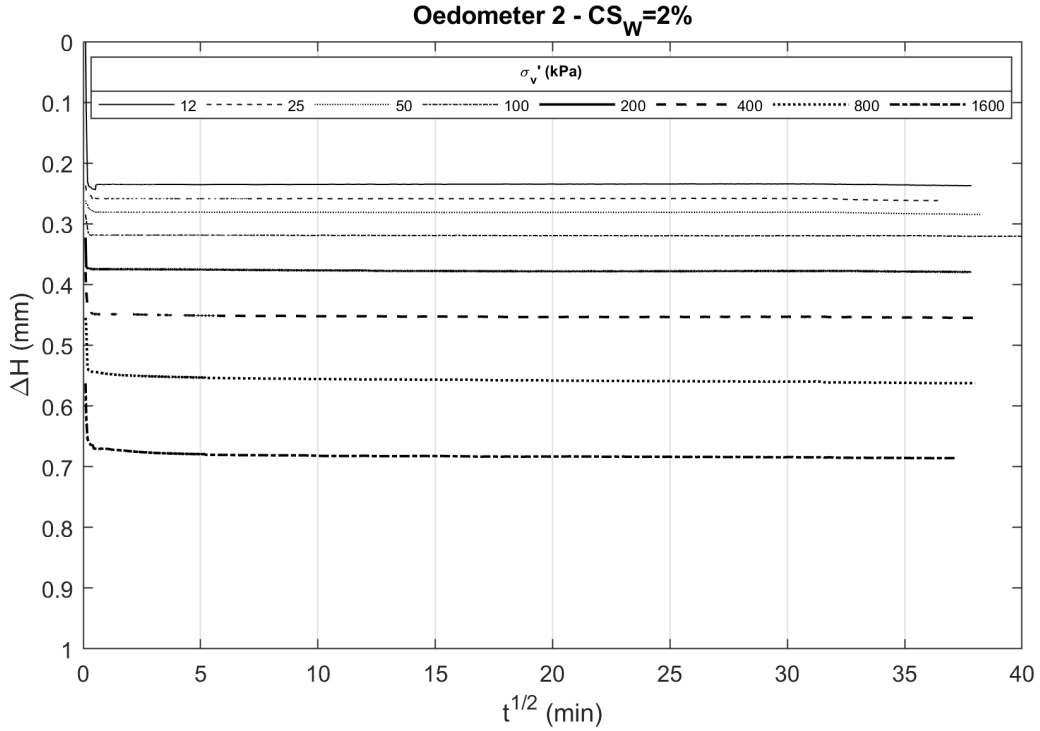

(a)

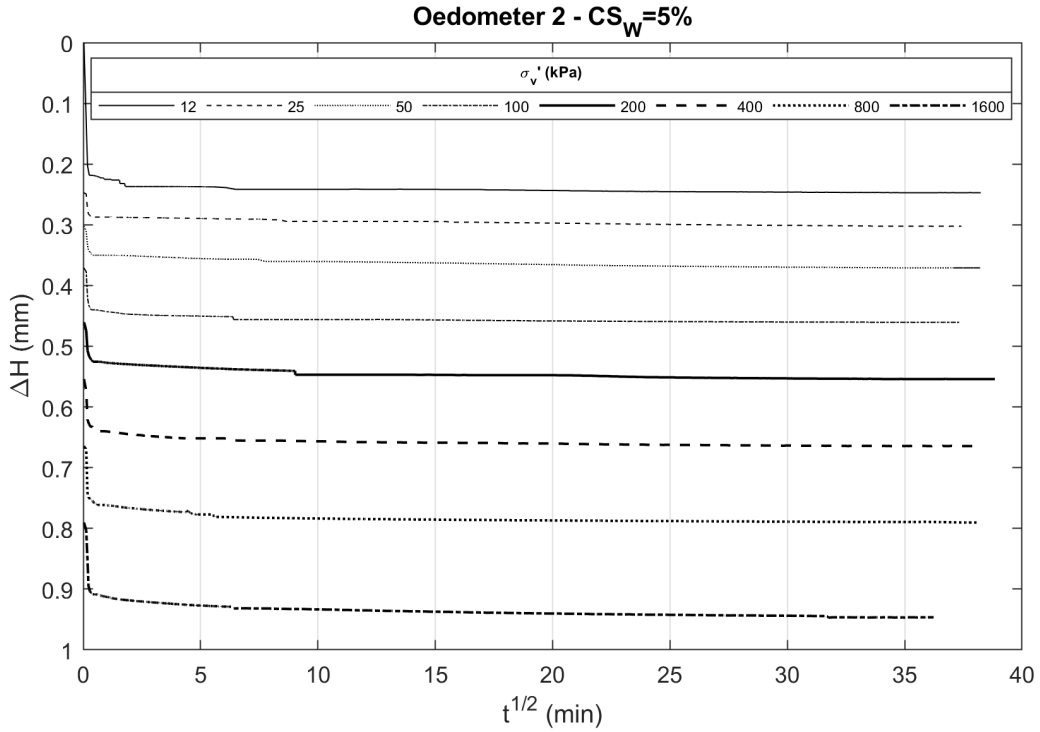

(b)

Figure 5.28: *Vertical displacement versus consolidation time for ID=11E (a) and ID=12E (b) (method A).*

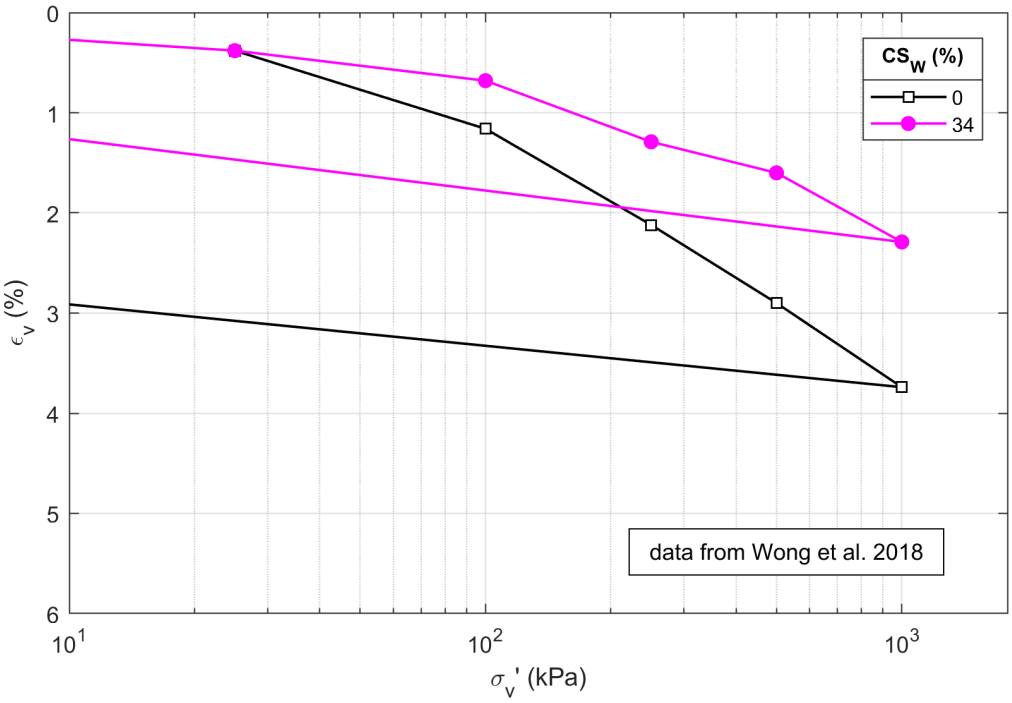

Figure 5.29: *Oedometer test results on treated and untreated sand (mod. from Wong et al., 2018).*

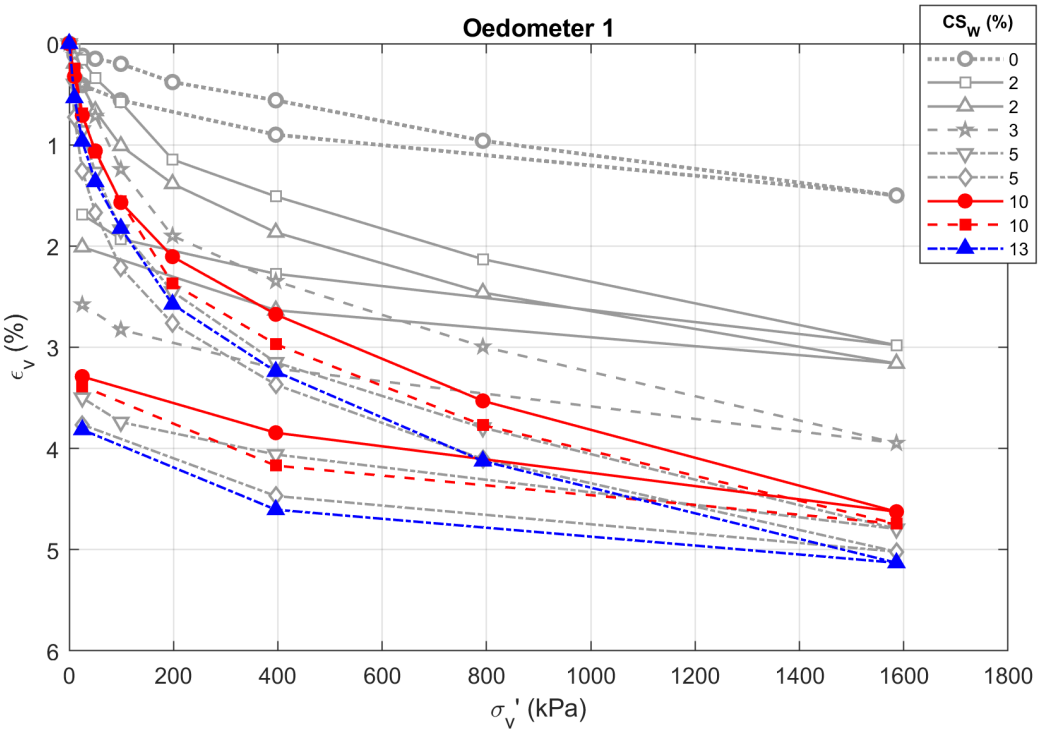

Figure 5.30: *Summary plot of oedometer tests on treated and untreated material (method A).*

is beneath 2% and 5%, confirming that above a certain threshold the compressibility properties of treated material change. Since the settlements of treated sand were higher than those of the untreated one, it was concluded that the specimens preparation method had no influence on it.

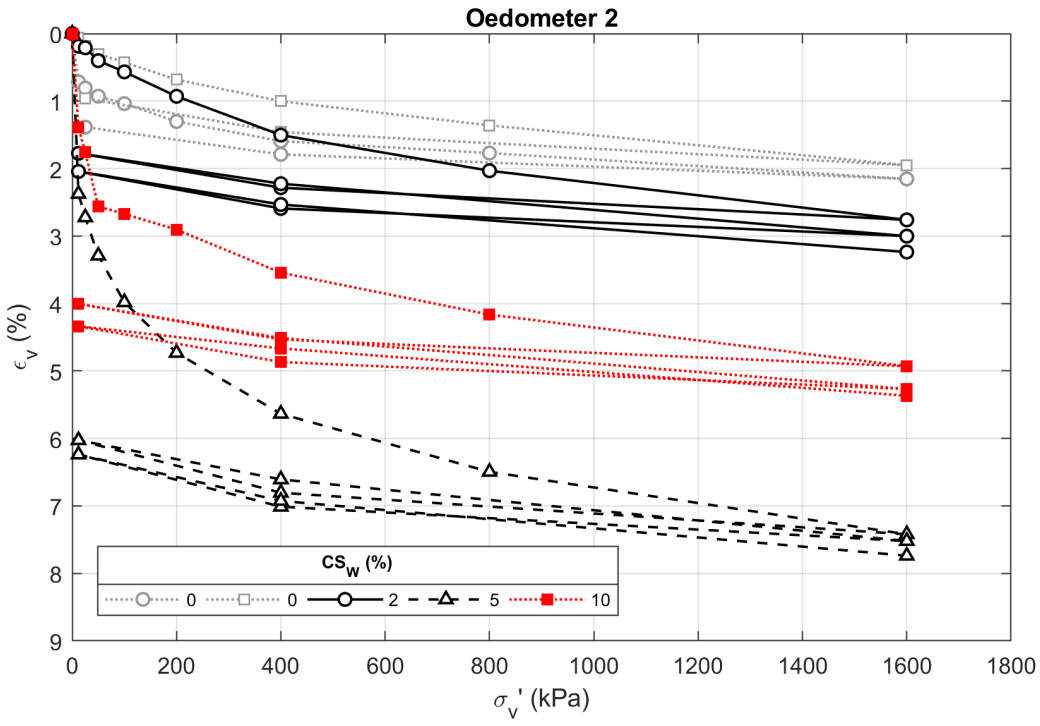

Figure 5.31: *Summary plot of oedometer tests on treated material (method B).*

Unloading and reloading

Unloading and reloading paths are practically coincident (Fig. 5.31): as reloading sequences were applied, the treated soil slightly densified. There was no significant strain development after the first compression phase, suggesting that the gel matrix was inert once loaded.

Compressibility modulus

Looking at Figures 5.26 and 5.30, the unloading sequence seemed to follow the same path for all tests, regardless of the initial CS content. To quantitatively match these results, the compressibility modulus, $m_v = \frac{\Delta\epsilon_v}{\Delta\sigma'_v}$, representing the slope of the stress-strain curve, was calculated for both the loading and unloading phases. For the loading phase, m_v was computed with reference to the last loading step, while the entire unloading stress range was used to calculate it for the unloading phase. The obtained values are plotted versus CS_W in Figure 5.32. The differences among the m_v values for loading and unloading paths between oedometer 1 and 2, reported in Figure 5.32, are due to the different set of devices used, as reported in Table 4.14. For tests 14E, 15E and 16E, m_v was calculated only for the first unloading sequence, for comparison with the remaining tests; furthermore, no distinction was made between $\Delta\sigma'_v = 1600 - 25kPa$ and $\Delta\sigma'_v = 1600 - 12kPa$, due to the great amplitude of the stress intervals. Data outcomes were then averaged when referred to the same CS_W. Figure 5.32 clearly shows that m_v, for both

oedometer 1 and 2, is strongly affected by CS content during loading while it is independent from CS content during unloading; moreover, it would be confirmed that, over a certain CS content threshold, the stress-strain response of treated material would change.

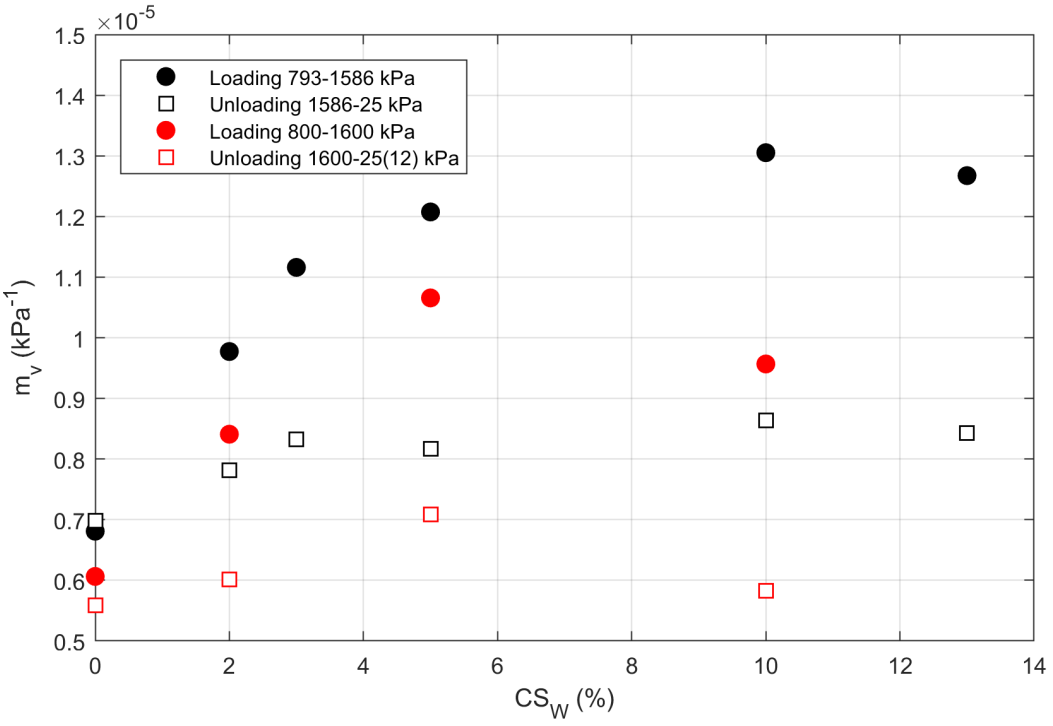

Figure 5.32: *Summary plot (oedometer 1 and 2) of compressibility modulus versus silica content for treated and untreated material.*

5.7 Summary

In this Chapter, the results of experimental testings, namely cyclic and monotonic triaxial tests, direct shear tests and oedometer tests on treated and untreated material were presented and discussed. Based on these analysis results, the following statements can be drawn.

- Low-content CS grouts can be successfully used to increase the liquefaction resistance of a clean, liquefiable sand and CS_W=2% is enough for this purpose.
- 'Weak' CS gel improves the shear strength of the material by providing a small cohesion to the sand particles, while the peak friction angle is practically unaffected by the presence of gel within pores, at least for $CS_W = 2\%$.
- The undrained static shear strength of treated soil increases as CS_W increases; this tendency is confirmed within the investigated range of effective confining stresses.
- As CS_W increases, $\Delta\epsilon_v$ increases for a given $\Delta\sigma'_v$, if compared to untreated sand.
- Untreated and treated sand exhibit similar settlements development over time and for treated material this is independent from CS_W.

- The increased compressibility of treated sand is characteristic of grouted material.
- It seems there is a threshold in CS content above which the compressibility properties of treated sand would change.

Therefore, to minimize the negative effects of pore gel on the compressibility of treated material, the use of low-CS content grout is recommended. From this study, CS_W=2% seems to be the optimal CS content to improve the performances of liquefiable material under cyclic and monotonic loading conditions, keeping the smallest increase of its compressibility.

Chapter 6

Conclusions and future developments

The present PhD study deals with the effects of high-diluted colloidal silica (CS) mixtures on the properties and mechanical behavior of a clean liquefiable sand. In order to evaluate these effects, laboratory investigations on treated and untreated material were carried out; several different colloidal silica contents, CS_W (the amount of silica solids, by weight, in the colloidal silica grout), were tested. It was proven that $CS_W = 2\%$ is sufficient to improve the soil behavior under both cyclic and monotonic loading conditions.

Understanding the rheological behavior of CS grout has been essential to correctly setup a meaningful laboratory campaign. For this purpose, the fundamental roles of gel time, t_g, and curing time, t_c, were extensively discussed in preliminary tests. Permeation tests confirmed that the rate of viscosity increase, namely the gelation process, is the main issue related to grout delivery; modifying the ratio between the accelerant and the total volume of grout in the stabilizing solution (α) allowed easy grouting of CS mixtures. Then, a dramatic decrease of hydraulic conductivity ($k_{T=10°C}$, with reference to a temperature of 10°C) of treated material was measured, revealing that even low CS content grout causes a significant (10^4 fold) $k_{T=10°C}$ reduction. Preliminary mechanical tests were used as a guideline for the following experimental investigations, especially concerning the role of samples formation in triaxial tests.

Tomography tests confirmed that CS gel is deposited among sand grains: it provides the sand with an artificial cohesion, which increases the drained shear strength of treated soil, as demonstrated by means of direct shear tests. The angle of peak shear resistance is practically unaffected by CS grouting, at least for the CS contents and effective consolidation stresses tested in this study. Both direct shear and monotonic triaxial tests showed that for $CS_W < 5\%$ the stress-strain response of treated sand at small strain levels is similar to that of the untreated material, while it is markedly different for $CS_W \geq 5\%$.

Cyclic triaxial tests confirmed the increase in liquefaction resistance of S3 sand with increasing D_r and CS_W. Therefore, the use of low CS content grout appears to be suitable to mitigate liquefaction hazard. In conclusion, the $CS_W = 5\%$ content originally proposed by Gallagher and Mitchell (2002) as a good compromise between effectiveness and economic cost of the treatment, can be surely reduced for practical applications.

Oedometer tests represent an important part of this study, since the evaluation of the CS treated sand behavior in terms of deformation had not been exhaustively analyzed by previous research. It was shown that, over the whole range of investigated CS contents, treated

soil is more compressible than the untreated one. This was demonstrated regardless of the method used to prepare the soil samples: the compressibility of treated material wasn't in any case lower than that of untreated sand. This aspect represents a significant shortcoming of the method for its practical use, especially for treatments under existing structures; however, this negative effect is minimized by using high-diluted CS mixtures, e.g. $CS_W = 2\%$.

Further research should demonstrate whether the increase of CS content up to high values (e.g. more than 10% by weight) can lead to a reduced compressibility of the stabilized soil; the existence of a threshold that discriminates the behavior in terms of compressibility could be in this study only hypothesized. If this is confirmed by future studies, however, the economic costs of a potential treatment would be unsustainable, if compared to other standard liquefaction mitigation techniques. Thus, colloidal silica grouting would be no more appealing. In addition, since CS gel is a compressible material, the applicability of the Effective Stress Principle for treated soil needs to be discussed and further research should provide dedicated constitutive models to characterize and predict the behavior of soil treated with colloidal silica mixtures.

Chapter 7

APPENDIX

7.1 Cyclic triaxial tests

Untreated medium-dense sand Figures 7.1, 7.2, 7.3, 7.4 (see Tab. 4.9).

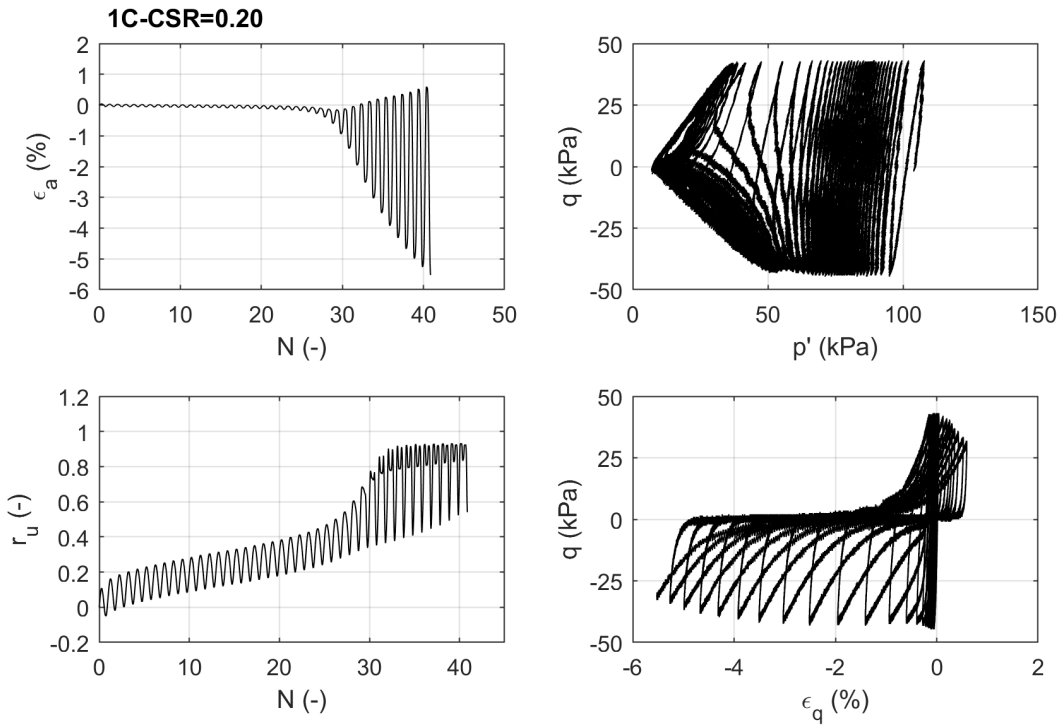

Figure 7.1: *ID=1C.*

Untreated loose sand Figures 7.5, 7.6, 7.7, 7.8, 7.9 (see Tab. 4.9).

CS_W**=5% treated sand** Figures 7.10, 7.11, 7.12, 7.13 (see Tab. 4.9).

CS_W**=2% treated sand** Figures 7.14, 7.15, 7.16, 7.17, 7.18 (see Tab. 4.9).

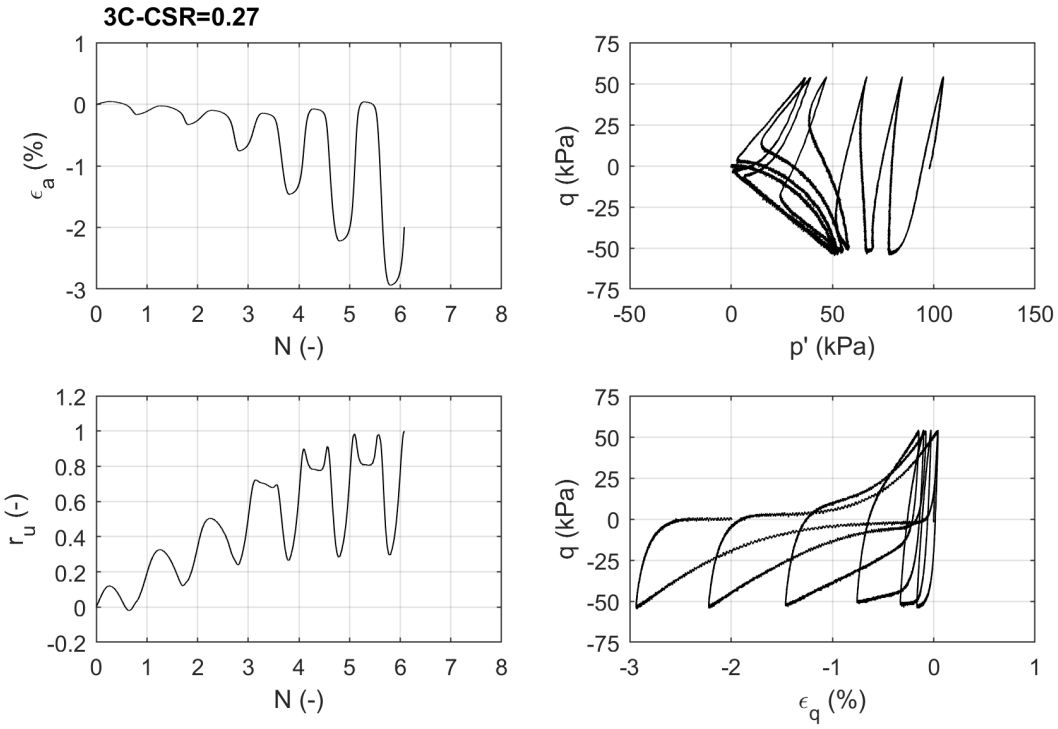

Figure 7.2: *ID=3C.*

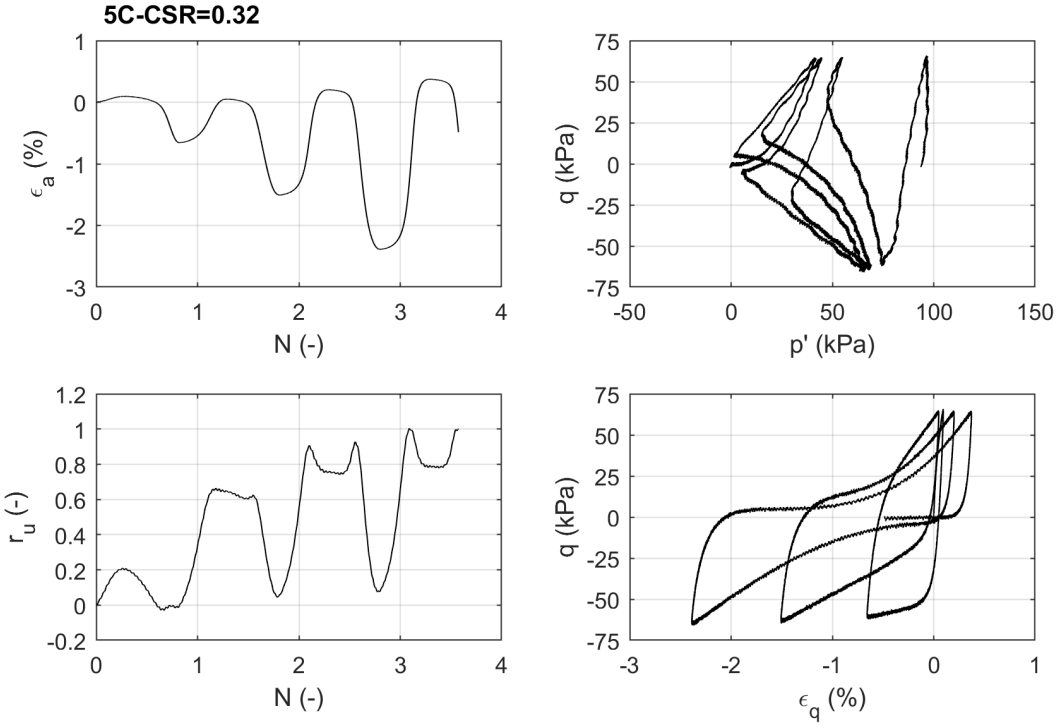

Figure 7.3: *ID=5C.*

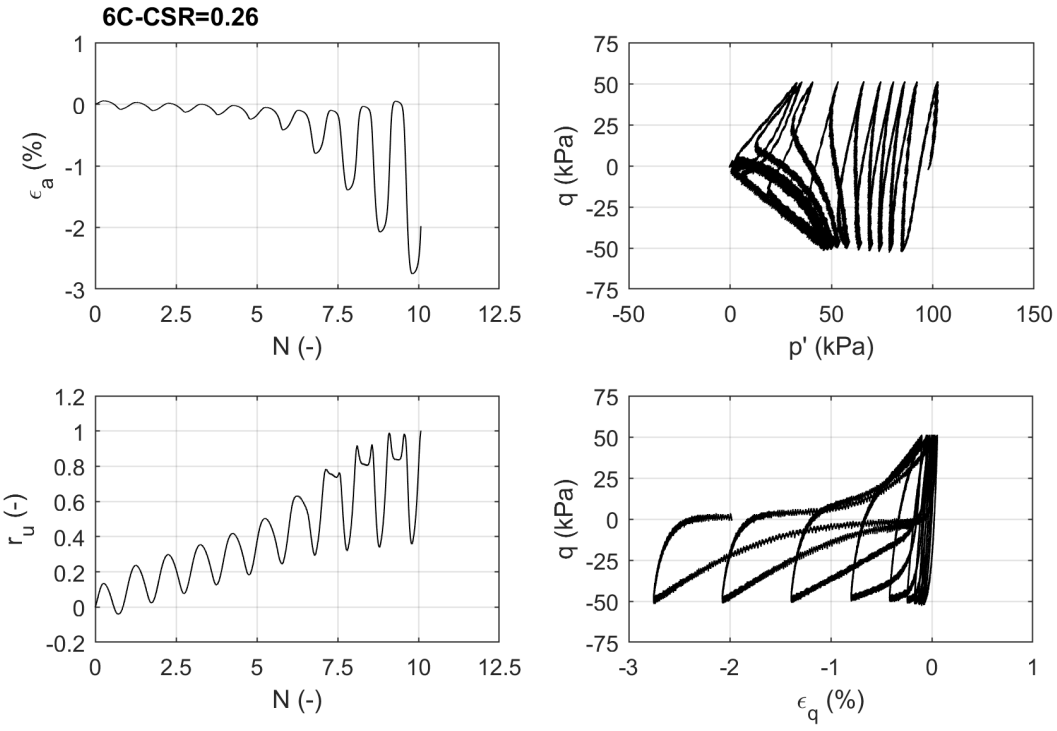

Figure 7.4: *ID=6C.*

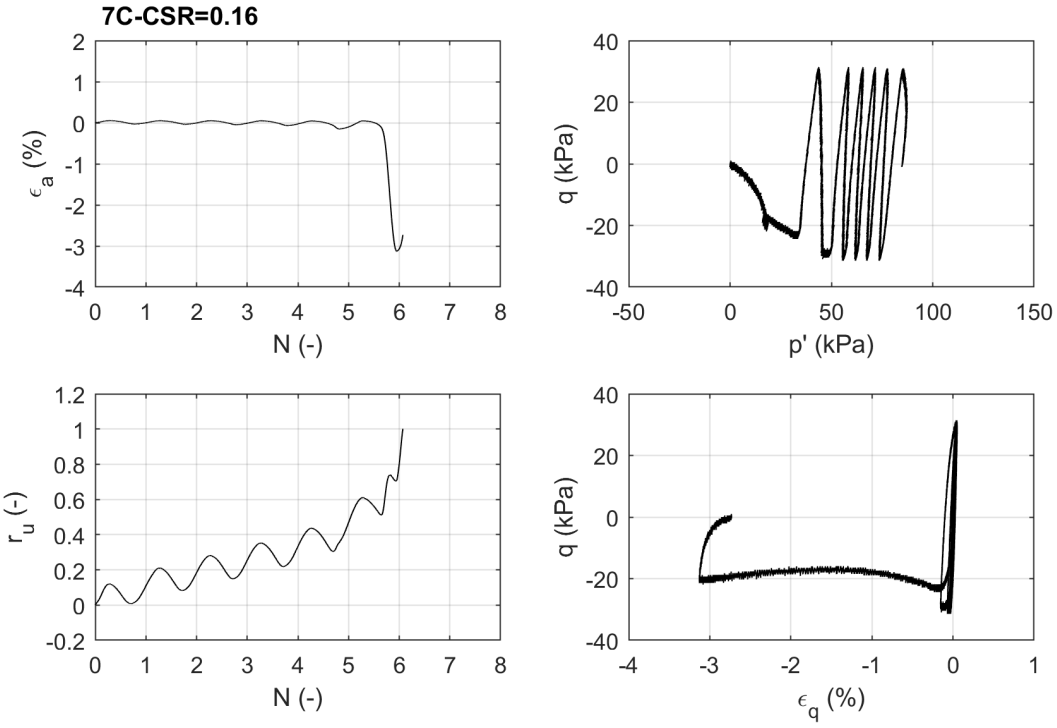

Figure 7.5: *ID=7C.*

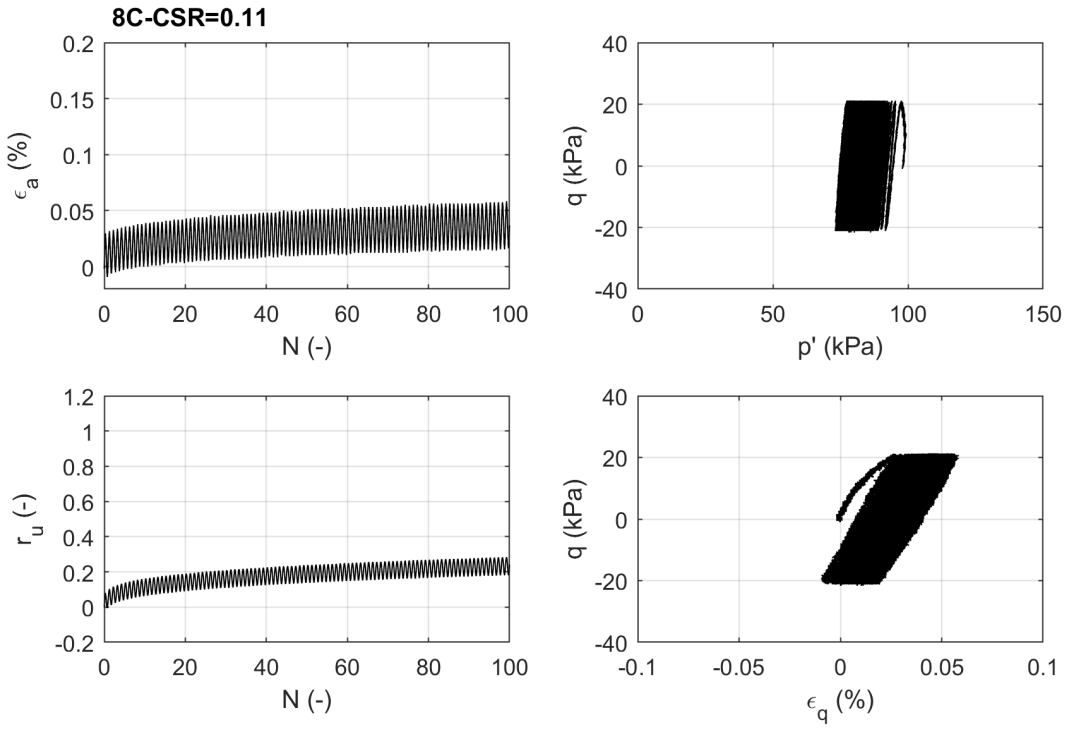

Figure 7.6: *ID=8C.*

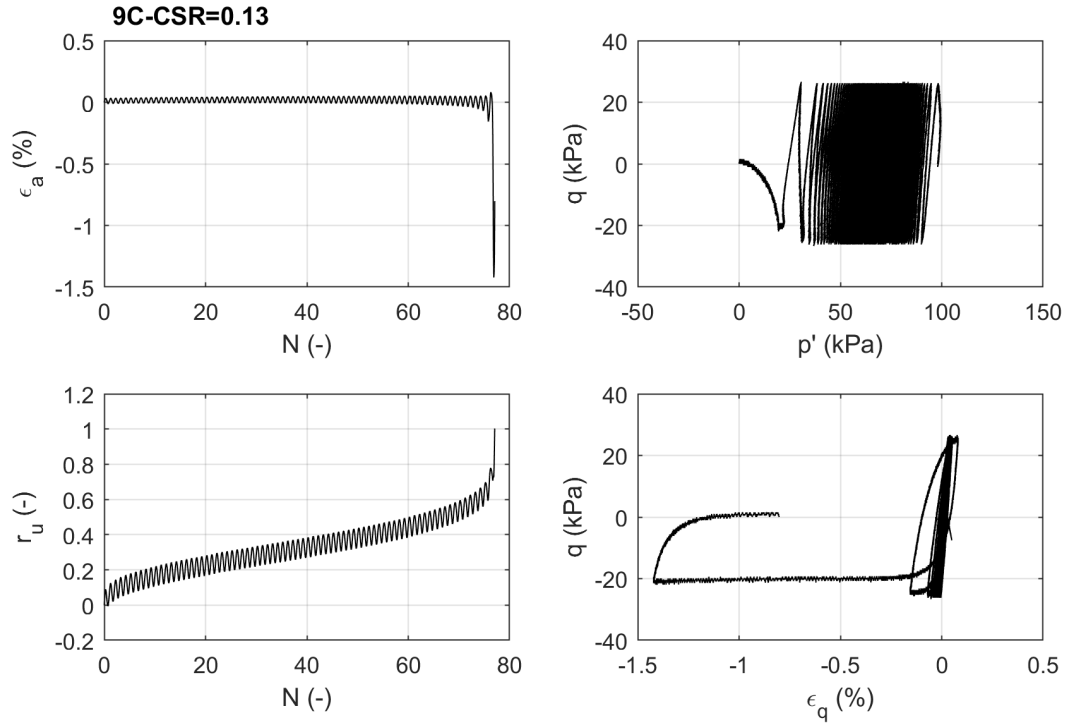

Figure 7.7: *ID=9C.*

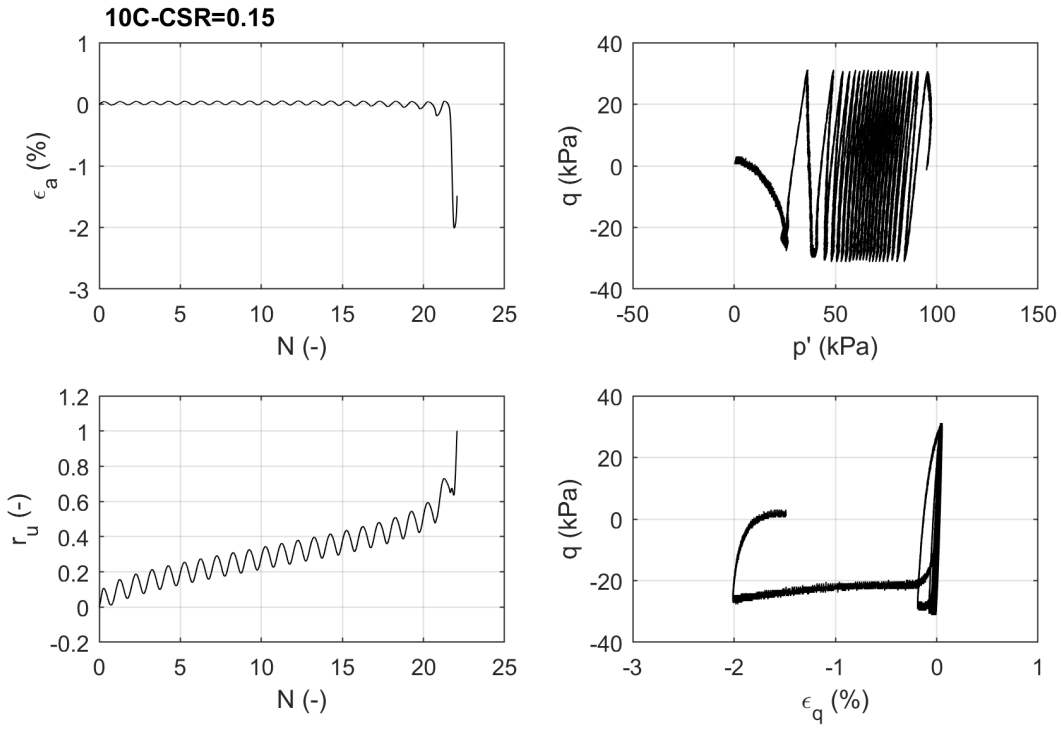

Figure 7.8: *ID=10C.*

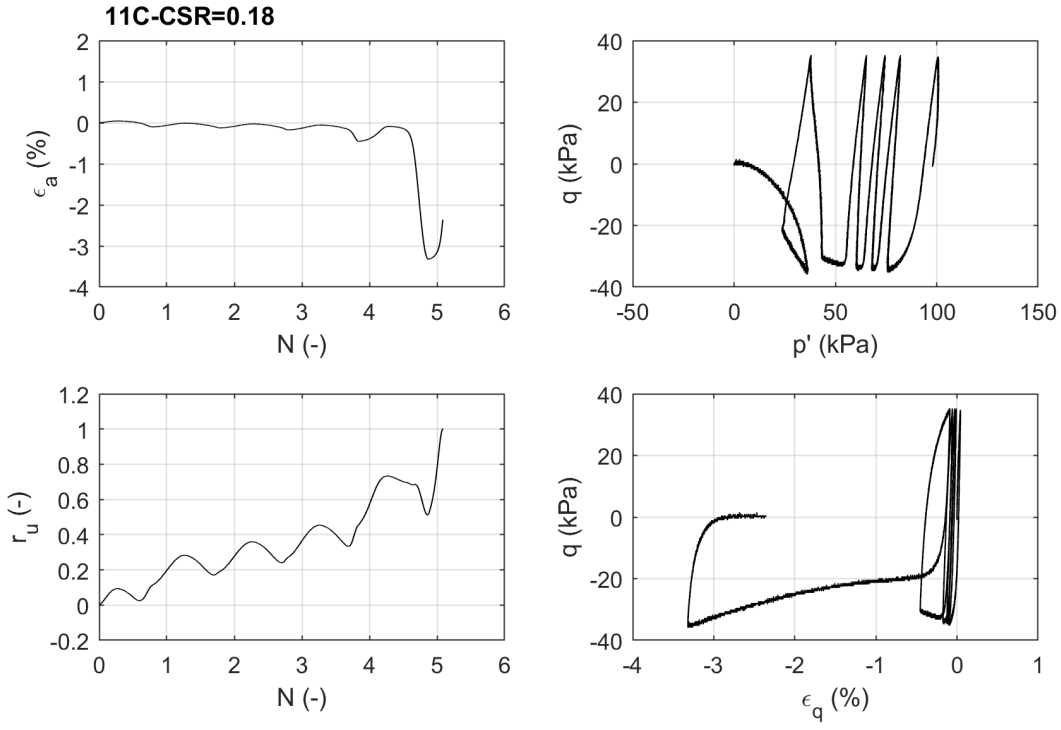

Figure 7.9: *ID=11C.*

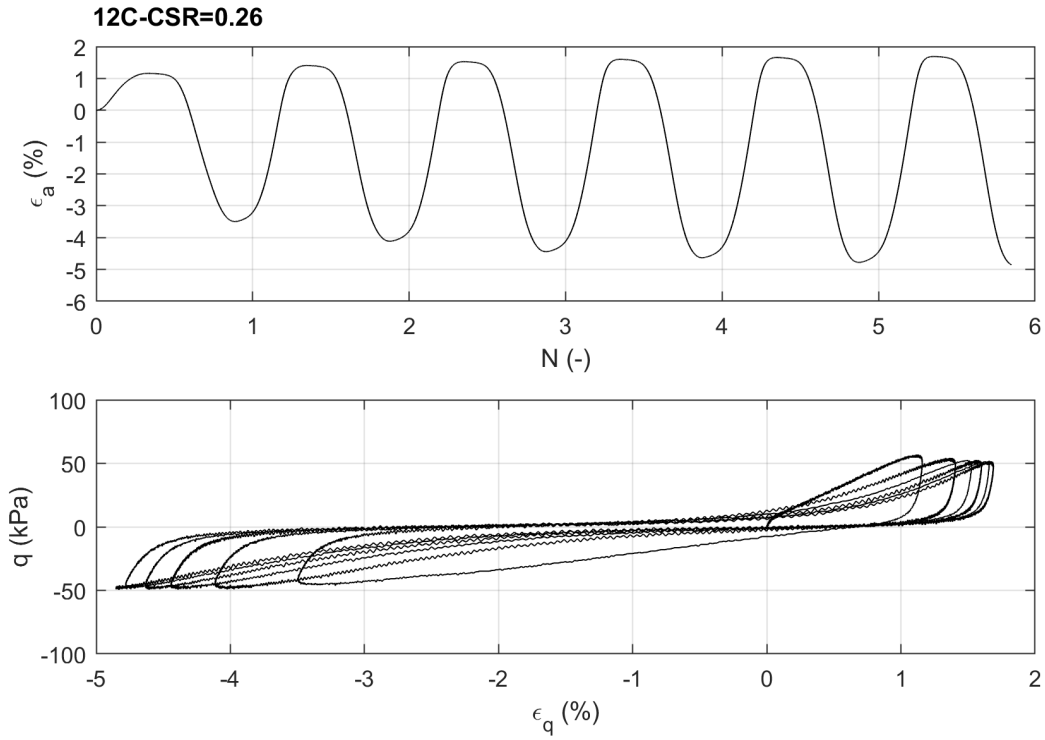

Figure 7.10: *ID=12C.*

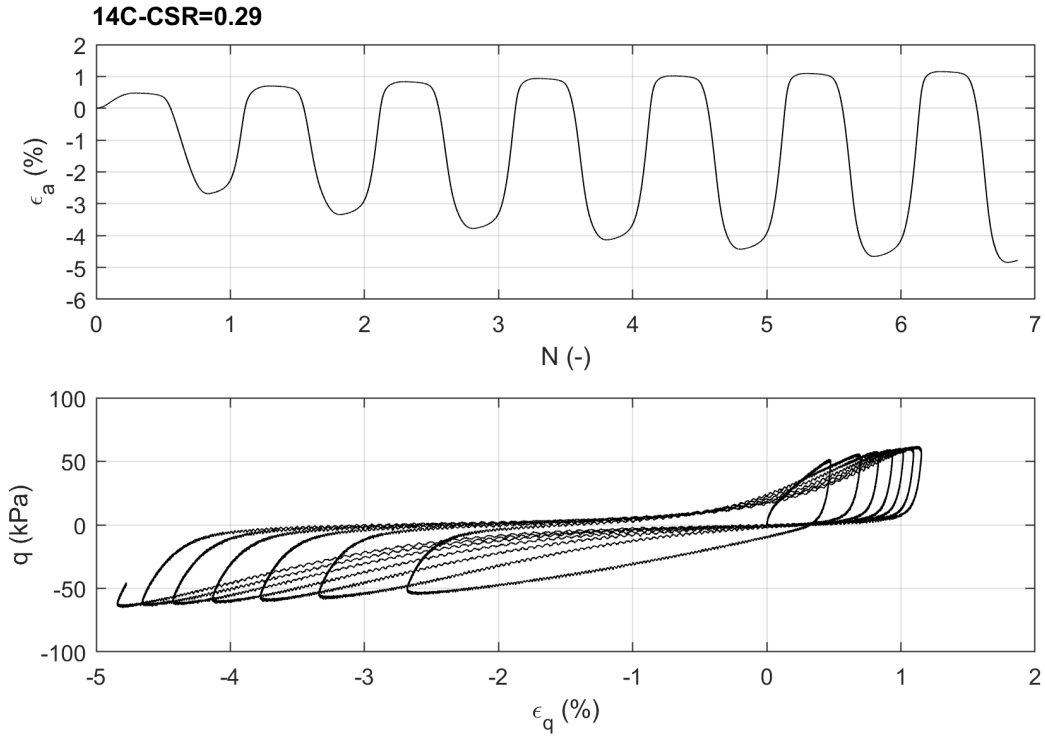

Figure 7.11: *ID=14C.*

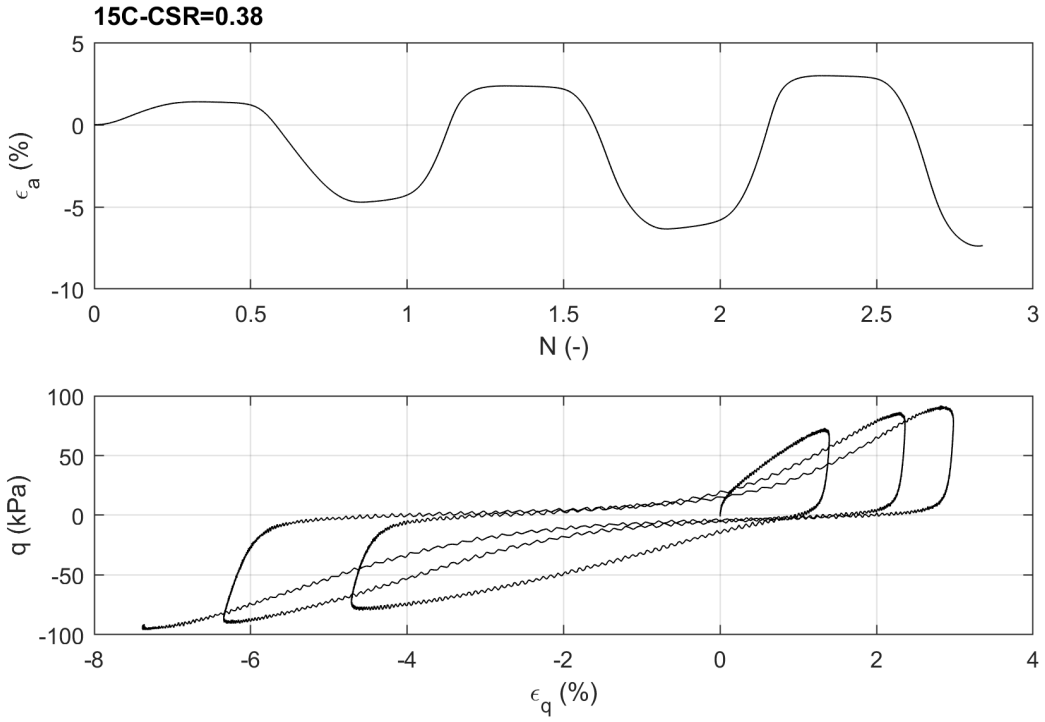

Figure 7.12: *ID=15C.*

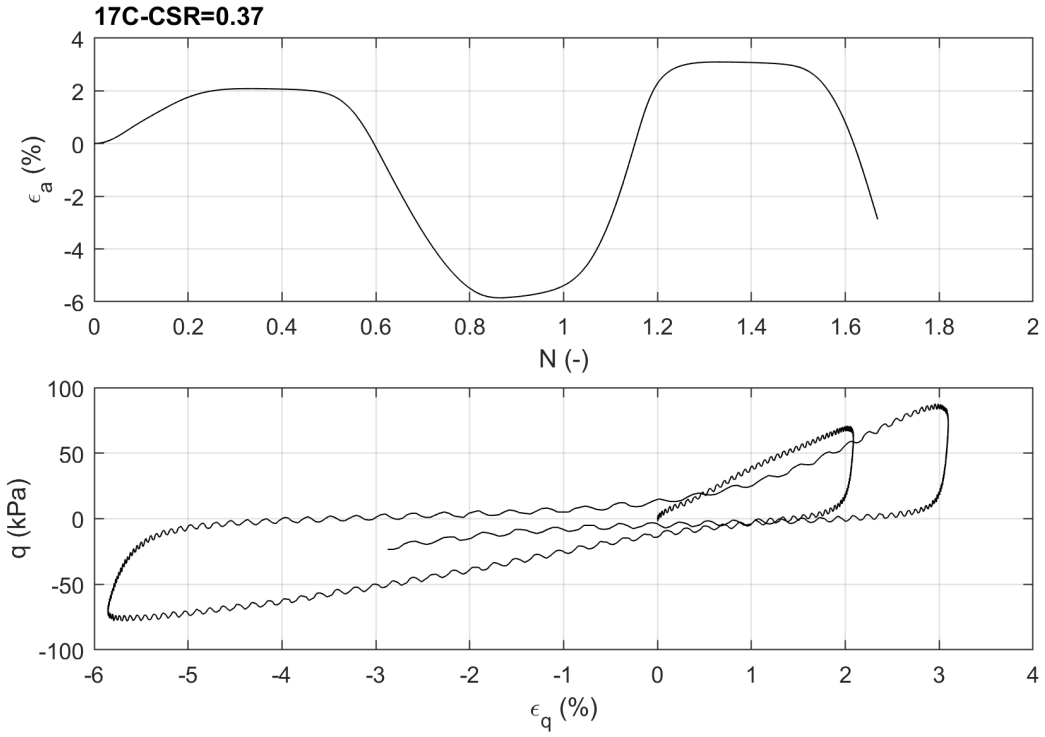

Figure 7.13: *ID=17C.*

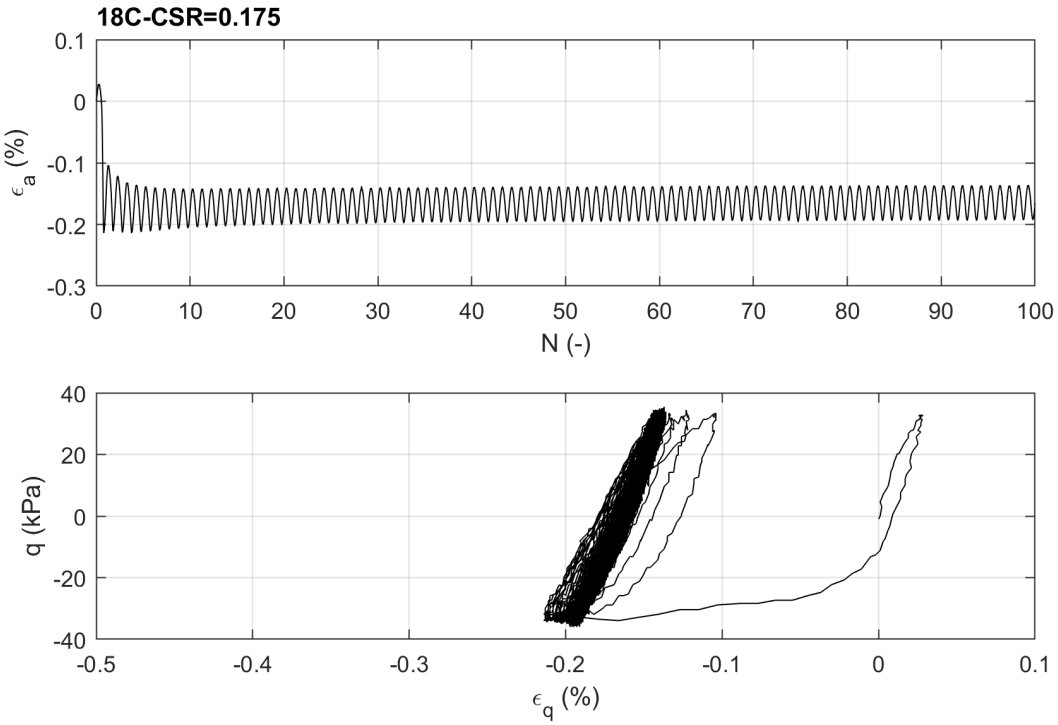

Figure 7.14: *ID=18C.*

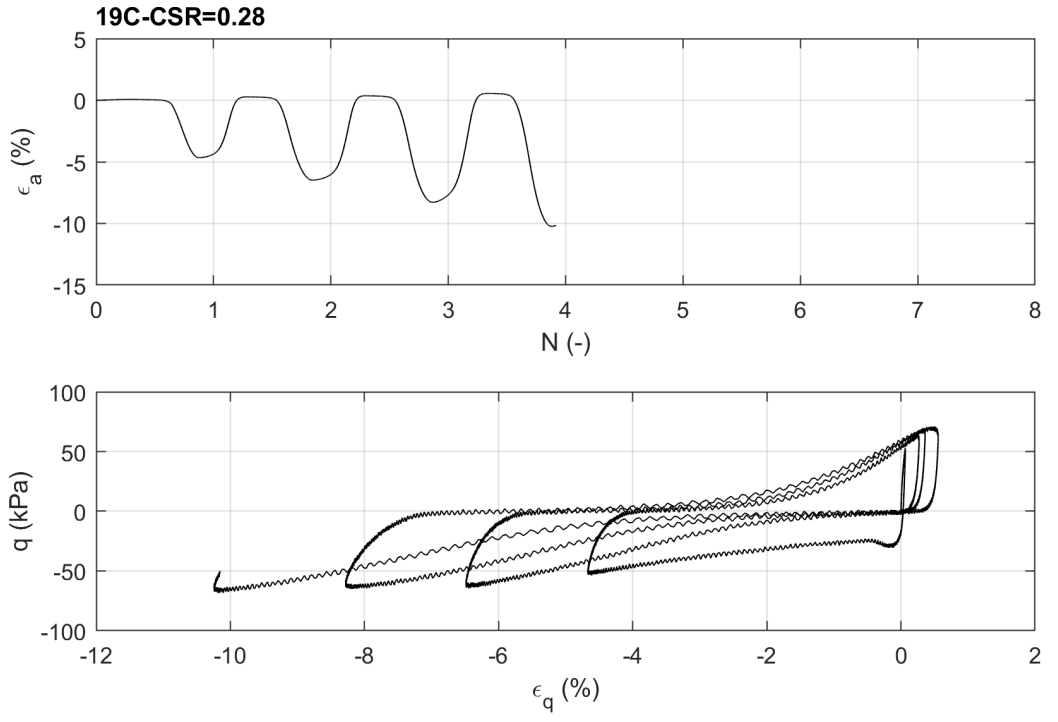

Figure 7.15: *ID=19C.*

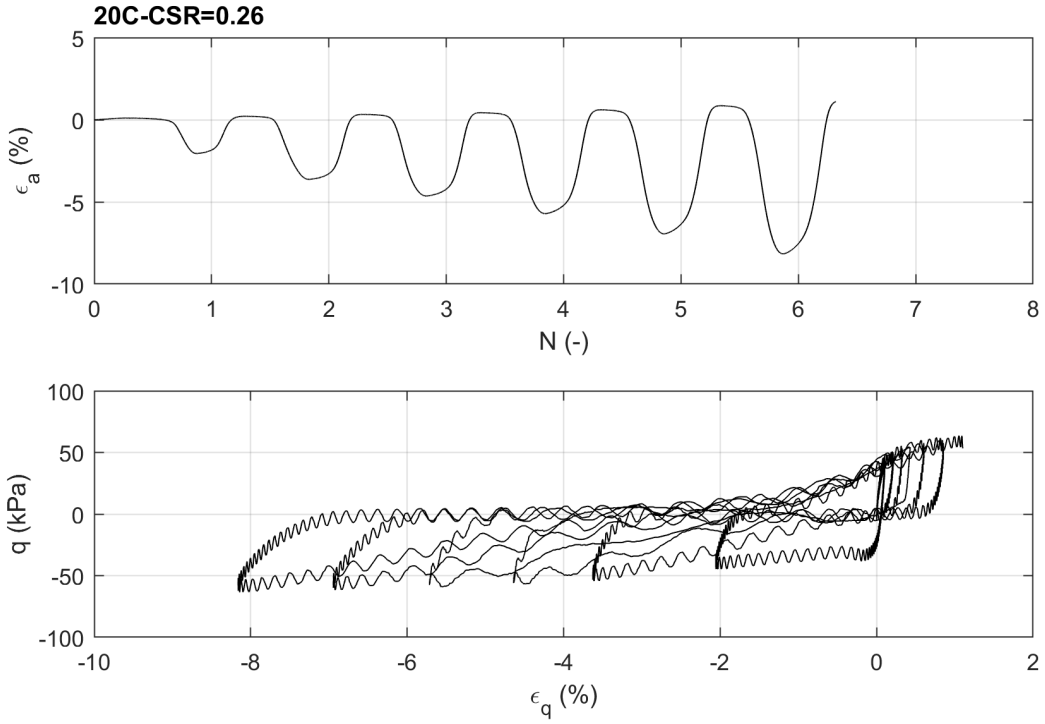

Figure 7.16: *ID=20C.*

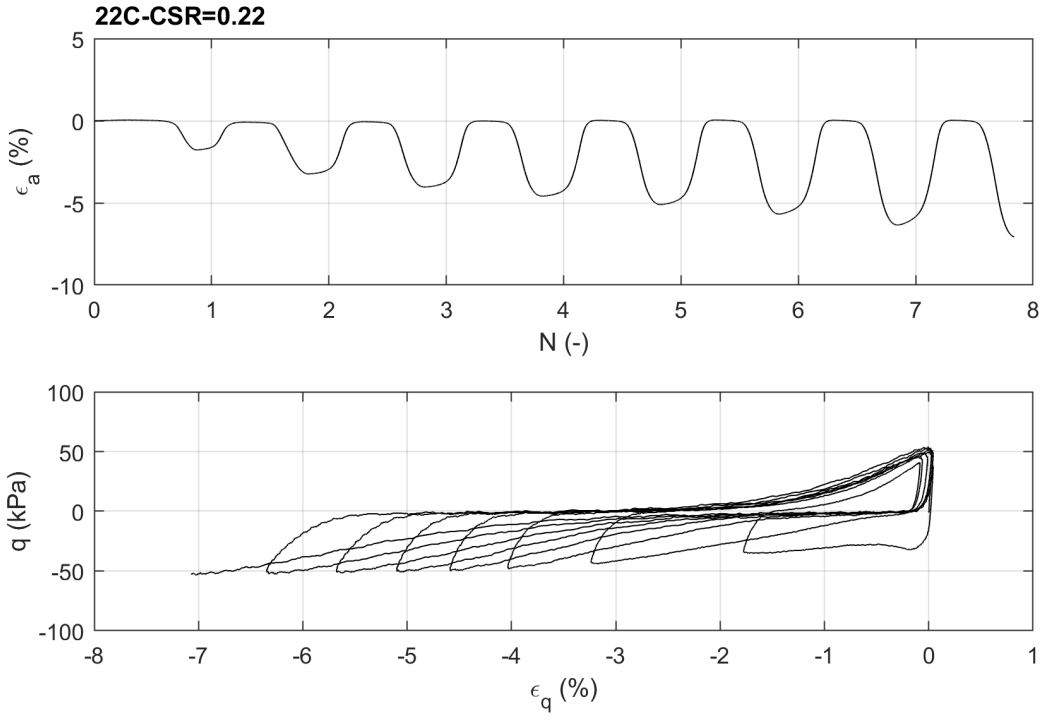

Figure 7.17: *ID=22C.*

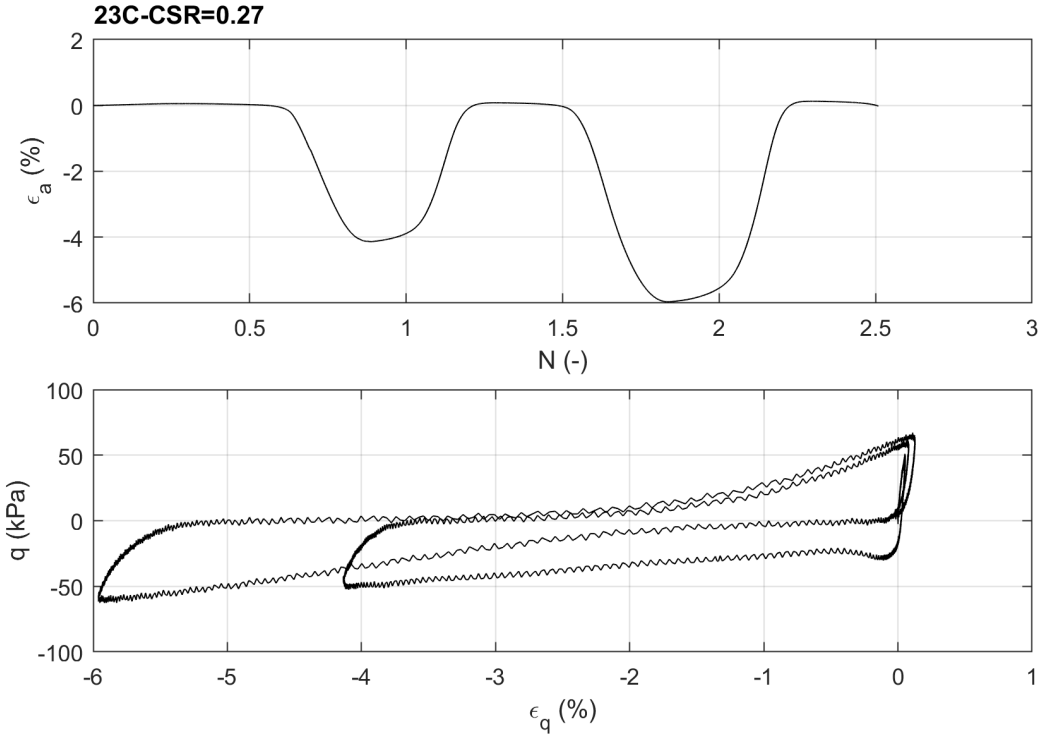

Figure 7.18: *ID=23C.*

Bibliography

Aboshi, H., Mizuno, Y., and Kuwabara, M. (1991). Present state of sand compaction pile in japan. In *Deep Foundation Improvements: Design, Construction, and Testing*. ASTM International.

Adalier, K. and Elgamal, A. (2004). Mitigation of liquefaction and associated ground deformations by stone columns. *Engineering Geology*, 72(3-4):275–291.

Agapoulaki, G. I. and Papadimitriou, A. G. (2015). Rheological properties of colloidal silica as a means for designing passive stabilization of liquefiable soils. In *Proceeding of XVI ECSMGE Geotechnical Engineering for Infrastructure and Development*, pages 2331–2336.

Agapoulaki, G. I. and Papadimitriou, A. G. (2018). Rheological properties of colloidal silica grout for passive stabilization against liquefaction. *Journal of Materials in Civil Engineering*, 30(10):04018251.

Akiyoshi, T., Fuchida, K., Matsumoto, H., Hyodo, T., and Fang, H. (1993). Liquefaction analyses of sandy ground improved by sand compaction piles. *Soil Dynamics and Earthquake Engineering*, 12(5):299–307.

Andrianopoulos, K. I., Agapoulaki, G. I., and Papadimitriou, A. G. (2016). Simulation of seismic response of passively stabilised sand. *Geotechnical Research*, 3(2):40–53.

Andrus, R. D. and Chung, R. M. (1995). *Ground improvement techniques for liquefaction remediation near existing lifelines*. National Institute of Standards and Technology, Gaithersburg.

Baggs, S. A. (1983). Remote prediction of ground temperature in australian soils and mapping its distribution. *Solar Energy*, 30(4):351–366.

Bahadori, H. and Manafi, S. (2013). Investigation on the dynamic properties of saturated sand-tire chips mixture by shaking table. In *Proceedings of the 18th International Conference on Soil Mechanics and Geotechnical Engineering, Paris*, pages 883–886.

Bao, X., Jin, Z., Cui, H., Chen, X., and Xie, X. (2019). Soil liquefaction mitigation in geotechnical engineering: An overview of recently developed methods. *Soil Dynamics and Earthquake Engineering*, 120:273–291.

Batilas, A., Pantazopoulos, I., and Athanasopoulos, G. (2018). Effects of colloidal silica grouting on the dynamic properties of sandy soils. In *Proceedings of the 16th European Conference on Earthquake Engineering, Thessaloniki*.

Been, K. and Jefferies, M. G. (1985). A state parameter for sands. *Géotechnique*, 35(2):99–112.

Bergna, H. E. and Roberts, W. O. (2005). *Colloidal silica: fundamentals and applications*. CRC Press.

Bolisetti, T., Reitsma, S., and Balachandar, R. (2009). Experimental investigations of colloidal silica grouting in porous media. *Journal of geotechnical and geoenvironmental engineering*, 135(5):697–700.

Boulanger, R. W. and Hayden, R. F. (1995). Aspects of compaction grouting of liquefiable soil. *Journal of geotechnical engineering*, 121(12):844–855.

Bradley, B. A. and Cubrinovski, M. (2011). Near-source strong ground motions observed in the 22 february 2011 christchurch earthquake. *Bulletin of the New Zealand Society for Earthquake Engineering*, 44(4):181–194.

Brennan, A. J. and Madabhushi, S. P. G. (2002). Effectiveness of vertical drains in mitigation of liquefaction. *Soil Dynamics and Earthquake Engineering*, 22(9-12):1059–1065.

Burbank, M., Weaver, T., Lewis, R., Williams, T., Williams, B., and Crawford, R. (2013). Geotechnical tests of sands following bioinduced calcite precipitation catalyzed by indigenous bacteria. *Journal of Geotechnical and Geoenvironmental Engineering*, 139(6):928–936.

Burbank, M. B., Weaver, T. J., Green, T. L., Williams, B. C., and Crawford, R. L. (2011). Precipitation of calcite by indigenous microorganisms to strengthen liquefiable soils. *Geomicrobiology Journal*, 28(4):301–312.

Butrón, C., Gustafson, G., Fransson, Å., and Funehag, J. (2010). Drip sealing of tunnels in hard rock: A new concept for the design and evaluation of permeation grouting. *Tunnelling and Underground Space Technology*, 25(2):114–121.

Cao, X., Cummins, H. Z., and Morris, J. F. (2010). Structural and rheological evolution of silica nanoparticle gels. *Soft Matter*, 6(21):5425–5433.

Castanier, S., Le Métayer-Levrel, G., and Perthuisot, J.-P. (1999). Ca-carbonates precipitation and limestone genesis—the microbiogeologist point of view. *Sedimentary geology*, 126(1-4):9–23.

Castro, G. (1975). Liquefaction and cyclic mobility of saturated sands. *Journal of the Geotechnical Engineering Division*, 101(6):551–569.

Castro, G., Enos, J. L., France, J. W., and Poulos, S. J. (1982). Liquefaction induced by cyclic loading. *NASA STI/Recon Technical Report N*, 83.

Castro, G. and Poulos, S. J. (1977). Factors affecting liquefaction and cyclic mobility. *Journal of Geotechnical and Geoenvironmental Engineering*, 103(6):501–516.

Chiaro, G., Modoni, G., and Salvatore, E. (2014). Prediction of the effects of compaction on granular materials. In *Proceedings of the International Symposium on Geomechanics from Micro to Macro, Cambridge, UK, Soga et al.(Eds), Taylor & Francis Group (London)*, pages 1189–1194.

Clough, G. W., Iwabuchi, J., Rad, N. S., and Kuppusamy, T. (1989). Influence of cementation on liquefaction of sands. *Journal of Geotechnical Engineering*, 115(8):1102–1117.

Conlee, C. T., Gallagher, P. M., Boulanger, R. W., and Kamai, R. (2012). Centrifuge modeling for liquefaction mitigation using colloidal silica stabilizer. *Journal of Geotechnical and Geoenvironmental Engineering*, 138(11):1334–1345.

De Groot, M., Kudella, M., Meijers, P., and Oumeraci, H. (2006). Liquefaction phenomena underneath marine gravity structures subjected to wave loads. *Journal of waterway, port, coastal, and ocean engineering*, 132(4):325–335.

DeJong, J. T., Fritzges, M. B., and Nüsslein, K. (2006). Microbially induced cementation to control sand response to undrained shear. *Journal of Geotechnical and Geoenvironmental Engineering*, 132(11):1381–1392.

DeJong, J. T., Mortensen, B. M., Martinez, B. C., and Nelson, D. C. (2010). Bio-mediated soil improvement. *Ecological Engineering*, 36(2):197–210.

Díaz-Rodríguez, J. A. and Antonio-Izarraras, V. M. (2004). Mitigation of liquefaction risk using colloidal silica stabilizer. In *13 th World Conference on Earthquake Engineering, Vancouver, Canada*.

Díaz-Rodríguez, J. A., Antonio-Izarraras, V. M., Bandini, P., and López-Molina, J. A. (2008). Cyclic strength of a natural liquefiable sand stabilized with colloidal silica grout. *Canadian Geotechnical Journal*, 45(10):1345–1355.

Ehrlich, H. L., Newman, D. K., and Kappler, A. (2015). *Ehrlich's geomicrobiology*. CRC press.

El Mohtar, C. S., Bobet, A., Drnevich, V. P., Johnston, C. T., and Santagata, M. C. (2014). Pore pressure generation in sand with bentonite: from small strains to liquefaction. *Géotechnique*, 64(2):108–117.

El Mohtar, C. S., Bobet, A., Santagata, M. C., Drnevich, V. P., and Johnston, C. T. (2013). Liquefaction mitigation using bentonite suspensions. *Journal of Geotechnical and Geoenvironmental Engineering*, 139(8):1369–1380.

El Mohtar, C. S., Clarke, J., Bobet, A., Santagata, M., Drnevich, V., and Johnston, C. (2008). Cyclic response of a sand with thixotropic pore fluid. In *Geotechnical earthquake engineering and soil dynamics IV*, pages 1–10.

Eseller-Bayat, E., Yegian, M. K., Alshawabkeh, A., and Gokyer, S. (2012a). Liquefaction response of partially saturated sands. i: Experimental results. *Journal of Geotechnical and Geoenvironmental Engineering*, 139(6):863–871.

Eseller-Bayat, E., Yegian, M. K., Alshawabkeh, A., and Gokyer, S. (2012b). Liquefaction response of partially saturated sands. ii: Empirical model. *Journal of Geotechnical and Geoenvironmental Engineering*, 139(6):872–879.

Eseller-Bayat, E. E., Yegian, M. K., Alshawabkeh, A., and Gokyer, S. (2009). A new mitigation technique for preventing liquefaction-induced building damages during earthquakes. In *WCCE–ECCE–TCCE Joint Conference: EARTHQUAKE & TSUNAMI*.

Facciorusso, J., Madiai, C., and Vannucchi, G. (2015). Cpt-based liquefaction case history from the 2012 emilia earthquake in italy. *Journal of Geotechnical and Geoenvironmental Engineering*, 141(12):05015002.

Facciorusso, J., Madiai, C., and Vannucchi, G. (2016). The 2012 emilia earthquake (italy): geotechnical characterization and ground response analyses of the paleo-reno river levees. *Soil Dynamics and Earthquake Engineering*, 86:71–88.

Finn, W. D., Pickering, D. J., and Bransby, P. L. (1971). Sand liquefaction in triaxial and simple shear tests. *Journal of Soil Mechanics and Foundations Division*, 97(SM4):639–659.

Fioravante, V., Giretti, D., Abate, G., Aversa, S., Boldini, D., Capilleri, P. P., Cavallaro, A., Chamlagain, D., Crespellani, T., Dezi, F., et al. (2013). Earthquake geotechnical engineering aspects of the 2012 emilia-romagna earthquake (italy). In *7th International Conference on Case Histories in Geotechnical Engineering*. Missouri University of Science and Technology.

Fujita, Y., Ferris, F. G., Lawson, R. D., Colwell, F. S., and Smith, R. W. (2000). Subscribed content calcium carbonate precipitation by ureolytic subsurface bacteria. *Geomicrobiology Journal*, 17(4):305–318.

Gallagher, P. M. (2000). *Passive site remediation for mitigation of liquefaction risk*. PhD thesis, Virginia Polytechnic Institute and State University, Blacksburg, VA, US.

Gallagher, P. M., Conlee, C. T., and Rollins, K. M. (2007a). Full-scale field testing of colloidal silica grouting for mitigation of liquefaction risk. *Journal of Geotechnical and Geoenvironmental Engineering*, 133(2):186–196.

Gallagher, P. M. and Finsterle, S. (2004). Physical and numerical model of colloidal silica injection for passive site stabilization. *Vadose Zone Journal*, 3(3):917–925.

Gallagher, P. M. and Koch, A. J. (2003). Model testing of passive site stabilization: A new grouting technique. In *Grouting and ground treatment*, pages 1478–1489.

Gallagher, P. M. and Lin, Y. (2005). Column testing to determine colloidal silica transport mechanisms. In *Innovations in grouting and soil improvement*, pages 1–10.

Gallagher, P. M. and Lin, Y. (2009). Colloidal silica transport through liquefiable porous media. *Journal of geotechnical and geoenvironmental engineering*, 135(11):1702–1712.

Gallagher, P. M. and Mitchell, J. K. (2002). Influence of colloidal silica grout on liquefaction potential and cyclic undrained behavior of loose sand. *Soil Dynamics and Earthquake Engineering*, 22(9):1017–1026.

Gallagher, P. M., Pamuk, A., and Abdoun, T. (2007b). Stabilization of liquefiable soils using colloidal silica grout. *Journal of Materials in Civil Engineering*, 19(1):33–40.

Gallagher, P. M., Pamuk, A., Koch, A. J., and Abdoun, T. H. (2002). Centrifuge modeling of passive site remediation. In *Proc., 7th United States National Conf. on Earthquake Engineering (7NCEE): Urban Earthquake Risk*. Earthquake Engineering Research Institute Oakland, CA, US.

Georgiannou, V. N., Pavlopoulou, E.-M., and Bikos, Z. (2017). Mechanical behaviour of sand stabilised with colloidal silica. *Geotechnical Research*, 4(1):1–11.

Ghionna, V. N. and Porcino, D. (2006). Liquefaction resistance of undisturbed and reconstituted samples of a natural coarse sand from undrained cyclic triaxial tests. *Journal of Geotechnical and Geoenvironmental Engineering*, 132(2):194–202.

Grozic, J. L., Robertson, P. K., and Morgenstern, N. R. (1999). The behavior of loose gassy sand. *Canadian Geotechnical Journal*, 36(3):482–492.

Grozic, J. L., Robertson, P. K., and Morgenstern, N. R. (2000). Cyclic liquefaction of loose gassy sand. *Canadian Geotechnical Journal*, 37(4):843–856.

Hamderi, M. and Gallagher, P. M. (2013). An optimization study on the delivery distance of colloidal silica. *Scientific Research and Essays*, 8(27):1314–1323.

Hamderi, M. and Gallagher, P. M. (2015). Pilot-scale modeling of colloidal silica delivery to liquefiable sands. *Soils and Foundations*, 55(1):143–153.

Hazarika, H., Hyodo, M., and Yasuhara, K. (2010). Investigation of tire chips-sand mixtures as preventive measure against liquefaction.

Hazarika, H., Yasuhara, K., Hyodo, M., Karmokar, A., and Mitarai, Y. (2008). Mitigation of earthquake induced geotechnical disasters using a smart and novel geomaterial. In *Proceedings of the 14th World Conference on Earthquake Engineering*.

Hazarika, H., Yasuhara, K., Karmokar, A., and Mitarai, Y. (2007). Shaking table test on liquefaction prevention using tire chips and sand mixture. In *Proceedings of the International workshop on scrap tire derived geomaterials—opportunities and challenges, Yokosuka, Japan*, pages 215–222.

He, J. and Chu, J. (2014). Undrained responses of microbially desaturated sand under monotonic loading. *Journal of Geotechnical and Geoenvironmental Engineering*, 140(5):04014003.

He, J., Chu, J., Wu, S.-f., and Peng, J. (2016). Mitigation of soil liquefaction using microbially induced desaturation. *Journal of Zhejiang University-SCIENCE A*, 17(7):577–588.

He, J., Ivanov, V., and Chu, J. (2013). Mitigation of liquefaction of saturated sand using biogas. *Géotechnique*, 63(4):267–275.

Huang, Y. and Wen, Z. (2015). Recent developments of soil improvement methods for seismic liquefaction mitigation. *Natural Hazards*, 76(3):1927–1938.

Hyodo, M., Murata, H., Yasufuku, N., and Fujii, T. (1991). Undrained cyclic shear strength and residual shear strain of saturated sand by cyclic triaxial tests. *Soils and Foundations*, 31(3):60–76.

Hyodo, M., Yamada, S., Orense, R., Okamoto, M., and Hazarika, H. (2007). Undrained cyclic shear properties of tire chip-sand mixtures. In *Proceedings of the international workshop on scrap tire derived geomaterials—opportunities and challenges, Yokosuka, Japan*, pages 187–196.

Idriss, I. M. and Boulanger, R. W. (2008). *Soil liquefaction during earthquakes*. Earthquake Engineering Research Institute, CA, US.

Iler, K. R. (1979). *The chemistry of silica*. John Wiley and Sons Inc, New York, US.

Indraratna, B., Chu, J., and Rujikiatkamjorn, C. (2015). *Ground Improvement Case Histories: Chemical, Electrokinetic, Thermal and Bioengineering*. Butterworth-Heinemann.

Ishihara, K. (1985). Stability of natural deposits during earthquakes. In *Proceedings of 11th International Conference on Soil Mechanics and Foundation Engineering*, pages 321–376.

Ishihara, K. (1996). *Soil behaviour in earthquake geotechnics*. Clarendon Press, Oxford, UK.

Ismail, M. A., Joer, H. A., Sim, W. H., and Randolph, M. F. (2002). Effect of cement type on shear behavior of cemented calcareous soil. *Journal of Geotechnical and Geoenvironmental Engineering*, 128(6):520–529.

Ivanov, V. and Chu, J. (2008). Applications of microorganisms to geotechnical engineering for bioclogging and biocementation of soil in situ. *Reviews in Environmental Science and Bio/Technology*, 7(2):139–153.

Ivanov, V., Chu, J., Stabnikov, V., He, J., and Naeimi, M. (2010). Iron-based bio-grout for soil improvement and land reclamation. In *Proceedings of the 2nd International Conference on Sustainable Construction Materials and Technologies, Italy*, pages 415–420.

Iwasaki, T., Tatsuoka, F., and Takagi, Y. (1978). Shear moduli of sands under cyclic torsional shear loading. *Soils and Foundations*, 18(1):39–56.

Japanese Geotechnical Society, J. G. S. (1998). *Remedial measures against liquefaction*. Balkema.

Kakavand, A. and Dabiri, R. (2018). Experimental study of applying colloidal nano silica in improving sand-silt mixtures. *International Journal of Nano Dimension*, 9(4):357–373.

Kananizadeh, N., Ebadi, T., Ehsan, S., Rizi, M., and Khoshniat, S. A. (2011). Behavior of nanoclay as an addetive in order to reduce kahrizak landfill clay permeability. In *Proceeding of 2nd International Conference on Environmental Science and Technology*, pages 26–28.

Kaneko, T., Orense, R. P., Hyodo, M., and Yoshimoto, N. (2012). Seismic response characteristics of saturated sand deposits mixed with tire chips. *Journal of Geotechnical and Geoenvironmental Engineering*, 139(4):633–643.

Karol, R. H. and Berardinelli, C. (2003). *Chemical grouting and soil stabilization*. M. Dekker New York.

Kavazanjian, E., O'Donnell, S. T., and Hamdan, N. (2015). Biogeotechnical mitigation of earthquake-induced soil liquefaction by denitrification: A two-stage process. In *Proceedings of the 6th International Conference on Earthquake Geotechnical Engineering*, pages 1–4.

Kodaka, T., Ohno, Y., and Takyu, T. (2005). Cyclic shear characteristics of treated sand with colloidal silica grout. In *Proceedings of the International Conference on Soil Mechanics and Geotechnical Engineering*, volume 16, pages 401–404. Aa Balkema Publishers.

Kramer, S. L. (1996). *Geotechnical Earthquake Engineering*. Prentice Hall, New York, US.

Ladd, R. S. (1978). Preparing test specimens using undercompaction. *Geotechnical Testing Journal*, 1(1):16–23.

Lade, P. V. (1993). Initiation of static instability in the submarine nerlerk berm. *Canadian Geotechnical Journal*, 30(6):895–904.

Liao, H. J., Huang, C. C., and Chao, B. S. (2003). Liquefaction resistance of a colloid silica grouted sand. In *Grouting and ground treatment*, pages 1305–1313.

Lu, Y. and Tan, Y. (2012). Examination of loose saturated sands impacted by a heavy tamper. *Environmental Earth Sciences*, 66(5):1557–1567.

Lupini, J. F., Skinner, A. E., and Vaughan, P. R. (1981). The drained residual strength of cohesive soils. *Géotechnique*, 31(2):181–213.

Mashiri, M. S., Vinod, J. S., and Sheikh, M. N. (2015). Liquefaction potential and dynamic properties of sand-tyre chip (stch) mixtures. *Geotechnical Testing Journal*, 39(1):69–79.

Matso, K. (1995). Lessons from kobe. *Civil Engineering*, 65(4).

Mitchell, J. K. and Wentz, F. J. (1991). *Performance of improved ground during the Loma Prieta Earthquake*, volume 91. Earthquake Engineering Research Center, University of California Berkeley.

Modoni, G. and Gazzellone, A. (2011). Experimental observations on the critical state of granular materials. In *Proceedings of the 5th International Symposium on Deformation Characteristics of Geomaterials, Seoul, Korea*, pages 850–857.

Mollamahmutoglu, M. and Yilmaz, Y. (2010). Pre-and post-cyclic loading strength of silica-grouted sand. In *Proceedings of the Institution of Civil Engineers-Geotechnical Engineering*, volume 163, pages 343–348.

Montoya, B. M., DeJong, J. T., and Boulanger, R. W. (2013). Dynamic response of liquefiable sand improved by microbial-induced calcite precipitation. *Géotechnique*, 63(4):302–312.

Moradi, G. and Seyedi, S. (2015). Effect of sampling method on strength of stabilized silty sands with colloidal nano silica. *Journal of Civil Engineering Research*, 5(6):129–135.

Moridis, G. J., Apps, J., Persoff, P., Myer, L., Muller, S., Yen, P., and Pruess, K. (1996). A field test of a waste containment technology using a new generation of injectable barrier liquids. *Spectrum'96, Seattle, WA, US*, pages 18–23.

Moridis, G. J., Persoff, P., Apps, J. A., Myer, L., Pruess, K., and Yen, P. (1995). A field test of permeation grouting in heterogeneous soils using a new generation of barrier liquids. Technical report, Lawrence Berkeley Lab., CA, US.

Nashed, R., Thevanayagam, S., Martin, G. R., and Shenthan, T. (2004). Liquefaction mitigation in silty soils using dynamic compaction and wick drains. In *Proceedings of 13th World Conference on Earthquake Engineering*.

Nemati, M. and Voordouw, G. (2003). Modification of porous media permeability, using calcium carbonate produced enzymatically in situ. *Enzyme and Microbial Technology*, 33(5):635–642.

Nikookar, M., Bahari, M., Nikookar, H., and Arabani, M. (2013). The strength characteristics of silty soil stabilized using nano-clay. In *Proc. of 7th Symposium on Advances in Science & Technology (7thsastech)*.

Noll, M. R., Bartlett, C., and Dochat, T. M. (1992). In situ permeability reduction and chemical fixation using colloidal silica. In *Proceeding of the Sixth National Outdoor Action Conference on Aquifer Restoration, Ground Water Monitoring, and Geophysical Method, National Ground Water Association*, pages 443–457.

Noll, M. R., Epps, D. E., Bartlett, C. L., and Chen, P. J. (1993). Pilot field application of a colloidal silica gel technology for in situ hot spot stabilization and horizontal grouting. In *Proc., 7th National Outdoor Action Conf*, pages 207–219.

Nouri Delavar, I. and Noorzad, R. (2017). Drained shear strength parameters of silty sand grouted by colloidal silica. *International Journal of Geotechnical Engineering*, pages 1–8.

Ohsaki, Y. (1970). Effects of sand compaction on liquefaction during the tokachioki earthquake. *Soils and Foundations*, 10(2):112–128.

Okamoto, M., Orense, R., Hyodo, M., and Kuwata, J. (2008). Monotonic shear behaviour of sand-tyre chips mixtures. In *Proceedings of the geotechnical symposium, New Zealand Geotechnical Society, Auckland, NZ*, pages 75–80.

Okamura, M., Ishihara, M., and Oshita, T. (2003). Liquefaction resistance of sand deposit improved with sand compaction piles. *Soils and Foundations*, 43(5):175–187.

Okamura, M., Ishihara, M., and Tamura, K. (2006). Degree of saturation and liquefaction resistances of sand improved with sand compaction pile. *Journal of geotechnical and geoenvironmental engineering*, 132(2):258–264.

Okamura, M. and Soga, Y. (2006). Effects of pore fluid compressibility on liquefaction resistance of partially saturated sand. *Soils and Foundations*, 46(5):695–700.

Okamura, M., Takebayashi, M., Nishida, K., Fujii, N., Jinguji, M., Imasato, T., Yasuhara, H., and Nakagawa, E. (2011). In-situ desaturation test by air injection and its evaluation through field monitoring and multiphase flow simulation. *Journal of Geotechnical and Geoenvironmental Engineering*, 137(7):643–652.

Onoue, A. (1988). Consolidation of multilayered anisotropic soils by vertical drains with well resistance. *Soils and Foundations*, 28(3):75–90.

Oumeraci, H. (1994). Review and analysis of vertical breakwater failures—lessons learned. *Coastal Engineering*, 22(1-2):3–29.

Pal, S. and Deb, K. (2018). Effect of stiffness of stone column on drainage capacity during soil liquefaction. *International Journal of Geomechanics*, 18(3):04018003.

Pamuk, A., Gallagher, P. M., and Zimmie, T. F. (2007). Remediation of piled foundations against lateral spreading by passive site stabilization technique. *Soil Dynamics and Earthquake Engineering*, 27(9):864–874.

Peacock, W. H. and Seed, H. B. (1968). Sand liquefaction under cyclic loading simple shear conditions. *Journal of Soil Mechanics & Foundations Division*, 94(SM3):689–708.

Pedrotti, M., Wong, C., El Mountassir, G., and Lunn, R. J. (2017). An analytical model for the control of silica grout penetration in natural groundwater systems. *Tunnelling and Underground Space Technology*, 70:105–113.

Peng, E.-x. and Zhang, D.-w. (2017). Prevention of liquefaction of saturated sand using biogas produced by *Pseudomonas stutzeri*. In *International Conference on Transportation Infrastructure and Materials*.

Persoff, P., Apps, J., Moridis, G., and Whang, J. M. (1999). Effect of dilution and contaminants on sand grouted with colloidal silica. *Journal of Geotechnical and Geoenvironmental Engineering*, 125(6):461–469.

Persoff, P., Moridis, G. J., Apps, J., Pruess, K., and Muller, S. J. (1994). Designing injectable colloidal silica barriers for waste isolation at the hanford site. In *Proceedings of the 33rd Hanford Symposium on Health and Environment—In situ Remediation: Scientific Basis for Current and Future Technologies*, pages 87–101. Part 1, Pasco, Wash,US.

Polito, C. P. and Martin II, J. R. (2001). Effects of nonplastic fines on the liquefaction resistance of sands. *Journal of Geotechnical and Geoenvironmental Engineering*, 127(5):408–415.

Popiel, C. O., Wojtkowiak, J., and Biernacka, B. (2001). Measurements of temperature distribution in ground. *Experimental thermal and fluid science*, 25(5):301–309.

Porcino, D., Ghionna, V. N., Granata, R., and Marcianò, V. (2015). Laboratory determination of mechanical and hydraulic properties of chemically grouted sands. *Geomechanics and Geoengineering*, 11(2):164–175.

Porcino, D., Marcianò, V., and Granata, R. (2011). Undrained cyclic response of a silicate-grouted sand for liquefaction mitigation purposes. *Geomechanics and Geoengineering*, 6(3):155–170.

Porcino, D., Marcianò, V., and Granata, R. (2012). Static and dynamic properties of a lightly cemented silicate-grouted sand. *Canadian Geotechnical Journal*, 49(10):1117–1133.

Poulos, S. J. (1981). The steady state of deformation. *Journal of Geotechnical and Geoenvironmental Engineering*, 107(GT5):553–562.

Promputthangkoon, P. and Hyde, A. F. L. (2007). Compressibility and liquefaction potential of rubber composite soils. In *Proceedings of the international workshop on scrap tire derived geomaterials—opportunities and challenges, Yokosuka, Japan*, pages 161–170.

Rao, G. V. and Dutta, R. K. (2006). Compressibility and strength behaviour of sand–tyre chip mixtures. *Geotechnical & Geological Engineering*, 24(3):711–724.

Rasouli, R., Hayashi, K., and Zen, K. (2016). Controlled permeation grouting method for mitigation of liquefaction. *Journal of Geotechnical and Geoenvironmental Engineering*, 142(11):04016052.

Rebata-Landa, V. and Santamarina, J. C. (2012). Mechanical effects of biogenic nitrogen gas bubbles in soils. *Journal of Geotechnical and Geoenvironmental Engineering*, 138(2):128–137.

Roscoe, K. H., Schofield, A., and Wroth, C. P. (1958). On the yielding of soils. *Geotechnique*, 8(1):22–53.

Rugg, D., Yoon, J., Hwang, H., and El Mohtar, C. (2011). Undrained shearing properties of sand permeated with a bentonite suspension for static liquefaction mitigation. In *Geo-Frontiers 2011: Advances in Geotechnical Engineering*, pages 677–686.

Saleh-Lakha, S., Shannon, K. E., Henderson, S. L., Goyer, C., Trevors, J. T., Zebarth, B. J., and Burton, D. L. (2009). Effect of ph and temperature on denitrification gene expression and activity in pseudomonas mandelii. *Applied and environmental microbiology*, 75(12):3903–3911.

Salvatore, E., Andò, E., Proia, R., Modoni, G., and Viggiani, G. (2018). Effect of strain localization on the response of granular materials subjected to monotonic and cyclic triaxial tests. *Rivista italiana di Geotecnica*, 52(2):30–43.

Salvatore, E., Modoni, G., Andò, E., Albano, M., and Viggiani, G. (2017). Determination of the critical state of granular materials with triaxial tests. *Soils and Foundations*, 57(5):733–744.

Saxena, S. K., Reddy, K. R., and Avramidis, A. S. (1988). Liquefaction resistance of artificially cemented sand. *Journal of Geotechnical Engineering*, 114(12):1395–1413.

Schnaid, F., Prietto, P. D. M., and Consoli, N. C. (2001). Characterization of cemented sand in triaxial compression. *Journal of Geotechnical and Geoenvironmental Engineering*, 127(10):857–868.

Schofield, A. and Wroth, P. (1968). *Critical state soil mechanics*, volume 310. McGraw-Hill, London, UK.

Schwarz, L. G. and Chirumalla, M. (2007). Effect of injection pressure on permeability and strength of microfine cement grouted sand. In *Grouting for ground improvement: Innovative concepts and applications*, pages 1–15.

Seed, H. B. and Booker, J. R. (1977). Stabilization of potentially liquefiable sand deposits using gravel drains. *Journal of Geotechnical and Geoenvironmental Engineering*, 103(7):757–768.

Seed, H. B. and Idriss, I. (1982). *Ground motions and soil liquefaction during earthquakes: engineering monographs on earthquake criteria, structural design, and strong motion records. MNO-5*. Earthquake Engineering Research Institute, Oakland, California.

Seed, H. B. and Idriss, I. M. (1971). Simplified procedure for evaluating soil liquefaction potential. *Journal of Soil Mechanics & Foundations Div*, 97(9):1249–1273.

Seed, H. B. and Lee, K. L. (1966). Liquefaction of saturated sands during cyclic loading. *Journal of Soil Mechanics and Foundations Division*, 92(SM6):105–134.

Seright, R. (1995). Reduction of gas and water permeabilities using gels. *SPE Production & Facilities*, pages 103–108.

Shenthan, T., Nashed, R., Thevanayagam, S., and Martin, G. R. (2004). Liquefaction mitigation in silty soils using composite stone columns and dynamic compaction. *Earthquake Engineering and Engineering Vibration*, 3(1):39–50.

Silver, M. L., Chan, C. K., Ladd, R. S., Lee, K. L., Tiedemann, D. A., Townsend, F. C., Valera, J. E., and Wilson, J. H. (1976). Cyclic triaxial strength of standard test sand. *Journal of Geotechnical and Geoenvironmental Engineering*, 102(5):511–523.

Šimek, M. and Cooper, J. E. (2002). The influence of soil ph on denitrification: progress towards the understanding of this interaction over the last 50 years. *European Journal of Soil Science*, 53(3):345–354.

Sladen, J. A., D'hollander, R. D., and Krahn, J. (1985). The liquefaction of sands, a collapse surface approach. *Canadian Geotechnical Journal*, 22(4):564–578.

Spencer, L., Rix, G. J., and Gallagher, P. M. (2008). Colloidal silica gel and sand mixture dynamic properties. In *Geotechnical Earthquake Engineering and Soil Dynamics IV*, pages 1–10.

Spencer, L. M., Glenn, J., and Gallagher, P. M. (2007). Dynamic properties of colloidal silica gel and sand mixtures. In *Proceedings of the 4th international conference on earthquake geotechnical engineering, Thessaloniki, GR*, number 1324.

Stabnikov, V., Ivanov, V., and Chu, J. (2015). Construction biotechnology: a new area of biotechnological research and applications. *World Journal of Microbiology and Biotechnology*, 31(9):1303–1314.

Stanford, G., Dzienia, S., and Vander Pol, R. A. (1975). Effect of temperature on denitrification rate in soils 1. *Soil Science Society of America Journal*, 39(5):867–870.

Stocks-Fischer, S., Galinat, J. K., and Bang, S. S. (1999). Microbiological precipitation of caco3. *Soil Biology and Biochemistry*, 31(11):1563–1571.

Taboada, V. (1995). *Centrifuge modeling of earthquake-induced lateral spreading using a laminar box*. PhD Thesis, Department of Civil Engineering, Rensselaer Polytechnic Institute.

Tamura, S., Tokimatsu, K., Abe, A., and Sato, M. (2002). Effects of air bubbles on b-value and p-wave velocity of a partly saturated sand. *Soils and foundations*, 42(1):121–129.

Tatsuoka, F., Muramatsu, M., and Sasaki, T. (1982). Cyclic undrained stress-strain behavior of dense sands by torsional simple shear test. *Soils and Foundations*, 22(2):55–70.

Terzaghi, K. v. (1936). The shearing resistance of saturated soils and the angle between the planes of shear. In *Proceedings of the 1st international conference on soil mechanics and foundation engineering*, volume 1, pages 54–56. Harvard University Press Cambridge, MA, US.

Tokimatsu, K., Yoshimi, Y., and Ariizumi, K. (1990). Evaluation of liquefaction resistance of sand improved by deep vibratory compaction. *Soils and Foundations*, 30(3):153–158.

Towhata, I. (2008). *Geotechnical Earthquake Engineering*. Springer Science & Business Media.

Towhata, I. and Kabashima, Y. (2001). Mitigation of seismically-induced deformation of loose sandy foundation by uniform permeation grouting. In *Proc. Earthquake Geotechnical Engineering Satellite Conference, XVth International Conference on Soil Mechanics and Geotechnical Engineering, Istanbul, Turkey*, pages 313–318.

Tsukamoto, Y., Ishihara, K., Nakazawa, H., Kamada, K., and Huang, Y. (2002). Resistance of partly saturated sand to liquefaction with reference to longitudinal and shear wave velocities. *Soils and foundations*, 42(6):93–104.

Uchimura, T., Chi, N., Nirmalan, S., Sato, T., Meidani, M., and Towhata, I. (2007). Shaking table tests on effect of tire chips and sand mixture in increasing liquefaction resistance and mitigating uplift of pipe. In *Proceedings of the International workshop on scrap tire derived geomaterials—opportunities and challenges, Yokosuka, Japan*, pages 179–186.

Vaid, Y. P. and Chern, J. (1983). Effect of static shear on resistance to liquefaction. *Soils and foundations*, 23(1):47–60.

Vaid, Y. P. and Negussey, D. (1988). Preparation of reconstituted sand specimens. In *Advanced triaxial testing of soil and rock*. ASTM International.

Vaid, Y. P. and Sivathayalan, S. (1996). Static and cyclic liquefaction potential of fraser delta sand in simple shear and triaxial tests. *Canadian Geotechnical Journal*, 33(2):281–289.

Van Paassen, L. A., Daza, C. M., Staal, M., Sorokin, D. Y., van der Zon, W., and van Loosdrecht, M. C. (2010). Potential soil reinforcement by biological denitrification. *Ecological Engineering*, 36(2):168–175.

Van Paassen, L. A., Harkes, M. P., Van Zwieten, G. A., Van der Zon, W. H., Van der Star, W. R. L., and Van Loosdrecht, M. C. M. (2009). Scale up of biogrout: a biological ground reinforcement method. In *Proceedings of the 17th international conference on soil mechanics and geotechnical engineering*, pages 2328–2333. Lansdale IOS Press.

Vannucchi, G., Crespellani, T., Facciorusso, J., Ghinelli, A., Madiai, C., Puliti, A., Renzi, S., et al. (2012). Soil liquefaction phenomena observed in recent seismic events in emilia-romagna region, italy. *International Journal of Earthquake Engineering*, 2(3):20–29.

Vranna, A. and Tika, T. (2015). Undrained monotonic and cyclic behaviour of a silty sand stabilized with colloidal silica. In *6th International Conference on Earthquake Geotechnical Engineering, Christchurch, NZ*.

Weaver, T. J., Burbank, M., Lewis, A., Lewis, R., Crawford, R., and Williams, B. (2011). Bio-induced calcite, iron, and manganese precipitation for geotechnical engineering applications. In *Geo-Frontiers 2011: Advances in Geotechnical Engineering*, pages 3975–3983.

Whang, J. M. (1995). Chemical-based barrier materials. *Assessment of barrier containment technologies for environmental remediation applications*, 9:211–247.

Whiffin, V. S. (2004). *Microbial CaCO3 precipitation for the production of biocement*. PhD thesis, Murdoch University, Western Australia.

Wong, C., Pedrotti, M., El Mountassir, G., and Lunn, R. J. (2018). A study on the mechanical interaction between soil and colloidal silica gel for ground improvement. *Engineering Geology*, 243:84–100.

Wood, D. M. (1990). *Soil behaviour and critical state soil mechanics*. Cambridge university press, UK.

Xia, H. and Hu, T. (1991). Effects of saturation and back pressure on sand liquefaction. *Journal of Geotechnical Engineering*, 117(9):1347–1362.

Yamamuro, J. A., Covert, K. M., and Lade, P. V. (2018). Static and cyclic liquefaction of silty sands. In *Physics and mechanics of soil liquefaction*, pages 55–65. Routledge.

Yang, J. (2002). Non-uniqueness of flow liquefaction line for loose sand. *Géotechnique*, 52(10):757–760.

Yang, J., Savidis, S., and Roemer, M. (2004). Evaluating liquefaction strength of partially saturated sand. *Journal of Geotechnical and Geoenvironmental Engineering*, 130(9):975–979.

Yegian, M. K., Eseller-Bayat, E., Alshawabkeh, A., and Ali, S. (2007). Induced-partial saturation for liquefaction mitigation: experimental investigation. *Journal of Geotechnical and Geoenvironmental Engineering*, 133(4):372–380.

Yonekura, R. and Miwa, M. (1993). Fundamental properties of sodium silicate based grout. In *Eleventh South East Asian Geotechnical Conference, Singapore*, pages 439–444.

Yoon, J. and El Mohtar, C. S. (2013). Dynamic rheological properties of sodium pyrophosphate-modified bentonite suspensions for liquefaction mitigation. *Clays and Clay Minerals*, 61(4):319–327.

Yoshimi, Y., Tanaka, K., and Tokimatsu, K. (1989). Liquefaction resistance of a partially saturated sand. *Soils and foundations*, 29(3):157–162.

Youd, T. L. and Idriss, I. M. (2001). Liquefaction resistance of soils: summary report from the 1996 nceer and 1998 nceer/nsf workshops on evaluation of liquefaction resistance of soils. *Journal of geotechnical and geoenvironmental engineering*, 127(4):297–313.

Zornberg, J. G., Cabral, A. R., and Viratjandr, C. (2004). Behaviour of tire shred sand mixtures. *Canadian Geotechnical Journal*, 41(2):227–241.